

Bacterially Derived Non-Ribosomally Synthesized Peptides:
Isolation, Structural Elucidation, Total Synthesis and Biological
Investigation

By
Andrew Tyler

A thesis submitted in partial fulfilment of the requirements
for the degree of
Doctor of Philosophy



September 2018

Abstract

Siderophores are non-ribosomally derived peptides, and are key components in bacterial virulence and in the bacterial endogenous secondary metabolome. Therefore, they provide a unique insight into bacterial infection and potential treatments.

As such, we have isolated two bacterial siderophores, the first being produced by a novel *Actinomadura* species. We carried out a de novo structural determination, utilising NMR, HMRS and Marfey's analysis, allowing us to identify the isolated siderophore as madurastatin C1. This work also allowed us to determine the absolute stereochemistry of madurastatin C1 and ultimately reassigned the structures of the madurastatin family of siderophores. This culminated in a publication in the ACS Journal of Natural Products in early 2017. As a continuation of this work, the total synthesis of madurastatin C1 has been completed.

A second novel bacterial strain yielded a novel siderophore like peptide, with structural similarities to the known siderophores; chlorocatechelins. Once again the structure was elucidated via NMR and HRMS with the stereochemistry assigned through Marfey's analysis. The total synthesis of this novel siderophore was completed, and the synthetic material used in biological studies, confirming the efficacy of the originally isolated natural product.

Acknowledgements

First and foremost, I would like to thank my supervisor Dr. Michael Hall for his support over the entire duration of my PhD. Over the last 4 years Dr. Hall has been an excellent mentor, teacher and friend. His patience and understanding have enabled me to overcome many of the challenges encountered over the course of my PhD, whilst his two favourite mantras “get back to the lab and do some work” and “pint?” have an uncanny ability to be said at the perfect moment. He has been a constant driving force behind my research whilst also allowing me to have the down time required to make the most of the research I have carried out over my time here, I owe him a great deal. Thank you, Dr. Hall.

Furthermore, I would like to extend my thanks to all of the members of the MJH research group, both past and present; who have been a pleasure to work with and whom I count amongst my closest friends. I would like to specifically thank Dr. Stephanie Morton-Laing and Dr. Joseph Cowell for their support during the pivotal first 6 months of my PhD. I would also like to thank all the current members of the MJH research group for your support in the lab and your assistance in enabling me to have a work-life balance outside of the laboratory.

I also wish to thank my colleagues at Demuris, CBCB and Pinnacle, particularly Dr. Hamed Mosaei Sejzi and Dr. Bernhard Kepplinger, for their assistance in providing the bacterial natural products and their analysis during the course of my PhD research, without which the project would not exist. I also wish to thank the staff at Newcastle university, particularly Dr. Corrine Wills and Professor William McFarlane for their excellent NMR work and Dr. Paul Waddell for his assistance in X-ray crystallography throughout my whole time here.

Finally I wish to thank my partner, Giorgia Fagnani. My family, in particular my mother and brother, and all my friends outside of Newcastle. You are all a constant source of support, your contribution to the successful completion of my PhD should not be underestimated.

List of abbreviations

aq.	Aqueous
Ar	Aromatic
Bn	Benzyl
calcd	Calculated
Cbz	Carboxybenzyl
COSY	Correlation spectroscopy
DCC	Dicyclohexylcarbodiimide
DCM	Dichloromethane
DIPEA	N,N-Diisopropylethylamine
DMF	Dimethyl formamide
DMSO	Dimethyl sulphoxide
eq	equivalents
Et ₂ O	Diethyl ether
Et ₃ N	Triethylamine
EtOAc	Ethyl Acetate
g	Grams
h	Hours
HATU	1-[Bis(dimethylamino)methylene]-1H-1,2,3-triazolo[4,5-b]pyridinium 3-oxid hexafluorophosphate
HMBC	Heteronuclear multiple bond correlation spectroscopy
HRMS	High Resolution Mass Spectrometry
HSQC	Heteronuclear single quantum correlation spectroscopy
IR	Infra Red
KOH	Potassium hydroxide
lit.	Literature
M	Molar
<i>m</i> CPBA	3-Chloroperbenzoic acid
Me	Methyl
mg	milligram
mL	millilitre
mol.	Molecular
MRSA	Methicillin-resistant <i>Staphylococcus aureus</i>
nm	nanometers
NMR	Nuclear Magnetic Resonance
O.N.	Over night
PPM	Parts per million
<i>R_f</i>	Retention factor
RT	Room temperature
SPE	Solid phase extraction
TFA	Trifluoroacetic acid
THF	Tetrahydrofuran
TLC	Thin layer chromatography
Tr	Trityl
UV-Vis	Ultra Violet- Visual

Chapter 1 – Introduction	1
1.1 Natural products	1
1.2 Bacteria and human health	2
1.3 Bacterial siderophores	7
1.4 Uses of siderophores.....	14
1.5 Conclusions.....	24
Chapter 2 - Isolation and Structural Determination of Madurastatin C1 (DEM31376/A)	26
2.1 Introduction.....	26
2.2 Demuris Ltd.	26
2.3 Actinomadura sp. DEM31376	26
2.4 DEM31376/A.....	26
2.6 Initial structural studies of DEM31376/A.....	27
2.7 Structural determination of DEM31376/A <i>via</i> ¹ H, ¹³ C and ¹⁵ N NMR.....	28
2.8 Marfey's analysis.....	40
2.9 Advanced Marfey's analysis of DEM31376/A	43
2.10 Resolution of the structure of madurastatin C1	48
2.11 Conclusions for chapter 2.....	56
Chapter 3. Total Synthesis of Madurastatin C1.....	57
3.1 Introduction.....	57
3.2 Relevant literature	57
3.3 Project aims.....	59
3.4 Retrosynthetic Analysis	59
3.5 Results and discussion.....	61
3.6 Synthesis of the left-hand half of madurastatin C1 (52)	61
3.7 Synthesis of the right-hand half of madurastatin C1 (53).....	66
3.8 Final reactions to generate madurastatin C1.....	74
3.9 Conclusions and future work	77
Chapter 4. Bioactivity, Structural Determination and Total Synthesis of DEM30616/A.....	79
4.1 Introduction.....	79
4.2 Current inhibitors of eLtaS	80
4.3 Screening for LtaS inhibitors	80
4.4 Project aims.....	82
4.5 Structural determination of DEM30616/A.....	83
4.6 Structural determination of DEM30616/A <i>via</i> ¹ H, ¹³ C and ¹⁵ N NMR.....	83
4.7 Advanced Marfey's Analysis of DEM30616/A.....	90
4.8 Conclusions on structural assignment of DEM30616/A	91

4.9 Total synthesis of DEM30616/A (79).....	92
4.10 Biological studies using syn.30616/A (79).....	100
4.11 Conclusions	101
Chapter 5. Conclusions and Future Work	103
5.1 Conclusions.....	103
5.2 Summary of research on DEM31376/A	103
5.3 Future research on DEM31376/A (madurastatin C1)	108
5.4 Summary of research on DEM30616/A	109
5.5 Future research on DEM30616/A (syn.30616).....	112
Chapter 6 – Experimental.....	115
6.1 General experimental information	115
References.....	161
Appendix	166

Chapter 1 – Introduction

1.1 Natural products

1.1.1 Introduction to natural products

Natural products are small molecules produced by a living organism whether it be a bacteria, fungi, plant or animal. Natural products have been shown to have diverse biological activities, acting as stimulants, depressants, hallucinogens, pain killers and antimicrobials. Due to their useful biological properties and production by readily available organisms, natural products have been useful to mankind for thousands of years, with records documenting the use of plant derived medicinal agents in ancient Egypt dating back to 2900 BC.¹

1.1.2 Natural products and chemical research

Not unlike early man, both the pharmaceutical industry and research chemists have looked to investigate natural products as a source of novel bioactive molecules. This is due to the wide range of chemical structures produced in nature, which has given us molecules capable of reducing and controlling pain (morphine, **1**)², therapeutic molecules used as anticancer agents (paclitaxel, **2**)³ and as antibiotics to fight infections (penicillin, **3**)⁴. In addition to their utility, the synthesis of natural products is seen by many organic chemists as an intellectual challenge. The complexity of natural products gives chemists a great opportunity to push known chemical reactions to their limits, forcing new synthetic methodologies and new reagents to be developed to tackle these challenging substrates.

An example of the total synthesis of a natural product utilising new methodological approaches can be seen in the total synthesis of tropinone (**4**). The first synthesis of tropinone was completed in 1901 in a 1% overall yield by Willstätter.⁵ This was then ultimately superseded by a synthesis carried out by Robert Robinson, in which he synthesised tropinone in a single step using what we would come to know as a biomimetic synthetic strategy, building a molecule using the route that nature has previously developed.⁶

Furthermore the use of new reagents to synthesise challenging substrates can be exemplified by the Dicyclohexylcarbodiimide mediated total synthesis of penicillin V. Peptide (amide) bonds cannot be generated by the direct combination of an amine and a carboxylic acid, due to the protonation of the amine by the carboxylic acid, forming a stable salt.⁷ This inherent difficulty in generating an amide bond can be overcome by the generation of a reactive

carboxylic acid derivative such as an acid chloride. Unfortunately, the β -lactam ring found in penicillin V is susceptible to ring opening under the acidic conditions used to generate such reactive carboxylic acid derivatives, preventing the desired ring closure from taking place. The use of a reagent, that could assist in the rapid generation of an amide bond, ideally at neutral pH and room temperature, was desired. The use of DCC to facilitate ring closure generated penicillin V in an aqueous solution at room temperature and was the first reported total synthesis of penicillin V.^{8,9}

Recently there has been increased interest in natural products due to the emergence of multi-drug resistant bacteria and the requirement for new anti-microbial agents with which to treat them.

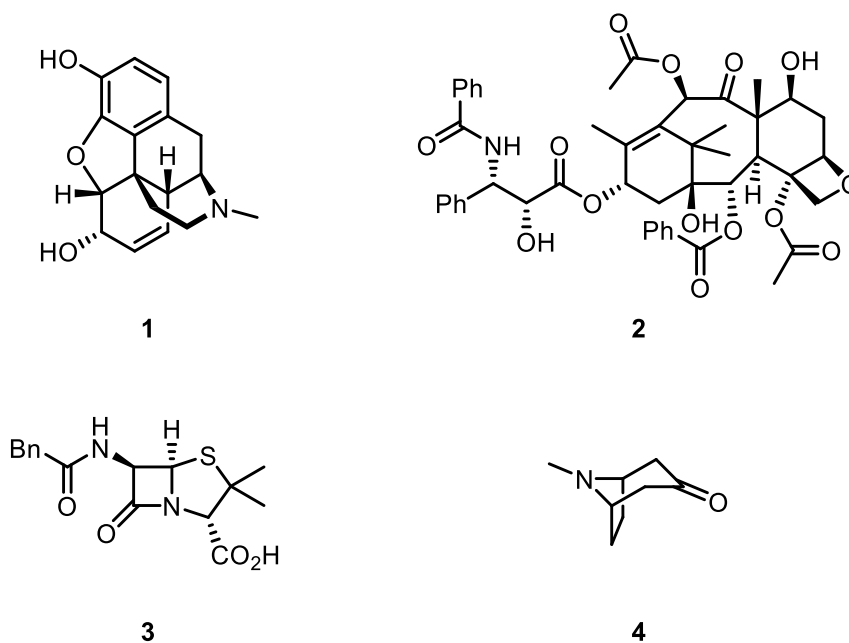


Figure 1. Chemical structures of morphine (1), paclitaxel (2), penicillin G (3) and tropinone (4)

1.2 Bacteria and human health

1.2.1 Introduction

Many bacteria can act as pathogens, posing a serious risk to human health. For more than half a century mankind has been able to treat bacterial infections using chemotherapeutic agents. This began with the serendipitous discovery of penicillin in 1929 for the treatment of infections by Gram-positive bacteria⁴ and the subsequent treatment of tuberculosis some 14 years later with the arrival of streptomycin.¹⁰ However bacteria are capable of evolving to become resistant to antibiotics. In fact, genes which encode for antibiotic resistance pre-date

the modern antibiotic era. Bacteria are known to produce antibiotics to provide a competitive advantage in the quest for resources they need to grow and thrive. As such other bacteria have evolved mechanisms to resist the action of these naturally occurring antibiotics.¹¹ In a similar way, our own advances in antibiotic discovery have been shadowed by the rise of bacteria that are resistant to known antibiotic treatments. This continual evolution of antibiotic resistant bacteria is of grave concern, as in the future once easily treatable bacterial infections could once again become deadly.

1.2.2 Antibiotic Resistance

Antibiotic resistance is now known against the vast majority of antibiotics currently in use, a timeline of which can be seen in Figure 2.

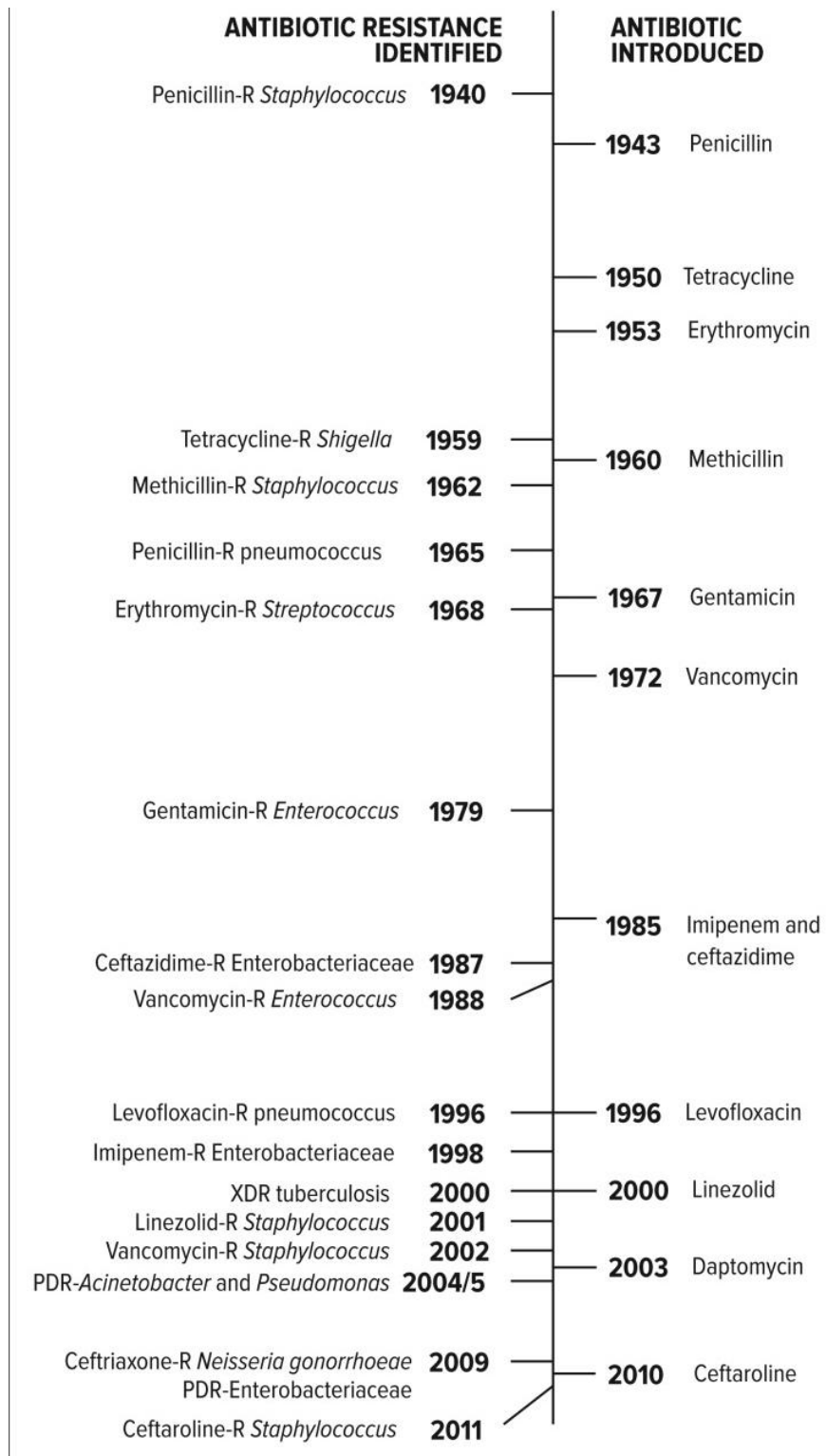


Figure 2. A timeline of antibiotic introduction and the first reports of observed resistance to the named drug. PDR = pan-drug-resistant; R = resistant; XDR = extensively drug-resistant. Figure taken from Ventola Ref: 12.

Resistance is even known for “drugs of last resort”. For example, antibiotic resistant strains of *Escherichia coli* have been discovered with resistance to polymyxin (colistin), an antibiotic

used for the treatment of Gram-negative infections.¹³ The *mcr-1* gene gives a plasmin-derived resistance against colistin. This is achieved by structurally altering lipid A, lowering its affinity toward colistin, and reducing the activity of this antibiotic agent.¹⁴ In addition, colistin resistance can be transferred between bacteria, including different species. This is achieved through a process known as horizontal gene transfer in which genes encoded on plasmid DNA are passed between bacterial cells. This has resulted in the rapid appearance of antibiotic resistant strains of *Salmonella enterica*, *Klebsiella pneumoniae*, *Enterobacter aerogenes* and *Enterobacter cloacae* against polymyxin all of which employ the *mcr-1* gene.¹³ Multiple resistance mechanisms in bacteria are now known, including alterations in the permeability of their cell membrane, alteration of the target site of an antibiotic, generation of enzymes capable of deactivating an antibiotic and the using of efflux mechanisms to pump drugs out of the bacterial cell.^{15,16}

Examples of mechanisms of antibiotic resistance

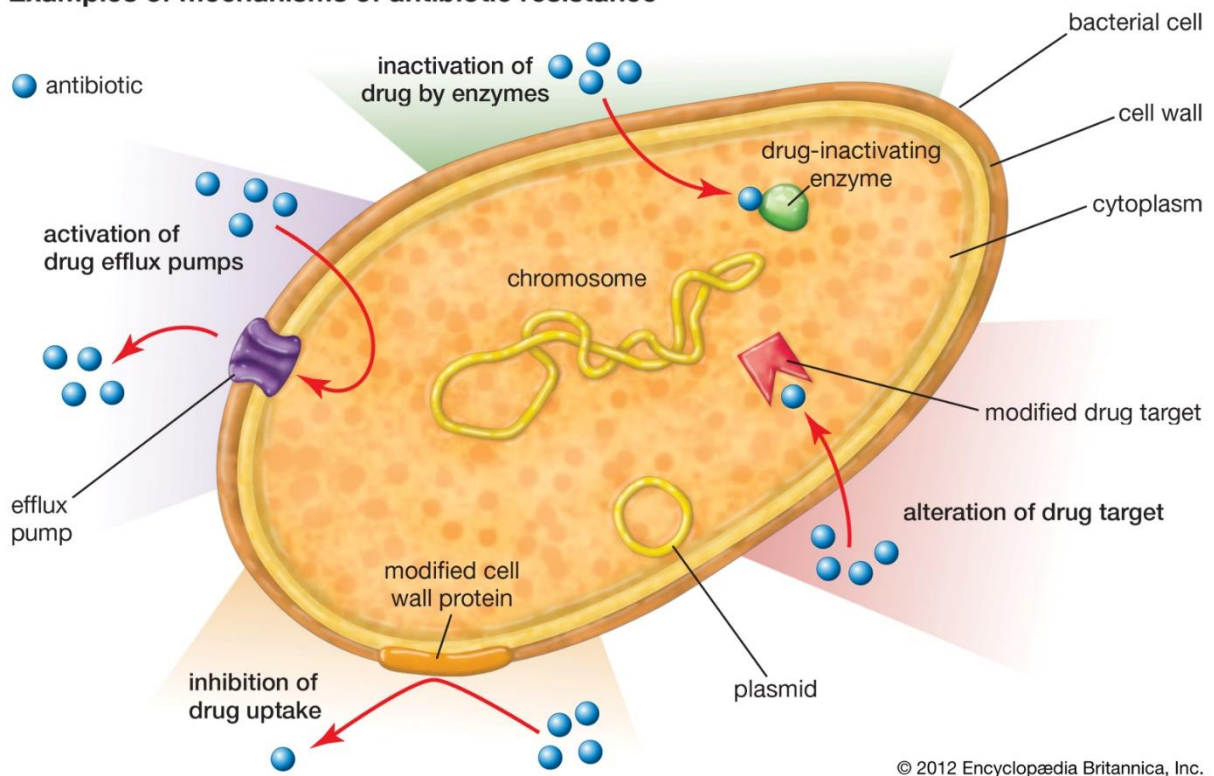


Figure 3. A diagram showing the various methods used by bacteria to incur antibiotic resistance, taken from the Encyclopædia Britannica Ref: 17.

Whilst the prevalence of antibiotic resistant bacteria has increased, very few new antibiotics have been produced in recent years.

1.2.3 Bacterial natural products as antibiotics

With an increasing need to develop novel antibiotics, many companies and research groups are now returning to investigating natural products as potential sources of new antibiotics. Traditionally plants provided the main source of natural products utilised by mankind, now however microorganisms are one of the key sources of bioactive natural products. Indeed, of the c. 50,000 known compounds produced by microbes, 46% are bioactive and 34% show antibiotic bioactivity.¹⁸ This greatly supersedes the percentages of bioactive natural products isolated from higher plants, with 16% of the total known number of plant derived natural products showing bioactivity and 2% showing antibiotic activity.¹⁸ As of 2005, up to 22,500 bioactive natural products had been isolated from microbes, with 17% of these isolated from unicellular bacteria, 38% by fungi and finally 45% from the bacterial genus actinomycetes.¹⁹ It is of no surprise then that the most thoroughly researched genus of bacteria is the actinomycetes, which were the origin of 75-80% of all microbially sourced natural products discovered in the latter half of the 20th century.¹⁸ Actinomycetes are known to produce some of our most essential antimicrobial agents, including the tetracyclines, rifamycins and streptomycins to name but a few.²⁰ The prevalence of antibiotic natural products from actinomycetes, coupled with the vast number of as yet unexplored bacterial species available (a single gram of soil can contain up to 5×10^4 species of bacteria, including many different actinomycete species),²¹ and the application of modern genomics and analytical techniques, has resulted in significant recent growth in the development of novel antibiotic natural products from bacteria.

However, despite the vast number of potential new antibiotic natural products available from bacterial sources, the development of any new antibiotic molecule will undoubtedly lead, sooner or later, to the evolution of resistant bacterial strains. Therefore, alternative approaches are needed in which an increased understanding of the life cycle of the bacteria could either reduce the ability of a pathogenic bacteria to infect a host or modulate the pathogenicity of an infectious bacteria.

1.2.4 Bacterial virulence

Whilst the need to develop new antibacterial drugs has been recognised, investigation of the methods used by bacteria to colonise human hosts is also of interest. Pathogenicity is the

ability of a microbe to cause disease. When considered in terms of their pathogenicity, bacteria can be divided into three groups. Primary pathogens are agents of disease, infections by *Vibrio cholerae* being the causative agent of cholera being one example.²² Opportunistic pathogens are organisms that have taken advantage of a hosts lowered immune system response, such as patients on immunosuppressants after an organ transplant or people suffering from HIV induced AIDS. Finally the vast majority of bacteria are classified as nonpathogens as they rarely or never cause human disease.²³

Bacterial virulence is the measure of pathogenicity, or the ability of the bacteria to cause damage to the host. The degree of virulence is governed by various factors including the number of infecting bacteria, the route of entry to the human body, the hosts defence mechanisms and the virulence factors of the bacterium. These virulence factors produced by bacteria are used, broadly speaking, to actively fight against the hosts immune system, from toxins (e.g. the *Botulinum* neurotoxins (BoNTs)), to more subtle bacterial cell surface modifications to evade immune system responses (e.g. to inhibit phagocytosis).²³ Ultimately, these virulence factors allow an invasive bacterium to colonise and replicate at the expense of the host. One class of bacterial virulence factors are known as siderophores, and interfering with the production, uptake and utilisation of siderophores by bacteria could suppress bacterial growth, reducing the rate of colonisation and allowing the immune system to tackle the bacterial infection without the need for the use of antibiotics. Due to their key role in bacterial virulence, we will now explore these natural products (bacterial siderophores) in more detail.

1.3 Bacterial siderophores

1.3.1 Introduction

Iron is an essential element for almost all life forms on the planet due to its key roles within the cell. This applies to all microorganisms, including bacteria and fungi, as well as plants and animals. Due to the favourable redox properties of iron, allowing exchange between two oxidation states (Fe^{2+} and Fe^{3+}), iron can partake in a large number of essential cellular processes including electron transport (e.g. cytochromes), oxygen transport (e.g. haemoglobin) and oxidative metabolism (e.g. P450s).^{24,25} However, despite the abundance of iron in the Earth's crust, iron is usually one of the limiting factors for bacterial cell growth and replication. In the case of bacterial cells, an internal cellular concentration of 10^{-7} to 10^{-5} M

ferrous iron (Fe^{2+}) is required.^{26–28} However, in aerobic environments Fe^{2+} is spontaneously oxidised to Fe^{3+} , going on to form ferric hydroxide ($\text{Fe}(\text{OH})_3$) in the presence of water.^{24,29,30} Ferric hydroxide is virtually insoluble in water and therefore the resulting free concentrations of Fe^{2+} (10^{-10} to 10^{-9} M) and Fe^{3+} (10^{-18} to 10^{-9} M) are very low in the environments in which many bacteria are normally found.^{26,27,31} Thus free Fe^{2+} and Fe^{3+} is effectively unavailable for utilisation by bacterial cells.

This low concentration of free iron in the environment also extends to the human body. The human body strives to keep concentrations of free iron very low ($< 10^{-24}$ M in human serum).³² Iron is stored within the human body, bound in tightly coordinated complexes such as lactoferrin, transferrin and haem. Normally, only 25–40% of the transferrin present in human serum is chelated to iron, enabling any free iron to be rapidly scavenged.²⁴ This low free iron concentration in human serum also helps to prevent colonisation of the human body by pathogenic bacteria. However, some pathogenic bacteria are capable of subverting the human iron storage systems to supply themselves with the iron they require. For example *Actinobacillus pleuropneumoniae* (the causative agent of porcine pleuropneumonia) expresses proteins that can uptake iron-containing transferrin for use by the bacteria.^{33,34} Similarly proteins associated with the uptake of haem have been found in the bacterial pathogens *Staphylococcus aureus*, *E. coli* and *Mycobacterium tuberculosis*.^{35,36}

Outside of a mammalian host, in order to utilise the insoluble Fe^{3+} found in aerobic environments, most bacteria biosynthesise and release extracellular iron scavengers that can chelate Fe^{3+} and transport it into the bacterial cell. These iron scavengers are called siderophores (from the Greek *sideros* meaning “iron” and *phores* meaning “bearer”),³¹ are typically low molecular weight molecules (500 – 1500 daltons) and are highly selective for the chelation of Fe^{3+} .^{24,37} Bacterial siderophores typically are hexa-dentate, employing three oxygen based bi-dentate chelating ligands, resulting in stable octahedral complexes with very high binding affinities for Fe^{3+} (Formation constant (K_f) values between 10^{22} to 10^{52} M^{-1}).^{24,29}

1.3.2 Structures of siderophores

Bacterial siderophores are structurally diverse with more than 500 different siderophores identified as of 2010, 270 of which had their chemical structures assigned, but this number continues to grow.²⁴ The structures of four representative siderophores are shown in Figure 4. Enterobactin (**5**) is one of the strongest iron chelators known, with a binding affinity

constant of $K_f = 10^{52} \text{ M}^{-1}$, and is known to be produced by two pathogenic bacteria *E. coli* and *Salmonella typhimurium*.^{38,39} Enterobactin comprises a cyclic ester back bone and three catecholate derived binding sites. Amychelin (**6**) is an example of a polypeptide siderophore, and one of the few siderophore-iron complexes to have been examined by X-ray crystallography.⁴⁰ The chelation motif of amychelin contains two hydroxamic acids in combination with an unusual 2-hydroxybenzoyl-oxazoline group. Deferoxamine B (**7**) is a linear polyamide with the three chelating hydroxamic acid functionalities built into the backbone of the siderophore. Deferoxamine B is one of the simplest hydroxamate siderophores and was for a time was used for the treatment of patients suffering from hemochromatosis (elevated levels of iron in the blood), through the chelation of free Fe^{3+} allowing it be excreted. Finally ferrichrome (**8**) is a siderophore produced by fungi, but is utilised by bacteria to acquire Fe^{3+} . Ferrichrome is a cyclic polypeptide with pendant hydroxamate groups used for iron chelation.

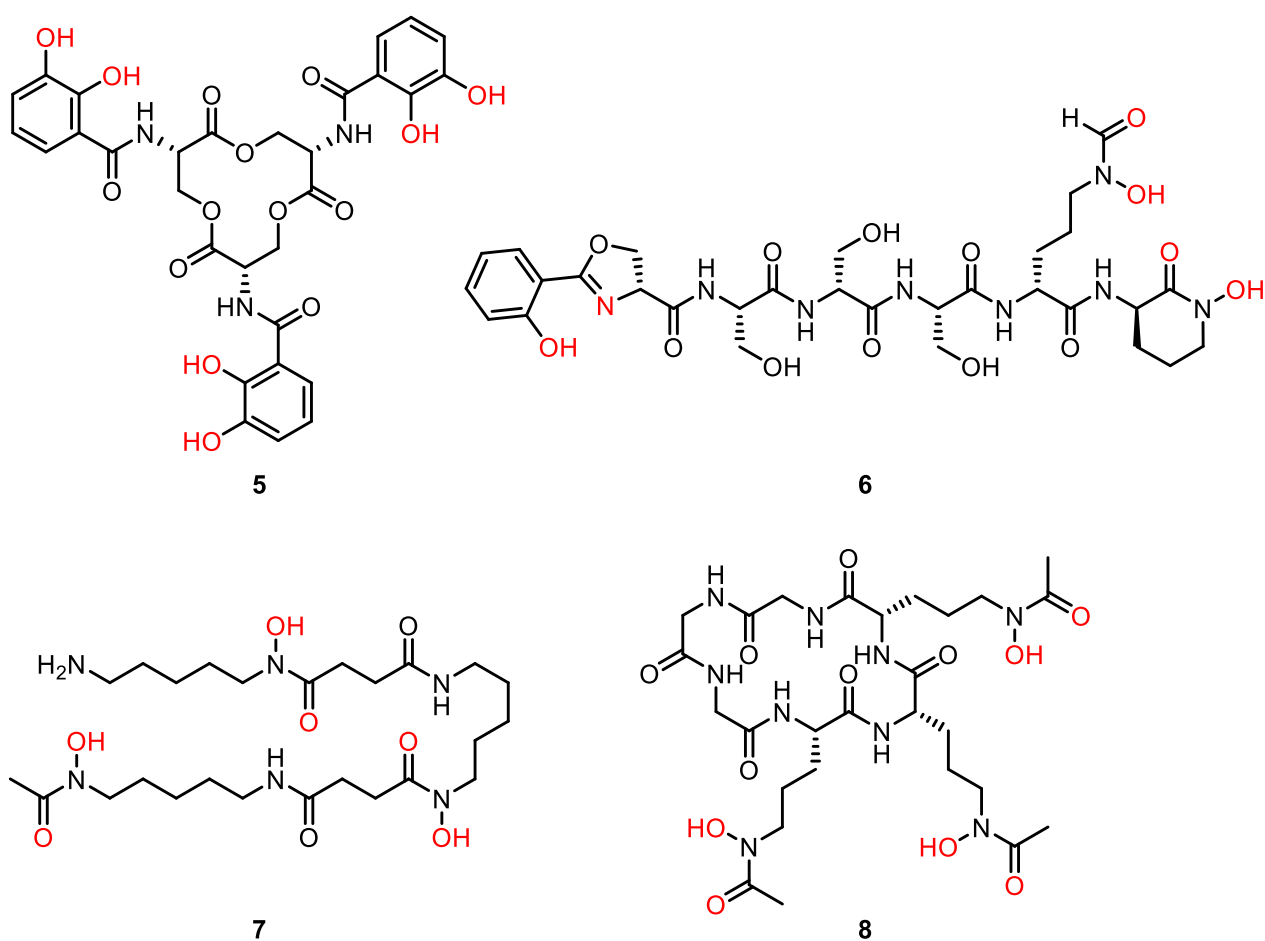


Figure 4. Chemical structures of siderophores enterobactin (**5**), amychelin (**6**), deferoxamine B (**7**) and ferrichrome (**8**).

As seen above, the chemical structures of bacterial siderophores are incredibly varied, and as such they are typically separated into three categories based on the chelating moieties they contain. These three categories are the catecholates (**9**), hydroxamates (**10**) and α -hydroxycarboxylates (**11**), there are also miscellaneous cases containing unusual chelation motifs, such as in amychelin (**16**). Although some bacterial siderophores contain a single type of chelation group, there are many examples of siderophores in which a mixture of each category of chelating group are employed in the chelation of the Fe^{3+} .

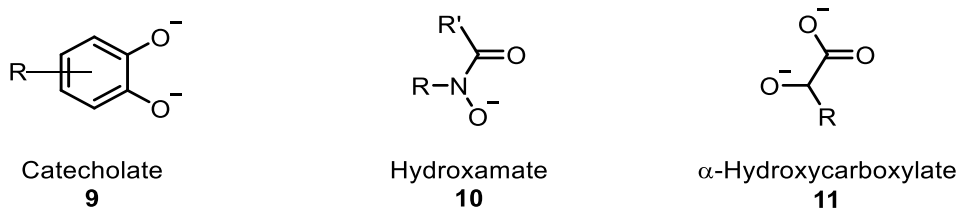


Figure 5. The chemical structures of three of the most common siderophore chelating groups, the catecholate (**9**) hydroxamate (**10**) and α -hydroxycarboxylate (**11**).

1.3.3 Biosynthesis of siderophores

The biosynthesis of many bacterial siderophores is carried out by nonribosomal peptide synthetase (NRPS) enzyme clusters. NRPS enzyme clusters typically only produce the corresponding siderophore during times of stress induced by low iron concentrations. In a typical NRPS several domains responsible for a specific transformation are arranged into an “assembly line”, and the growing peptide chain is passed from one domain to the next, with each adding a new amino acid. In some cases specific epimerisation, methylation and cyclisation domains are also used to further modify the growing polypeptide. In the case of enterobactin, the biosynthetic process begins with the production of 2,3-dihydroxybenzoic acid and its loading into one of the biosynthesis domains. 2,3-Dihydroxybenzoic acid is then coupled to serine to give the corresponding amide bound to the NRPS. Three of these amide units are then sequentially combined to give the linear siderophore, before cyclisation leads to release of the completed enterobactin molecule from the NRPS cluster.⁴¹

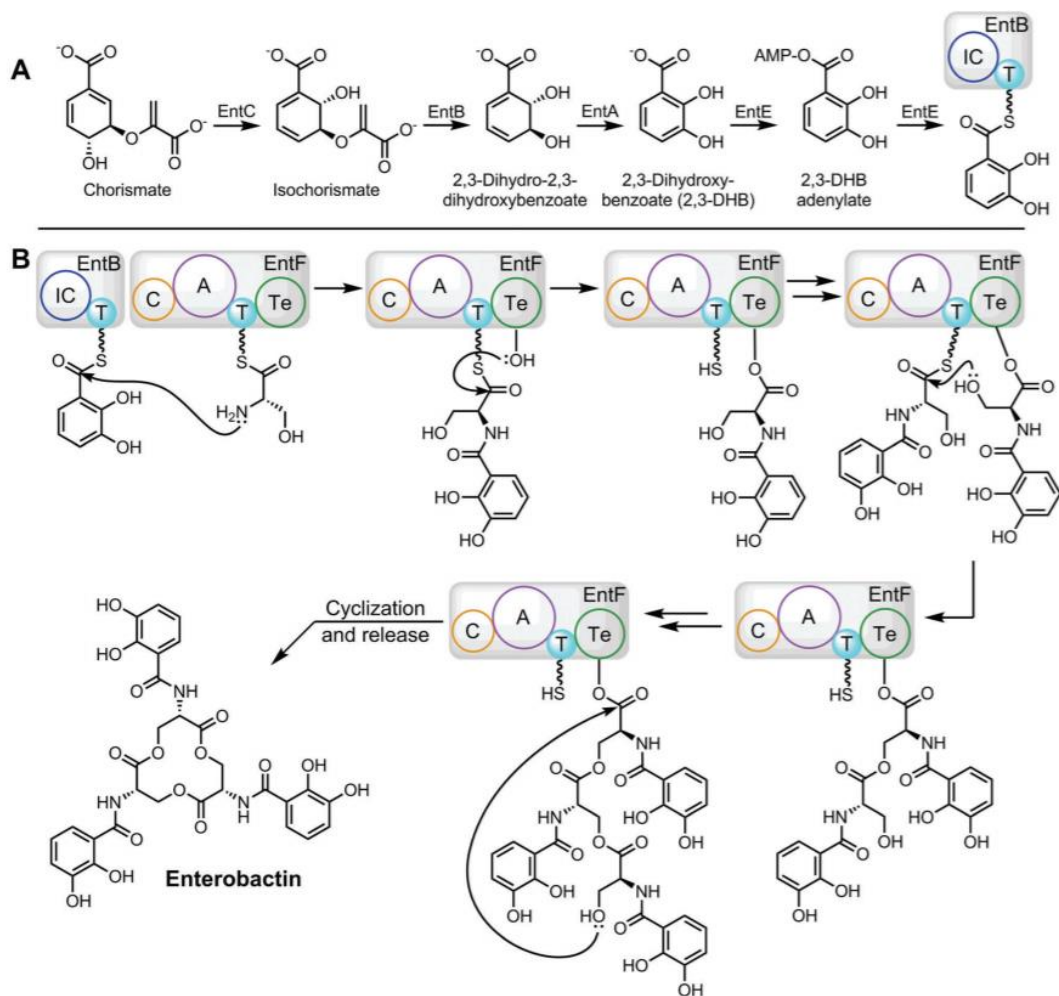


Figure 6. Biosynthesis of enterobactin. (A) Synthesis and activation of 2,3-dihydroxybenzoate by EntABCE. (B) Assembly of enterobactin by NRPS: EntF. IC – isochorismatase; C – condensation domain; A – adenylation domain; T – thiolation domain; Te – thioesterase domain. Taken from Reitz et al. Ref: 41.

1.3.4 Bacterial-iron uptake processes.

After chelation of Fe^{3+} by a siderophore, the producing bacteria then has to reabsorb the siderophore-iron complex from its environment. This uptake process differs between Gram-positive and Gram-negative bacteria. The majority of siderophore uptake studies have been centred around pathogenic Gram-negative bacteria, such as *E. coli* and *S. typhimurium*. These Gram-negative bacteria have an internal cytoplasmic membrane which is shielded by a thicker outer membrane, with the area between dubbed the periplasmic space. The outer membrane is a lipid bilayer made up with lipopolysaccharides and phospholipids, and contains a number of different proteins.^{42,43} Proteins specially used for the uptake of molecules can be passive, as in the case of porins which are permanently open channels that let low molecular weight compounds into the periplasmic space, or active, such as energy dependant active transporters.²⁴

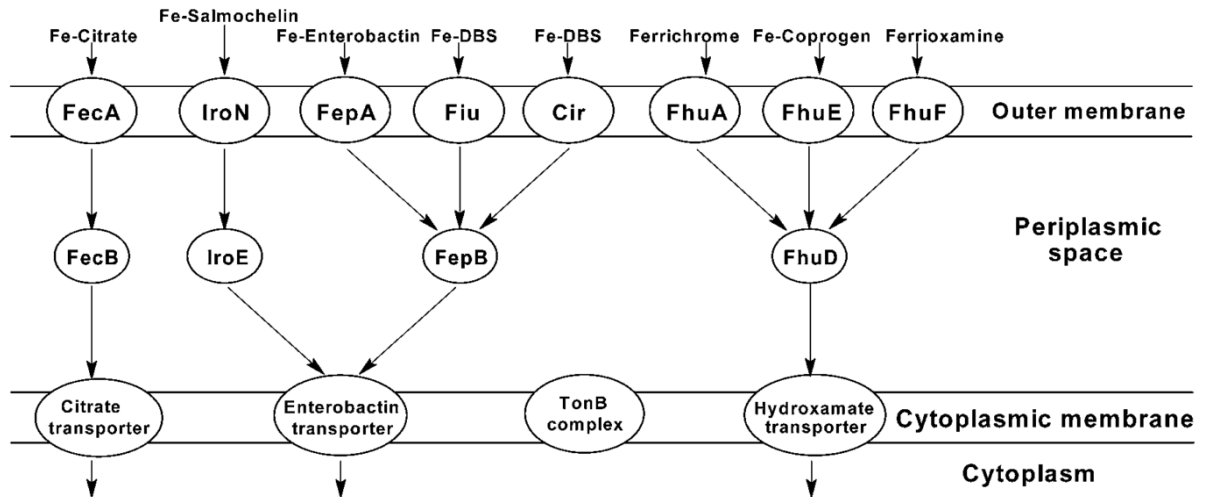


Figure 7. The Fe^{3+} transport system of *E. coli* and related *Enterobacteriaceae*. Taken from Hider et al. Ref: 24.

As can be seen in Figure 7, there are multiple outer membrane proteins that are used to actively transport siderophores across the outer membrane. Once an external siderophore binds to one of these transport proteins, (FepA for example) a conformational change in the protein occurs. This change then allows the TonB protein to bind to the periplasmic side of the siderophore/transport protein complex, opening a channel and allowing the siderophore into the periplasmic space.²⁴ Some of these siderophore binding proteins like ferric-enterobactin permease (FepA) are highly selective and only allow a specific siderophore-iron conjugate to pass through them.⁴⁴ Meanwhile others such as the Ferrichrome outer membrane transporter (FhuA, Figure 8) are non-selective and allow uptake of many different siderophore-iron complexes.

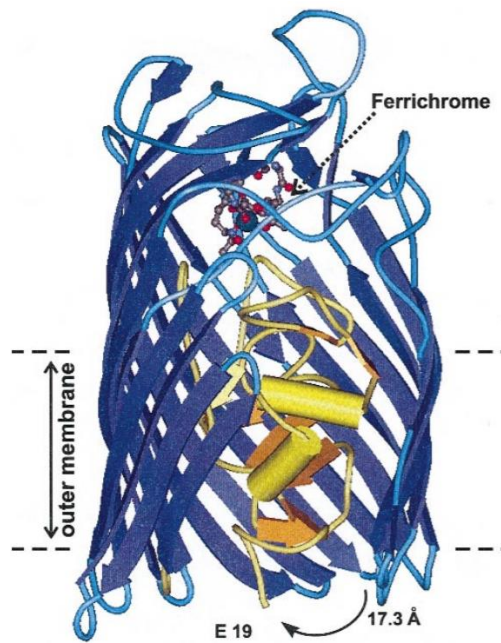


Figure 8. Crystal structure of the FhuA transport protein with ferrichrome bound. Resolution 2.7 Å. Taken from Braun et al. Ref: 45.

Once the siderophore-iron complex is inside the periplasmic space, it is transported to a periplasmic siderophore binding protein (FepB in the case of Fe-enterobactin) which delivers the siderophore across the periplasmic space to the cytoplasmic membrane (Figure 7).⁴⁶ Once here, ATP mediated transport across the cytoplasmic membrane carries the siderophore into the bacterial cell cytoplasm.⁴⁷

The siderophore-iron complex uptake pathway of Gram-positive bacteria is not as well studied. However, it is believed to be a similar process to the way in which a siderophore-iron complex moves from the cytoplasmic membrane into the cytoplasm in a Gram-negative bacterium. More specially, in Gram-positive bacteria, siderophore binding proteins are tethered to the outside of the cytoplasmic membrane and are able to catch and bind siderophore-iron complexes. Once bound, the siderophore-iron complex is then imported by siderophore permeases that span the cytoplasmic membrane through an ATP mediated process.⁴⁷ It has also been suggested that some of these siderophore binding proteins tethered to the outside of the cytoplasmic membrane contain an *apo*-siderophore (a siderophore without a chelated iron atom). Upon capture of an extracellular siderophore-iron complex by the siderophore binding protein, the iron atom is transferred from the extracellular siderophore to the *apo*-siderophore and it is this, now iron chelated, *apo*-siderophore that is transferred into the bacterial cell cytoplasm.^{47,48}

Once inside the cytoplasm of either a Gram-positive or Gram-negative bacterium, release of siderophore bound iron is proposed to occur almost exclusively *via* reduction of Fe³⁺ to Fe²⁺. Bacterial siderophores have low binding affinity for Fe²⁺, hence iron in the reduced Fe²⁺ form can then be more easily released from the complex.^{49,50} This method is common for both the hydroxamate and α -hydroxy carboxylate siderophores, with the siderophore then being re-excreted for reuse in iron uptake. However, catecholate siderophores, such as enterobactin, are unable to undergo redox based iron release processes. In this case, it is proposed that the cyclic ester backbone of enterobactin is hydrolysed by an esterase, to convert the hexadentate siderophore into three independent bi-dentate ligands. The resulting complex is more easily reduced to release Fe²⁺ into the cell.⁵¹

1.4 Uses of siderophores

Bacterial siderophores have found applications in a number of areas of science and medicine. This includes their use as growth factors for unculturable bacteria, the detection of microbial pathogens, treatment of iron overload and their use as antibiotics, these are discussed below.

1.4.1 Siderophores as growth factors

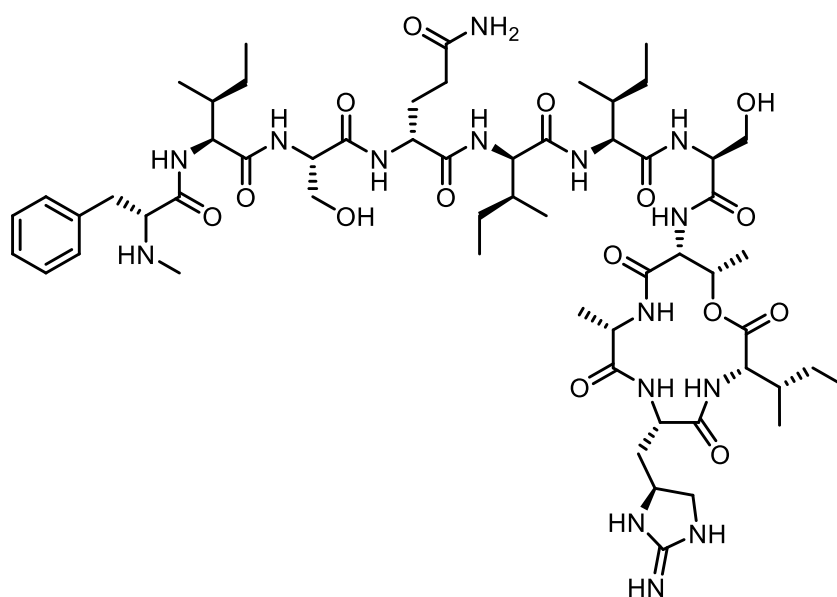
1.4.1.1 Introduction

Metagenomics sequencing of environmental samples (e.g. soils or marine sediments) supports the postulate that less than 1% of the prokaryotes present can be easily grown in isolation in the laboratory using current methodologies.⁵² New methods for the isolation and growth of these “unculturable” bacteria would be of significant benefit, not only aiding in the general study of the bacterial world, but also potentially resulting in the discovery of many new natural products arising from these previously unstudied bacteria.

1.4.1.2 Natural products from “unculturable” bacteria

Some approaches to cultivating these “unculturable” bacteria involve growing the bacteria in an alternative medium to agar, for example in sand, in an agar-marine sediment mix sandwiched between semi-permeable membranes, and so on.⁵² Some research groups have focused on the growth of these “unculturable” bacteria alongside other species from the same environment, postulating that signalling molecules released by the growing bacterial species can induce growth of the “unculturable” bacterial neighbours.^{53,54} It has also been found that

siderophores from these neighbouring bacterial species can also induce growth of “unculturable” bacteria.^{52,55} Indeed some of the first bacterial siderophores to be isolated; mycobactin and ferrichrome were identified as bacterial growth factors.^{56,57} It is possible that many of these “unculturable” bacteria do not actively produce their own siderophores, instead they elect to steal the iron they need from siderophore-iron complexes produced by other bacteria.⁵² In 2015 the use of iChip technology allowed the cultivation of an “unculturable” bacteria (*Eleftheria terraes*), resulting in the isolation of a novel Gram-positive antibiotic teixobactin (**12**). Experiments showed that teixobactin had antibiotic activity against methicillin-resistant *S. aureus* and vancomycin-resistant *Enterococci*. Furthermore no detectable resistance to teixobactin (**12**) was observed during these studies. Finally, Ling and Schneider showed that teixobactin (**12**) could be effective in an MRSA animal infection model (mice) with no observable toxicity.⁵⁸



12

Figure 9. Molecular structure of teixobactin (**12**)

With such a promising novel antibiotic isolated from an “unculturable” bacterium, it is hoped that other approaches, such as the use of siderophores as growth factors for “unculturable” bacteria, could be used to enable access to the bioactive natural products produced from the 99% of bacteria currently considered “unculturable”.

range of siderophores trialled in these studies described to date, it is difficult to say if the use of immobilised siderophores could be applied clinically for rapid bacteria detection. Optimisation of these techniques will therefore be required before the use of such systems could be applied in a clinical setting.

1.4.3 Siderophores as clinical iron chelators

1.4.3.1 Introduction

Iron is an essential element in the human body, and its concentration is tightly regulated.⁶² Iron overload disorder is caused by the presence of excess iron in the body, in particular in the organs and serum, and can be caused by frequent blood transfusions, chronic hepatitis, or through genetic disorders such as hemochromatosis.^{31,62} The excess iron accumulates in vital organs such as the liver and brain, where free radical production causes severe organ damage which can be fatal to the patient.⁶²

1.4.3.2 Siderophores in the treatment of iron overload

Deferoxamine was used clinically as a treatment for iron overload disorder for several years and was approved by the FDA in 1969. Due to the non-toxic nature of this siderophore it proved to be an effective method for the treatment of iron overload disorder. It could be administered as an oral, intramuscular or continuous intravenous infusion and allowed excess iron to be excreted through the urine and faeces. Unfortunately, the physiological side effects of using this siderophore and the requirement for continuous doses caused a decline in its use. In addition to the direct health risks of using deferoxamine as an iron chelator in patients, it was also shown that the presence of deferoxamine in the blood could lead to increased risk of bacterial infection due to the availability of siderophore bound iron. Currently non-siderophore based iron chelators such as deferiprone and deferasirox are used as an effective method of treatment for iron overload disorder.⁶³

1.4.4 Siderophores as “Trojan Horse” antibiotics

1.4.4.1 Introduction

Since the uptake of Fe^{3+} is essential for bacterial growth, then the targeting of this pathway is a potential route for the development of novel antibiotic molecules. Furthermore these active uptake pathways can be highly selective for a specific bacterial species. This then presents an opportunity for the development of highly selective antibiotics. If the siderophore uptake

process could be subverted as a means to carry an antibiotic payload into the bacterial cell. Thus a “Trojan Horse” approach in which the modification of a siderophore to incorporate an antibiotic molecule (Figure 11) that is released upon uptake into a bacterial cell, *via* a cleavable linker, could prove to be a viable method for the selective treatment of bacterial infections.

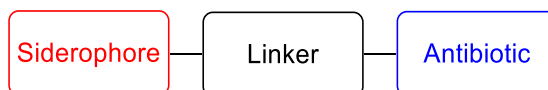


Figure 11. Schematic representation of a siderophore-linked antibiotic “Trojan Horse”

Looking to nature, it appears that this “Trojan Horse” approach of using a siderophore as a vector to transport a chemically bound antibiotic into a bacterial cell, which is then released to cause an antibiotic effect, is already used in the form of the natural product sideromycins.⁶⁴

1.4.4.2 Sideromycins

The sideromycins are a class of natural products that include the antibiotic siderophore families the albomycins and salmycins (Figure 12). The siderophore component of the albomycins is structurally similar to ferrichrome (**8**) and is bound through a serine moiety to a thioribosyl pyrimidine, which acts as the antibiotic warhead.⁶⁴ Similarly the siderophore component of the salmycins is structurally similar to deferoxamine B (**7**) and linked through an ester to an aminodisaccharide, which also acts as the active antibiotic in this case.⁶⁴

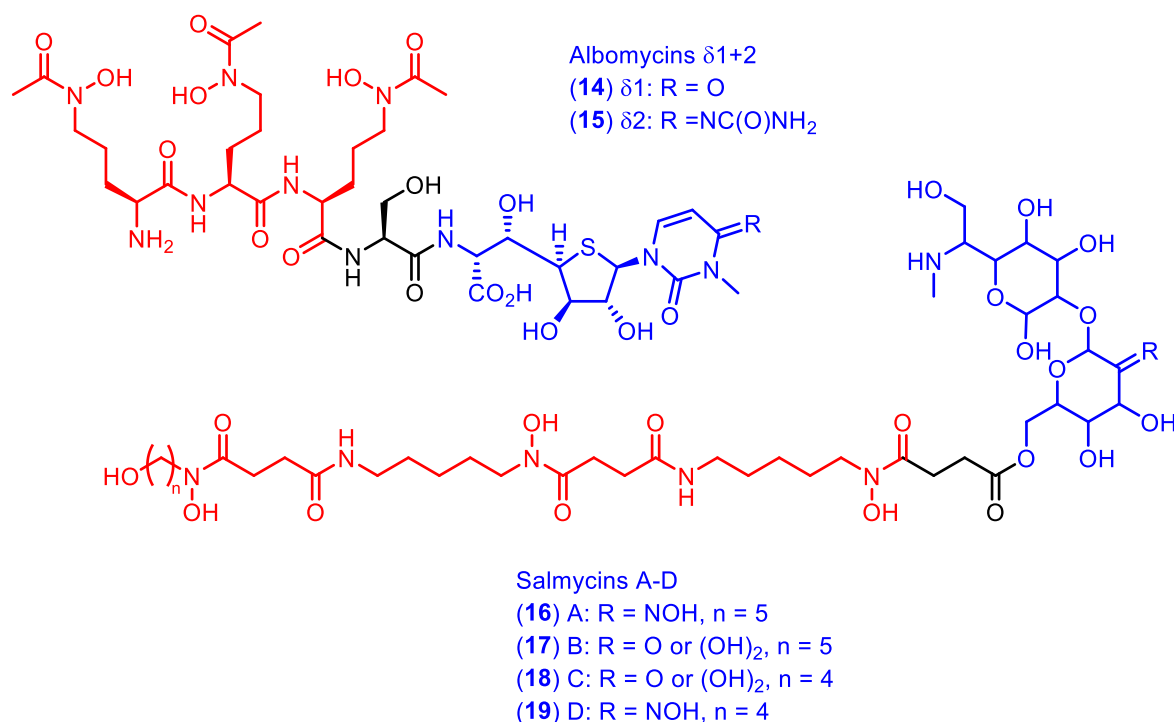


Figure 12. Chemical structures of the albomycins (**14+15**) and salmycins (**16-19**). (Red - siderophore component, black – linker, blue – antibiotic compound)

Due to the ability of the albomycins and the salmycins to chelate Fe³⁺ and to mimic the naturally occurring ferrichrome (**8**) and deferoxamine B (**7**) respectively, it is postulated that they are transported into bacterial cells *via* the same proteins used in the native siderophore uptake process. In *E. coli*, ferrichrome is actively transported into the cell *via* the outer membrane transport protein FhuA. In the case of the albomycins, it has been shown *via* X-ray crystallography that albomycin can complex with the outer membrane transport protein FhuA, suggesting that this protein can actively uptake the albomycins into the bacterial cell alongside its native siderophore.⁶⁵

In the case of albomycin $\delta 2$ (**15**), once transported into *E. coli* cells *via* FhuA, peptidase N cleaves the siderophore-serine amide bond, releasing the thioribosyl pyrimidine antibiotic warhead and leading to cell death (Figure 13). Mutant *E. coli* strains that were devoid of peptidase N activity were shown to be resistant to albomycin, and instead albomycin simply acted as a siderophore, delivering iron into the bacterial cell.^{66,67}

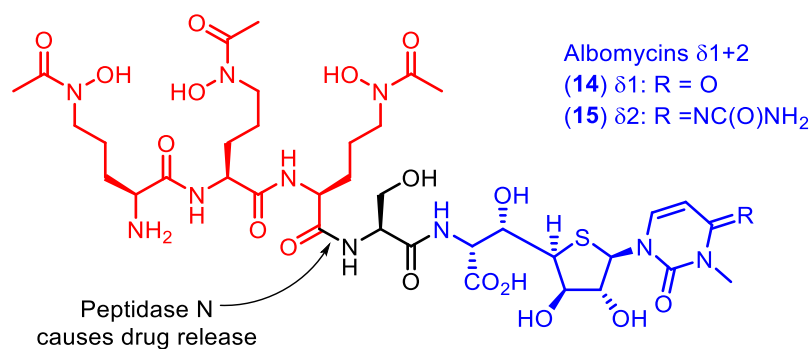


Figure 13. Proposed method of antibiotic release in the albomycins. (Red - siderophore component, black – linker, blue – antibiotic compound)

The combination of a siderophore and antibiotic has been shown to be considerably more effective than the antibiotic alone. For example albomycin $\delta 2$ (**15**) is 30,000 times more effective as an antibiotic against *S. aureus* and *E. coli* than the isolated thioribosyl pyrimidine antibiotic.⁶⁴ Inspired by these antibiotic siderophores, much research has gone into the synthesis and development of both natural and unnatural siderophore-antibiotic conjugates, an overview of which will now be given.

There are of course a number of ongoing challenges within the field of siderophore-antibiotic conjugates. For a successful siderophore-antibiotic conjugate, the molecule must:

- 1) be recognised by the native siderophore uptake machinery, e.g. surface receptor proteins, in order to be actively transported across the cell membrane.
- 2) be cleaved from the linker, once inside the periplasmic space or cell cytoplasm, by an enzyme that can release the antibiotic component.
- 2) be bioactive once released from the linker within the cell.⁶⁸

1.4.4.3 Man made sideromycin analogues

With the discovery of the sideromycins, much research has been undertaken to generate novel siderophore-antibiotic conjugates as potential antibiotic therapeutics. The use of a siderophore-antibiotic conjugate over a classical antibiotic has several potential advantages:

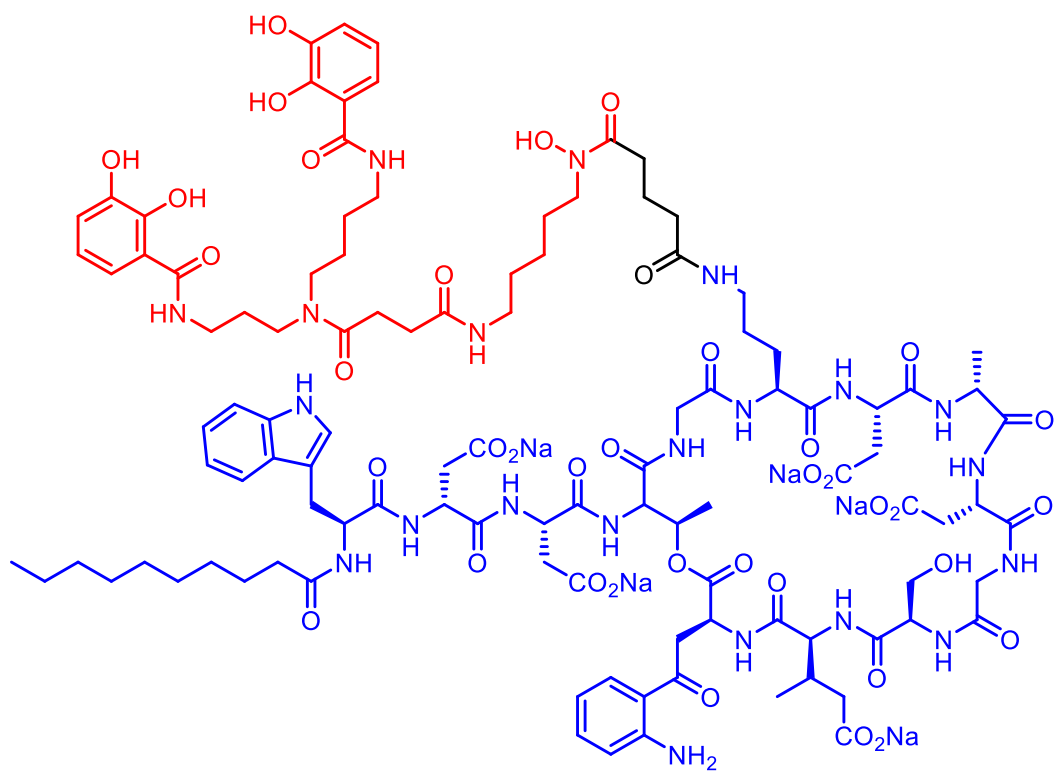
- 1) **Increased potency.** One of the limiting factors for the efficacy of antibiotic drugs is the rate of uptake of the antibiotic into the bacterial cell. Usually this is governed by the concentration gradient leading to passive diffusion of the drug through the cell membrane.⁶⁹ This uptake rate is countered by the bacteria through the use of efflux

pumps which are used to remove toxic substrates (such as antibiotics) from the bacterial cell. This means that very high doses of antibiotics are often required to give a sufficient concentration of the antibiotic inside the bacterial cell to induce cell death. Siderophore-antibiotic conjugates have the potential to greatly increase the rate of uptake of the antibiotic component into the bacterial cell, due to their hijacking of the bacterial active transport systems. As a consequence lower overall doses of the antibiotic component would be required for the same therapeutic effect, reducing off-target toxicity.

- 2) **Selective targeting of pathogenic bacteria.** Due to the presence of selective siderophore receptors on the surface of the bacterial cell, one could imagine the use of a specific siderophore-antibiotic conjugate to target a specific pathogenic bacteria. This would result in a very narrow spectrum antibiotic capable of killing the unwanted pathogenic bacteria in a patient, whilst leaving the naturally occurring “friendly” bacteria of the human microbiome unscathed.

1.4.4.4 Broadening the activity of Gram-positive antibiotics

Gram-negative bacteria are usually less sensitive to antibiotics due to their thicker cell walls, slowing the rate of diffusion of antibiotics into the bacterial cell.⁷⁰ However if antibiotic molecules could be helped across the cell wall of a Gram-negative bacteria this could allow the use of molecules previously only used for Gram-positive infections to be re-tasked for the treatment of Gram-negative infections. Daptomycin is a Gram-positive antibiotic that, due to its large size, has difficulty in diffusing through the outer membrane of a Gram-negative bacteria.⁷¹ Indeed when *Acinetobacter baumannii* is treated with daptomycin, no antibiotic effect is observed at the maximum tested concentrations of 100 μM . However, when bound to a synthetic siderophore, the siderophore-daptomycin conjugate (**20**) showed much improved antibiotic activity against *A. baumannii* with a MIC value of 0.5 μM , suggesting that the siderophore component had been recognized by the siderophore transport proteins, successfully carrying the antibiotic into the cell. Thus an antibiotic commonly reported to only be active against Gram-positive bacteria can show antibiotic activity against Gram-negative bacterial species through the incorporation into a siderophore-antibiotic conjugate.⁷¹



20

Figure 14. Chemical structure of **20**, a siderophore - daptomycin conjugate

1.4.4.5 Increasing the potency of known antibiotics

Siderophore-antibiotic conjugates of β -lactam antibiotics have also been prepared, including an enterobactin-ampicillin (**21**) and an enterobactin-amoxicillin (**22**) conjugate. Against uropathogenic *E. coli* CFT073 the siderophore-antibiotic conjugates were 1000 fold more potent than the parent antibiotics ampicillin and amoxicillin, with MIC values of 10 nM.⁷² The siderophore-antibiotic conjugate was selective for *E. coli* with a general lack of activity shown against Gram-negative strains *K. pneumoniae* ATCC 13883 and *P. aeruginosa* PAO1, and Gram-positive strains *Bacillus cereus* ATCC 14579 and *S. aureus* ATCC 25923.

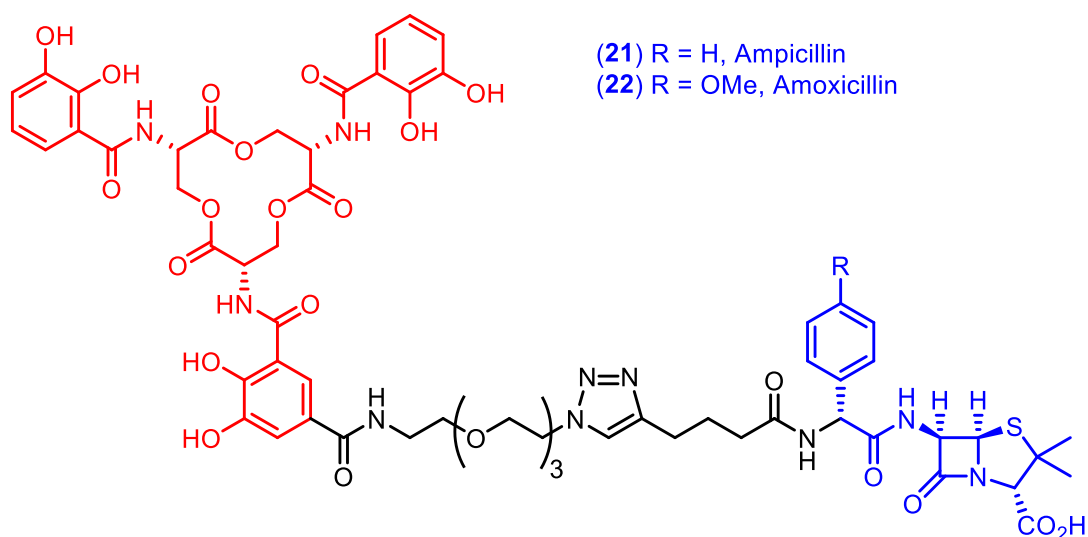


Figure 15. Chemical structures of **21** and **22**, siderophore - β -lactam conjugates

The role of the siderophore component in facilitating uptake into the bacterial cell was highlighted by the decrease in effectiveness of the siderophore-antibiotic conjugate in the presence of high concentrations of Fe^{3+} or when an excess of parent siderophore was used in growth inhibition studies.

Unfortunately, bacteria which have already developed resistance to β -lactam antibiotics through the generation of β -lactamase enzymes also show resistance against these siderophore- β -lactam conjugates. For example, the treatment of the bacterial strain *A. baumannii* ATCC 17978 using a siderophore like- β -lactam antibiotic (**23**) was successful with MIC values of 0.4 μM , whilst the treatment of the β -lactamase producing *A. baumannii* mutant (ATCC 17978 pNT255: ADC-1) was not (MIC >50 μM).⁷³ As such, alternative antibiotics have been utilised to generate novel siderophore like-antibiotic conjugates.⁷³

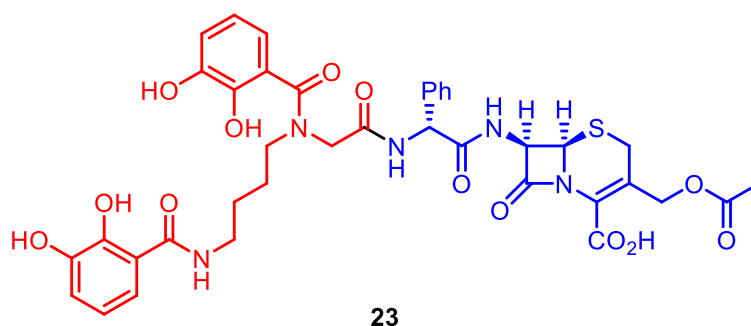


Figure 16. Chemical structure of the siderophore - cephalosporin conjugate (**23**).

mutations will ultimately render many of these new antibiotic agents ineffective for the treatment of bacterial infections.

The ability of bacteria to acquire iron is essential to bacterial growth and therefore virulence. In order to obtain the concentrations of iron required for bacterial growth and replication, bacteria have developed specialist natural products for the chelation of Fe^{3+} . These chelating agents are called siderophores and are used by bacteria to solubilize and transport Fe^{3+} to the bacterial cell surface. Once here, specialist proteins transport the siderophore-iron complex across the cell membrane and into the bacterial cell.

Siderophores have found use in a variety of applications from the treatment of iron overload disorder and pathogen detectors, to assisting in the growth of “unculturable” bacteria and the development of sideromycin like “Trojan horse” antibiotics. Due to the essential role that iron uptake processes and siderophores play in the growth of bacterial cells, we have developed an interest in this area of research. The isolation of novel siderophores, their structural determination and their total synthesis is therefore a valuable addition to the growing body of research focused around bacterial siderophores.

1.6 Project aims

Therefore, the overall aims of this project are to investigate the siderophores produced by two bacterial species, *Actinomadura sp.* (DEM31376) and *Streptomyces sp.* (DEM30616). These investigations will include the isolation of the siderophores produced by these two bacterial strains. After isolation, a de-novo structural determination will be carried out to assign the chemical structure and absolute stereochemistry of the isolated natural products. Finally, the total synthesis of both of these siderophores will be carried out. The total synthesis should allow access to large quantities of siderophore and potentially modified derivatives of these siderophores, with which to carry out further experimentation.

Chapter 2 - Isolation and Structural Determination of Madurastatin C1 (DEM31376/A)

2.1 Introduction

In this chapter we will start by discussing the bacteria DEM31376, which is responsible for producing the siderophore madurastatin C1 (DEM31376/A), including attempts to identify the bacteria *via* 16S rRNA analysis. We will then discuss the isolation and structural determination of the siderophore madurastatin C1 (DEM31376/A). Finally, we will discuss our investigation of the stereochemistry of DEM31376/A and the correction of the literature structure for madurastatin C1.

2.2 Demuris Ltd.

The MJH research group work closely with the microbiology and antibiotic discovery company Demuris Ltd. based in the medical school at Newcastle University. They maintain a collection of bacterial strains from extreme and/or unusual environments, with the intention that these unusual strains of bacteria might produce novel antibiotics with unusual or unique modes of action. The prefix DEM followed by the identification number is assigned to each bacterial strain in Demuris' catalogue.

2.3 *Actinomadura* sp. DEM31376

Actinomadura sp. DEM31376 was isolated from a deep sea marine sediment found at Canary Basin in the Atlantic Ocean.⁷⁴ 16S rRNA analysis of DEM31376 was carried out by Dr. Hamed Mosaei Sejzi and revealed that DEM31376 was a novel member of the *Actinomadura* genus, most closely related to *Actinomadura mexicana* A290^T and *Actinomadura citrea* IFP 14678^T.

2.4 DEM31376/A

The original rationale for investigating *Actinomadura* sp. DEM31376 was to identify and isolate novel antibiotic molecules. Preliminary work on DEM31376 was carried out at Demuris by Dr. Hamed Mosaei Sejzi, resulting in the isolation of a compound, assigned as DEM31376/A, through a bioassay guided fractionation approach. Initial testing of DEM31376/A suggested that this molecule had antibiotic activity. However, subsequent work revealed that DEM31376/A was not in fact bioactive, the observed bioactivity arising from a minor contamination of the sample with a co-eluting natural product GE23077 (a known and highly

active RNAP inhibitor, also produced by DEM31376). Due to this misleading bioactivity we had already begun to examine DEM31376/A to gain understanding of its structure and biological role, prior to our identification of the presence of GE23077. However due to our interest in the structure and biology of bacterial siderophores, we decided to continue our investigations into this bacterial natural product.

2.5 Isolation of DEM31376/A

Early in our investigations into DEM31376/A we required the production of large (>100mg) quantities of the molecule in order to undertake structural elucidation. To achieve this I worked with Dr. Hamed Mosaei Sejzi at Demuris Ltd. to grow *Actinomadura sp.* DEM31376 on large scale, followed by isolation of DEM31376/A. Therefore DEM31376 was grown in liquid ISP2 media on a 20 L scale over seven days. After this time the fermentation broth was decanted from the bioreactor, Amberlite XAD16N beads were added to the broth and the mixture left overnight to absorb any organic compounds present. After 12 hours the Amberlite XAD16N beads were collected by filtration, washed with methanol and the resulting filtrate evaporated under reduced pressure. The concentrated filtrate was then fractionated on C₈ SPE cartridges through stepwise elution with 25%, 50% and 75% methanol in water with a final elution with 100% methanol. HPLC-MS revealed two related compounds in the 75% and 100% methanol fractions. The major compound, with a retention time of 12 minutes, gave a signal in MS with $m/z = 592$ (M+H)⁺ whilst the minor compound, at 9 minutes, gave $m/z = 610$ (M+H)⁺. The minor compound gave an m/z of 18 more than that for the major compound, thus we postulated that they may be related through hydrolysis. The 75% methanol in water and 100% methanol fractions were combined and further purified *via* reverse phase C₁₈ column chromatography, with the major compound eluting between 4.5 and 6 minutes to give 283 mg of DEM31376/A. From here, we sought to determine the chemical structure of DEM31376/A *via* a combination of high resolution mass spectrometry and NMR spectroscopy.

2.6 Initial structural studies of DEM31376/A

2.6.1 Mass spectrometry of DEM31376/A

High-resolution mass-spectrometry of DEM31376/A gave $m/z = 592.27315$ for the proposed [M+H]⁺ ion, resulting in a calculated molecular formula of C₂₆H₃₇O₉N₇. MSⁿ experiments also revealed major fragmentation ions with m/z values of 462.19, 434.20, 403.16, 349.15 and 318.11, more discussion of which will be given later in section 2.7.9.

2.6.2 Calculation of double bond equivalents

Based on the proposed molecular formula of DEM31376/A, we established that there were twelve double bond equivalents (DBE) present in DEM31376/A.

$$\text{DBE} = C - \left(\frac{H}{2}\right) + \left(\frac{N}{2}\right) + 1 = 26 - 18.5 + 3.5 + 1 = 12.$$

Equation 1. Calculation of the number of double bond equivalents in DEM31376/A ($C_{26}H_{37}O_9N_7$)

2.7 Structural determination of DEM31376/A via ^1H , ^{13}C and ^{15}N NMR

2.7.1 Introduction

In this section, we will discuss the structural elucidation of DEM31376/A. At this stage we suspected that DEM31376/A was a polypeptide due to the presence of several nitrogen atoms and the ease of fragmentation during HRMS. This therefore allowed us to attempt to solve the structure of DEM31376/A as a number of discrete sections corresponding to each amino acid. To begin, we started our assignment by comparing our NMR data to our HRMS and DBE calculations. Initial examination of the ^1H NMR spectrum (Figure 18) revealed a total of 23 hydrogen atoms *via* integration, suggesting that 3 hydrogen atoms had undergone deuterium exchange. The ^{13}C NMR spectra showed 26 carbon environments, matching the proposed chemical formula. Further to this, we were able to assign 10 of the 12 calculated DBE with the combined NMR data through the presence of a 6 membered aromatic ring (4 DBE) and 6 carbonyl like carbons (6 DBE). Due to the high number of heteroatoms in DEM31376/A, long range ^{15}N - ^1H correlation experiments were also performed. ^{15}N NMR experiment gave signals corresponding to 7 nitrogen atoms, which is consistent with our assigned chemical structure. These 7 nitrogen atoms were found in four discrete chemical shift ranges: 20-40, 110-120, 170-180 and 200-220 ppm suggesting four different nitrogen environments. With the initial NMR data corroborating our HRMS and DBE calculations, we next moved on to detailed examination of both 1D and 2D NMR spectra to conclusively assign the chemical structure of DEM31376/A.

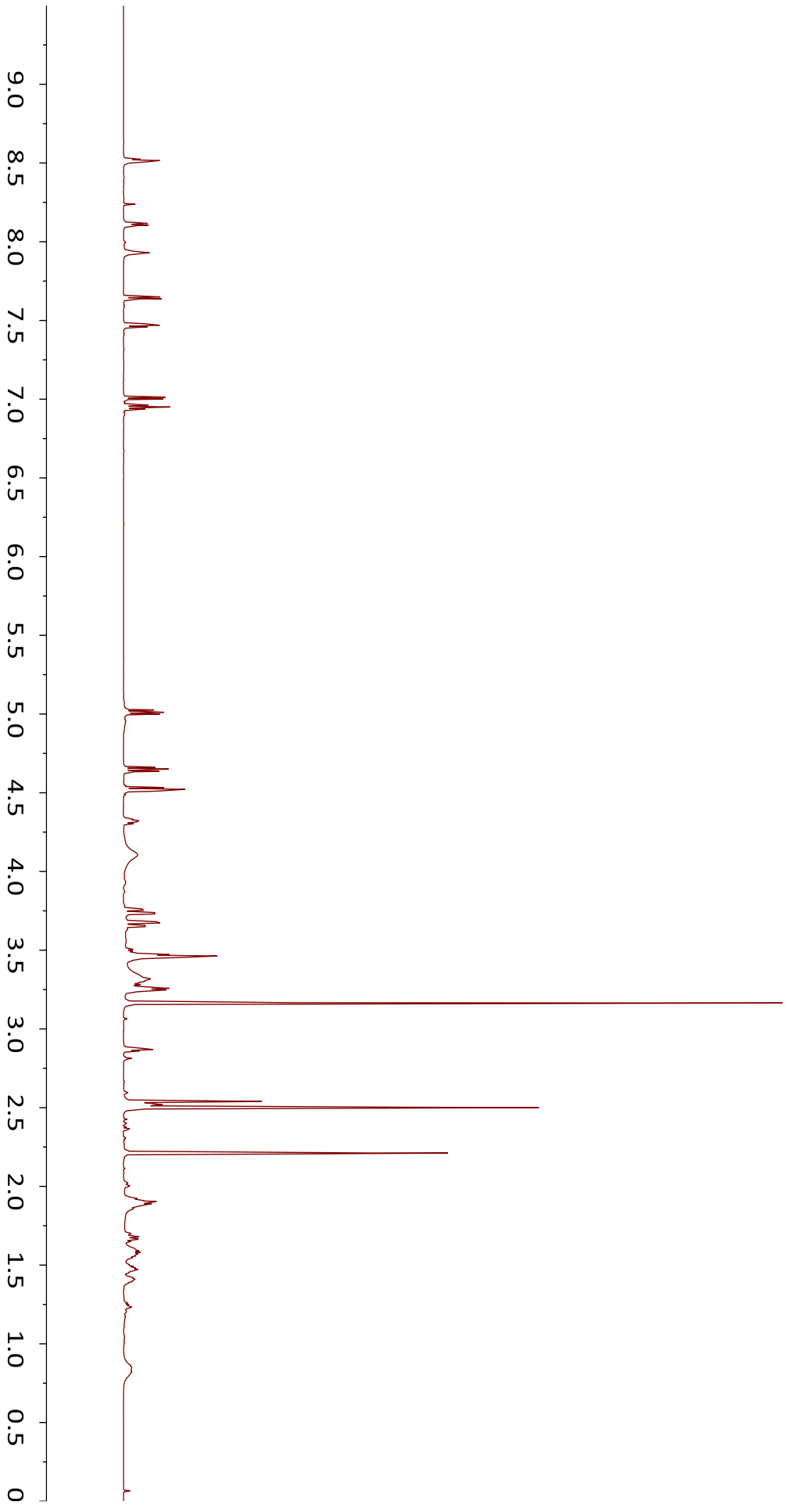


Figure 18. ¹H NMR of DEM31376/A in D₆-DMSO 298 K, 700 MHz

2.7.2 Fragment 1

Inspection of the ^1H NMR showed a four proton spin system (assigned *via* COSY) with signals at 7.65, 7.47, 7.01 and 6.95 ppm. The splitting pattern was indicative of a 1,2-disubstituted aromatic ring, with the two quaternary carbons identifiable by ^{13}C and HMBC experiments (position 1 and position 6). HMBC experiments showed that an additional deshielded carbon atom at 165.9 ppm (P-7) was connected to the aromatic ring at position 6. The chemical shift of the carbon signal at position 1 was higher than normal for a benzene derived aromatic ring at 159.1 ppm. We concluded that the carbon at position 1 was therefore substituted with an electron withdrawing hydroxyl group, explaining the high chemical shift. This assignment was supported by a lack of any additional HMBC correlations from the hydrogen at position 2. In summary, fragment 1 consists of a 1,2-disubstituted benzene ring, with a hydroxyl group at position 1 and a carbonyl group position 6 (Figure 19).

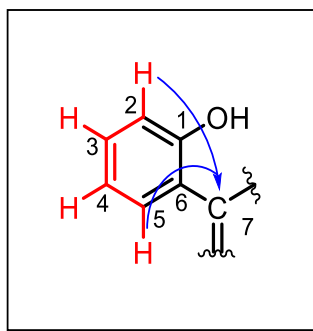


Figure 19. Proposed structural assignment for fragment 1 of DEM31376/A (COSY = red, selected HMBC = blue)

Table 1. ^1H and ^{13}C signals associated with fragment 1

Position	$\delta_{1\text{H}}$ multiplicity, (J in Hz)	$\delta_{13\text{C}}$	HMBC
1	-	159.1	-
2	7.01 dd ($J = 8.4, 1.1$ Hz, 1H)	116.6	H to C6, 4, 1, 7
3	7.47 ddd ($J = 8.7, 7.2, 1.8$ Hz, 1H)	134.1	H to C6, 5, 1
4	6.97 – 6.93 (m, 1H)	119.1	H to C6, 2, 5, 3, 1
5	7.65 dd ($J = 7.9, 1.8$ Hz, 1H)	128.1	H to C2, 3, 1, 7
6	-	109.9	-
7	-	165.9	-

2.7.3 Fragment 2

For fragment 2, a three-proton spin system was observed in the ^1H NMR spectrum with signals at 5.01 (P-9), 4.65 and 4.52 ppm (P-10). The two signals at 4.65 and 4.52 ppm showed J values

of 10.5 Hz, suggesting a geminal coupling between two diastereotopic protons, which was confirmed through an HSQC experiment (Figure 20).

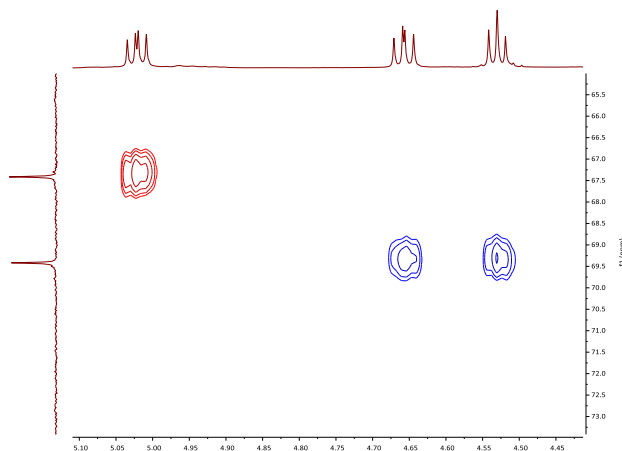


Figure 20. HSQC correlation between the diastereotopic methylene signals 4.65 & 4.52 ppm (P-10) and carbon 69.4 ppm (P-9).

HMBC data revealed that all three proton signals were coupled to a new deshielded carbon at 170.2 ppm (P-11) and to the previously described deshielded carbon at position 7 in fragment 1. Long range ^{15}N - ^1H experiments showed correlations between all three protons to a deshielded tertiary nitrogen atom at 208.2 ppm which, combined with the lack of an amide proton signal, suggested that this tertiary amine may be incorporated into some sort of heterocycle. The presence of a geminal methylene adjacent to an apparent alpha proton, a carbonyl like carbon and a nitrogen atom lead us to assign fragment 2 as a cyclised serine. This assignment would also count toward one of the two rings we anticipated from our DBE calculations. However, we were unable to conclusively assign this ring as either a five membered oxazoline ring, or a three membered aziridine – amide. At this stage, both of these could be assigned from the data (Figure 21).

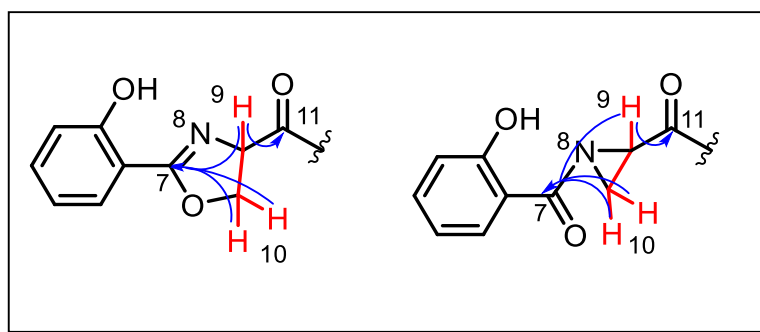


Figure 21. The two possible structural configurations of fragment 2. Oxazoline left and aziridine right. (COSY = red, selected HMBC = blue)

Upon investigation of literature structures, we found several examples of salicylic acid – oxazoline containing natural products. All of these had ^{13}C chemical shifts matching that of our natural product (see Table 2). We therefore preliminarily assigned fragment 2 as an oxazoline ring.

Table 2. ^{13}C NMR signals at positions 7, 9 and 10 of DEM31376/A and several oxazoline containing natural products

Name	Assignment	Solvent	^{13}C chemical shift (ppm) for positions:		
			7	9	10
DEM31376/A	oxazoline	d_6 -DMSO	165.9	67.4	69.4
amyachelin	oxazoline	d_6 -DMSO	168.7	64.9	72.2
transvalecin Z	oxazoline	d_6 -DMSO	168.6	67.4	69.7
nocardichelin A	oxazoline	d_6 -DMSO	165.6	67.2	69.0

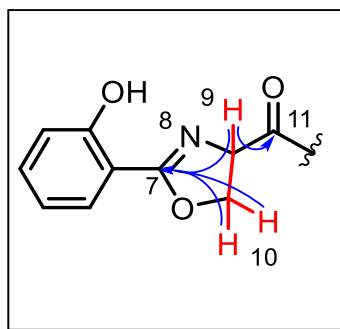


Figure 22. Proposed structural assignment for fragment 2 of DEM31376/A (COSY = red, selected HMBC = blue)

Table 3. ^1H , ^{13}C and ^{15}N signals associated with fragment 2

Position	$\delta_{1\text{H}}$ multiplicity, (J in Hz)	$\delta_{13\text{C}}$	$\delta_{15\text{N}}$	HMBC
7	-	165.9	-	-
8	-	-	208.2	N to H9, 10
9	5.01 dd, ($J = 10.4, 7.7$ Hz, 1H)	67.4	-	H to C10, 6, 7, 11
10	4.65 dd ($J = 10.5, 8.4$ Hz, 1H)	69.4	-	H to C9, 7, 11, 10
	4.52 t ($J = 8.0$ Hz, 1H)	-	-	H to C9, 7, 11, 10
11	-	170.2	-	-

2.7.4 Fragment 3

In the ^1H NMR spectrum, two distinctive double doublets were observed at 3.75 and 3.67 ppm (P-13) with J values of 16.5 Hz, again indicating geminal coupling. COSY experiments showed coupling between this geminal methylene and an amide proton signal at 8.52 ppm (P-12), with the corresponding nitrogen atom at 109.2 ppm in the ^{15}N - ^1H spectrum. With no further coupling, we assigned this fragment as a glycine derived unit. HMBC data showed correlations between the geminal methylene and a new deshielded carbon at 168.4 ppm (P-14) and to the deshielded carbon previously reported at position 11 in fragment 2 (Figure 23).

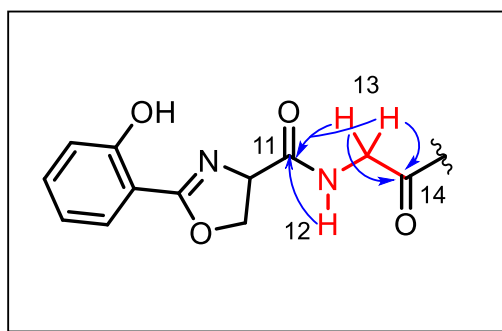


Figure 23. Proposed structural assignment for fragment 3 of DEM31376/A. (COSY = red, selected HMBC = blue)

Table 4. ^1H , ^{13}C and ^{15}N signals associated with fragment 3

Position	$\delta_{1\text{H}}$ multiplicity, (J in Hz)	$\delta_{13\text{C}}$	$\delta_{15\text{N}}$	HMBC
11	-	170.2	-	-
12	8.52 t ($J = 5.9$ Hz, 1H)	-	109.2	H to C13, 14, 11 N to H13
13	3.75 dd ($J = 16.5, 6.1$ Hz, 1H) 3.67 dd ($J = 16.5, 5.7$ Hz, 1H)	42.2 -	- -	H to C14, 11 H to C14, 11
14	-	168.4	-	-

2.7.5 Fragment 4

In the ^1H NMR spectrum a second suspected amide signal can be seen at 7.93 ppm (P-15). COSY correlation spectra showed coupling between this amide proton and a two proton methylene signal at 3.25 ppm (P-16). This methylene group (P-16) showed coupling through a COSY experiment to a second methylene signal at 2.52 ppm (P-17). Both methylene groups showed HMBC correlations to a new deshielded quaternary carbon at 170.9 ppm (P-18), whilst the methylene at position 16 and the amide signal at position 15 showed a correlation to the previously reported carbonyl carbon at position 14 in fragment 3. We therefore assigned fragment 4 as a β -alanine unit (Figure 24).

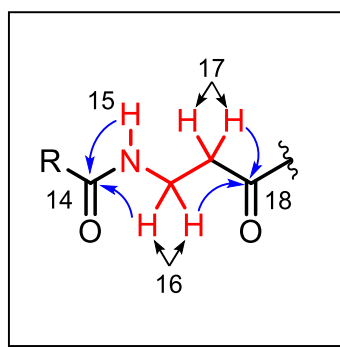


Figure 24. Proposed structural assignment for fragment 4 of DEM31376/A (COSY = red, selected HMBC = blue)
R = fragments 1 - 3

Table 5. ^1H , ^{13}C and ^{15}N signals associated with fragment 4

Position	$\delta_{1\text{H}}$ multiplicity, (J in Hz)	$\delta_{13\text{C}}$	$\delta_{15\text{N}}$	HMBC
14	-	168.4	-	-
15	7.93 t ($J = 5.8$ Hz, 1H)	-	112.5	H to C16, 14 N to H13, 17
16	3.28 – 3.22 (m, 2H)	34.6	-	H to C17, 14, 18
17	2.53 – 2.51 (m, 2H)	32.0	-	H to C16, 18
18	-	170.9	-	-

2.7.6 Fragment 5

A distinctive singlet with an integration of 3 was observed at 2.21 ppm (P-25) in the ^1H NMR spectrum, indicating the presence of a methyl group. A correlation was observed in the ^{15}N - ^1H NMR spectrum between this methyl group and a nitrogen atom with a chemical shift of 29.1 ppm (P-24). This led us to assign the signal as an *N*-methyl group, with the lack of coupling and therefore splitting of the methyl signal attributed to deuterium exchange of the amine hydrogen. This methyl group showed a correlation *via* a HMBC experiment to a one proton triplet at 2.87 ppm (P-23). This in turn showed a HMBC signal to a new deshielded quaternary carbon at 173.5 ppm (P-26). The COSY correlation spectrum showed that this triplet (P-23) was the first of 5 proton-proton coupled ^1H signals, with the first correlation from the triplet at 2.87 ppm (P-23) to a diastereotopic methylene group split into two signals at 1.40 and 1.48 ppm (P-22). Both signals attributed to position 22 showed proton-proton coupling to a second methylene group at 1.58 ppm (P-21). This penultimate methylene signal (P-21) was coupled to a broad multiplet signal with an integration of four between 3.49-3.42 ppm (P-20). Thorough inspection of this signal *via* HMBC experiments showed that it was in fact two overlapping methylene signals (Figure 25), only one of which was part of the coupled spin system we were interested in. This terminal methylene group (P-20) showed correlations

to the previously reported carbonyl carbon at position 18 in fragment 4 and to a nitrogen atom at 175.9 ppm (P-19). However, no amide proton was observed as anticipated, whilst the chemical shift of the nitrogen atom was significantly higher than our previously assigned amide nitrogen's, at 175.9 ppm vs c.110 ppm.

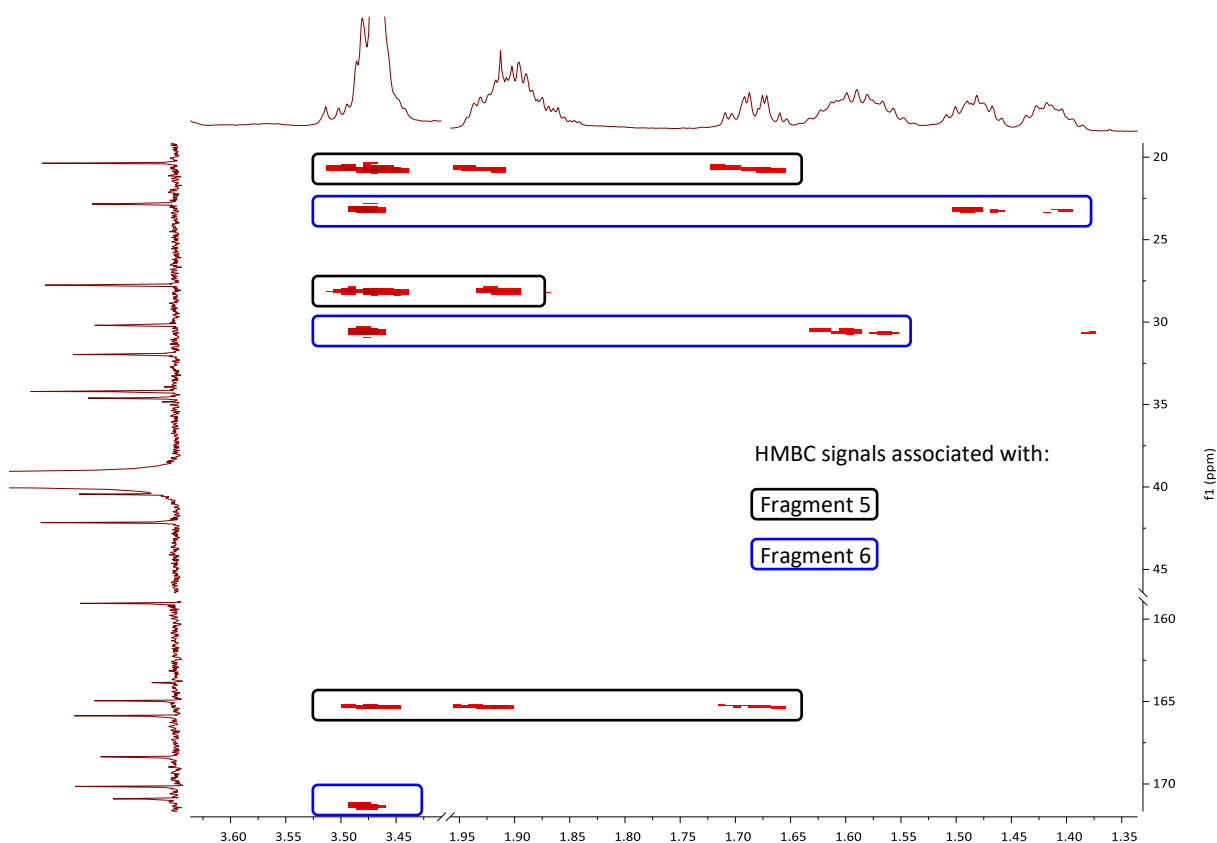


Figure 25. A HMBC experiment showing correlations of the two overlapping methylene groups between 3.49-3.42 ppm to fragments 5 and 6.

In summary for fragment 5, we identified an *N*-methyl group, as well as a spin system consisting of an α -proton at 2.87 ppm (P-23) and 3 methylene groups at 3.49-3.42, 1.58 and 1.40/1.48 ppm (P's 20-22). The lack of the expected amide proton was unsettling, as a HMBC correlation between the methylene at position 20 and the previously assigned carbonyl at position 18 (fragment 4) was observed. The chemical shift of the nitrogen at position 19 was higher than that previously observed for amide nitrogen signals, so we deferred the assignment of this nitrogen atom until more data was available.

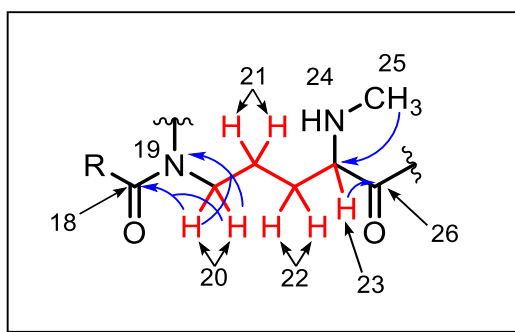


Figure 26. Proposed structural assignment for fragment 5 of DEM31376/A (COSY = red, selected HMBC = blue)
R = Fragments 1 – 4

Table 6. ^1H , ^{13}C and ^{15}N signals associated with fragment 5

Position	$\delta_{1\text{H}}$ multiplicity, (J in Hz)	$\delta_{13\text{C}}$	$\delta_{15\text{N}}$	HMBC
18	-	170.9	-	-
19	-	-	175.9	N to H20, 21
20	3.49 – 3.42 (m, 4H)(2H)	47.0	-	H to C21, 22, 18
21	1.58 tt ($J = 16.5, 6.7$ Hz, 2H)	22.8	-	H to C22, 20, 23
22	1.40 ddd ($J = 15.9, 13.1, 6.8$ Hz, 1H) 1.48 ddt, ($J = 11.7, 9.8, 5.9$ Hz, 1H)	30.2	-	H to C20, 23, 26 H to C20, 23, 26
23	2.87 t ($J = 6.6$ Hz, 1H)	63.7	-	H to C21, 22, 25, 26
24	-	-	29.1	N to H25, 22
25	2.21 (s, 3H)	34.2	-	H to C23
26	-	173.5	-	-

2.7.7 Fragment 6

The final amide signal in the ^1H NMR spectrum was observed at 8.11 ppm (P-27) and showed COSY coupling to an apparent α -proton signal at 4.32 ppm (P-28). This α -proton at position 28 showed HMBC correlations to a new deshielded carbon at 165.0 ppm (P-33). In a similar fashion to fragment 6, a spin system containing an α -proton and an additional three methylene groups was observed (*via* COSY). To expand, the α -proton (P-28) was coupled to a diastereotopic methylene group (P-29) which was split into two signals at 1.67 ppm and 1.96–1.82 ppm. The signal at 1.96–1.82 ppm was a multiplet with an integration of 3 (Figure 27), with HSQC confirming that the additional two hydrogens were a result of an additional methylene group (P-30).

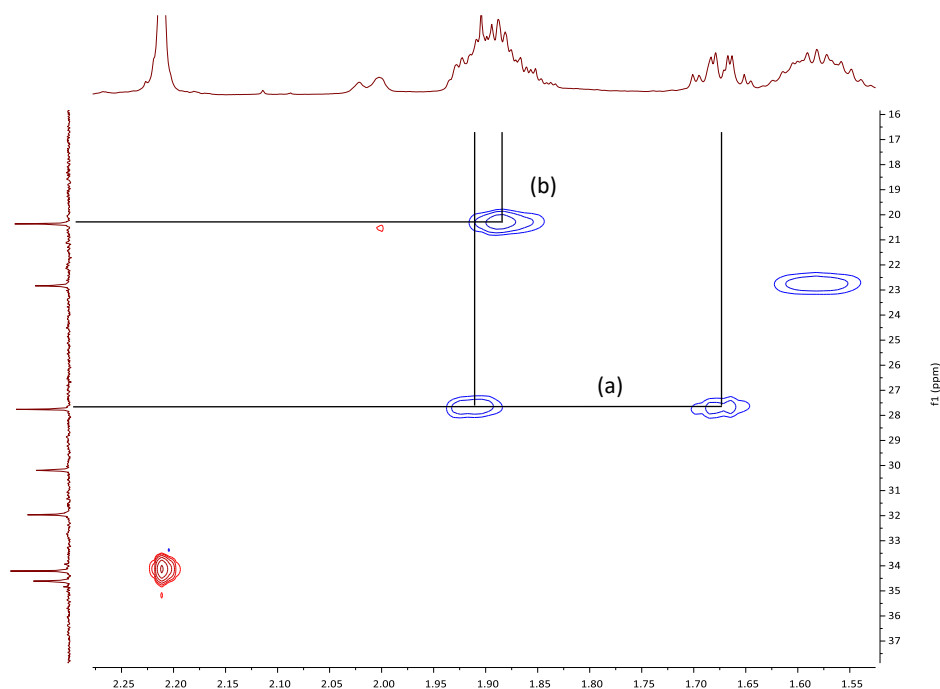


Figure 27 HSQC showing that the multiplet at 1.89 ppm is a mixture of one and a half methylene groups found on carbons 27.8 ppm (a, P-29) and 20.4 ppm (b, P-30)

The methylene group at position 30 (b in Figure 27) was shown *via* COSY and HMBC experiments to couple to the final methylene group in the chain at 3.49-4.42 ppm (P-31). This is the overlapping signal in the ^1H NMR that we previously discussed in fragment 5 (Figure 25). This methylene group (P-31) correlated to a nitrogen at 171.8 ppm (P-32), allowing us to provisionally construct fragment 6 as shown in Figure 28 below.

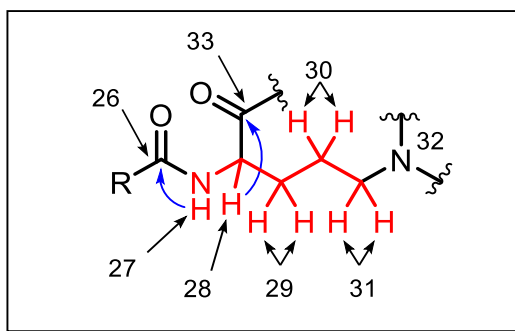


Figure 28. Preliminary assignment of NMR data for fragment 6 (COSY = red, selected HMBC = blue) R = Fragments 1 – 5

The chemical shift of the nitrogen at position 32 (171.8 ppm) is similar to that of the partially assigned tertiary nitrogen at position 19 in fragment 5 (175.9 ppm) and as such it is probably also tertiary in nature. In addition, HMBC data showed a correlation between the protons at

position 31 and the carbonyl like carbon at position 33. This suggested that the fragment is cyclic, and as such would satisfy the final DBE calculated for the molecule. As such a cyclic ornithine amino acid can be assigned for fragment 6.

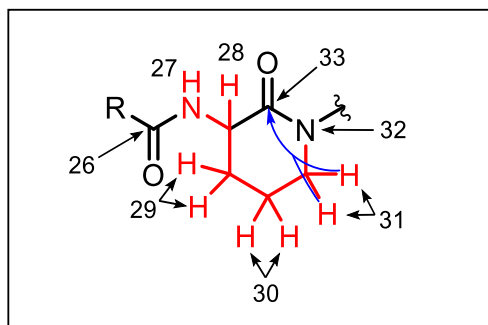


Figure 29. Proposed structural assignment for fragment 6 of DEM31376/A as a cyclic ornithine (COSY = red, selected HMBC = blue) R = Fragments 1 – 5

Table 7. ^1H , ^{13}C and ^{15}N signals associated with fragment 6

Position	$\delta_{1\text{H}}$ multiplicity, (J in Hz)	$\delta_{13\text{C}}$	$\delta_{15\text{N}}$	HMBC
26	-	173.5		
27	8.11 d ($J = 8.3$ Hz, 1H)	-	118.8	H to C28, 33, 26 N to H27, 28, 23, 29
28	4.32 ddd ($J = 10.9, 8.2, 5.3$ Hz, 1H)	49.4		H to C30, 29, 33, 26
29	1.96 – 1.82 (m, 3H) (1H) 1.67 qd ($J = 12.5, 4.3$, 1H)	27.8		H to C30, 29, 33
30	1.96 – 1.82 (m, 3H) (2H)	20.4		
31	3.49 – 3.42 (m, 4H) (2H)	51.2		H to C30, 29, 33
32	-	-	171.8	N to H31, 29
33	-	165.0		

2.7.8 Final assignments

Comparison of the calculated chemical formula for DEM31376/A against the atoms assigned for fragments 1-6 reveals that all seven nitrogen and twenty-six carbon atoms have been assigned. However, two oxygen and two hydrogen atoms are yet to be assigned. We know that the two nitrogen atoms at 171.8 and 175.9 ppm (positions 19+32) do not have a proton attached to them, and the high nitrogen chemical shifts suggest an electronegative atom is attached to these nitrogen atoms instead. As such a hydroxamic acid functionality can be assigned to these two nitrogen atoms. This assignment not only satisfies our molecular formula, but also satisfies the four different ^{15}N chemical shift ranges observed: 29.1 ppm for the methyl amine, 110-120 ppm for the amides, 170-180 ppm for the hydroxamic acids and

208.2 ppm for the oxazoline nitrogen. The hydroxamic acid group is a common structural feature in siderophores.²⁴ Whilst siderophores are specific Fe³⁺ chelators they are also well documented to chelate Ga³⁺.^{75–78} This is due to the similar ionic radii of Ga³⁺ (0.62 Å) and Fe³⁺ (0.65 Å).⁷⁵ The role of DEM31376/A as a siderophore was confirmed by metal chelation studies, with the mixing of DEM31376/A in methanol with both Fe(acac)₃ and Ga(acac)₃ to form two 1:1 metal to ligand complexes. These complexes were then subjected to HPLC-MS, resulting in the appearance of both an [M-3H⁺+Fe³⁺+H]⁺ signal at *m/z* = 645 and a [M-3H⁺+Ga³⁺+H]⁺ signal at *m/z* = 658 corresponding to the respective 1:1 molecule:metal chelates, confirming the biological role of DEM31376/A as a siderophore.

2.7.9 Conclusions for the structural assignment of DEM31376/A

The combination of each individual fragment *via* the HMBC data allows us to propose the full structure for DEM31376/A (**25**, Figure 30). This is a pentapeptide siderophore, constructed from the amino acids serine (which has been capped with a salicylic acid), glycine, β-alanine, Nα-methyl-ornithine and ornithine. This assignment fulfils the twelve double bond equivalents (DBEs) calculated for DEM31376/A *via* the three rings (one aromatic) and 6 double bonds. In addition, the three “OH” groups (two hydroxamic acid and one phenolic) and methylamine proton account for the four exchangeable protons that were not observed in the ¹H NMR spectrum.

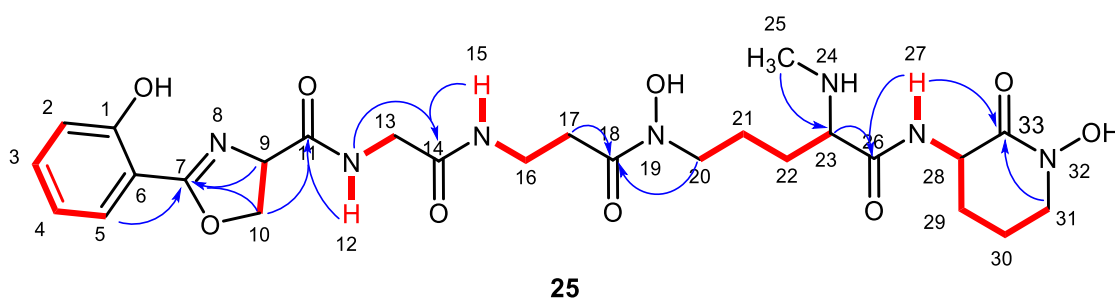


Figure 30. Structural assignment of DEM31376/A (**25**) (COSY = red, selected HMBC = blue)

This assignment is also supported by the original MS and HRMS fragmentation data. Ring opening of the oxazoline under acidic conditions explains the [M+H₂O+H]⁺ peak observed in our original HPLC and mass spectrometry data. Whilst fragmentation of DEM31376/A at the amide bonds, as this is a common feature in mass spectrometry of peptides,⁷⁹ yields the daughter ions we observed and detailed previously (Figure 31).

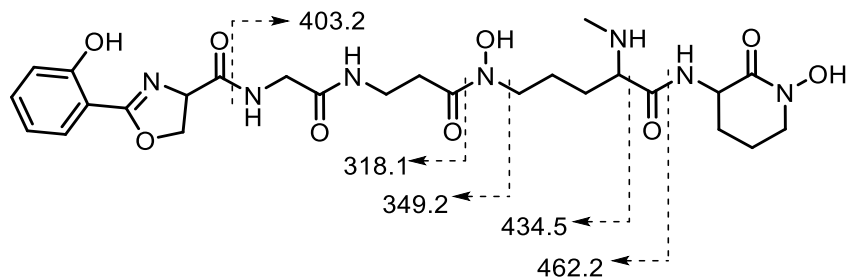


Figure 31. Proposed assignment of the fragmentation ions of DEM31376/A (**25**)

With the chemical structure of DEM31376/A successfully assigned, we next decided to assign the stereochemistry of DEM31376/A using Marfey's analysis.

2.8 Marfey's analysis

2.8.1 Introduction to Marfey's analysis

Marfey's analysis is a technique used for the determination of the absolute stereochemistry of amino acids.⁸⁰ This is done *via* functionalization of the amino acid in question with Marfey's reagent and comparing the HPLC retention time of the resulting diastereomer against Marfey's functionalised L and D amino acid standards.

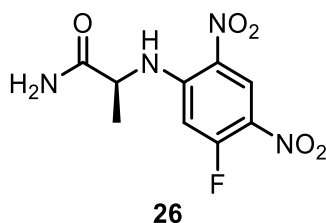


Figure 32. Marfey's reagent

Marfey's reagent (N_{α} -(2,4-dinitro-5-fluorophenyl)-L-alaninamide) (**25**) has an electron deficient aromatic ring which serves two purposes. First, it allows for nucleophilic aromatic substitution to occur *via* attack by the amino acid nitrogen. Second, the aromatic ring provides a chromophore to allow detection *via* UV-Vis absorption at 340 nm. Synthesis of standards of both L and D amino acids with Marfey's reagent will give diastereomers with different HPLC retention times, without the need to use a chiral HPLC column (Figure 33).

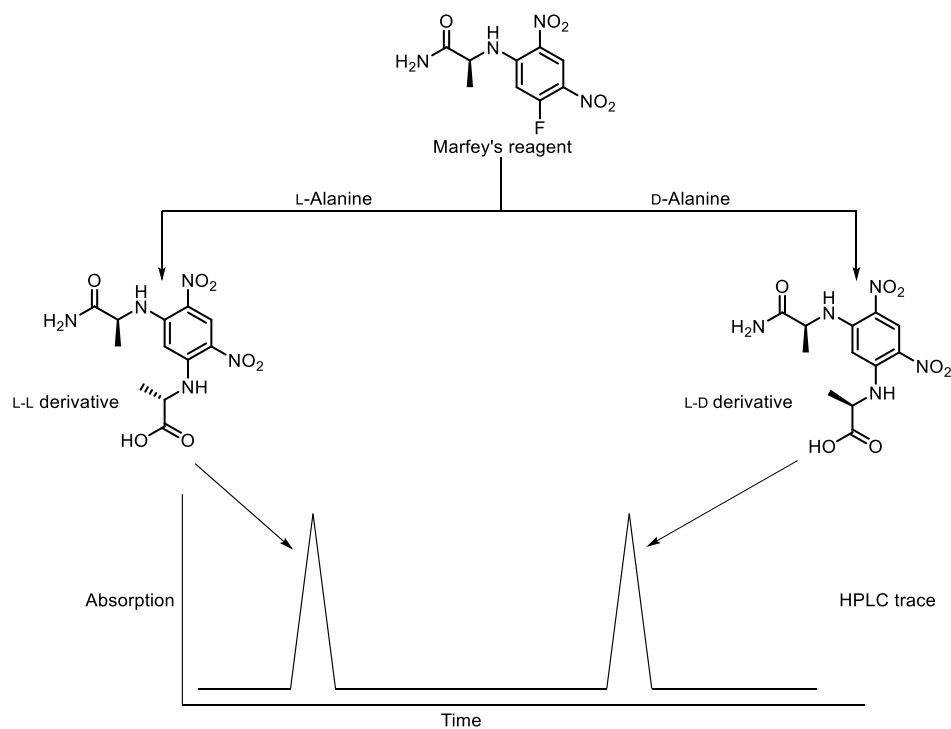


Figure 33. Graphical representation of the separation of L and D Alanine via Marfey's analysis

Comparing the retention time of the Marfey's functionalised amino acid standards against the functionalised, unknown-chirality, amino acid under investigation allows assignment of the absolute stereochemistry of that amino acid (Figure 34).

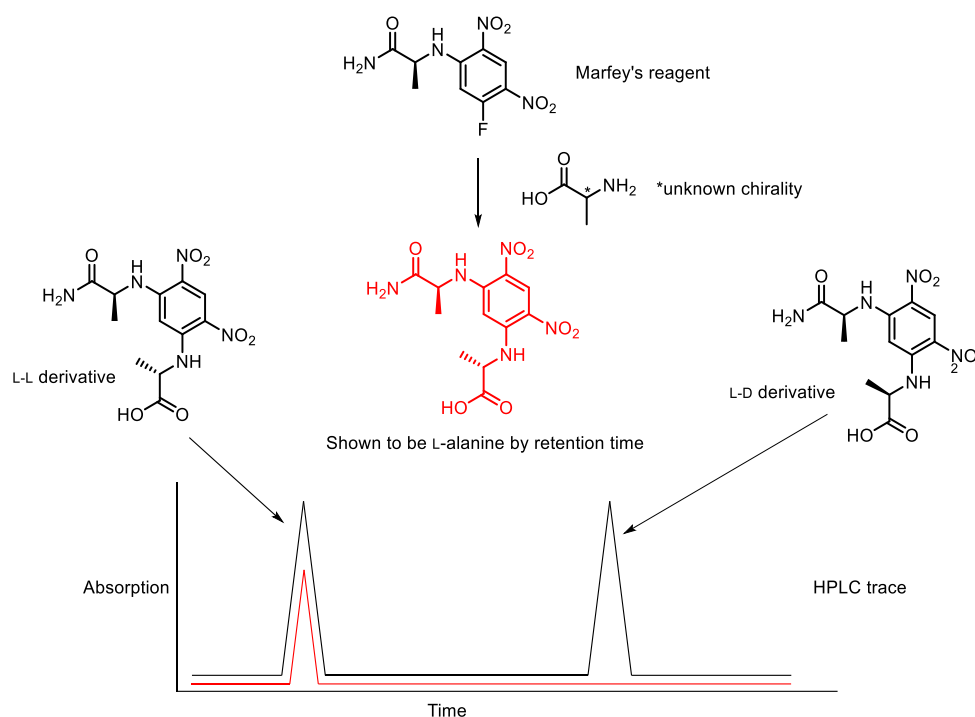


Figure 34 Graphical representation of the assignment of the absolute stereochemistry of alanine via Marfey's analysis

2.8.2 Advanced Marfey's method

Marfey's method was improved by Harada and co-workers and coined the "Advanced Marfey's Method".⁸¹ In the original technique, the Marfey's reagent always bore the same chirality (L-alanine) and the two standards were synthesised *via* reaction of this L-Marfey's reagent (L_M) with L and D amino acids (L_{aa} or D_{aa}) to give an L_M-L_{aa} diastereomer and an L_M-D_{aa} diastereomer. The insight of Harada and co-workers was that the relationship between an L_M-L_{aa} derivative and a D_M-D_{aa} derivative would be enantiomeric, giving one class of Marfey's derivatives with identical retention times. Likewise, the relationship between an L_M-D_{aa} derivative and a D_M-L_{aa} derivative would be enantiomeric as well. However, these two groups of enantiomeric Marfey's derivatives would be diastereomers in relation to each other and therefore have different retention times (Figure 35).

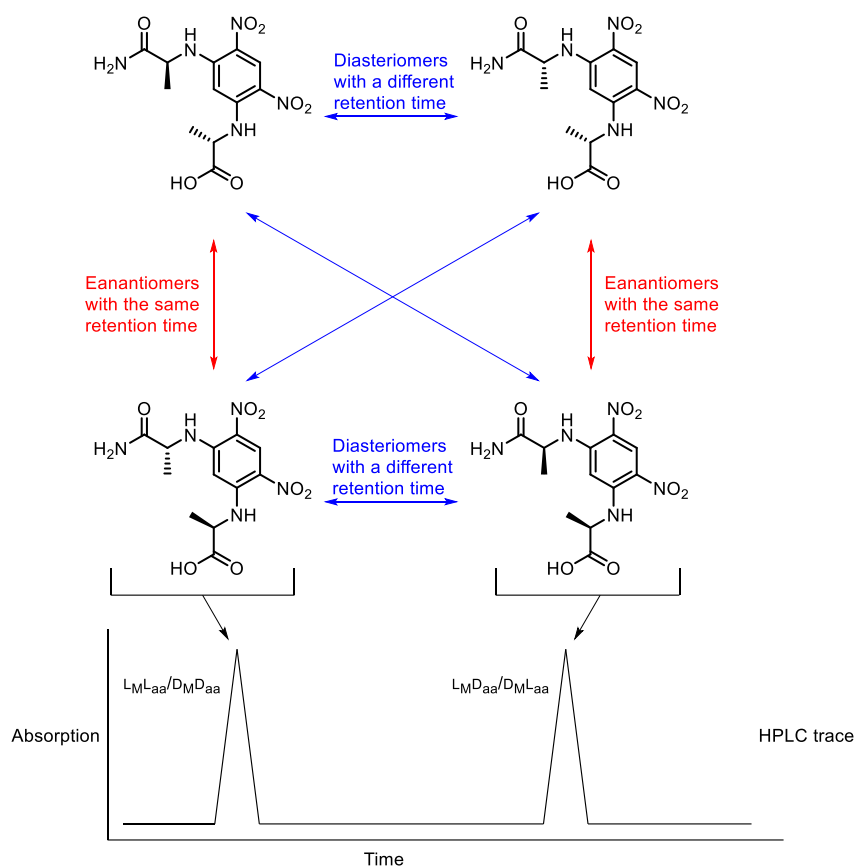


Figure 35. Graphical representation of the separation of L and D Alanine via advanced Marfey's analysis.

This means that Marfey's standards can be produced by changing the chirality of the Marfey's reagent whilst using the same chiral amino acid. This is incredibly useful if the amino acid to be analysed has been functionalised or modified in some way, making access to both chiral enantiomers (either commercially or synthetically) difficult or prohibitively expensive.

2.9 Advanced Marfey's analysis of DEM31376/A

2.9.1 Introduction

There are three chiral amino acids in DEM31376/A that need to be assigned: serine (blue), $N\alpha$ -methyl-ornithine (red) and ornithine (green).

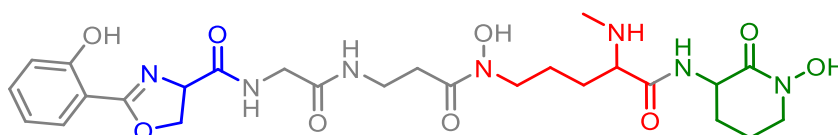


Figure 36. Structure of DEM30616/A (**25**) showing the three chiral amino acids: serine (blue), $N\alpha$ -methyl-ornithine (red) and ornithine (green), chiral centres are marked with an asterisk.

In order to determine the absolute stereochemistry of DEM31376/A, we will first need to generate a series of L and D Marfey's amino acid standards for L-serine, L-ornithine and L-N α -methyl-ornithine and record their HPLC retention times. After this, DEM31376/A could then be hydrolysed and reacted with L-Marfey's reagent and the HPLC retention times obtained could then be compared to those of the amino acid standards, in order to determine the chirality of the amino acids in DEM31376/A.

2.9.2 Preparation of Marfey's standards for DEM31376/A

To prepare our Marfey's amino acid standards, we functionalised L-serine, L-ornithine and L-N α -methyl-ornithine with both N α -(5-fluoro-2,4-dinitrophenyl)-L-leucinamide and N α -(5-fluoro-2,4-dinitrophenyl)-D-leucinamide in water and in the presence of base. Due to the presence of the two nitrogen atoms in the ornithine derived amino acids, the functionalisation reaction generated three products. These were the mono- α -functionalised, the mono- δ -functionalised, and the bi- α,δ -functionalised products. After the synthesis of our standards, they were each subjected to HPLC-MS and their retention times recorded.

2.9.3 Marfey's analysis of DEM31376/A

With the synthesis and HPLC retention times of the required amino acid standards completed, hydrolysis of the natural product was carried out.

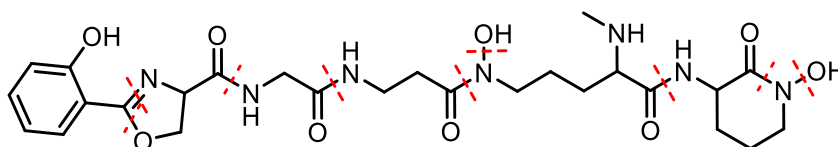


Figure 37. Graphical representation of the hydrolysable bonds in **25** in the presence of concentrated HI.

For the hydrolysis we elected to react DEM31376/A in concentrated hydroiodic acid. The use of concentrated hydroiodic acid causes first the hydrolysis of the amide bond to the hydroxylamine, followed by the reduction of said hydroxylamine to the free amine.^{25,82} This allowed commercially available ornithine and N α -methyl-ornithine to be used for the synthesis of the Marfey's standards.

Complete hydrolysis of DEM31376/A was achieved in concentrated hydroiodic acid, and the residue was functionalised with N α -(5-fluoro-2,4-dinitrophenyl)-L-leucinamide. Analysis by

HPLC-MS gave a multitude of peaks *via* detection with UV-Vis, scanning between 190-640 nm. This was due to the presence of all 5 functionalised amino acid residues as well as hydrolysed Marfey's reagent and other side-products. The chromatogram was simplified by searching for the exact masses of the Marfey's functionalised amino acids we were interested in. The masses selected were 400.14 for serine, 427.19 (mono) and 721.28 (bi) for ornithine and 441.20 (mono) and 735.30 (bi) for *N*-methyl-ornithine, generating the extracted ion chromatogram overleaf (Figure 38).

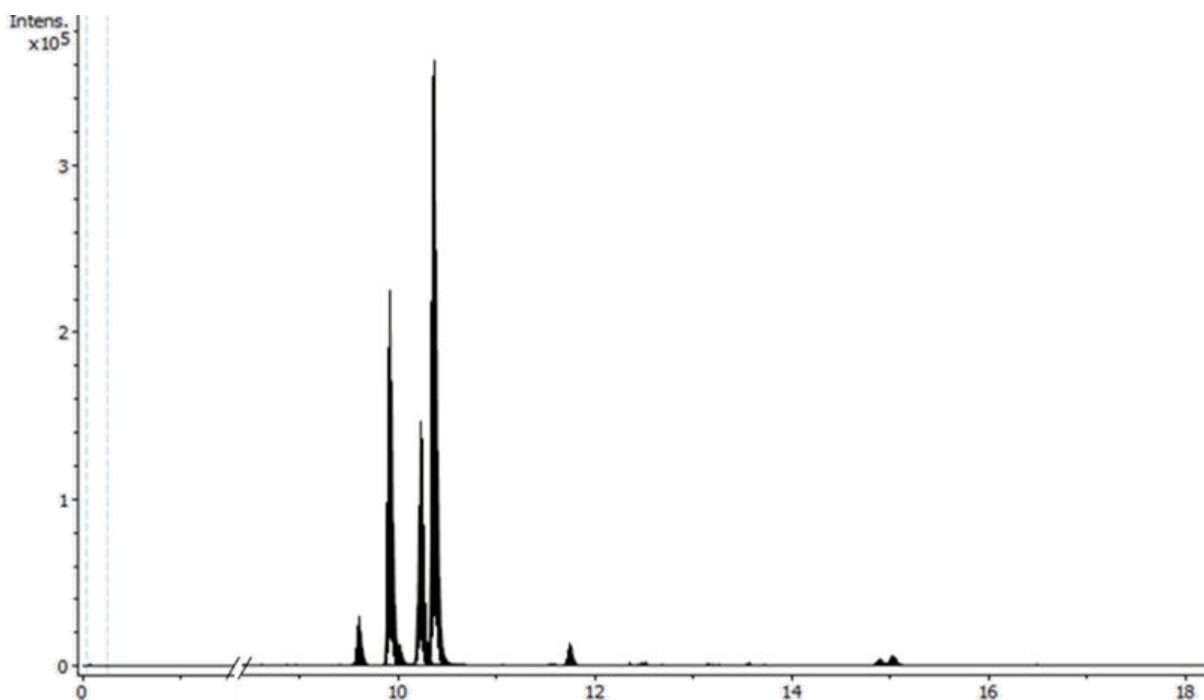


Figure 38. Extracted ion chromatogram of hydrolysed DEM31376/A functionalised with *N* α -(5-fluoro-2,4-dinitrophenyl)-L-leucinamide showing the ions with *m/z* values of 400.14, 427.19, 721.28, 441.20 and 735.30.

Graphical comparison of the retention times of the Marfey's functionalised amino acid standards with Marfey's functionalised DEM31376/A (Figure 39), as well as direct comparison of the retention times in Table 8 showed that DEM31376/A is comprised of D-serine (*R*), L-ornithine (*S*) and L-*N* α -methyl-ornithine (*S*).

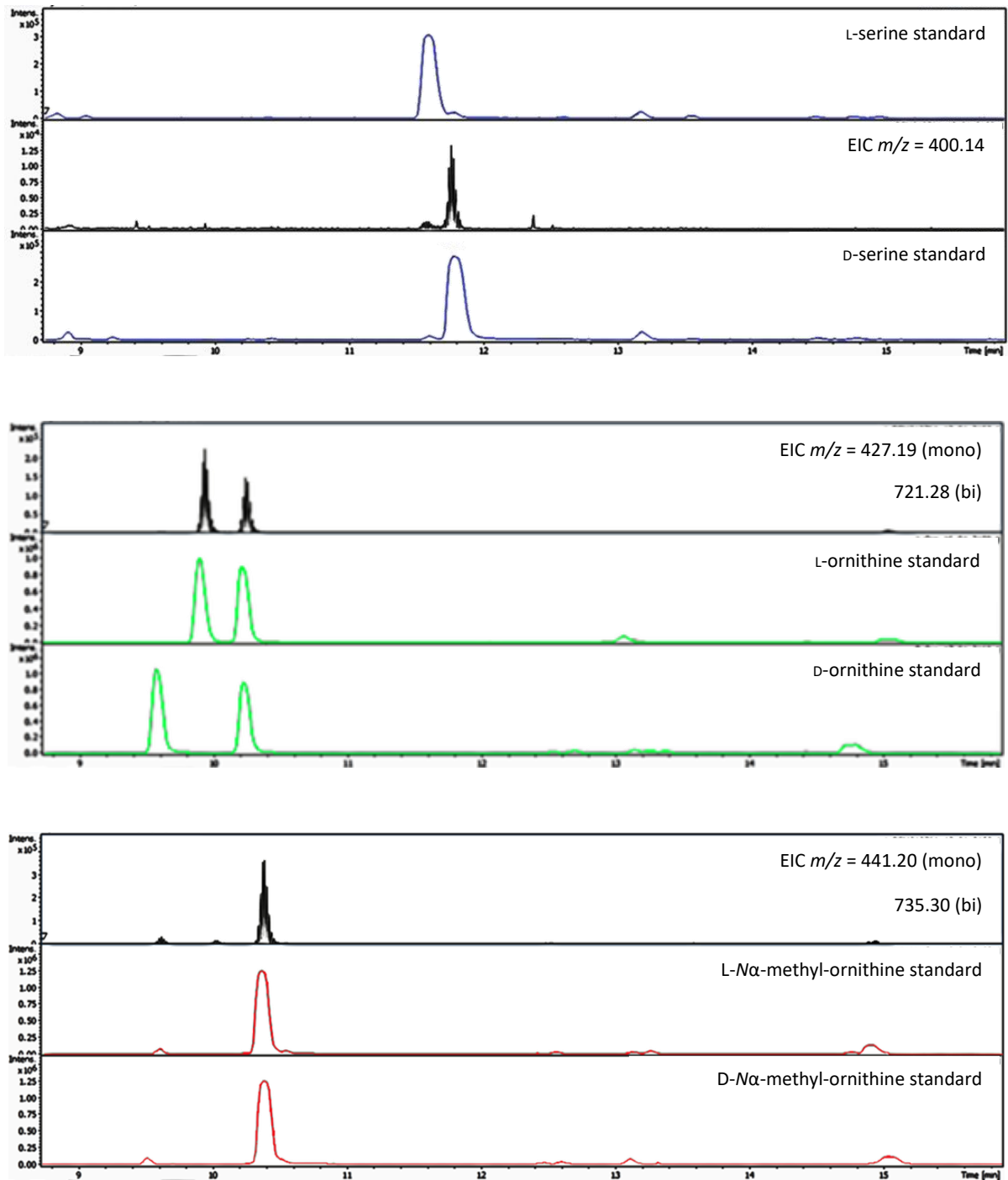
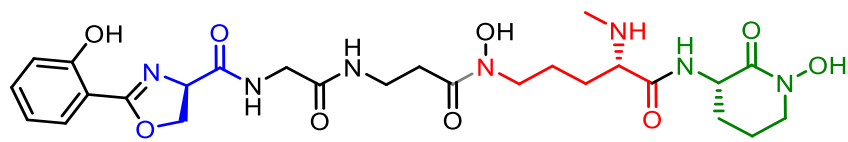


Figure 39. Extracted ion chromatograms from Marfey's analysis of DEM31376/A showing the experimental peaks (black), and amino acid standards: serine (blue), ornithine (green) and N α -methyl-ornithine (red).

Table 8. Retention times of Marfeys functionised amino acid standards and hydrolysed DEM31376/A

Amino acid	Marfey's Chirality	Retention Time (mins)	Separation (mins)
L-Serine	L	11.6	0.2
L-Serine	D	11.8	
L-Ornithine α	L	9.9	0.3
L-Ornithine α	D	9.6	
L-Ornithine δ	L	10.2	0
L-Ornithine δ	D	10.2	
L-Ornithine $\alpha+\delta$	L	15.1	0.4
L-Ornithine $\alpha+\delta$	D	14.7	
L- N_{α} -methyl-ornithine α	L	9.6	0.1
L- N_{α} -methyl-ornithine α	D	9.5	
L- N_{α} -methyl-ornithine δ	L	10.4	0
L- N_{α} -methyl-ornithine δ	D	10.4	
L- N_{α} -methyl-ornithine $\alpha+\delta$	L	14.9	0.4
L- N_{α} -methyl-ornithine $\alpha+\delta$	D	15.3	
DEM31376/A Serine	D	11.8	-
DEM31376/A Ornithine α	L	9.9	-
DEM31376/A Ornithine δ	L	10.2	-
DEM31376/A Ornithine $\alpha+\delta$	L	15.1	-
DEM31376/A N_{α} -methyl-ornithine α	L	9.6	-
DEM31376/A N_{α} -methyl-ornithine δ	L	10.4	-
DEM31376/A N_{α} -methyl-ornithine $\alpha+\delta$	L	14.9	-

2.10 Resolution of the structure of madurastatin C1

2.10.1 Introduction

Upon completion of our structural assignment of DEM31376/A, we discovered the family of structurally similar siderophores named ‘madurastatins’ all of which had been isolated from the culture broths of *Actinomadura sp.* bacteria. This family of molecules also included madurastatin C1 (**30**), which bore a near identical structure to DEM31376/A (**25**).^{83,84} Indeed the only difference in structure between DEM31376/A (**25**) and madurastatin C1 (**30**) was in the structural assignment of the serine moiety. We had assigned this serine derived component as an oxazoline ring, which conflicted with the published structures of madurastatins A1, B1, B3 and C1, which had all been assigned with an aziridine ring.^{83,84,85}

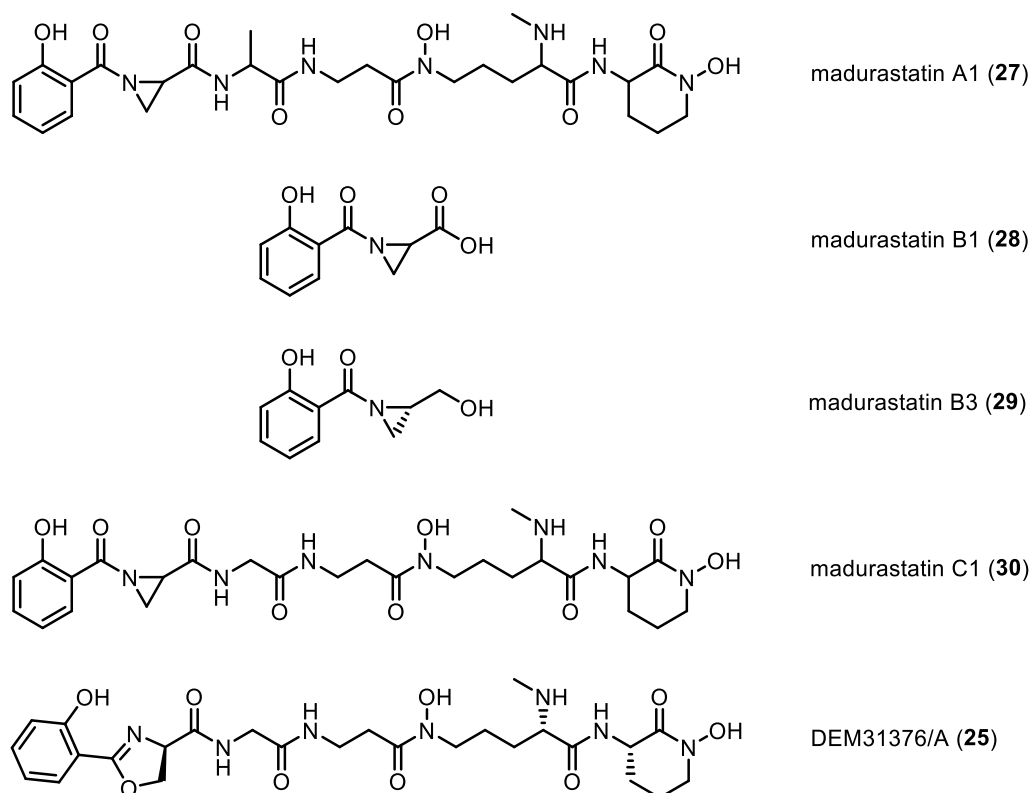


Figure 40. Published structures of madurastatins A1, B1, B3 and C1 and our proposed structure for madurastatin C1 (**24**)

Correctly assigning the structure at this position is important, as madurastatins A1, B1 and C1 showed mild antibiotic activity *via* inhibition of the growth of *M. luteus* (and *S. aureus* in the case of madurastatin C1) whilst madurastatin B3 (**29**) showed toxicity against *Bacillus subtilis*, *E. coli*, *Mycobacterium tuberculosis* and methicillin resistant *S. aureus*. Conversely, hydrolysed (ring-opened) madurastatins showed little to no antimicrobial activity at all. This led the

authors to conclude that the aziridine ring played an important role in the antimicrobial activity of the madurastatins, and as such the chemical structures of the madurastatins should be reviewed and re-assigned if necessary.⁸³⁻⁸⁵

2.10.2 Assignment of DEM31376/A

To this end, we went back to our assignment, wherein we had elected to classify the cyclised serine as an oxazoline ring. This was due to the ¹³C chemical shifts of the α and β carbons being 67 and 69 ppm respectively. These chemical shifts were in line with other oxazoline containing siderophores including amyachelin,⁴⁰ gobichelin A,⁸⁶ nocardichelin A,⁸⁷ transvalecin Z⁸⁸. The assignment of an oxazoline ring was further supported in the case of amyachelin, through resolution of the structure *via* single crystal X-ray crystallography.⁴⁰ Conversely to oxazoline rings, aziridine rings typically have lower ¹³C chemical shifts, in the range of 25-45 ppm. With these published structures lending support to our assignment of an oxazoline ring, we decided to finally prove through synthesis that the oxazoline assignment was correct.

In order to confirm our assignment, we decided to synthesise two salicylate capped serine models, as both the oxazoline (**31** or **32**) and aziridine (**33** or **34**) and compare their NMR data against the isolated natural products.

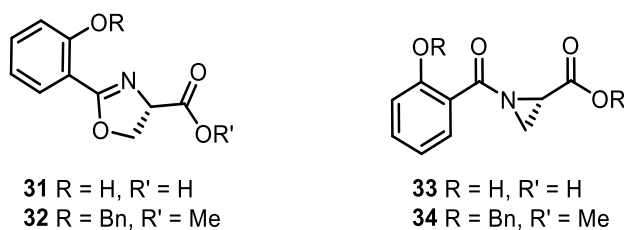
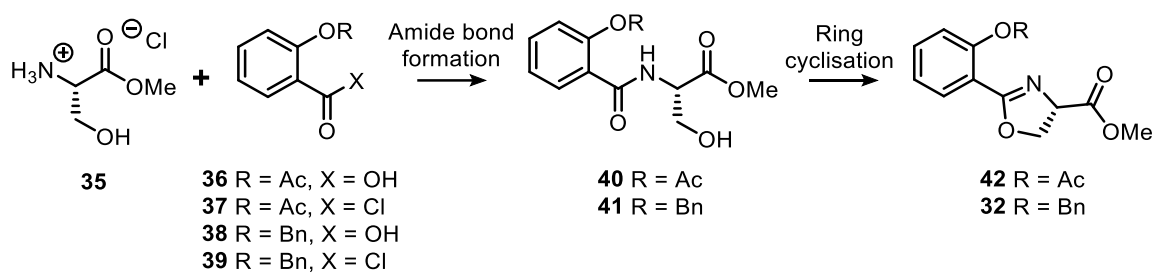


Figure 41. Structures of the target oxazoline models (**31** + **32**) and aziridine models (**33** + **34**).

2.10.3 Synthesis of model oxazoline

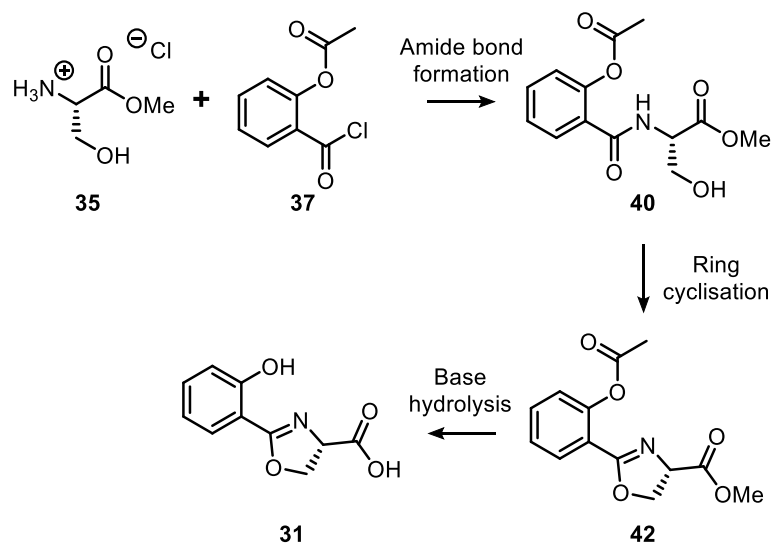
As the model we wished to construct was derived from the amino acid serine, we decided to utilise this amino acid in the form of serine methyl ester **35**. This would be coupled *via* reaction with a protected derivative of salicylic acid to generate an amide bond, through either an acid chloride or peptide coupling.⁷ Cyclisation could then be carried out using thionyl chloride.⁸⁹



Scheme 1. Proposed general synthetic route to the model oxazoline precursors **42** and **33**.

2.10.4 Synthesis of model oxazoline **31**

Our first synthetic attempts to generate the oxazoline model involved the reaction of *O*-acetylsalicyloyl chloride (**37**) with L-serine methyl ester hydrochloride (**35**) at room temperature in the presence of base. We elected to use an acetyl group to protect the phenolic alcohol as it would enable easy removal at a later stage *via* base mediated hydrolysis, the same conditions used to remove the methyl ester, to generate oxazoline model **31** (Scheme 2).



Scheme 2. Proposed synthetic route to oxazoline **30**

Interestingly, the amide generated from the reaction of serine methyl ester **35** and acid chloride **37** failed to undergo ring cyclisation to generate oxazoline **42**. As a result, 2D NMR experiments were carried out on amide **40** revealing that the attempted amide bond formation had in fact produced ester **43** as an unexpected product. Thus explaining the failure

of the attempted ring-cyclisation reactions. We therefore chose to utilise a new protecting group for the aromatic-hydroxyl group to circumvent this issue.

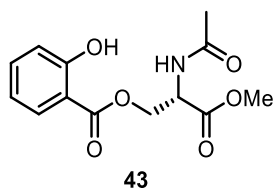
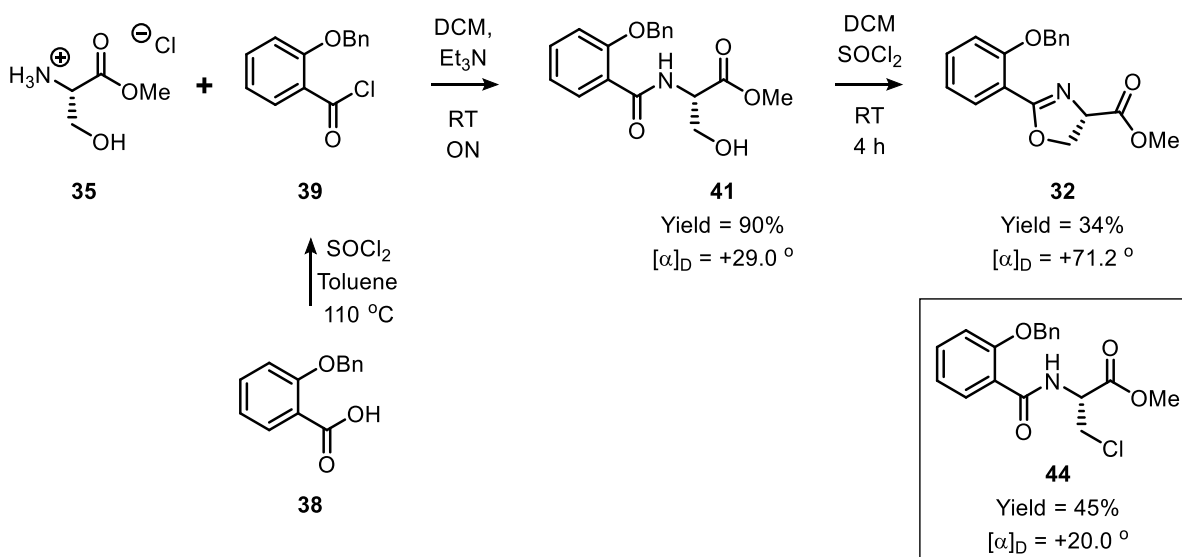


Figure 42. Resulting product from the reaction of serine methyl ester **35** and salicylic acid derivative **37**

2.10.5 Alternative synthesis to generate model oxazoline (**32**)

Due to the difficulty in generating amide **40** we therefore chose to use a benzyl protecting group in our second synthetic attempt, to generate target amide **41**. Amide **41** was synthesised by reacting serine methyl ester **35** with either acid chloride **39** or through a DCC mediated peptide coupling with acid **38**.⁸⁹ Whilst DCC mediated peptide coupling between serine methyl ester **35** and acid **38** resulted a high yield of amide **41** (70%), the product required several rounds of purification to remove the DCU by-product. Conversely, reaction of serine methyl ester **35** and acid chloride **39** successfully gave higher yields of amide **41** (c. 90%) and was significantly easier to purify.



Scheme 3. Alternative synthetic route to generate model oxazoline **32**

With the synthesis of amide **41** completed we next looked to complete the required intramolecular ring closure to generate oxazoline **32** using thionyl chloride.⁸⁹ Initial attempts

in both dry THF and DCM gave exclusively an unwanted alkyl chloride by-product **44**.⁹⁰ By monitoring the reaction *via* TLC we observed the formation of oxazoline **32** was being mirrored by the generation of alkyl chloride **44**. We therefore elected to quench the reaction after one hour by the addition of water, enabling us to isolate oxazoline **32** in 34% yield. Whilst this result was promising we looked to improve the yield of oxazoline by using DAST to accomplish the desired ring cyclisation.⁹¹ Using DAST in dry DCM afforded exclusively oxazoline **32** in 79% yield with no observable by-products generated.

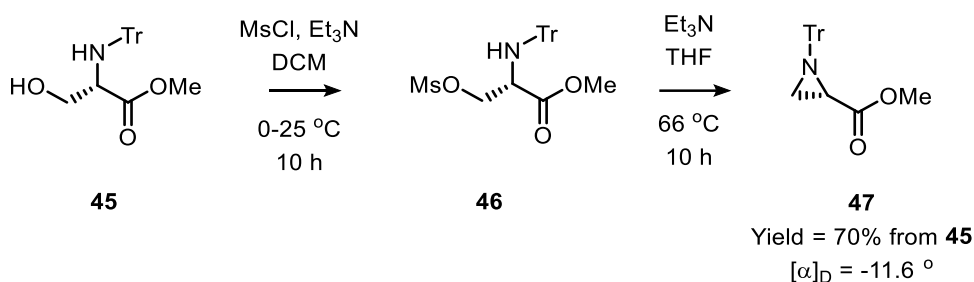
*Table 9. Reaction conditions and results for the reaction of amide **41** with SOCl₂ to generate **32** and **44***

Reagent	Temperature (°C)	Solvent	Time (hours)	Yield (%) oxazoline (32)	Yield (%) chloride (44)
SOCl ₂	-78	THF	18	0	95
SOCl ₂	-78	DCM	18	0	84
SOCl ₂	-78	DCM	1	34	45
DAST	-78	DCM	2	79	0

The quantity of oxazoline produced was enough to allow us to fully characterise **32** *via* NMR, HRMS and X-ray crystal analysis. With the synthesis of oxazoline **32** completed, we next turned our attention to the synthesis of the aziridine model (**34**).

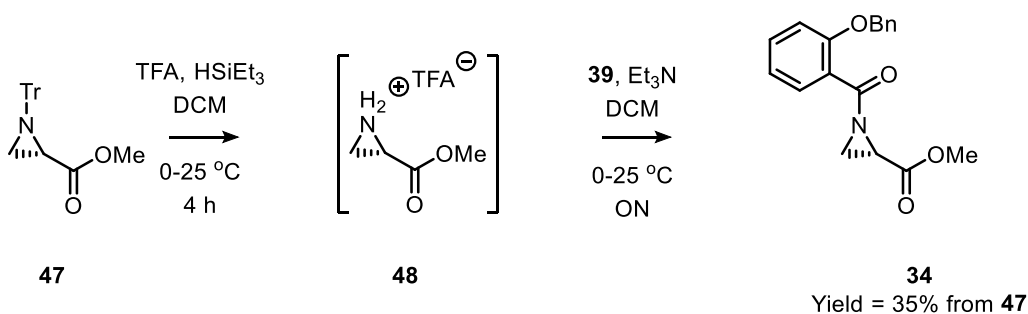
2.10.6 Synthesis of model aziridine (**34**)

To allow direct NMR comparison between the oxazoline and aziridine models, we elected to synthesise model aziridine **34**. To synthesise **34**, we first had to construct an aziridine ring followed by reaction with benzyl protected acid chloride **39**. We therefore began with an *N*-trityl (Tr) protected L-serine (**45**) which was reacted with mesyl chloride in order to activate the alcohol, making it a better leaving group (**46**). This mesylate was not isolated, but evaporated to dryness and dissolved in THF and heated in the presence of Et₃N. This resulted in the mesylate being displaced *via* an intramolecular S_N2 reaction to give the required aziridine (**47**) in 70% yield over two steps after isolation via trituration (Scheme 4).^{92–95}



Scheme 4. Synthetic route to generate aziridine 47

The next step was the removal of the trityl protecting group. This is usually achieved *via* the use of TFA in chloroform/methanol 1:1,^{93,96,97} however, in our hands this reaction proved unsuccessful with exclusively unreacted starting material observed by TLC. Modification of this procedure to include the use of triethylsilane in the presence of TFA cleanly cleaved off the trityl protecting group, yielding the free amine (**48**).^{92,98} With our freshly deprotected amine in hand we reacted this, without purification, with freshly prepared acid chloride (**39**) to form oxazoline model (**34**) in a 20% yield from aziridine (**47**).



Scheme 5. Synthetic route to generate aziridine 34

2.10.7 Structural confirmation of DEM31376/A and the madurastatins

With the synthesis of the oxazoline (**32**) and aziridine (**34**) model systems completed, NMR studies of both of these compounds were carried out. We then compared this data against the NMR data obtained for DEM31376/A and the literature values for madurastatin C1 (Table 10). The ¹³C chemical shifts for the synthesised aziridine ring come at 37.5 ppm (P-2) and 33.1 ppm (P-3), far lower than the corresponding signals observed for DEM31376/A and madurastatin C1. Meanwhile the ¹³C chemical shift for the quaternary carbon (P-1) is at 178.1 ppm and thus too deshielded in comparison to the isolated natural products. Happily, the ¹³C signals for the synthesised oxazoline ring were found to be at 70.8 ppm (P-2), 69.3 ppm (P-3)

and 168.1 ppm (P-1), all of which are near perfect matches to the shifts seen in the natural products (Table 10)

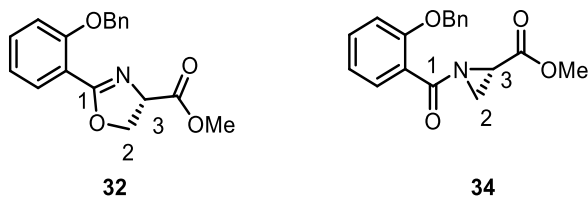


Table 10 ¹³C NMR data for model systems (**32**) and (**34**) versus madurastatin C1 and DEM31376/A

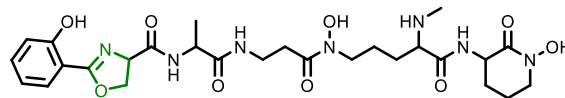
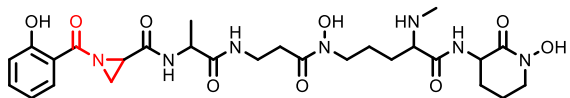
Name	Solvent	Carbon chemical shift (ppm)		
		1	2	3
Synthesised Oxazoline (32)	CD ₃ OD	168.1	70.8	69.3
Synthesized Aziridine (34)	CD ₃ OD	178.1	37.5	33.1
DEM31376/A (25)	CD ₃ OD	165.9	69.4	67.4
Madurastatin C1 (30)	CD ₃ OD	167.0	69.3	67.9

As a result of our studies, we propose that DEM31376/A (**25**) and madurastatin C1 (**30**) are the same molecule. In addition, we have proven that madurastatin C1 (**30**) contains an oxazoline ring, not the previously reported aziridine. Similarly, the chemical structures of madurastatin A1 (**27**), B1 (**28**) and MBJ-0035 (**49**) are also incorrect and each has had its structures revised to contain an oxazoline ring in our publication from early 2017.⁹⁹ We also propose that the reported isolation and antibacterial studies of madurastatin B3 (**29**) are in fact the isolation and bacterial studies of spoxazomicin C (see Figure 43).

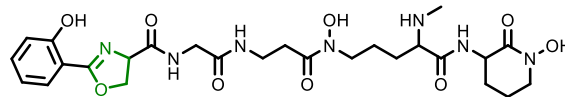
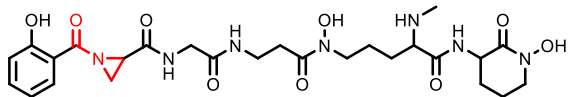
Old assignment

New assignment

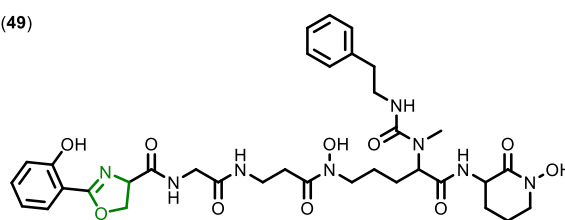
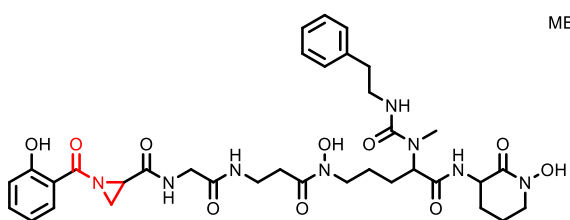
Madurastatin A1 (27)



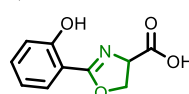
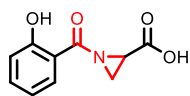
Madurastatin C1= MBJ-0034= DEM31376/A (25)



MBJ-0035 (49)



Madurastatin B1 (28)



Madurastatin B3 (29)

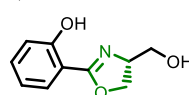
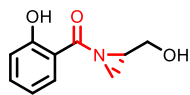


Figure 43. Original structures of madurastatins A1, B1, B3, C1 and MBJ-0035 left, red and their new proposed structural assignments right, green

2.11 Conclusions for chapter 2

In this chapter, we have highlighted our work to isolate and identify the potentially bioactive bacterial siderophore DEM31376/A from a novel *Actinomadura sp.* itself isolated from deep sea marine sediment found at Canary Basin in the Atlantic Ocean. After initial investigation it was realised that the antibiotic nature of samples of DEM31376/A arose from a co-eluting natural product GE23077. However, due to our interest in the structure and biology of bacterial siderophores, we decided to continue our investigations into this bacterial natural product. Investigations therefore began with a large scale fermentation of the bacterial strain DEM31376 and isolation of the bioactive compound through solid phase capture with Amberlite XAD16N beads and elution with methanol. This was followed by fractionation *via* solid phase extraction (C8 cartridge) and a final reverse phase chromatography step to yield 283 mg of DEM31376/A. After Isolation we determined the chemical structure of DEM31616/A *via* a *de novo* structural determination utilising a series of techniques including HRMS, 1D and 2D NMR and Marfey's analysis. This allowed us to assign DEM31376/A as a pentapeptide siderophore with three chiral centres (D-Serine, L-N- α -Methyl-Ornithine and L-Ornithine). Comparison of this natural product to known siderophores informed us that we had in fact re-isolated the known siderophore madurastatin C1. However, our structural assignment differed slightly to that of madurastatin C1, with our assignment containing an oxazoline ring as opposed to an aziridine-amide. Synthesis of model compounds **32** + **34** and comparison of their carbon chemical shift data allowed us to prove that our assignment was indeed correct. With that we propose that the chemical structures of madurastatins A1, B1, C1 and B3 be changed to incorporate an oxazoline ring instead of an aziridine-amide functionality.

With the chemical structure fully assigned, we next turned our attention to the total synthesis of madurastatin C1 which as of yet has not been reported in the literature.

Chapter 3. Total Synthesis of Madurastatin C1

3.1 Introduction

With the chemical structure and stereochemistry of madurastatin C1 (**25**) assigned by ourselves in Chapter 2, we next sought to complete the total synthesis of this natural product. The total synthesis of madurastatin C1 was deemed rewarding for several reasons. Primarily, at the time of writing the total synthesis of madurastatin C1 has not yet been reported in the literature. As organic chemists this represented an exciting opportunity to be the first to synthesise a natural product. In addition to this, total synthesis would allow us to access pure siderophore without the dependency on fermentation of bacterial strain DEM31376. This would remove the potential for contamination from the natural product GE23077 (described in Chapter 2) in any bioassay or feeding experiments we may wish to carry out in future. Furthermore, total synthesis would allow us to easily generate structural derivatives of madurastatin C1 by modification of the constituent amino acids either prior to their utilisation in the total synthesis, or *via* post synthetic modification. With this rationale for the total synthesis of madurastatin C1, we looked to the literature for the synthesis of other similar natural products.

3.2 Relevant literature

3.2.1 Total synthesis of Exochelin MN (**50**).

Exochelin MN (**50**) is an extracellular siderophore produced by *Mycobacterium neoaurum* and has been shown to facilitate iron uptake in *Mycobacterium leprae*, the causative agent of leprosy.^{100,101} Chelation of Fe³⁺ occurs at the hydroxamic acid groups (red) and either the *threo*- β -hydroxy-L-histidine or hydroxyl/amine positions (blue) depending on pH.¹⁰²

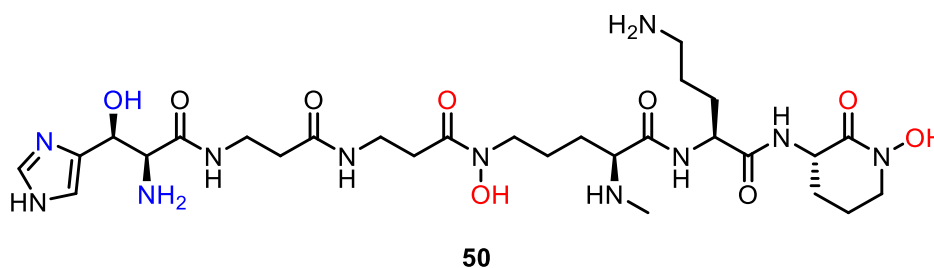


Figure 44. Chemical structure of Exochelin MN (**50**)

The reported total synthesis of exochelin MN (**50**) was completed in 2002 by Dong and Miller in an excellent overall yield of 4.7% and there are several structural similarities between exochelin MN and madurastatin C1.¹⁰³ These include the cyclised hydroxamic acid derived from ornithine (blue) and the *N*- α -methyl functionalised ornithine with a hydroxamic acid functionality at the δ position (red) (Figure 45). Due to these similarities, the total synthesis of exochelin MN (**50**) will provide a valuable resource in the total synthesis of madurastatin C1.

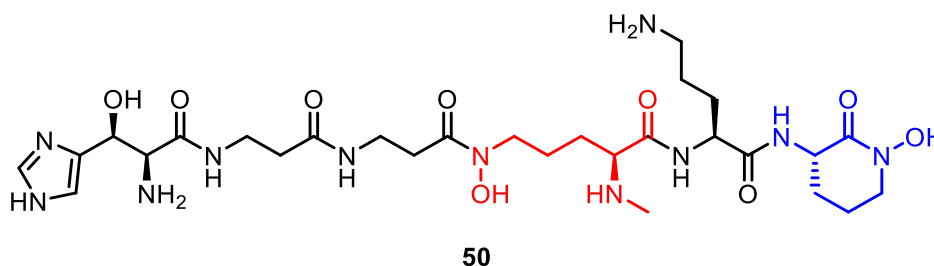


Figure 45. The structure of exochelin MN with the structurally similar amino acid components found in madurastatin C1 highlighted (cyclised ornithine blue, *N*- α -methyl ornithine red).

In the total synthesis of exochelin MN a key intermediate was used to access both the methylated and cyclised ornithine components. This intermediate, nitrone **51** is an oxidised amino acid synthesised from *N*- α -Cbz-L-ornithine, and was developed from the indirect oxidation chemistry used in the synthesis of D-ferrichrome by Naegeli and Keller-Schierlein.¹⁰⁴

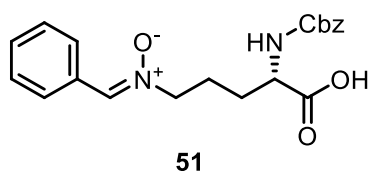


Figure 46. The key intermediate "nitron" **51** used in the synthesis of exochelin MN.

The synthesis of this key intermediate was completed *via* conversion of the primary amine in *N*- α -Cbz-L-ornithine to an imine, followed by oxidation of said imine to the corresponding oxaziridine using *m*-CPBA and finally acid catalysed hydrolysis to the nitrone **51**.¹⁰⁵ Using this route, Miller and co-workers synthesized nitrone **51** in 80% yield from L-*N*- α -methyl-ornithine on a 30 g scale. In addition to the large scale, this key intermediate was isolated over three steps without the use of column chromatography. This significantly sped up the synthetic process, allowing for large scale preparation and kept losses due to purification steps to a

minimum. This therefore seemed like an ideal candidate for use in the synthesis of madurastatin C1 (**25**).

3.3 Project aims

The aim of this part of the project was to carry out retrosynthetic analysis of madurastatin C1 (**25**) to give synthetic targets that could be obtained by simple chemical reactions, that could also be scaled up to enable access to madurastatin C1 (**25**) in gram scale quantities if needed. Once this is achieved we would synthesise our required modified amino acids. These modifications include the synthesis of hydroxamic acids, a mono-*N*-methylation and cyclisation reactions. Upon generation of our modified amino acids, we could then carry out the total synthesis of madurastatin C1 (**25**).

3.4 Retrosynthetic Analysis

Initial retrosynthetic analysis of madurastatin C1 shows that the disconnections should be relatively routine, owing to its poly-peptide nature. Disconnection at the amide and hydroxamic acid bonds leads us to basic amino acids and the key nitron intermediate (**51**) already discussed. In order to maximise yields we elected to use a convergent synthetic route (Figure 47).

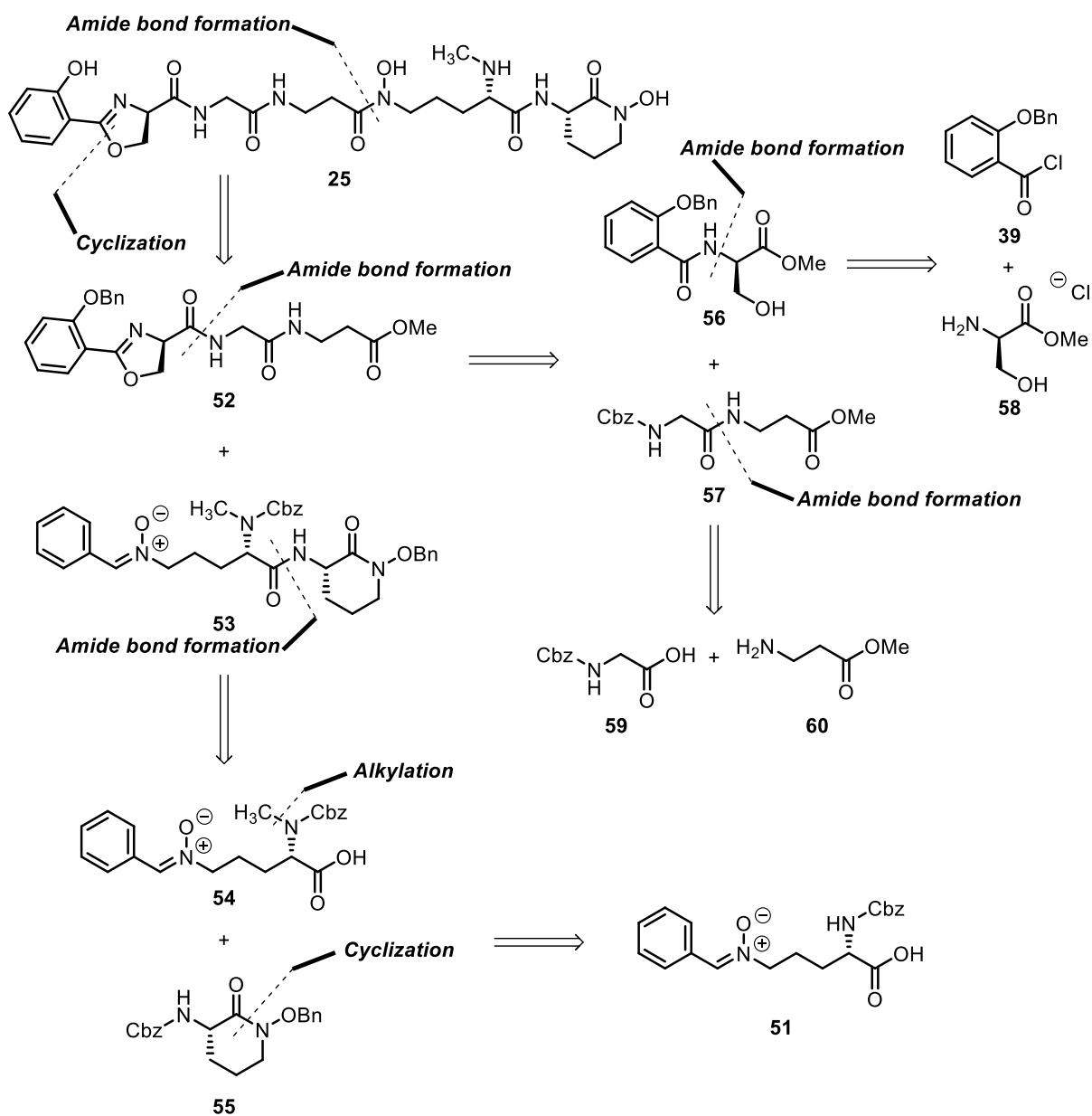


Figure 47. Retrosynthetic analysis of madurastatin C1 (25).

3.5 Results and discussion

3.5.1 Introduction

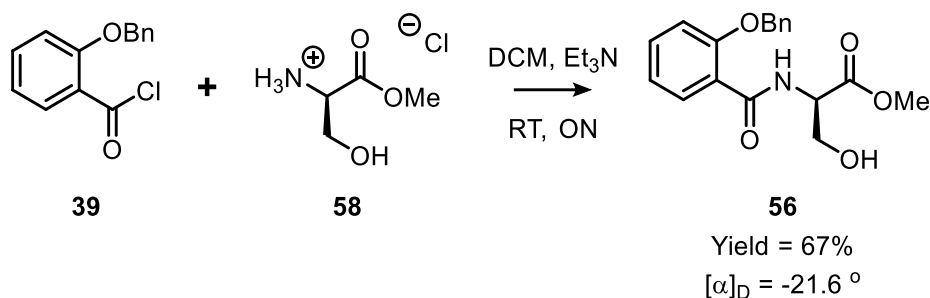
Due to the assembly line nature of polypeptide synthesis, the total synthesis of madurastatin C1 will revolve around the synthesis of modified amino acids and the coupling of these amino acids through amide bonds, as is shown in our retrosynthesis. We have already discussed the synthesis of a similar natural product, exochelin MN (**50**), utilising a similar process of amino acid synthesis followed by amide coupling. To this end, we will begin by synthesising the required modified amino acids derived from a salicylic acid capped serine (**56**), a glycine and β -alanine dipeptide (**57**) and the methylated (**54**) and cyclised (**55**) ornithines, produced from the key nitron intermediate **51** (Figure 47). The generation of intermediates **56** and **57** required amide bond coupling reactions to be carried out and as such the serine, glycine and β -alanine amino acids had their carboxylic acid functionality protected through a methyl ester group. Methyl esters are common protecting groups in amide/peptide chemistry, as they are stable to mild acids, bases and the reaction conditions required for amide bond coupling. These protecting groups prevent unwanted amide coupling reactions occurring at the carboxylic acid, preventing polymerisation. In addition, methyl esters are relatively easy to remove, utilising either strong acid or strong base catalysed cleavage of the methyl ester. Saponification, reaction with a base such as sodium hydroxide, is among the most common methods for cleavage of methyl esters. However, reaction with a strong base for extended periods of time can result in partial or total racemisation of a chiral amino acid, owing to the acidic nature of the α -proton. This will not be a problem in the synthesis of dipeptide **57** as it utilises two non-chiral amino acids. Whereas the synthesis of **56** and **52** include the chiral amino acid serine, and as such will need to be monitored to ensure racemisation has not occurred. With these points in mind, we began with the synthesis of the left hand side of madurastatin C1 (**52**).

3.6 Synthesis of the left-hand half of madurastatin C1 (**52**)

3.6.1 Synthesis of salicylic acid capped serine (**56**)

The synthesis of **56** required that a carboxyl-protected D-Serine be coupled to a suitably protected derivative of salicylic acid *via* an amide bond. Due to our previous experience in the synthesis of amide **41** (all be it with the opposite stereochemistry, see Chapter 2), we elected

to use the same methods in the synthesis of **56**, specifically the utilisation of an acid chloride and base to generate salicylic acid capped serine **56**.



Scheme 6. Synthetic route to generate salicylic acid capped serine methyl ester **56**

To this end acid chloride **39** was generated *via* refluxing 2-benzyloxybenzoic acid (**38**) in toluene in the presence of a slight excess of thionyl chloride for 3 h. This was then stirred with D-serine methyl ester hydrochloride (**58**) in the presence of Et₃N, yielding the desired amide after column chromatography with an average yield of 74%. This yield is slightly lower than we anticipated and we attributed this to hydrolysis of acid chloride **39** back to the corresponding carboxylic acid (**38**) prior to reaction with D-serine methyl ester hydrochloride (**58**). Retention of the chirality at the α -proton was confirmed *via* optical rotation measurements (-21.6°) and single crystal X-ray crystallography of the purified material. Confirmation of the stereochemistry of a molecule using X-ray crystal analysis is completed *via* calculation of the Flack parameter. The Flack parameter is used to estimate the absolute configuration of a molecule from the data obtained *via* X-ray crystal analysis. "A crystal of enantiomerically pure compound in the correct absolute configuration has a value of the Flack parameter of zero."¹⁰⁶ A calculated Flack parameter of 0 means that the absolute stereochemistry of the drawn structure is almost certainly correct, whilst a Flack parameter of 1 means that the assigned absolute stereochemistry is almost certainly inverted. As the flack parameter value of (**56**) was 0.08(\pm 5), and therefore very close to 0, we were confident that the stereochemistry of **56** was in the *R* (*D*) configuration.

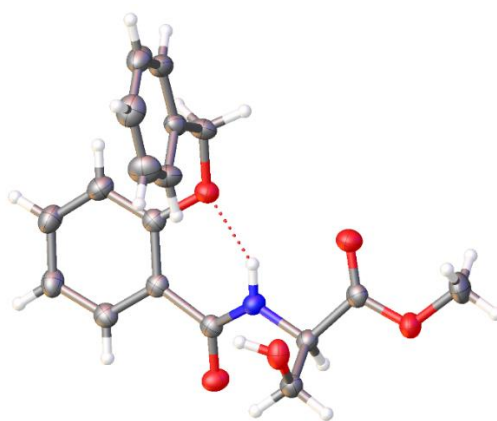
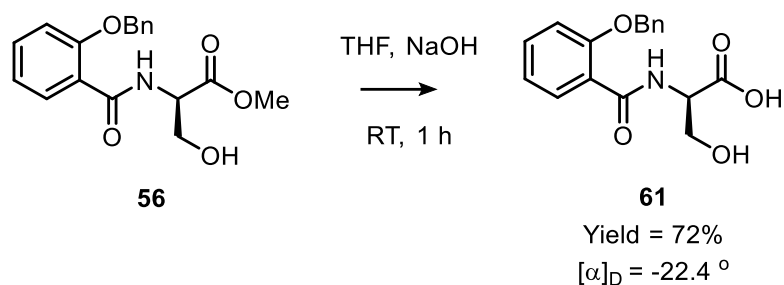


Figure 48. X-ray crystal structure of **56**.

3.6.2 Deprotection of **56**

Our next step was the conversion of methyl ester **56** to its corresponding carboxylic acid.

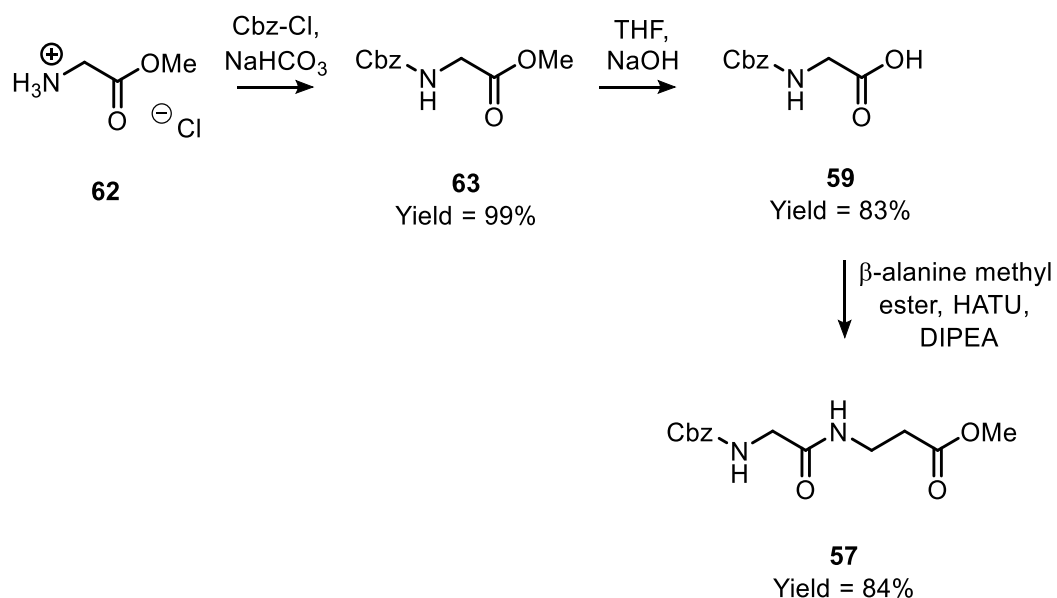


Scheme 7. Synthetic route to generate salicylic acid capped serine **61**.

We elected to saponify methyl ester **56** *via* base mediated hydrolysis, generating the carboxylate, followed by acidification during work up to yield the carboxylic acid. Due to the presence of a chiral centre in D-serine we wished to limit the degree of racemisation by using the lowest possible reaction time. As such the reaction mix was monitored *via* TLC every 10 minutes over the course of an hour. After one hour the TLC showed a complete loss of starting material with a new spot stuck to the baseline, corresponding to the generation of the carboxylate. Carboxylic acid **61** was then isolated in a quantitative conversion from **56** after acid/base extraction. Carboxylic acid **61** showed the clear loss of the methyl ester peak found at 3.69 ppm in the ^1H NMR spectrum of methyl ester **56** and gave an optical rotation measurement of -22.4° . This is very close to that of the starting methyl ester (-21.6°) and we were therefore satisfied that we had not racemised the chiral centre via the base mediated hydrolysis of **56**.

3.6.3 Synthesis of glycine- β -alanine di-peptide **57**

With carboxylic acid **61** synthesised, we now proceeded with the synthesis of dipeptide **57** consisting of glycine and β -alanine.



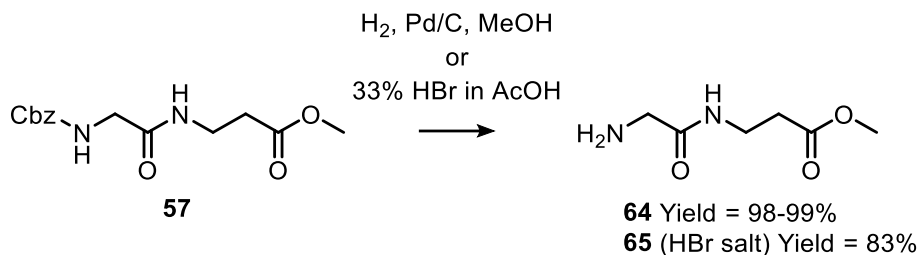
Scheme 8. Synthetic route to generate di-peptide **57**

The synthesis began with the protection of the primary amine of glycine methyl ester hydrochloride with a Cbz group by mixing **62** with benzyl chloroformate in water in the presence of sodium hydrogen carbonate. The appearance of a new UV visualised spot on TLC indicated formation of our product, which was then isolated in a 99% yield *via* column chromatography. Carboxylic acid **59** was then generated in the same manner as for **61**, *via* hydrolysis of methyl ester **63** with aqueous sodium hydroxide and monitoring *via* TLC over 1 hour. Carboxylic acid **59** was then subjected to peptide coupling conditions in the presence of β -alanine methyl ester hydrochloride (**60**). Initially EDC hydrochloride was used as our amide coupling reagent with Et₃N as base, giving average yields of 63%. Changing from EDC to HATU allowed access to methyl ester **57** in 84% after isolation *via* silica gel column chromatography.

3.6.4 Deprotection of **57**

With the synthesis of di-peptide **57** completed, we next had to remove the Cbz protecting group. Removing the Cbz group would allow us to couple carboxylic acid **61** to the newly

generated amine (**64/65**). Removal of a Cbz group is commonly achieved *via* acidic deprotection with HBr in acetic acid or through hydrogenation.¹⁰⁷

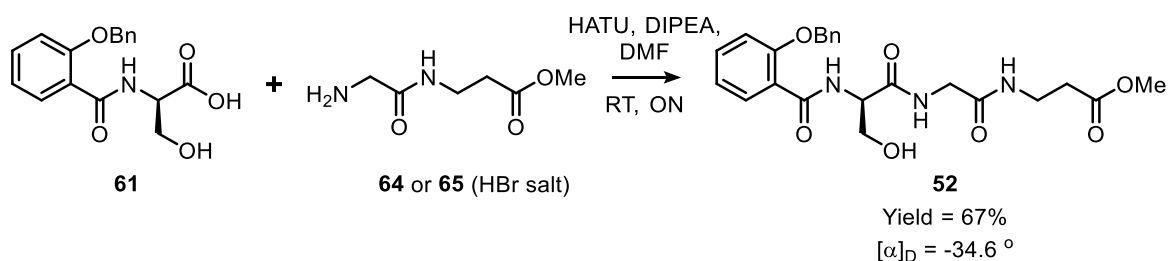


*Scheme 9. Synthetic route to generate salicylic acid capped serine **64** and **65***

Both of these methods were experimented with, and reaction with HBr in acetic acid was easier to carry out, owing to the use of liquid reagents instead of gaseous hydrogen. The reaction of **57** with 33% HBr in acetic acid with DCM as solvent afforded the corresponding HBr salt as a red solid (**65**). This solid was hygroscopic however, which lead to difficulties in handling and characterisation. We therefore also attempted the deprotection of **57** *via* hydrogenation which consistently gave near quantitative yields. Hydrogenation was carried out using hydrogen gas (1 atm) in methanol with palladium on carbon as catalyst for 6 hours and gave a quantitative conversion to the free amine (**64**). Both **64** and **65** were used in future reactions in the synthesis of madurastatin C1.

3.6.5 Synthesis of the left-hand half of madurastatin C1 (**52**)

With the synthesis of both carboxylic acid **61** and amines **64/65** completed, we could now carry out the peptide coupling reaction to generate tripeptide **52** and finish the synthesis of the left-hand half of madurastatin C1.



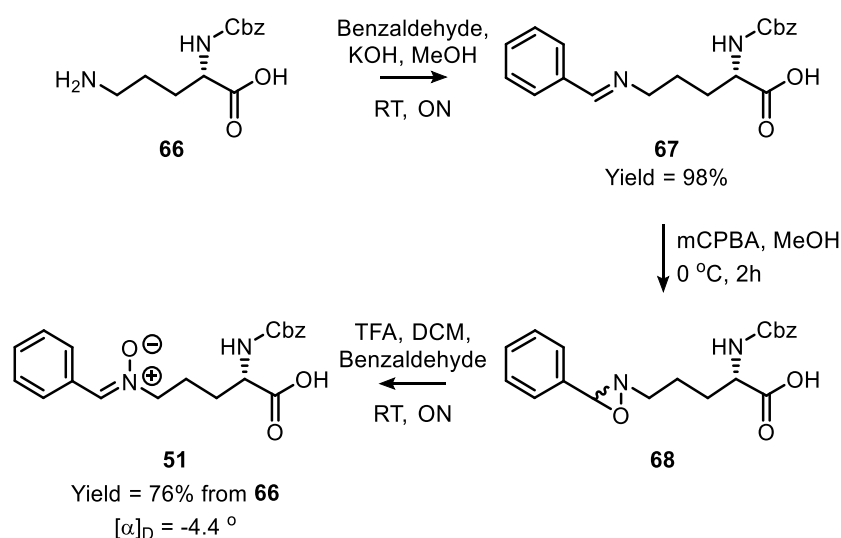
*Scheme 10. Synthetic route to (**52**).*

For the synthesis of tri-peptide **52**, HATU was used as the peptide coupling reagent, with DMF as solvent and DIPEA as base. DMF was chosen due to the hydrobromide salt **65** being insoluble in DCM. These reaction conditions generated the corresponding amide in 67% yield after isolation *via* silica gel column chromatography. The optical rotation of **52** was -34.6° , showing that we had retained *R* (*D*) stereochemistry at the serine. With the left hand half of madurastatin C1 completed we next moved on to the synthesis of key nitron **51**.

3.7 Synthesis of the right-hand half of madurastatin C1 (**53**)

3.7.1 Synthesis of key nitron intermediate **51**

In order to generate our oxidised ornithine amino acids, we looked to the oxidation chemistry that we discussed in the introduction of this chapter in section 3.2.1. This chemistry involves converting *N*- α -Cbz-L-ornithine into imine (**67**), followed by oxidation to the corresponding oxaziridine using *m*CPBA **68**. This oxidation to an oxaziridine inserts the desired nitrogen-oxygen bond, with acid catalysed rearrangement of the oxaziridine affording the desired nitron **51** (Scheme 11).



Scheme 11. Synthetic route to generate the key intermediate nitron **51**.

3.7.2 Synthesis of imine **67**

We therefore began the synthesis with *N*- α -Cbz-L-ornithine **66** as it contained a suitable protecting group for the α amine whilst also being commercially available. This was reacted with benzaldehyde in the presence of potassium hydroxide. During the reaction, water is generated as a by-product and we therefore included 3 Å molecular sieves in the reaction mix.

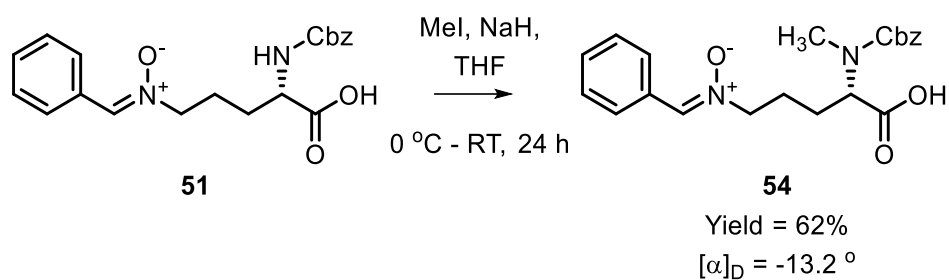
These remove the generated water and help to push the reaction equilibrium toward the generation of products, rather than returning from the hemiaminal intermediate to benzaldehyde and *N*- α -Cbz-L-ornithine starting materials (**66**). After the reaction had completed, the pulverised molecular sieves were removed *via* filtration. We discovered that filtration through celite, a commonly used technique for the capture of molecular sieves, leads to decomposition of imine **67**. Filtration of the molecular sieves through a sinter funnel and evaporation of the methanol yielded imine **67** as a hygroscopic white foam with quantitative conversion from ornithine starting material **66**.

3.7.3 Synthesis of nitronone **51**

With imine **67** generated we moved on to the oxidation step followed by the immediate conversion to the nitronone (**51**), owing to the unstable nature of the oxaziridine intermediate. Oxidation of the imine was accomplished *via* reaction of **67** with *m*CPBA in methanol. After removal of the solvent and extraction to remove the benzoic acid by-product the crude material was then stirred in the presence of TFA in DCM. Initial attempts at this reaction gave very low yields of the desired nitronone. After repeating the experiment several times, we realised that commercially available *m*CPBA contains both *m*-chlorobenzoic acid and water as stabilisers to reduce the danger of this potentially explosive material. We therefore purified the *m*CPBA *via* extraction with diethyl ether and washing with buffered basic solution to remove the *m*-chlorobenzoic acid and water impurities and generate higher purity *m*CPBA. Repeating the oxidation step with this batch of *m*CPBA and reaction of the crude mixture with TFA gave the corresponding nitronone (**51**) in significantly higher yields (76%), which was isolated *via* trituration from EtOAc and hexane as a white precipitate. Retention of the chirality at the α -proton was again confirmed *via* optical rotation measurements (-4.4 °). Whilst the optical rotation value appears to be close to zero, suggesting racemisation of the sample, a Flack parameter of -0.05(\pm 10) was obtained from single crystal X-ray crystallography of the purified material, suggesting that the crystal had *S* (*L*) chirality.

With significant quantities of our key intermediate nitronone (**51**) available, we next looked to synthesise the required methylated ornithine **54** and cyclised ornithine **55**

3.7.4 Synthesis of methylated ornithine **54**



Scheme 12. Synthetic route to generate methylated ornithine 54.

For the synthesis of methylated ornithine **54**, we reacted nitron **51** with methyl iodide in the presence of sodium hydride as base. Once again, owing to the product being a zwitterion, **54** was isolated *via* trituration in 62% yield. Despite the use of a strong base in the form of sodium hydride, optical rotation measurements showed that the sample still retained mostly D chirality (-13.2°). The original ^1H NMR of this material revealed a new peak at 2.83 ppm corresponding to the new methyl group. However, this and many other ^1H and ^{13}C NMR signals were duplicated due to the methyl group causing hindered rotation of the nitrogen-carbon bonds at the α position. This was overcome by heating the NMR sample to 70°C , causing the peaks to coalesce and giving a clear spectrum (Figure 49).

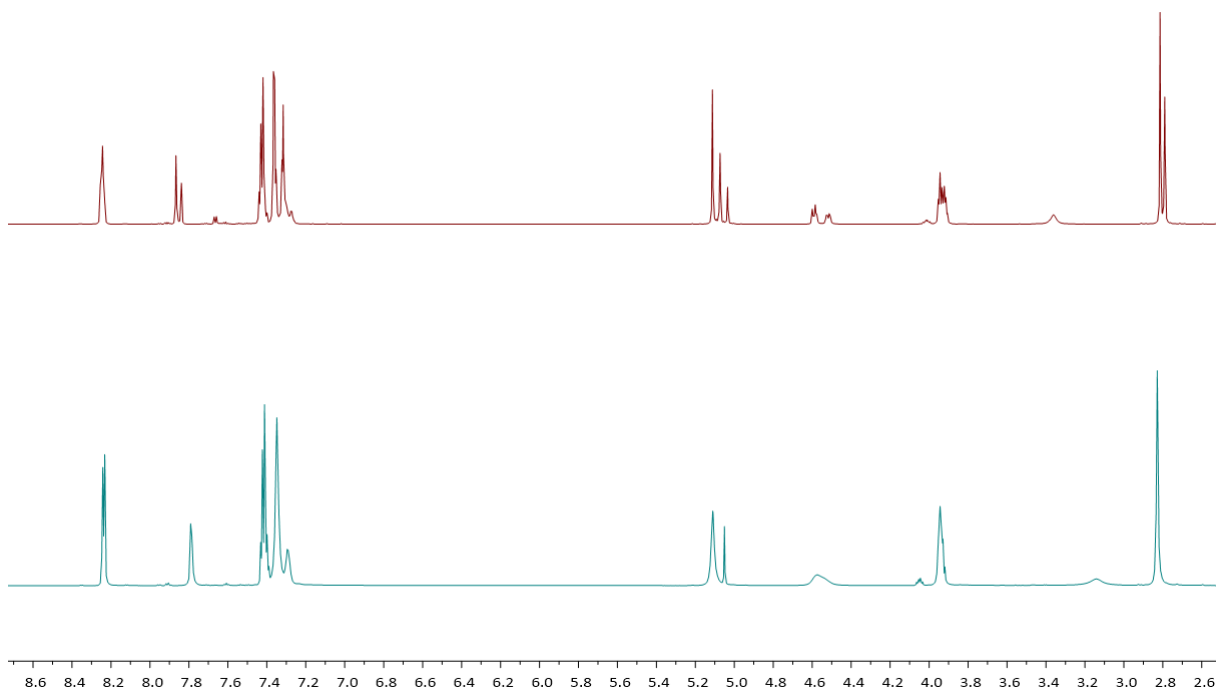
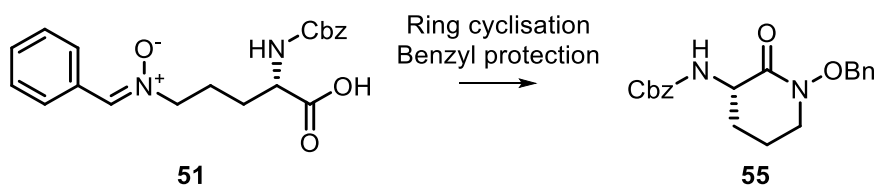


*Figure 49. ^1H NMR of **54** at 298 K top, and 343 K bottom (D_6 -DMSO, 700 MHz) showing the coalescence of the duplicated ^1H NMR signals at higher temperature.*

3.7.5 Synthesis of cyclised ornithine **55**

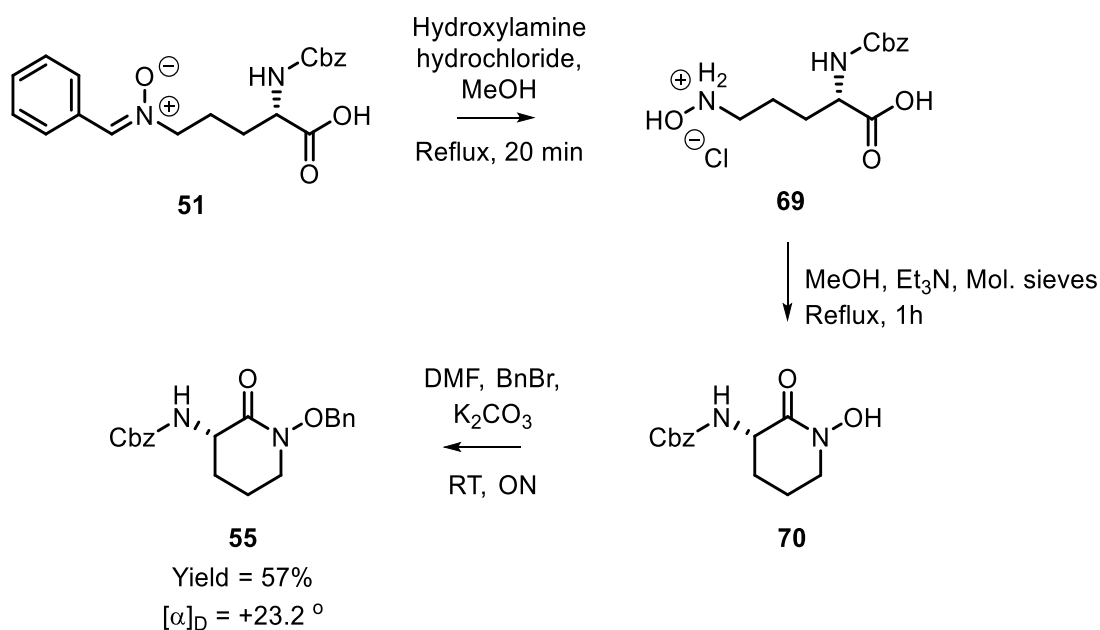
For the synthesis of cyclised ornithine **55**, a one pot deprotection, cyclisation and benzylation was carried out (Scheme 13).



Scheme 13. Proposed generalised synthetic route to cyclised ornithine **55**.

Benzyl protection of the hydroxylamine oxygen is required as the hydroxylamine generated by cyclisation of **51** is very polar and also capable of chelating metal ions, significantly hindering its purification. Protecting the hydroxyl component of the hydroxamic acid with a benzyl group will prevent metal chelation whilst also decreasing polarity therefore allowing for isolation *via* silica gel column chromatography.

To begin, nitrone (**51**) was dissolved in methanol and refluxed in the presence of hydroxylamine hydrochloride, generating hydroxylamine **69**. This was then followed by addition of Et₃N and 3 Å molecular sieves with the mixture continuing under reflux. After an hour the cyclised hydroxamic acid (**70**) was isolated *via* extraction and washing of the reaction mix, after which the crude material was stirred in the presence of benzyl bromide in DMF using K₂CO₃ as catalyst, yielding fully protected cyclised ornithine (**55**) in 57% yield from **51** (Scheme 14).

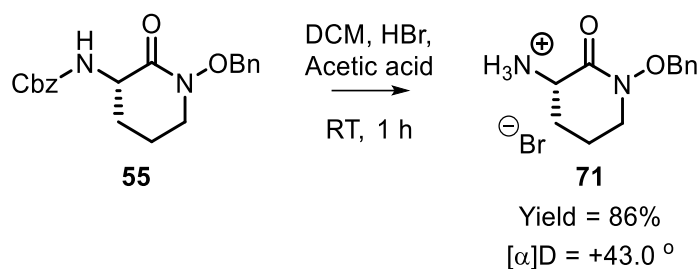


Scheme 14. Synthetic route to cyclised ornithine **55** via a one pot deprotection, cyclisation and benzylation reaction.

Upon measuring the optical rotation of cyclised ornithine **55** (+23.2 °), we noted that our experimental value was opposite to that found in the literature.¹⁰³ Indeed further inspection of the literature for the synthesis of **55** gave both positive and negative optical rotation values for each of the *R* and *S* enantiomers.^{103,108,109} As we could not therefore confidently assign the stereochemistry of cyclised ornithine **55** using optical rotation, we elected to try and confirm the stereochemistry *via* X-ray crystallography. To this end, after the optical rotation of **54** was recorded the sample was allowed to slowly evaporate, yielding crystals suitable for single crystal X-ray analysis. Unfortunately, the Flack parameter for this crystal was not close to zero and had a large margin of error (Flack parameter = 0.35(±12)). As a result we could not confidently show that the chiral centre in **55** was in the expected *S* configuration.

3.7.6 Deprotection of cyclised ornithine **55**

With the fully protected cyclised ornithine now completed, we had to remove the Cbz protecting group and generate the corresponding amine (Scheme 15).



Scheme 15. Synthetic route to deprotected cyclised ornithine 71.

As discussed for the deprotonation of **57**, it is well documented that the removal of a Cbz group can be completed *via* hydrogenation or with a solution of HBr in acetic acid.¹⁰⁷ As *O*-Benzyl groups can be removed *via* hydrogenation but are resistant to strongly acidic conditions, the use of HBr in acetic acid was employed to selectively remove the Cbz group whilst leaving the benzyl group intact. To this end we reacted cyclised ornithine **55** with 33% HBr in acetic acid for 2 hours, yielding **71**, which was isolated *via* trituration from ether and chloroform in 86% yield.¹⁰³ The optical rotation of **71** was +43 ° and the structure was also resolved *via* X-ray crystallography (Figure 50). This time, the Flack parameter was much more acceptable at -0.030(±9), supporting the assignment of the stereocentre in an *S* configuration as we had anticipated.

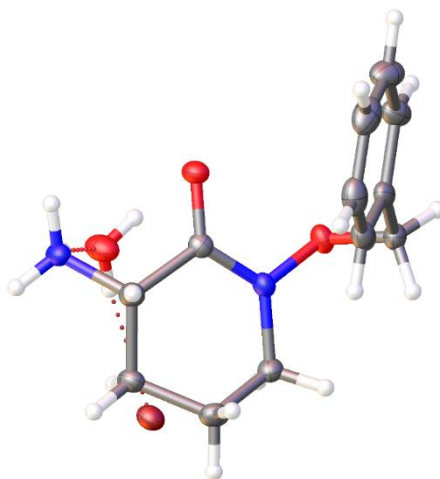
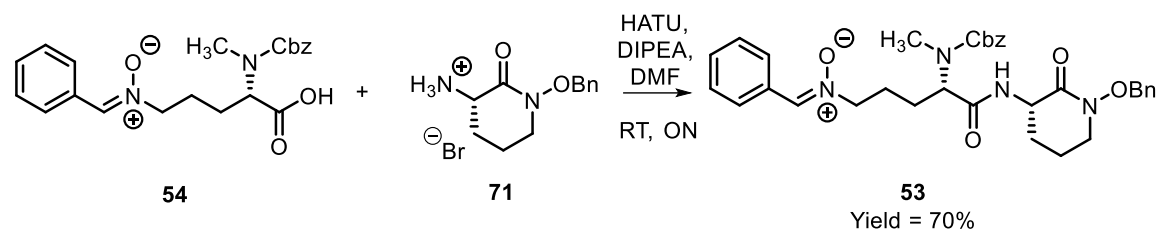


Figure 50. X-ray crystal structure of 71.

With the required free amine now available, we could proceed to the amide coupling of **54** and **71** to generate the right hand half of madurastatin C1.

Synthesis of dipeptide 53.

With our two modified ornithine amino acids **54** and **71** now completed, we could now carry out the peptide coupling required to synthesise dipeptide **53**.



Scheme 16. Synthetic route to dipeptide **53**.

To begin, methylated ornithine **54** was stirred in the presence of the peptide coupling agent HATU in DMF. This was followed by the addition of cyclised ornithine **71** and DIPEA, generating the desired di-peptide. The structure was confirmed by HRMS and NMR studies, but in a similar fashion to the characterisation of methylated ornithine **54**, numerous peaks were duplicated presumably due to hindered rotation. ^1H and ^{13}C NMR studies at a variety of temperatures showed some signal coalescence (as shown in Figure 51), leading to easier to interpret spectra. However, even at high temperatures the ^{13}C NMR data still showed duplicated peaks whilst other appeared to broaden and disappear into the baseline.

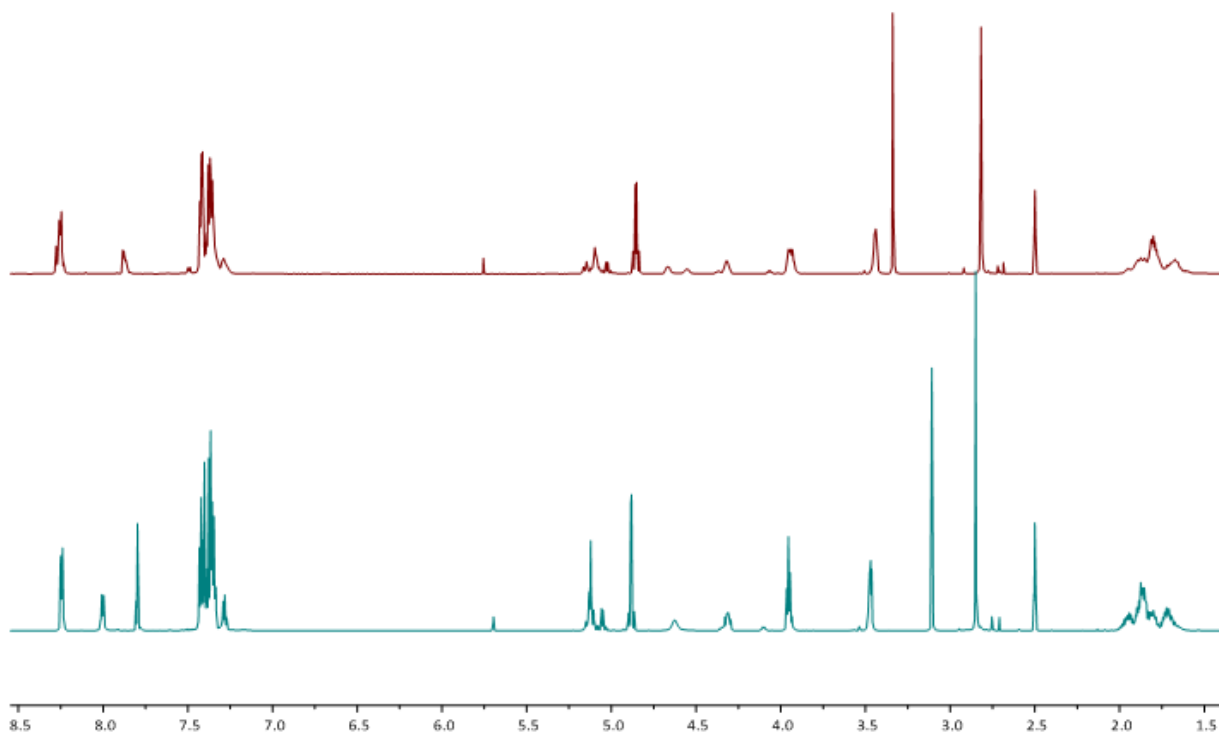
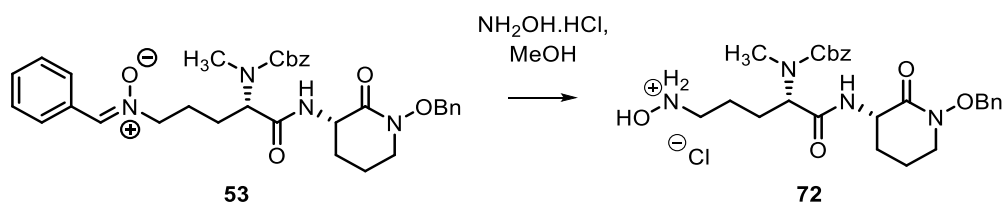


Figure 51. ^1H NMR of **53** at 298 K top, and 348 K bottom (D_6 -DMSO, 700 MHz) showing the coalescence of the duplicated ^1H NMR signals at higher temperature.

3.7.8 Deprotection to generate hydroxylamine (72)

With the fully protected dipeptide (**53**) in hand, we now had to remove the aromatic-imine group to give a hydroxylamine. This could then be used to couple the two halves of madurastatin C1 together *via* a hydroxamic acid group.

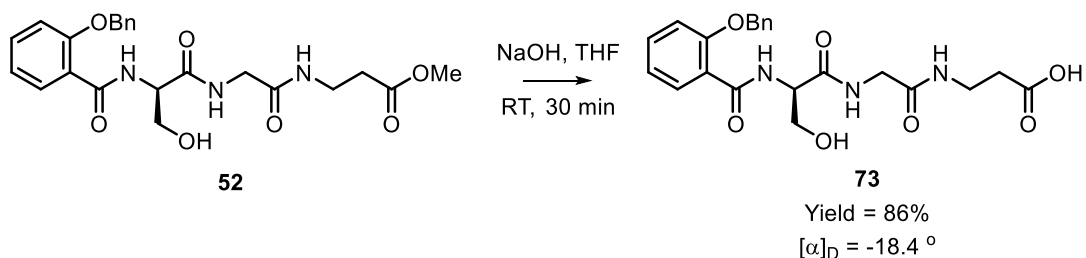


Scheme 17. Synthetic route to dipeptide **72**.

In a similar fashion to the synthesis of ornithine hydroxylamine **69**, generation of hydroxylamine **72** was completed *via* stirring dipeptide **53** in the presence of hydroxylamine hydrochloride. This afforded the corresponding hydroxylamine **72** as the hydrochloride salt that could be easily isolated *via* trituration and filtration. Due to the instability of this intermediate, no further purification was carried out and instead the material was carried through and used immediately in the next coupling reaction.

3.7.9 Deprotection of 52

Prior to the coupling of both half's of madurastatin C1, tripeptide **52** had to be converted from the methyl ester to the corresponding carboxylic acid **73**.



Scheme 18. Synthetic route to generate carboxylic acid **73**.

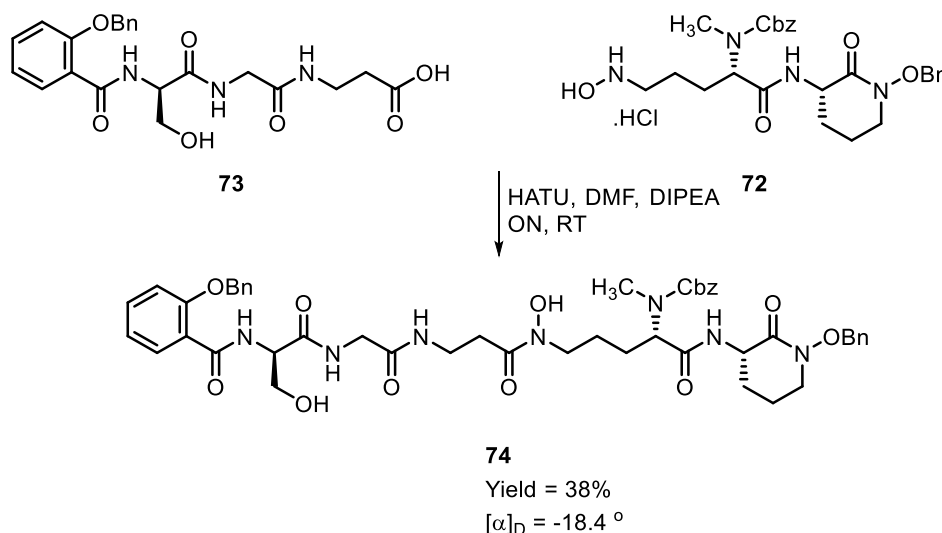
To synthesise carboxylic acid **73**, methyl ester **52** was dissolved in THF and hydrolysis of the methyl ester was carried out using aqueous sodium hydroxide. TLC monitoring every 10 minutes showed that the hydrolysis was complete after 30 minutes. Acid/base extraction

afforded the carboxylic acid as a clear oil, with ^1H NMR analysis showing that the methyl group had been removed through loss of the singlet at 3.65 ppm from the starting material (**52**). Retention of the predominantly D enantiomer was again shown *via* optical rotation, with an $[\alpha]_{\text{D}}$ value of -18.4° .

3.8 Final reactions to generate madurastatin C1

3.8.1 Synthesis of pentapeptide **74**

With the synthesis of both of our target carboxylic acid **73** and hydroxylamine **72**, we were now ready to move on to the amide coupling to generate pentapeptide **74** through a central hydroxamic acid.



Scheme 19. Synthetic route to pentapeptide **74** via HATU mediated peptide coupling of **73** and **72**.

We therefore began with dissolving carboxylic acid **73** in DMF and stirring in the presence of the peptide coupling reagent HATU. This was then followed by the addition of hydroxylamine **72** with DIPEA used as base. Unfortunately, TLC showed that several by-products were made over the course of the reaction with a similar R_f to that of our desired product **74**, leading us to believe that we had synthesised diastereomers. This mixture of diastereomers proved difficult to separate *via* silica gel column chromatography, due to their highly polar nature and the similar R_f to that of our product. After two rounds of silica gel column chromatography we managed to partially isolate pentapeptide **74** in a 35% yield. This yield was disappointing considering that our previous HATU mediated amide coupling reactions had typically proceeded on average in 80% yields. The low yield could be attributed to the multiple

diastereomer by-products formed as well as the multiple rounds of silica gel column chromatography used to isolate **74**. In addition to the suspected diastereomers produced, an additional by-product yielded crystals that were suitable for X-Ray single crystal analysis. Resolution of the crystal structure showed that we had generated the intramolecular cyclised ester **75** over the course of the reaction. The molecular ion of **75** was also observed *via* HRMS but due to the similar *R_f* of **75** to the other by-products generated in the reaction we were not able to isolate **75** for full characterisation by NMR.

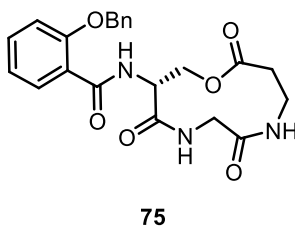
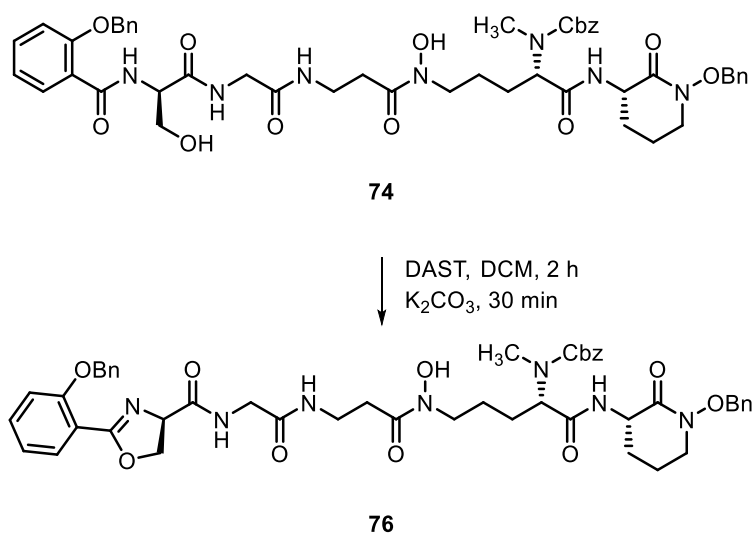


Figure 52. Chemical structure of cyclised tripeptide **75** formed via intramolecular cyclisation of HATU activated carboxylic acid **73**.

We propose that the cyclisation occurred *via* nucleophilic attack by the serine hydroxyl group at the HATU activated carboxylic acid, generating the corresponding eleven membered ring. Whilst it is unfortunate to lose material at this late stage of the synthesis, this could be prevented in future *via* protecting the serine alcohol with a selective and easily removable oxygen protecting group, such as a TBDMS. With the synthesis and isolation of pentapeptide **74** complete, we could now complete the oxazoline ring cyclisation to generate fully protected madurastatin C1.

3.8.2 Synthesis of oxazoline pentapeptide (**76**)

Drawing on our experience of the synthesis of oxazoline model **32**, we felt confident that we could complete the ring closure of **74** with DAST. Using DAST gave the highest yields of oxazoline during the synthesis of model oxazoline **32** without the formation of by-products such as alkyl chloride **44**, generated when thionyl chloride was used.

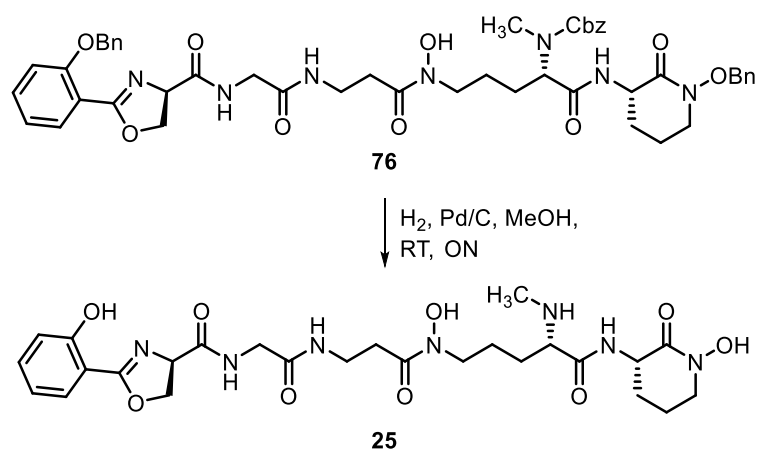


Scheme 20. Synthetic route to oxazoline pentapeptide **76** via DAST mediated oxazoline formation from **74**.

Due to the low yield of pentapeptide **74** from the previous reaction, we had no choice but to carry out the oxazoline ring cyclisation reaction on a small scale. Unfortunately, half of starting pentapeptide **74** was lost due to experimental error. Despite this, oxazoline pentapeptide **76** was successfully synthesised *via* reaction of **74** with DAST and the molecular ion of **76** was observed *via* HRMS (m/z value of 906.4036 for the proposed $[M+H]^+$ ion). Due to the low quantity of material and its high polarity we elected not to purify *via* column chromatography, instead immediately moving on to the final reaction, the global deprotection of oxazoline pentapeptide **76**.

3.8.3 Global deprotection to generate synthetic madurastatin C1 (**25**).

With our oxazoline ring now in place, we looked to carry out a global deprotection using gaseous hydrogen with Pd/C as catalyst. We anticipated this would remove both the *N*-Cbz and the two *O*-benzyl protecting groups in a single step.



Scheme 21. Global deprotection of **76** via hydrogenation over Pd/C to generate synthetic madurastatin C1 **25**

The deprotection reaction was carried out in methanol under 1 atmosphere of hydrogen gas and 20 mg of palladium on carbon. With the desire to remove all three protecting groups at once we left the sample overnight, with the catalyst removed *via* filtration through celite. The initial crude NMR showed complete removal of the protecting groups, with only four aromatic ¹H signals present. These aromatic signals had an identical splitting pattern to that of the natural product madurastatin C1.

With our global deprotection completed we sought to purify synthetic madurastatin C1 (**25**), however the sample appeared to change colour inside the NMR tube, from clear to yellow. A second NMR experiment was carried out, showing that the sample had begun to degrade, with the ratios of ¹H NMR signals changing between both NMR experiments. This degradation was attributed to the presence of celite in the sample which, despite our best efforts, had passed through to our sample during the filtration process used to remove the palladium catalyst.

With no additional pentapeptide starting material to hand, we were unable to complete a second synthesis of madurastatin C1 within the project timeline.

3.9 Conclusions and future work

In this chapter we aimed to develop a synthetic route to generate madurastatin C1 that was high yielding and scalable. We then aimed to synthesise the required modified amino acids and ultimately complete the total synthesis of madurastatin C1. Retrosynthetic analysis provided a viable convergent synthetic route to madurastatin C1 based around amide coupling chemistry and utilisation of amino acid oxidation chemistry. The synthesis of the

required modified amino acids was successful and coupling reactions were completed in high yields *via* utilisation of HATU as our amide coupling reagent of choice. Whilst we tentatively believe that we had completed the total synthesis of madurastatin C1 on a test scale, we were unsuccessful in the isolation or characterisation of any pure material due to the degradation of synthetic madurastatin C1. In future we would look to improve our reaction yields to allow access to larger volumes of synthetic material. In particular we would look to utilise a protecting group, such as TBDMS, for the serine hydroxyl. This would prevent the intramolecular cyclisation reaction we observed in the synthesis of pentapeptide **72**. Finally, after the global deprotection reaction to yield madurastatin C1 we would look to utilise either size exclusion chromatography or HPLC to isolate pure material and to remove any celite or palladium catalyst that may have contaminated the sample.

For the final part of this project, we look to a new bioactive bacterial natural product DEM30616/A.

Chapter 4. Bioactivity, Structural Determination and Total Synthesis of DEM30616/A

4.1 Introduction

Lipoteichoic acid (LTA) is an important component of the cell wall of Gram positive bacteria and plays an essential role in bacterial growth and therefore virulence. One of the key enzymes responsible for the synthesis of lipoteichoic acid is known as LTA synthase (LtaS).¹¹⁰ LtaS is located on the cell membrane of Gram-positive bacteria and can be divided into two parts, the trans membrane domain and the extracellular domain (eLtaS). The eLtaS domain is responsible for the enzymatic activity of LtaS, and the X-ray crystal structure of eLtaS was resolved in 2008 (Figure 53).¹¹¹ Due to the role of LtaS in bacterial growth, compounds that could inhibit eLtaS are interesting as potential novel antibiotics, as blocking the activity of eLtaS would prevent the production of the essential lipoteichoic acid, limiting bacterial growth and could therefore lead to new treatments of bacterial infections.

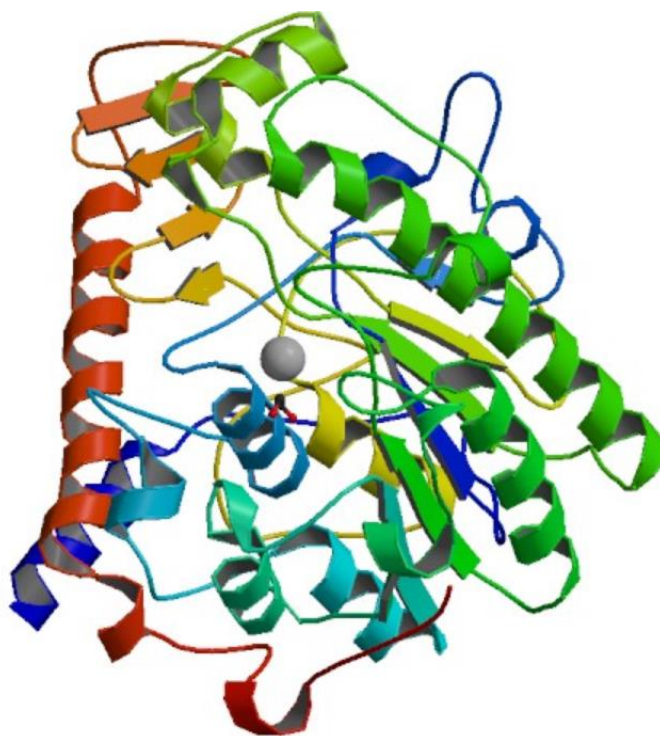


Figure 53. X-ray crystal structure of the eLtaS enzyme in a ribbon representation taken from Freemont et al. Ref:

111

4.2 Current inhibitors of eLtaS

Current inhibitors of eLtaS include the poly aromatic compound 1771 (**77**) and the azo dye Congo red (**78**).^{112,113} When incubated with *S. aureus*, compound 1771 (**77**) showed the ability to reduce the abundance of LTA and also inhibited growth, however the binding site of **77** was not identified.¹¹² A dual-drug approach of using LtaS inhibitor 1771 (**77**) in combination with known antibiotics has been shown to abrogate the growth of multi-drug resistant *Enterococcus faecium*.¹¹⁴ The azo dye Congo red (**78**) has been shown to exhibit a dose-dependent decrease in LTA production with inhibition of LtaS demonstrated both *in vitro* and *in cellulo*, however the exact mode of action is unclear.¹¹³

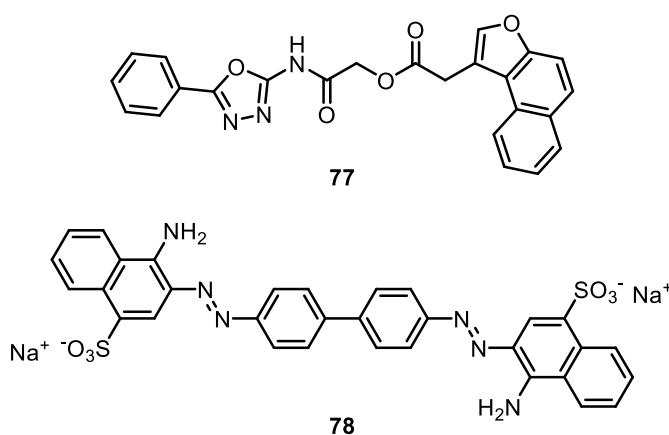


Figure 54. Chemical structures of eLtaS inhibitors 1771 (**77**) and Congo red (**78**).

Despite these two examples and the potential for computer aided drug design due to the availability of the X-ray crystal structure of eLtaS, no commercial drug is currently available based on a small molecule inhibitor of LtaS.

4.3 Screening for LtaS inhibitors

Our collaborators (Dr. Bernhard Kepplinger, Prof. Jeff Errington) at the Centre for Bacterial Cell Biology have developed a novel screening approach for the detection of potential LtaS inhibitors. It was observed that a *Bacillus subtilis* mutant with a deleted *mbl* gene (Δmbl) yielded cells that failed to grow in their correct shape and had poor viability (C-Figure 55).^{115,116} Normal growth of these cells could be restored when grown in the presence of a high concentrations of Mg²⁺ (D-Figure 55).

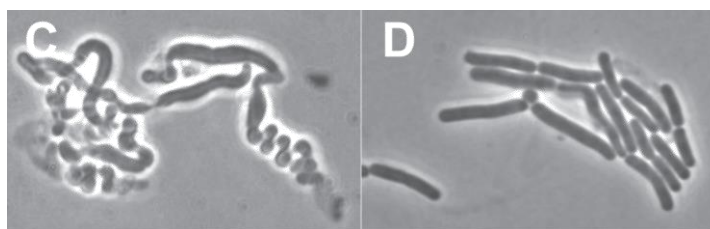


Figure 55. *Bacillus subtilis* ΔmbI mutant showing abnormal growth (C) and the same ΔmbI mutant grown with an additional 20 mM Mg^{2+} (D).

A second mutation of the ΔmbI mutant resulted in the restoration of normal growth of the bacterial cells without the requirement for additional Mg^{2+} . This second mutation being the deletion of the genes encoding for the LtaS enzyme. As the deletion of LtaS genes appeared to restore the normal growth and viability of these cells, it was postulated that the ΔmbI mutant could serve as a useful test to screen for inhibitors of the LtaS enzyme. Any compound that inhibits LtaS in the ΔmbI mutant should mimic the deletion of the LtaS gene, restoring normal growth and viability of these cells without the requirement for additional Mg^{2+} .

To this end the ΔmbI mutant was used in a high throughput screen to identify novel natural product inhibitors of LtaS. Extracts from approximately two thousand bacterial strains were screened by Dr. Kepplinger, to see if they caused recovery of the ΔmbI mutant in the absence of additional Mg^{2+} . This would mean that these extracts may contain a compound or compounds that inhibit LtaS. Three of these two thousand extracts showed reproducible activity, with one (the extract from bacterial strain DEM30616) being selected for further study. After isolation of the bioactive compound (assigned as DEM30616/A), samples were sent to Fundación Medina for preliminary structural assignment. Based on mass spectrometry data in conjunction with the known literature, the structure was putatively assigned as a dipeptide formed from two ornithine amino acids, one of which contained a hydroxamic acid and the other capped with a 2,3-dihydroxybenzoic acid moiety (**79**, Figure 56).

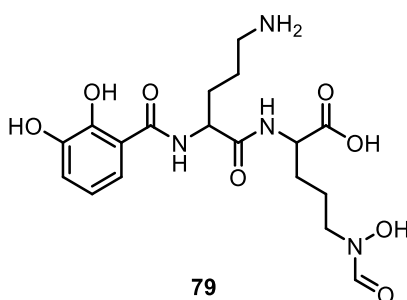


Figure 56. Preliminarily assigned structure of DEM30616/A.

Upon inspection of the preliminarily assigned structure, DEM30616/A appeared to be a structural derivative of chlorocatechelins A (**80**) and B (**81**) and mirubactin (**82**) (Figure 57).^{117–119} Chlorocatechelin A and mirubactin are both hexadentate siderophores and are produced from a *Streptomyces* sp. and *Actinosynnema mirum* respectively.

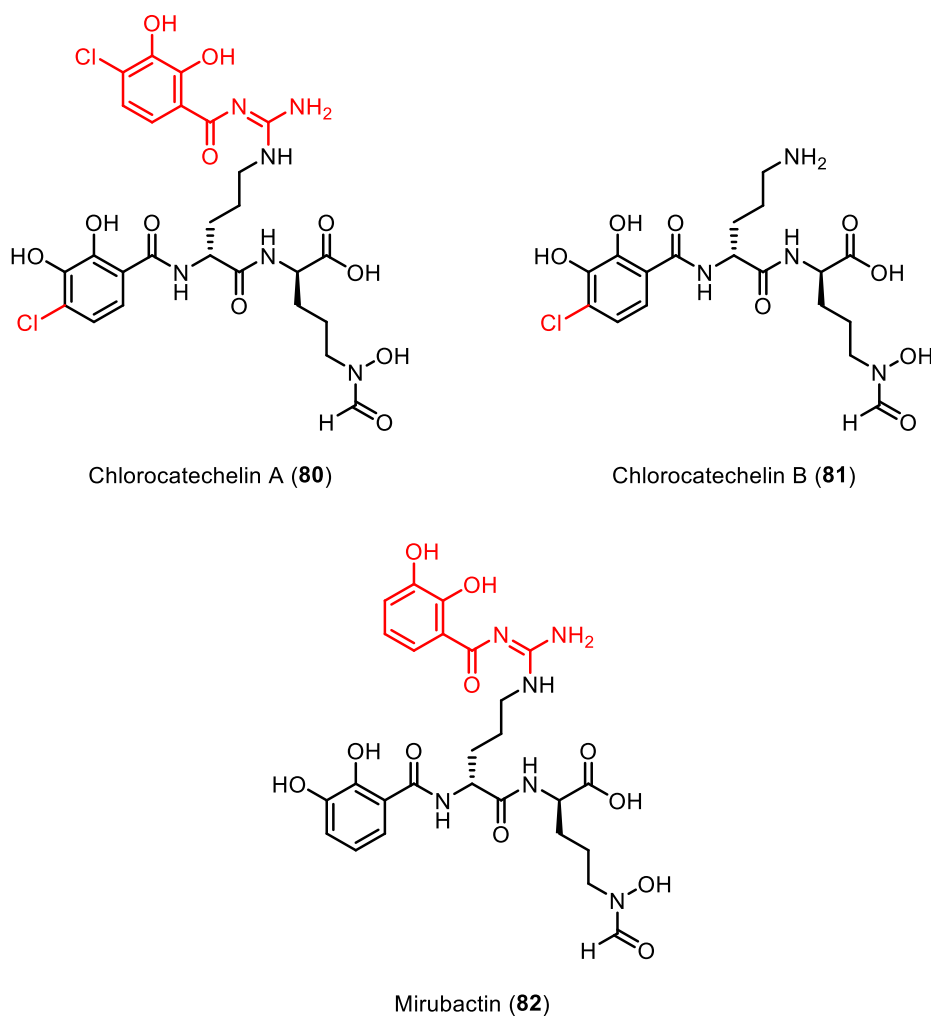


Figure 57. Chemical structures of chlorocatechelins A (**80**) and B (**81**) and mirubactin (**82**). Structural differences vs DEM30616/A are highlighted in red.

4.4 Project aims

Our first priority was to carry out a detailed *de novo* structural elucidation of DEM30616/A, including the determination of the absolute stereochemistry. Our proposed structural assignment would then be compared to the preliminarily assigned structure provided by Fundación Medina. Second, due to the structural similarity to known siderophores, and our previous experiences, we were concerned that the observed activity of DEM30616/A may

have been due to the presence of minor quantities of other bioactive compounds in the tested samples. To address this, we decided to undertake the total synthesis of DEM30616/A. This would allow a comparison of our synthetic material against the natural isolate. If the same activity is observed between the natural product and synthetic DEM30616/A then we will have proven the efficacy of DEM30616/A.

4.5 Structural determination of DEM30616/A.

4.5.1 Mass Spectrometry of DEM30616/A

Our first task in the structural elucidation of DEM30616/A was to validate the MS data provided by Fundación Medina. Therefore, we subjected DEM30616/A to High Resolution Mass Spectrometry studies. HRMS of DEM30616/A gave $m/z = 427.1805$ for the proposed $[M+H]^+$ ion, resulting in a calculated molecular formula of $C_{18}H_{25}O_8N_4$. This result was in keeping with the proposed molecular formula of **79**.

4.5.2 Calculation of double bond equivalents

Based on the proposed molecular formula of DEM30616/A, we established that there were eight double bond equivalents present in DEM30616/A. Again this result was in keeping with the preliminarily assigned structure for DEM30616/A (**79**).

$$DBE = C - \left(\frac{H}{2}\right) + \left(\frac{N}{2}\right) + 1 = 18 - 13 + 4 + 1 = 8.$$

Equation 2. Calculation of the number of double bond equivalents in DEM30616/A ($C_{18}H_{25}O_8N_4$).

4.6 Structural determination of DEM30616/A via 1H , ^{13}C and ^{15}N NMR

4.6.1 Introduction

In this section, we will discuss the structural elucidation of DEM30616/A. To begin, we started our assignment by comparing our NMR data to our HRMS data. Initial examination of the 1H NMR spectrum in D_2O revealed a total of 18 hydrogen atoms *via* integration, suggesting that 7 hydrogen atoms had undergone deuterium exchange (Figure 58). The use of D_2O as NMR solvent also meant that there were no amide proton signals present in the 1H NMR spectrum to help in the assignment of the chemical structure. The ^{13}C NMR spectra showed multiple duplicated carbon signals, making interpretation difficult, however a combination of HMBC and HSQC experiments allowed us to identify the main ^{13}C signals associated with

DEM30616/A, totalling 18 carbon atoms which was consistent with the proposed chemical formula. With this initial examination completed, we next looked to assign the chemical structure of DEM30616/A *via* 2D NMR analysis, as a series of individual fragments.

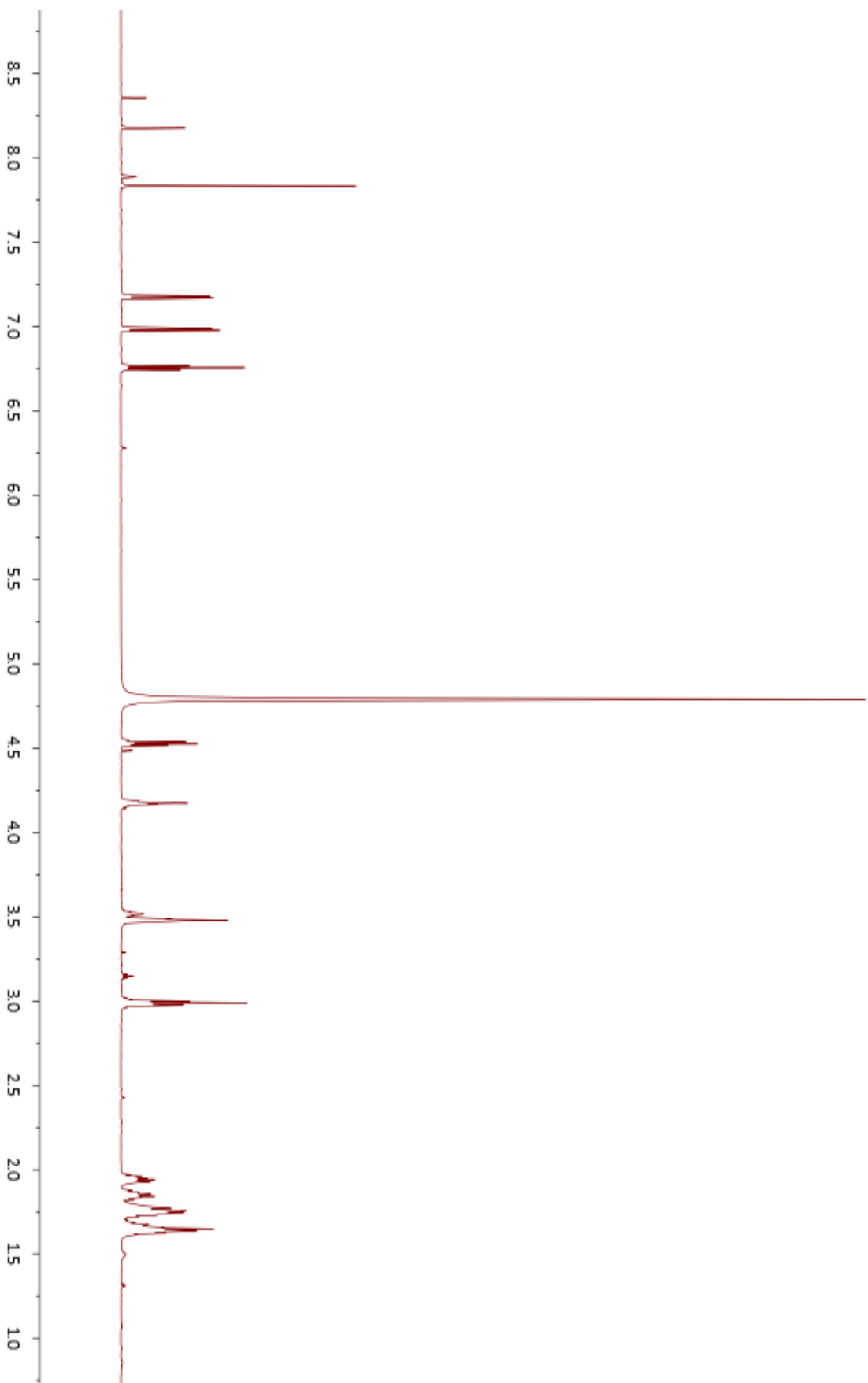


Figure 58. ^1H NMR of DEM30616/A in D_2O 298 K, 700 MHz

4.6.2 Fragment 1

Inspection of the ^1H NMR showed a three proton spin system (assigned *via* COSY) with signals at 7.18, 6.98, and 6.76 ppm. The splitting pattern was indicative of a 1,2,3-trisubstituted aromatic ring, with the three quaternary carbons identifiable by ^{13}C and HMBC experiments (P-1 to P-3). HMBC experiments showed that an additional deshielded carbon atom at 169.8 ppm (P-7) was connected to the aromatic ring at position 1. The chemical shifts of the carbon signals at positions 2 and 3 were in line with what we would expect for an aromatic ring substituted with a hydroxyl group, however we were not able to conclusively assign which ^{13}C signal corresponded to positions 2 and 3. In summary, fragment 1 consists of a 1,2,3-trisubstituted benzene ring, with two hydroxyl groups at positions 2 and 3 and a carbonyl group position 7 (Figure 59).

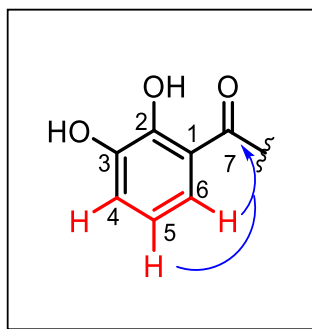


Figure 59. Proposed structural assignment for fragment 1 of DEM30616 (COSY = red, selected HMBC = blue).

Table 11. ^1H and ^{13}C signals associated with fragment 1.

Position	$\delta_{1\text{H}}$ multiplicity, (J in Hz)	$\delta_{13\text{C}}$	HMBC
1	-	116.4	
2	-	146.3 or	
3	-	144.4	
4	6.98 (dd, $J = 7.9, 1.5$ Hz, 1H)	119.5	H to C1, 2, 3, 5, 6
5	6.76 (t, $J = 8.0$ Hz, 1H)	119.6	H to C1, 2, 3, 4, 6, 7
6	7.18 (dd, $J = 8.1, 1.6$ Hz, 1H)	119.2	H to C 1, 2, 3, 4, 5, 7
7	-	169.8	

4.6.3 Fragment 2

An apparent α -proton was observed at 4.53 ppm in the ^1H NMR spectrum (P-9). This showed a HMBC signal to a new deshielded quaternary carbon at 172.6 ppm (P-10) and a correlation to an amide nitrogen through a ^{15}N - ^1H correlation experiment (-260.5 ppm, P-8). A COSY

experiment showed that this α -proton was the first of 5 proton-proton coupled ^1H signals, with the first correlation from position 9 at 4.53 ppm to a diastereotopic methylene group split into two signals between 1.98-1.91 and 1.89-1.82 ppm (P-11). Both of the signals attributed to position 11 showed proton-proton coupling to a second methylene group at 1.76 ppm (P-12). This signal was an overlapping multiplet with an integration of 3. Despite the signal overlap, the presence of the methylene group was established through HSQC and HMBC experiments. This penultimate methylene signal (P-12) was coupled to the final methylene group (P-13) at 2.99 ppm. This final methylene group was shown through a ^{15}N - ^1H experiment to correlate to a primary amine ^{15}N signal at -348.8 ppm (P-14).

In summary for fragment 2, we identified a spin system consisting of an α -proton at 4.53 ppm (P-9) and 3 methylene groups at 1.98-1.91 and 1.89-1.82, 1.80-1.71 and 2.99 ppm (P's 11, to 13). We observed HMBC correlations between the proton at position 9 and two suspected amide carbonyl carbons at 169.8 ppm (P-7) and 172.6 ppm (P-10). In addition, we also observed correlations to two nitrogen atoms corresponding to the amide nitrogen at position 8 and the primary amine nitrogen at position 14.

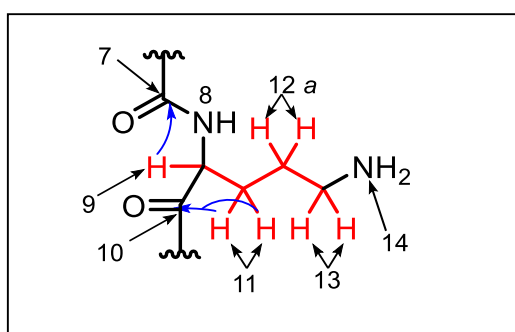


Figure 60. Proposed structural assignment for fragment 2 of DEM30616/A (COSY = red, selected HMBC = blue).

Table 12. ^1H , ^{13}C and ^{15}N signals associated with fragment 2.

Position	$\delta_{1\text{H}}$ multiplicity, (J in Hz)	$\delta_{13\text{C}}$	$\delta_{15\text{N}}$	HMBC
8	-	-	-260.5	-
9	4.53 (dd, $J = 7.8, 6.4$ Hz, 1H)	53.2	-	H to C1, 7, 10, 11, 12
10	-	172.6	-	-
11	1.98 – 1.91 (m, 1H) 1.89 – 1.82 (m, 1H)	27.8	-	H to C9, 10, 12, 13
12	1.80 – 1.71 (m, 3H) ($\alpha = 2\text{H}$)	23.1	-	*
13	2.99 (ddd, $J = 8.6, 6.9, 2.1$ Hz, 2H)	38.8	-	H to C11, 12
14	-	-	-348.8	-

*Unknown due to signal overlap

4.6.4 Fragment 3

For the final fragment, a similar approach was employed as for fragment 2. We noted an apparent α -proton multiplet between 4.21 and 4.13 ppm in the ^1H NMR spectrum (P-16). This showed a HMBC signal to a new deshielded quaternary carbon at 178.1 ppm (P-17) which, due to its chemical shift, we assigned as a carboxylic acid. The α -proton at position 16 also showed a correlation to an amide nitrogen through a ^{15}N - ^1H correlation experiment (-252.9 ppm, P-15). A COSY experiment showed that this α -proton was the first of 5 proton-proton coupled ^1H signals, with the first correlation from the α -proton (P-16) to a diastereotopic methylene group split into two signals between 1.80-1.71 and 1.69-1.60 ppm (P-18). The peak between 1.80-1.71 ppm was part of the overlapping signal used for the assignment of position 12. Similarly, the peak found between 1.69-1.60 ppm was an overlapping multiplet, with an integration of 3. The two extra hydrogen signals attributed to this multiplet formed the penultimate methylene group at position 19. The final methylene group (P-20) was represented by a multiplet between 3.56-3.44 ppm. And showed HMBC coupling to a deshielded carbon atom at 159.5 ppm. This was shown to be a formyl carbonyl *via* a HSQC signal to a highly deshielded singlet in the ^1H NMR. This highly deshielded singlet had been split into two signals, a major peak at 7.83 ppm and a minor one at 8.18 ppm, that when taken together gave an integration of one. Both the methylene group at position 20 and the formyl proton at position 20 showed correlations in the ^{15}N - ^1H spectrum to a deshielded nitrogen atom at -199.3 ppm. We assigned this nitrogen as a hydroxamic acid.

In summary for fragment 3, we identified a spin system consisting of an α -proton between 4.21-4.13 ppm (P-16) and 3 methylene groups at 1.80-1.71 and 1.69-1.60, 1.69-1.60 and finally 3.56-3.44 (P's 18 to 20). We observed HMBC correlations between the proton at position 16 and an amide carbonyl carbon at 172.6 ppm (P-10) and a carboxylic acid carbonyl carbon at 178.1 ppm (P-17). In addition, we also observed correlations from the methylene group at position 20 and the formyl proton at position 22 to a nitrogen atom corresponding to a hydroxamic acid at position 21.

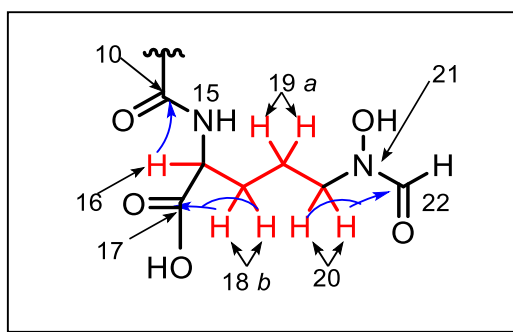


Figure 61. Proposed structural assignment for fragment 3 of DEM30616/A (COSY = red, selected HMBC = blue).

Table 13. ^1H , ^{13}C and ^{15}N signals associated with fragment 2.

Position	$\delta_{1\text{H}}$ multiplicity, (J in Hz)	$\delta_{13\text{C}}$	$\delta_{15\text{N}}$	HMBC
15	-	-	-252.9	-
16	4.21 – 4.13 (m, 1H)	54.6	-	H to C10, 17 18, 19
17	-	178.1	-	-
18	1.80 – 1.71 (m, 3H) ($b = 1\text{H}$) 1.69 – 1.60 (m, 3H) ($b = 1\text{H}$)	28.2	-	*
19	1.69 – 1.60 (m, 3H) ($a = 2\text{H}$)	22.7	-	*
20	3.56 – 3.44 (m, 2H)	50.0	-	H to C16, 18, 19, 22
21	-	-	-199.3	-
22	7.83 and 8.18 (s, 1H)	159.4	-	H to C20

*Unknown due to signal overlap

With the assignment of the final fragment accomplished, we completed the full assignment of the chemical structure of DEM30616/A (**77**). This is a di-peptide which contains a catechol aromatic ring and a hydroxamic acid group. Our assignment is in keeping with that previously provided by Fundación Medina.

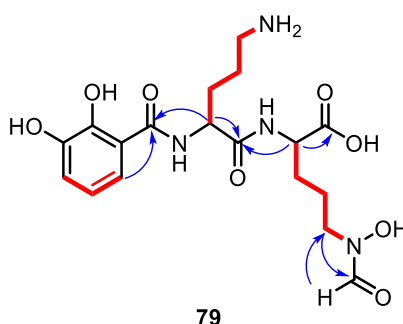


Figure 62 Structural assignment of DEM30616/A (**77**) (COSY = red, selected HMBC = blue).

4.7 Advanced Marfey's Analysis of DEM30616/A

With the chemical structure of **79** now completed, we next wished to assign the absolute stereochemistry of the two ornithine residues found within DEM30616/A. Amino acid standards were prepared *via* functionalisation of L-ornithine with both *N* α -(5-Fluoro-2,4-dinitrophenyl)-L-leucinamide and *N* α -(5-Fluoro-2,4-dinitrophenyl)-D-leucinamide and the retention times recorded (Table 14). With the synthesis and HPLC retention times of the ornithine amino acid standards completed, hydrolysis and functionalisation of DEM30616/A was carried out. DEM30616/A was hydrolysed using hydroiodic acid, followed by functionalisation with *N* α -(5-fluoro-2,4-dinitrophenyl)-L-leucinamide. Comparison of the retention times of the Marfey's functionalised amino acid standards against Marfey's functionalised DEM30616/A revealed the presence of solely D-ornithine, which is consistent with the assigned absolute stereochemistry of the related siderophores chlorocatechelin A (**79**) and B (**80**) and mirubactin (**81**).

Table 14. Retention times of Marfey's functionalised amino acid standards and hydrolysed DEM30616/A.

Amino acid	Marfey's Chirality	Retention Time (mins)	Separation (mins)
L-Ornithine α	L	10.8	0.6
L-Ornithine α	D	10.2	
L-Ornithine δ	L	11.2	0.0
L-Ornithine δ	D	11.2	
L-Ornithine $\alpha+\delta$	L	16.8	0.3
L-Ornithine $\alpha+\delta$	D	16.5	
DEM30616/A Ornithine α	L	10.2	-
DEM30616/A Ornithine δ	L	11.2	-
DEM30616/A Ornithine $\alpha+\delta$	L	16.5	-

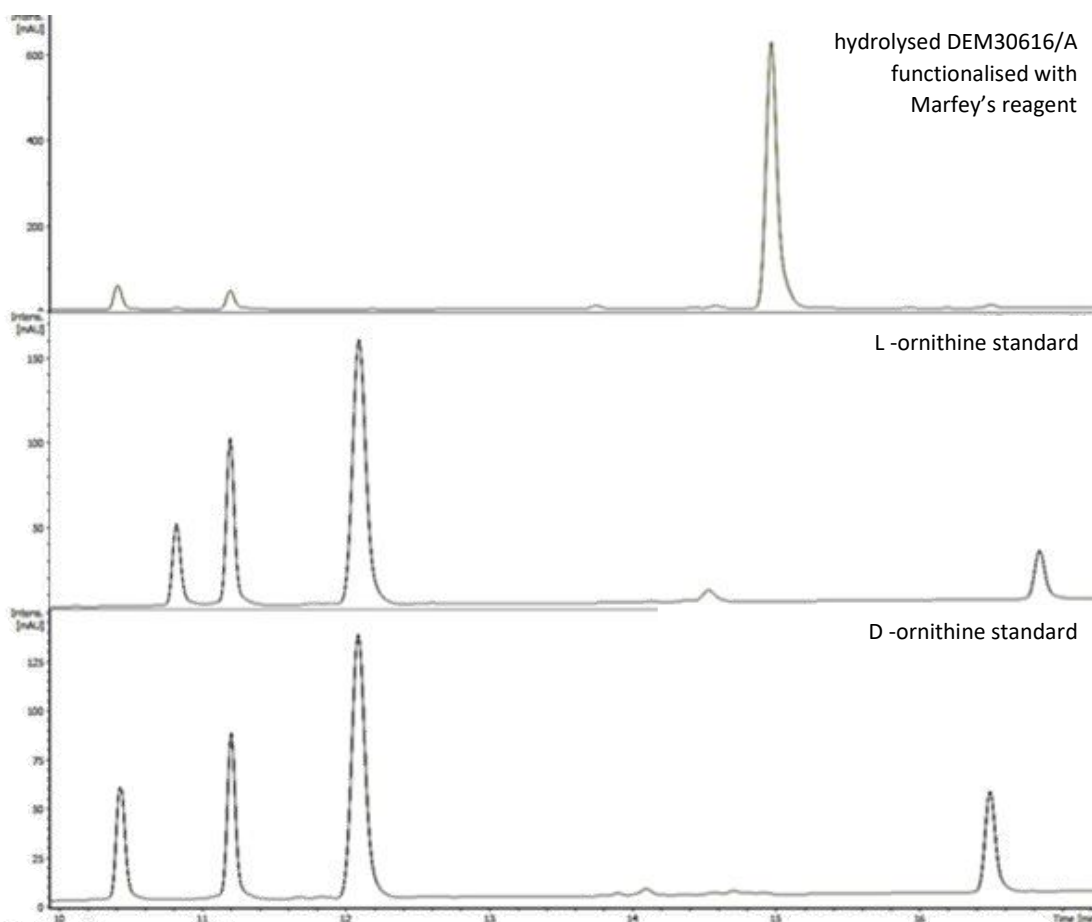


Figure 63. HPLC chromatogram showing the products of $N\alpha$ -(5-fluoro-2,4-dinitrophenyl)-L-leucinamide derivitized DEM30616/A (top), L-derivitized L-ornithine (middle) and D-derivitized L-ornithine (bottom).

4.8 Conclusions on structural assignment of DEM30616/A

We have completed a *de novo* structural assignment of DEM30616/A (**77**) through a combination of high-resolution mass spectrometry, NMR studies and Marfey's analysis. Through this work we have assigned the chemical structure of DEM30616/A, a potential LtaS inhibitor, and its absolute stereochemistry (Figure 64). Now we sought to complete the total synthesis of (**77**) to generate synthetic material for use in bioassays to determine the efficacy of (**77**) as an LtaS inhibitor

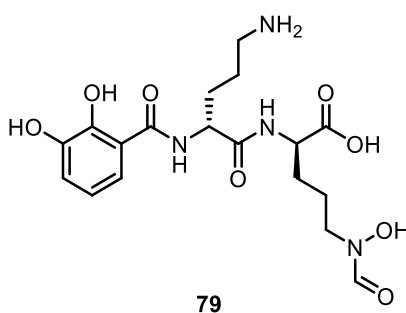


Figure 64. Structure of DEM30616/A including absolute stereochemistry.

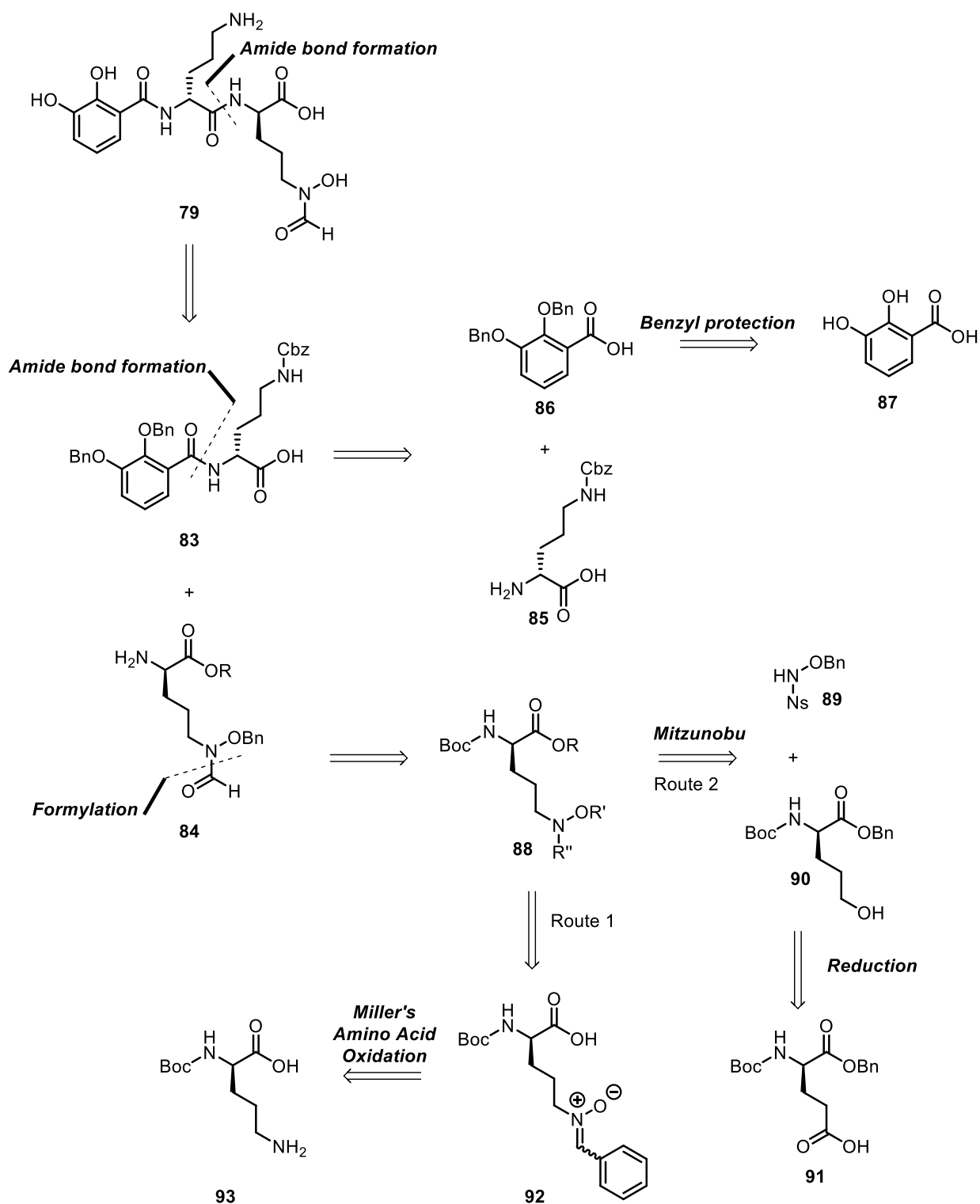
4.9 Total synthesis of DEM30616/A (79)

4.9.1 Introduction

Since DEM30616/A may indeed be a LtaS inhibitor, and having confirmed its chemical structure, we elected to complete the total synthesis of DEM30616/A. This would allow for a repeat of bioassays utilising synthetic material and subsequently prove the efficacy of isolated DEM30616/A. Throughout the remainder of this chapter in a bid to avoid confusion, the isolated, bacterially derived natural product will be referred to exclusively as DEM30616/A and any material produced in the laboratory will be referred to exclusively as syn.30616/A.

4.9.2 Retrosynthesis of DEM30616/A (79)

Similarly to the retrosynthesis of madurastatin C1 (**25**), we envisaged disconnections at the amide bonds of DEM30616/A (**79**) to be most appropriate to generate our synthetic targets. This would generate a 2,3-dihydroxybenzoic acid which is commercially available and can be easily protected. The central ornithine in DEM30616/A is unmodified and so can be inserted easily *via* amide bond coupling, with a suitable protecting group being employed for the free amine at the α position. For the synthesis of the final ornithine-hydroxamate we envisaged two different synthetic routes. The first route was influenced by our previous work outlined for the synthesis of madurasatin C1, through the use of Miller's ornithine oxidation chemistry, we hoped to generate the required hydroxamic acid group. The second synthetic route was inspired by the total synthesis of the aforementioned chlorocatechelins and mirubactin see Scheme 22

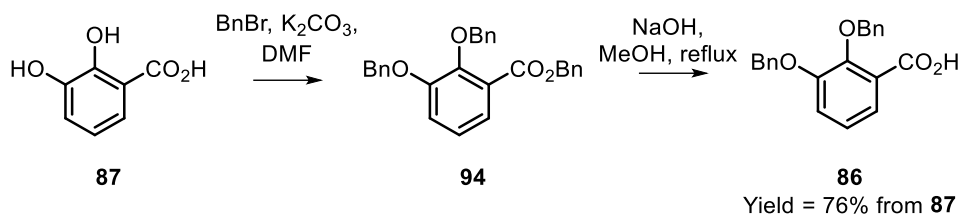


Scheme 22. Retrosynthetic analysis of DEM30616/A with two routes to generate intermediate **83**.

4.9.3 Synthesis of amide **83**

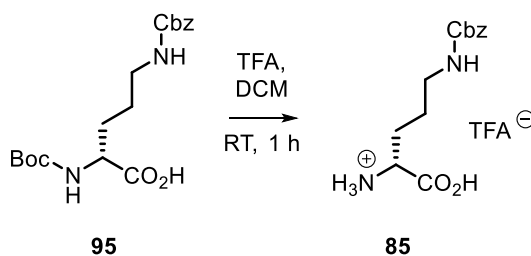
To begin the total synthesis of DEM30616/A, we looked to protect the hydroxyl groups in 2,3-dihydroxybenzoic acid (**87**). To this end, **87** was reacted with benzyl bromide in the presence

of potassium carbonate to generate the corresponding benzyl ester (**94**). Benzyl ester **94** was then refluxed in the presence of aqueous NaOH to generate the desired carboxylic acid (**86**).



*Scheme 23. Synthetic route to aromatic carboxylic acid **86** via benzylic protection and ester hydrolysis.*

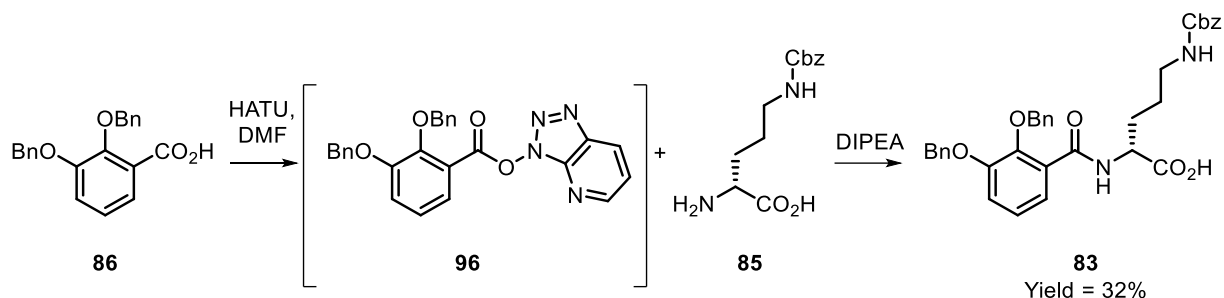
With carboxylic acid **86** now available, we next needed to incorporate a Cbz protected D-ornithine in order to generate amide **83**. We began with the removal of the Boc group in *N*α-Boc-*N*δ-Cbz-L-ornithine **95**, *via* reaction with TFA in DCM, giving near quantitative conversion to the TFA salt (**85**).



*Scheme 24. Synthetic route to deprotected ornithine **85** via TFA mediated Boc removal.*

The final step for the synthesis of amide **83** was therefore to use a HATU mediated peptide coupling of carboxylic acid (**86**) with our newly prepared ornithine **85**. Due to the presence of both a free amine and an unprotected carboxylic acid in ornithine **85**, we planned to pre-treat carboxylic acid **86** with HATU generating intermediate **96**. This, followed by the addition of ornithine **85**, would generate the desired amide (**83**) and prevent self-polymerisation of ornithine **85**. As such, carboxylic acid **86** was reacted with HATU in DMF for 10 minutes followed by the addition of ornithine **85** and DIPEA (Scheme 25). ¹H NMR of the crude reaction mix showed signals corresponding to our desired product, with no signals indicating that polymerisation had occurred. Due to the presence of a highly polar carboxylic acid group, purification of **83** via silica gel column chromatography proved to be non-trivial, with much of the crude product lost during this purification step resulting in a relatively low yield of 32%.

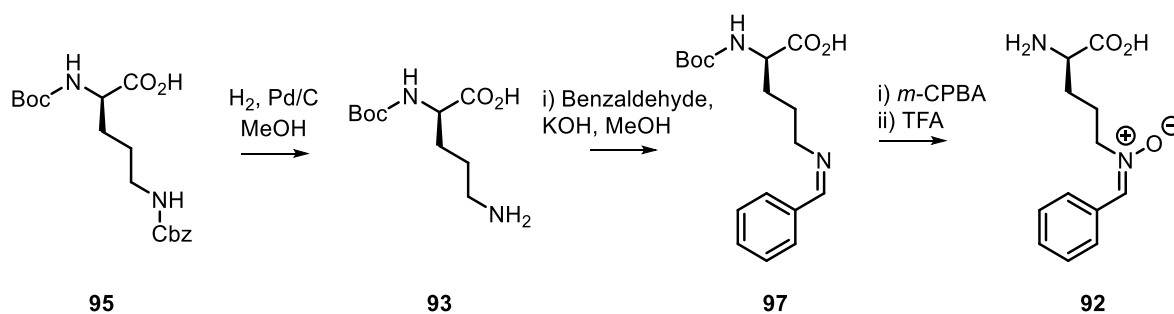
With our desired amide **83** completed, we could then look to synthesising formylated ornithine **84**.



Scheme 25. Synthetic route to dipeptide **78** via HATU mediated coupling of **81** to **80**.

4.9.4 Synthesis of the nitron **92** Route 1.

As discussed in our retrosynthetic analysis, we envisaged two separate routes to generate formylated ornithine **84**. Drawing on our experience in hydroxamic synthesis used in the total synthesis of madurastatin C1, we elected to begin with the method of oxidation and acid catalysed rearrangement (Route 1). Starting from the same protected ornithine (**95**) used for the synthesis of amide **83**, we envisaged that removal of the Cbz protecting group would yield the free amine (**93**) required to generate imine **97**. We could then carry out the subsequent oxidation and acid catalysed rearrangement to give nitron **92**.



Scheme 26. Synthetic route to nitron **92** via removal of the Cbz group, imine formation and oxidation/acid catalysed rearrangement of **95**.

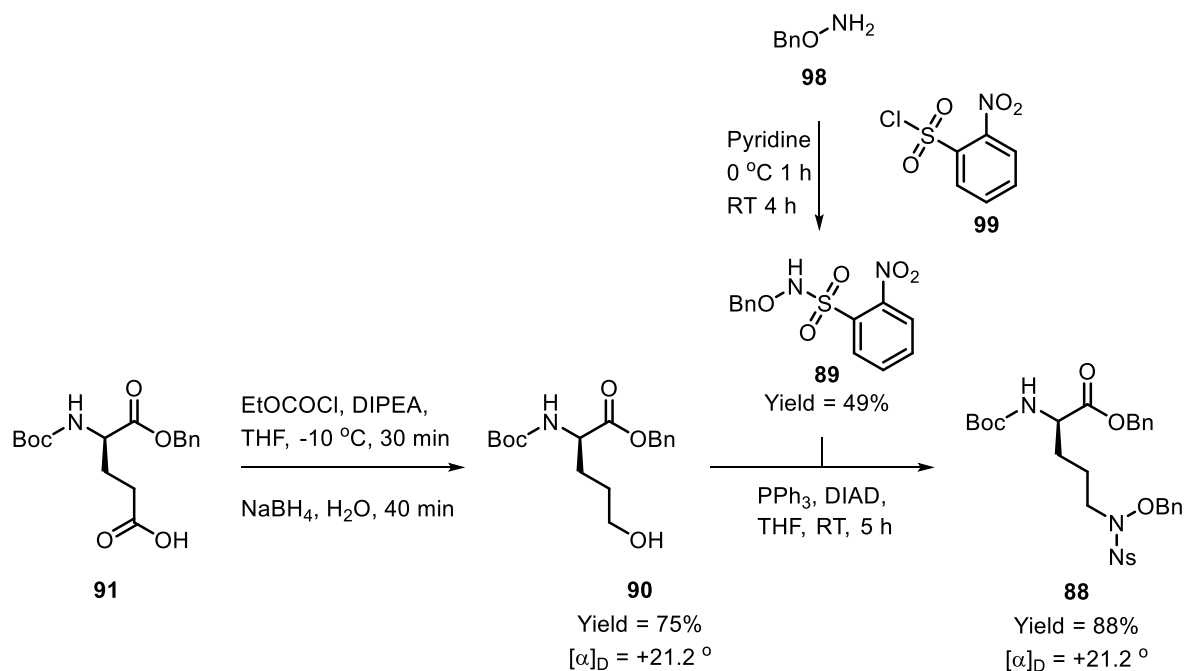
Starting from the protected ornithine **95**, hydrogenation gave the corresponding free amine **93** in a quantitative conversion, highlighted by a complete loss of aromatic signals in the ^1H NMR. From here imine **97** was generated *via* stirring **95** in the presence of benzaldehyde, KOH and 3 Å molecular sieves. The final step was the indirect oxidation of imine **97** using *m*CPBA

to generate the corresponding oxaziridine, immediately followed by acid catalysed rearrangement with TFA to generate nitrene **92**. Unfortunately, nitrene **92** was isolated in low yields and with rapid degradation of the product observed.

In addition to the problems in isolating nitrene **92**, we had foreseen that the acid catalysed rearrangement to make nitrene **92** would also result in the loss of the *N*-Boc group. Whilst this initially seemed advantageous as it would allow incorporation of nitrene **92** into our previously synthesised peptide **83**. We later realised that we would need to re-protect this amine to ensure the selective formylation of the hydroxylamine. The additional synthetic steps required in this already low yielding synthetic route coupled with the expensive nature of the ornithine starting material **95** lead us to conclude that this synthetic route was not viable. We therefore elected to use our second proposed approach (Route 2) taken from the synthesis of the chlocatechelins.¹¹⁸

4.9.5 Synthesis of ornithine **88** via Route 2.

As discussed in our retrosynthetic analysis, the second route to formylated ornithine **84** was based on the total synthesis of the chlocatechelin's.¹¹⁸ This involved the reduction of *D*-glutamic acid **91** to alcohol **90**, followed by a Mitsunobu type reaction between alcohol **90** and sulphonamide **89** to generate ornithine **88** (Scheme 27).

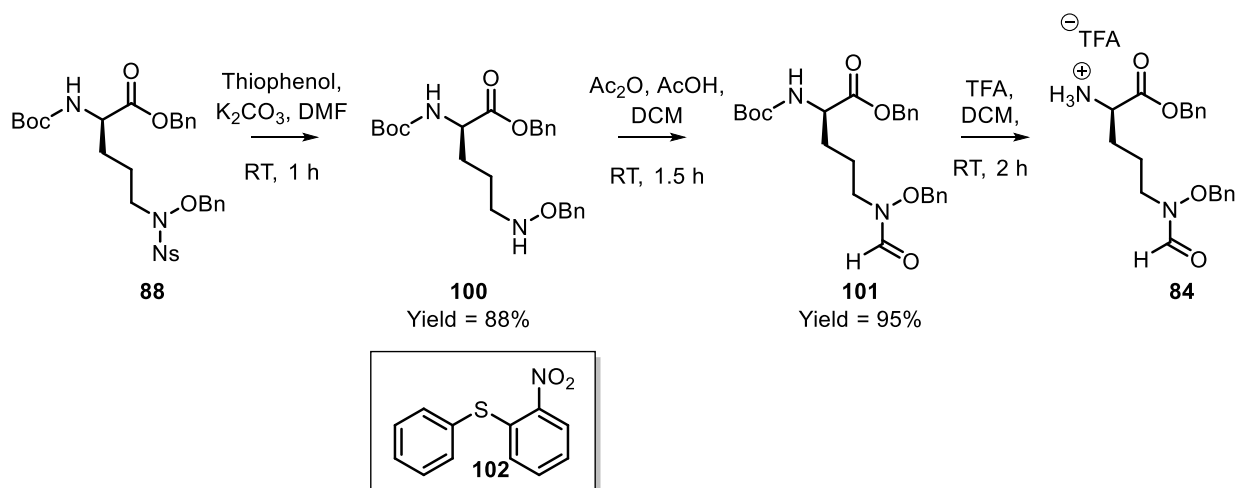


Scheme 27. Synthetic route to fully protected ornithine **88** via reduction of glutamic acid and subsequent Mitsunobu type reaction.

We began with the reduction of protected D-glutamic acid **91** to alcohol **90**. This was completed by activating the carboxylic acid with ethyl chloroformate to generate the corresponding anhydride. This was then reduced *via* reaction with sodium borohydride to generate alcohol **90** with an average yield of 75%. Due to the inexpensive nature of the starting material and the simplicity of the reaction, we were able to generate hundreds of milligrams of alcohol **90**. In parallel to the preparation of alcohol **90**, we completed the synthesis of sulphonamide **89**. This was achieved by stirring 2-nitrobenzenesulfonyl chloride (**99**) with O-benzylhydroxylamine (**98**) using pyridine as both solvent and base. Sulphonamide **89** was purified *via* crystallisation and the structure confirmed *via* NMR and X-ray crystallography. With the preparation of alcohol **90** and sulphonamide **89** completed, a Mitsunobu type coupling was carried out, substituting the alcohol for the nosylated hydroxylamine, generating fully protected ornithine **88** in 88% yield.

4.9.6 Synthesis of formylated ornithine **84**

With the synthesis of fully protected ornithine **88** completed, we could next move on to the removal of the nosyl group followed by formylation and removal of the Boc group to generate formylated ornithine **84**.



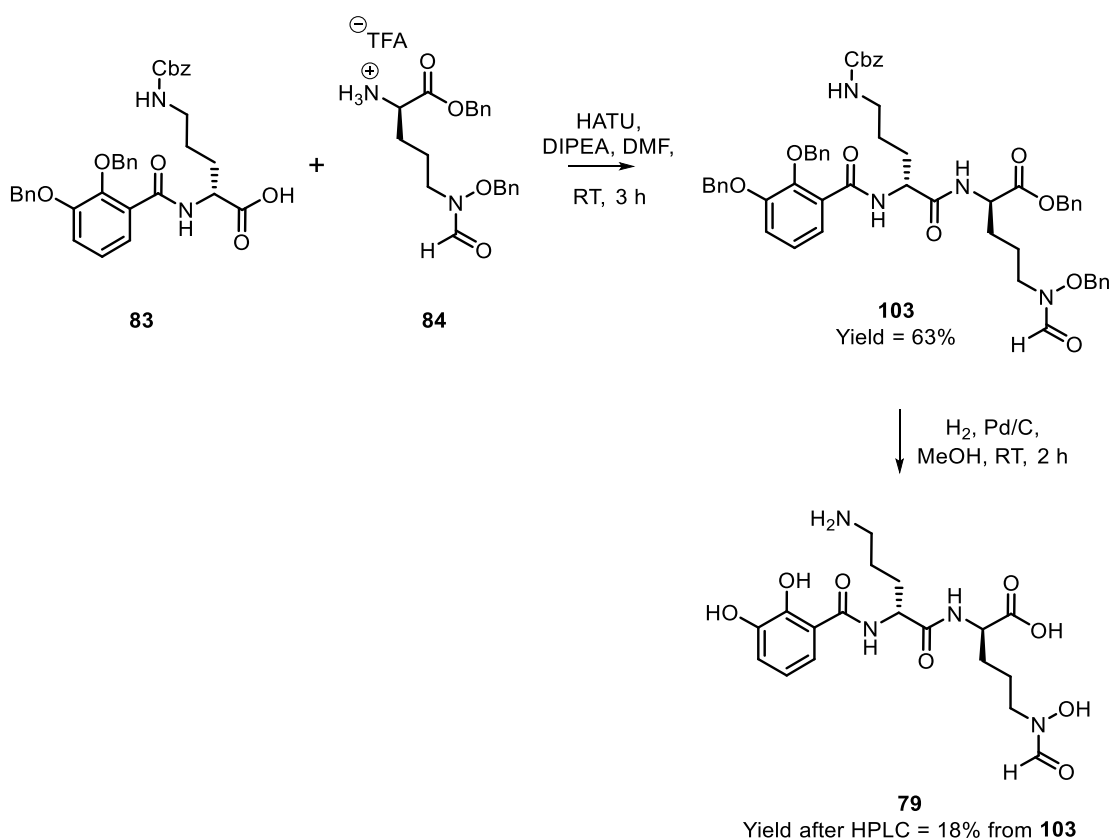
Scheme 28. Synthetic route to formylated ornithine **84** via de-nosylation, formylation and deprotection of **88**.

To this end we reacted the fully protected ornithine **88** with thiophenol in the presence of base, leading to complete loss of starting material *via* TLC. After purification *via* column

chromatography we obtained both our desired ornithine derived hydroxylamine **100** and by-product **102**, which is consistent with the proposed mechanism for this reaction. Formylation was carried out *via* a mixed anhydride approach. A mixture of formic acid and acetic anhydride was prepared and added to ornithine **100** yielding formylated ornithine **101** in 95% yield. Finally, the Boc protecting group was removed from the amine at the α -position *via* stirring a solution of **101** in DCM with TFA to yield **84** as the TFA salt.

4.9.7 Synthesis of syn.30616/A79

With the synthesis of formylated ornithine **84** and carboxylic acid **83** completed, the coupling together of these two intermediates could now be carried out to generate fully protected DEM30616/A **103**. This, followed by a global hydrogenation/deprotection would give syn.30616/A **79**.



Scheme 29 Synthetic route to syn.30616/A (**79**) via HATU mediated peptide coupling followed by global hydrogenation/deprotection.

To accomplish this we mixed carboxylic acid **83** with HATU, and subsequently added formylated ornithine **84** and DIEPEA as base. This afforded our desired di-peptide (**103**) in 63%

yield after purification *via* column chromatography. The final deprotection reaction was carried out *via* hydrogenation over palladium on carbon, leading to complete removal of both the benzyl groups and the Cbz group to generate syn.30616/A (**79**). Due to our experiences using celite as a filtration method to remove palladium on carbon causing degradation of synthetic madurastatin C1 (**25**), we looked to find an alternative filtration method that would avoid using celite. As such we employed the use of C₈ SPE cartridges. These reverse phase cartridges allowed for effective filtration of the palladium on carbon, whilst circumventing the problem of celite contaminating our sample.

Syn.30616/A (**79**) was then isolated and purified *via* HPLC. The HPLC sample containing our synthetic material contained multiple compounds, which were all isolated. Each was then subjected to an analytical HPLC experiment, with the retention time of one of these isolated compounds matching that of DEM30616/A. The HPLC peak containing what we suspected to be syn.30616/A (**79**) was collected, and analysed *via* mass spectrometry and ¹H NMR, all of which matched that of the natural product DEM30616/A. We therefore had succeeded in synthesising syn.30616/A. One of the additional peaks collected had the same *m/z* value as DME30616/A but had a differing retention time. We therefore assigned this compound as a diastereomer.

Whilst the completion of the synthesis of syn.30616/A was satisfying, HPLC isolation did not give perfectly clean material, as two extra aromatic signals were observed *via* ¹H NMR. Due to the small quantity of sample obtained, (c. 1mg) further analytical experiments to try and determine the identity of the contaminant were not carried out.

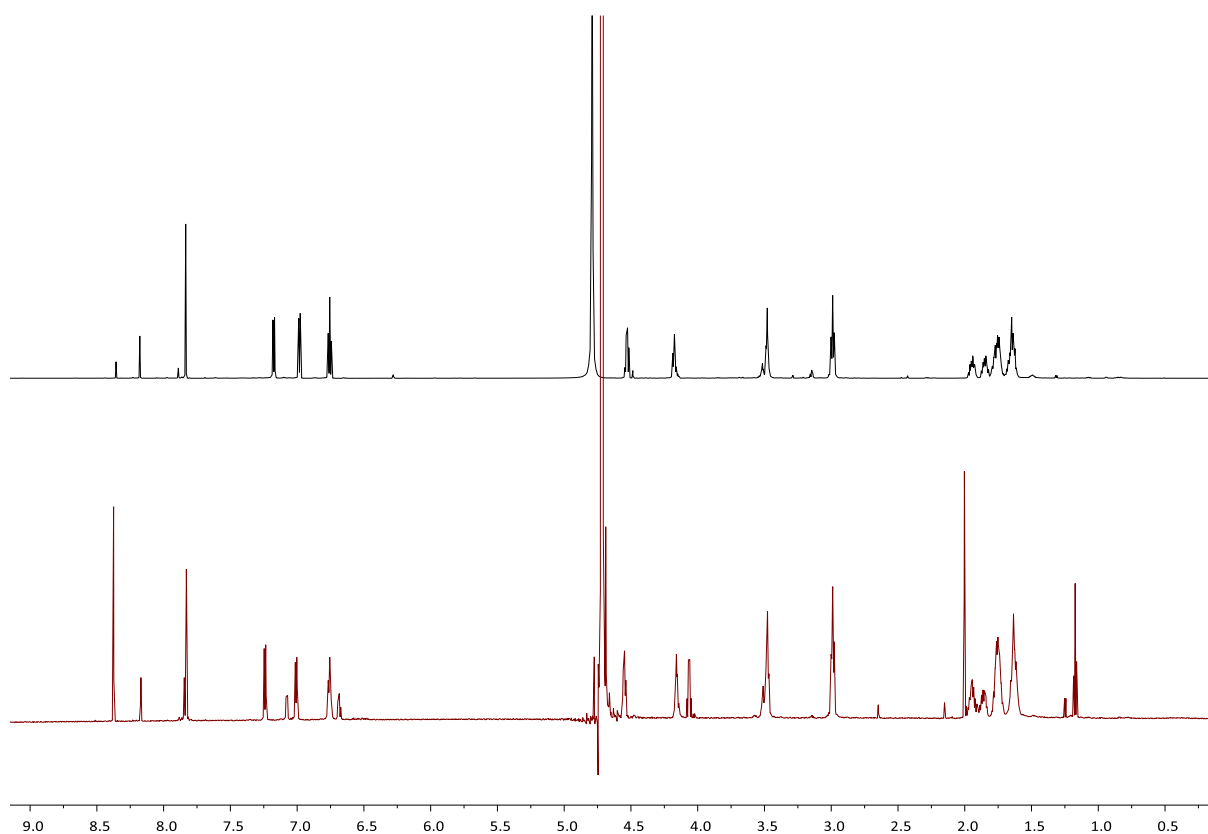


Figure 65. NMR comparison of DEM31376/A (top) and syn.30616/A (bottom) in D₂O, 700 MHz, 298 K.

4.10 Biological studies using syn.30616/A (79)

With synthetic material in hand, repeats of the bioassay experiments that had originally used DEM30616/A could be carried out using syn.30616, to establish the efficacy of DEM30616/A as a LtaS inhibitor. We would expect the same recovery of the ΔmbI mutant observed when the bacterial cells were grown in the presence of DEM30616/A when using syn.30616/A.

Micobiological studies were carried out by Dr. Bernard Keplingher at the Centre for Bacterial Cell Biology, the outcome of which showed that this was the indeed case. The incubation studies carried out using syn.30616/A caused the same recovery observed when the ΔmbI mutant was incubated with DEM30616/A without any additional Mg²⁺ required.

Although the ΔmbI mutant has been used as a screening method to detect potential LtaS inhibitors, we do not yet have any idea on the mode of action of DEM30616/A. Due to the structural similarity of DEM30616/A to known siderophores (chlorocatechelins A, B and mirubactin) and the classical chelating groups present in DEM30616/A (a catecholate and a hydroxamic acid) the role of DEM30616/A as a potential metal chelator should be taken into account. Indeed, given the reliance of the ΔmbI mutant on high concentrations of Mg²⁺ to

grow properly, a bi-dentate siderophore could act as a growth factor for the ΔmbI mutant, chelating Mg^{2+} and carrying it into the bacterial cell, giving a false positive result. Further research on the biological role of DEM30616/A will therefore need to be carried out. One approach would be the synthesis of non-metal chelating mimics of DEM30616/A, which are now accessible due to our work on the total synthesis of syn.30616/A. If these non-metal chelating mimics also cause recovery of the ΔmbI mutant, then we would be confident that we have indeed discovered a novel LtaS inhibitor.

4.11 Conclusions

Lipoteichoic acid (LTA) plays an essential role in bacterial growth and virulence, and disruption of the production of this molecule could prove to be an effective antibacterial treatment. In the search for inhibitors of LtaS enzyme responsible for the production of LTA, we have identified a compound of interest: DEM30616/A. Using a combination of mass spectrometry, NMR and Marfey's analysis, we have determined the chemical structure and assigned the absolute stereochemistry of DEM30616/A. With the structure assigned, we have also completed the total synthesis of DEM30616/A (syn.30616/A).

During our total synthesis of DEM30616/A, we investigated two separate approaches to synthesise the formyl containing ornithine amino acid **84**. The first approach utilising Millers oxidative strategy gave poor yields and required a high number of reaction steps, making this synthetic route unattractive. As a result, we completed the total synthesis of syn.30616/A *via* a new synthetic route based around the synthesis of chlorocatechelin. Results from biological assays utilising synthetic material (syn.30616/A) showed recovery of the ΔmbI mutant, matching the results observed when using the natural product DEM30616/A. This proved the efficacy of the natural product *via* the recovery of the ΔmbI mutant. Whilst we were successful in the total synthesis of DEM30616/A, improvements need to be made to reduce diastereomer production.

Whilst we were satisfied that DEM30616/A causes recovery of the ΔmbI mutant there is some concern that the observed recovery may not be due to inhibition of LtaS. Due to the chemical structure of DEM30616/A bearing classical siderophore like chelating groups, and the dependency of the ΔmbI mutant on high concentrations of Mg^{2+} one could make the argument that DEM30616/A may be acting as a Mg^{2+} siderophore, transporting Mg^{2+} ions into the bacterial cell and allowing for normal growth of the mutant, without additional Mg^{2+} being

added to the growth media. Further research will be needed to establish whether DEM30616/A is acting as either a LtaS inhibitor or a Mg²⁺ siderophore growth factor.

Chapter 5. Conclusions and Future Work

5.1 Conclusions

5.1.1 Introduction

Over the course of this project the isolation, structural determination and total synthesis of two bacterially derived natural products has been completed. The first of these natural products (DEM31376/A) being a pentapeptide siderophore and the other (DEM30616/A) a dipeptide that was investigated as a potential LtaS inhibitor. Siderophores are secondary metabolites that are produced by bacteria in order to acquire iron from their natural environment. Iron is an essential element for bacterial cell growth and function, but is relatively inaccessible as a nutrient for bacteria due to the rapid oxidation of Fe^{2+} to Fe^{3+} in aqueous aerobic environments. This leads to the production of insoluble iron oxide salts which then precipitate out of aqueous environments at neutral pH's. This low availability of iron is a limiting factor in the growth of bacteria. DEM31376/A is the pentapeptide siderophore produced by the novel bacterial strain DEM31376.

The second siderophore investigated in this project was DEM30616/A, a compound found as a result of an antibiotic screening study to identify novel LtaS inhibitors. Lipoteichoic acid is a vital component of the bacterial cell wall in Gram positive bacteria. Inhibition of one of the enzymes responsible for producing lipoteichoic acid, namely LtaS, could lead to the discovery of new antibiotic compounds.

5.2 Summary of research on DEM31376/A

A large-scale fermentation of the bacterial strain DEM30616 was carried out by us in collaboration with Demuris Ltd. and lead to the isolation of 283 mg of DEM31376/A. With this, structural determination was carried out *via* a wide range of analytical techniques. High resolution mass spectrometry was used to identify the molecular ion for DEM31376/A, and the resulting chemical formula and double bond equivalents were calculated. From here, 1D and 2D NMR experiments allowed us to assign the chemical structure of DEM31376/A, whilst the stereochemistry was assigned *via* advanced Marfey's analysis showing that DEM31376/A was comprised of D-serine, and two L-ornithine amino acids.

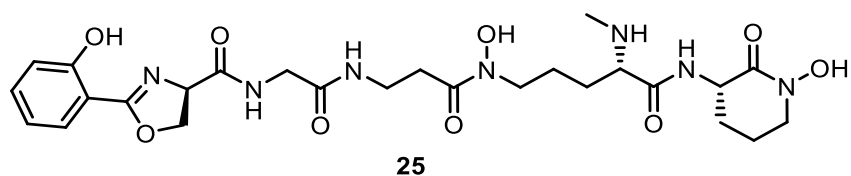


Figure 66. Chemical structure of madurastatin C1 (DEM31376/A)

With this completed we discovered that we had re-isolated the known natural product madurastatin C1. However, the structure of madurastatin C1 described in the literature was different to that assigned by us. This was due to differing structural assignments of the cyclised serine, assigned as a three-membered aziridine ring in the literature, and as a five-membered oxazoline ring by ourselves. Synthesis of two standards containing a five-membered oxazoline (**32**) and a three membered aziridine (**47**) were completed and their ^{13}C NMR spectra compared to that of madurastatin C1. With this we were able to show not only that the assigned chemical structure of madurastatin C1 was incorrect, but the entire family of madurastatin siderophores (A1, B1, B3) and the related natural product MBJ-0035 should be re-assigned to contain a five-membered oxazoline as opposed to the currently reported three-membered aziridine. This work culminated in a publication in the ACS Journal of Natural Products in 2017.

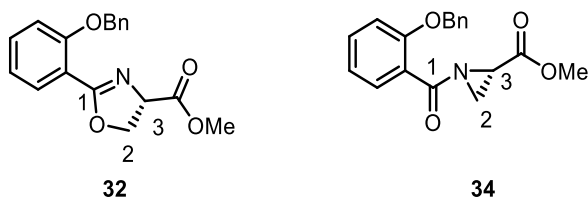
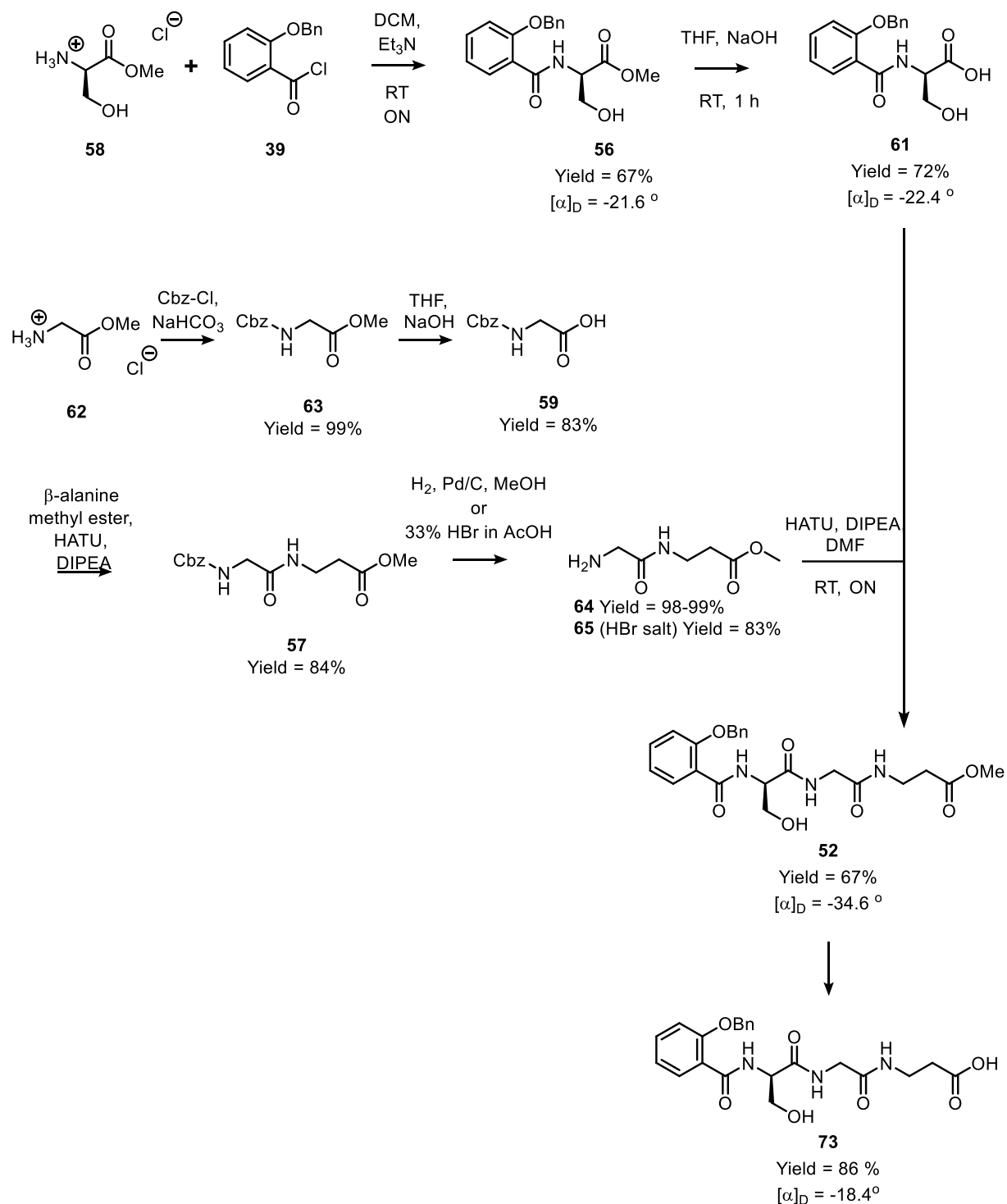


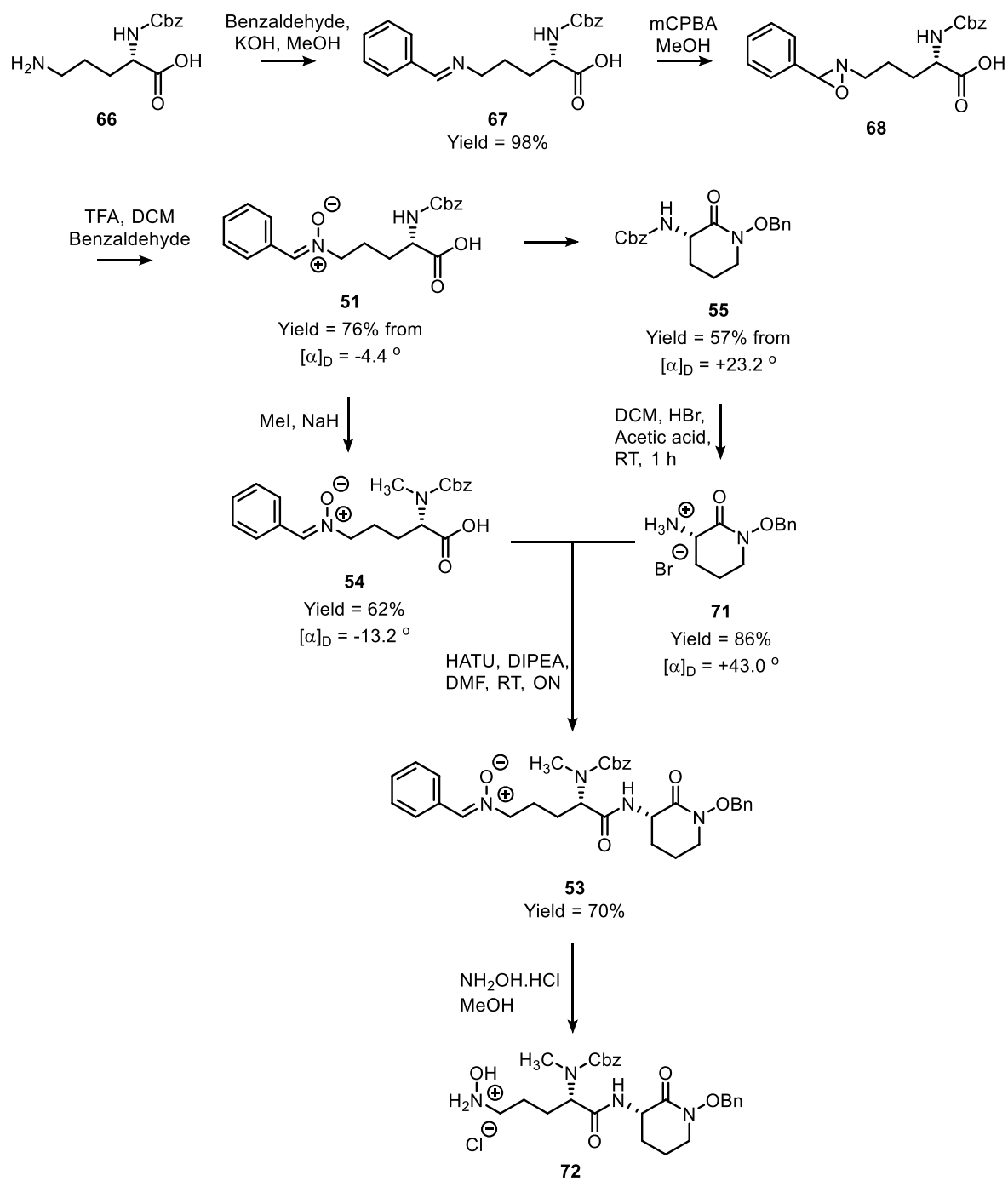
Figure 67. Chemical structures of our synthesised oxazoline model (**32**) and aziridine model (**34**)

With the structure of DEM31376/A now fully assigned, we next moved our attention to the total synthesis of DEM31376/A. This began with a retro-synthetic analysis of madurastatin C1, which allowed us to come up with a viable synthetic route based around disconnections at the amide/hydroxamic acid bonds. In order to generate the required hydroxamic acids, we elected to use oxidation chemistry at the ornithine amino acids. Meanwhile, the amide bond coupling reactions carried out utilising DCC, EDC and HATU. A convergent strategy designed around building the two halves of madurastatin C1 separately and then joining these together in a

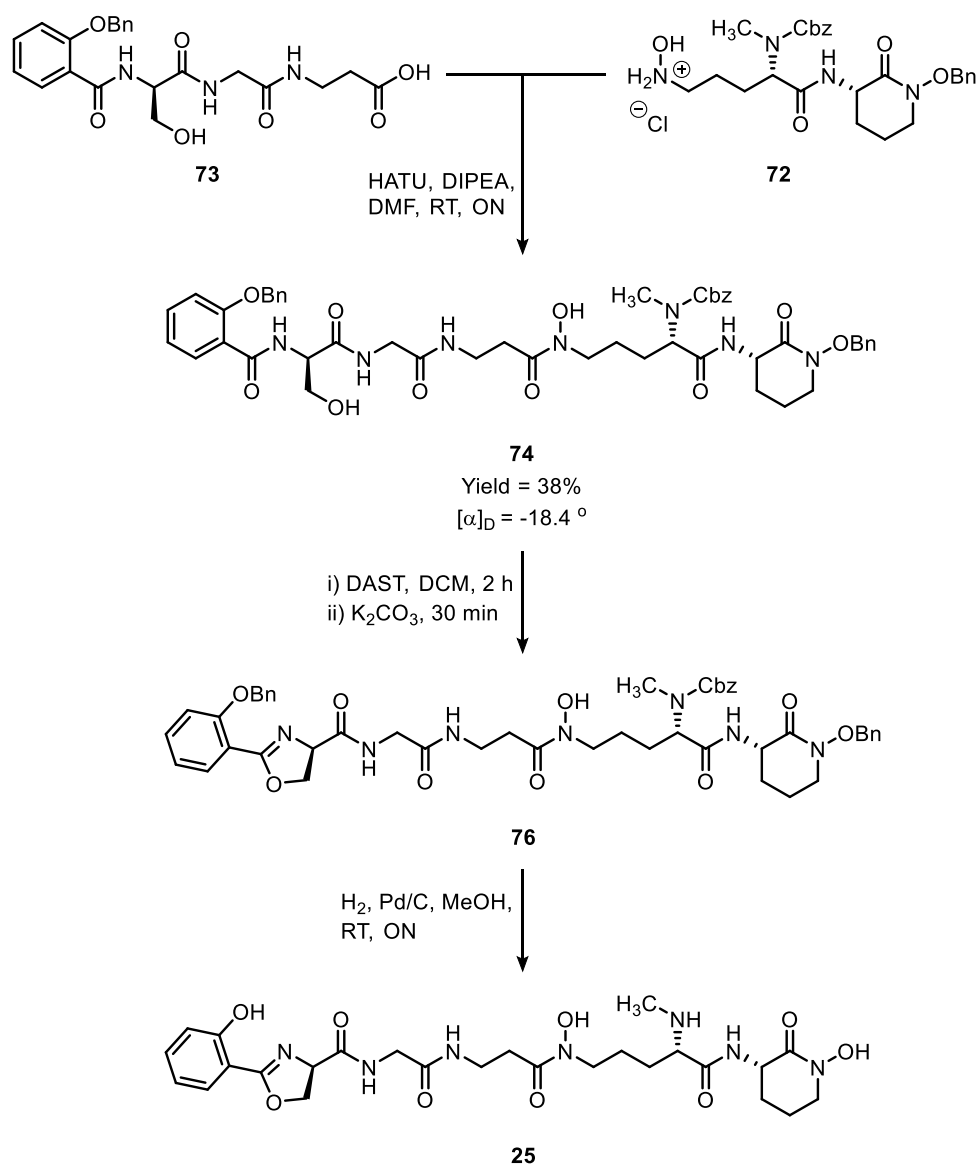
late stage peptide coupling reaction was carried out in a bid to maximise yields and reduce the risk of diastereomer formation (see schemes 30-32).



Scheme 30. Synthetic route to the left-hand half (**73**) of madurastatin C1 (DEM31376/A)



Scheme 31. Synthetic route to the right-hand half (**72**) of madurastatin C1 (DEM31376/A)



Scheme 32. Synthetic route showing the coupling of the left (**73**) and right (**72**) halves of madurastatin C1 (DEM30616/A), followed by a ring cyclisation and global deprotection to yield the final product madurastatin C1 (DEM31376/A) (**25**)

The synthetic route allowed us to generate the constituent amino acids in large quantities (100's of milligrams) and in good overall yields. We also showed that ring cyclisation through the use of DAST was an appropriate step to generate the five-membered oxazoline ring without generating unwanted by-products as was the case with thionyl chloride. Whilst the total synthesis was not fully achieved as the final product degraded in the presence of celite and palladium on carbon after the filtration step, we do believe that this synthetic procedure would yield the correct natural product, provided a more efficient filtration step was used after the final hydrogenation step.

5.3 Future research on DEM31376/A (madurastatin C1)

5.3.1 Improvements to overall yield.

First and foremost, the total synthesis of madurastatin C1 would need to be completed. As we were unsuccessful in the isolation of synthetic madurastatin C1 during this project, that would be the primary objective of any future research. During the total synthesis of madurastatin C1 there are several notable steps in which synthetic yields were reduced, which could be mitigated via new approaches. In the coupling of the left (**73**) and right (**72**) hand half's of madurastatin C1, we also observed the cyclised by-product (**75**). In order to mitigate this in future, the alcohol group on serine should be protected from the outset with an easily removable protecting group. As there are other alcohol functionalities present in madurastatin C1, the protecting group used for the serine hydroxyl should be different from these to allow for selective removal. The use of a silicon protecting group such as a TBDMS group would allow for selective late stage deprotection of the serine hydroxyl group, to allow for the ring cyclisation reaction to occur, without causing the other benzyl and Cbz protecting groups to be removed. The protection of the serine-hydroxyl functionality would give increased yields via preventing any unwanted side reactions occurring at this position. In addition to the use of a serine protecting group, we would also employ a similar strategy used after the global deprotection of our other natural product, DEM30616/A, to remove the palladium on carbon after the global deprotection reaction. This would involve filtration of the reaction mix through a SPE C8 cartridge as opposed to filtration through celite. This was shown to successfully trap the palladium on carbon in the synthesis of DEM30616/A and would prevent the degradation observed at the end of our total synthesis of madurastatin C1.

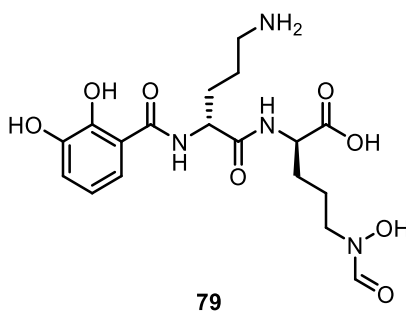
5.3.2 Alternate synthetic targets.

As discussed in Chapter 1 section 1.4.4.3, sideromycins have been generated in the laboratory by coupling antibiotic compounds to known siderophores. These antibiotics can have extremely large surface area or molecular weight but are still taken up by some bacterial species. This would be an interesting avenue to explore, as the *N*-methyl group in madurastatin C1 could easily be substituted for a *N*-R functionality. This R group could be a linked antibiotic compound to generate a novel synthetic sideromycin analogue. This approach could be completed by either incorporating the antibiotic molecule into the *N*-

methyl ornithine amino acid (**54**) during a total synthesis or via coupling of an antibiotic molecule with bacterially derived madurastatin C1.

5.4 Summary of research on DEM30616/A

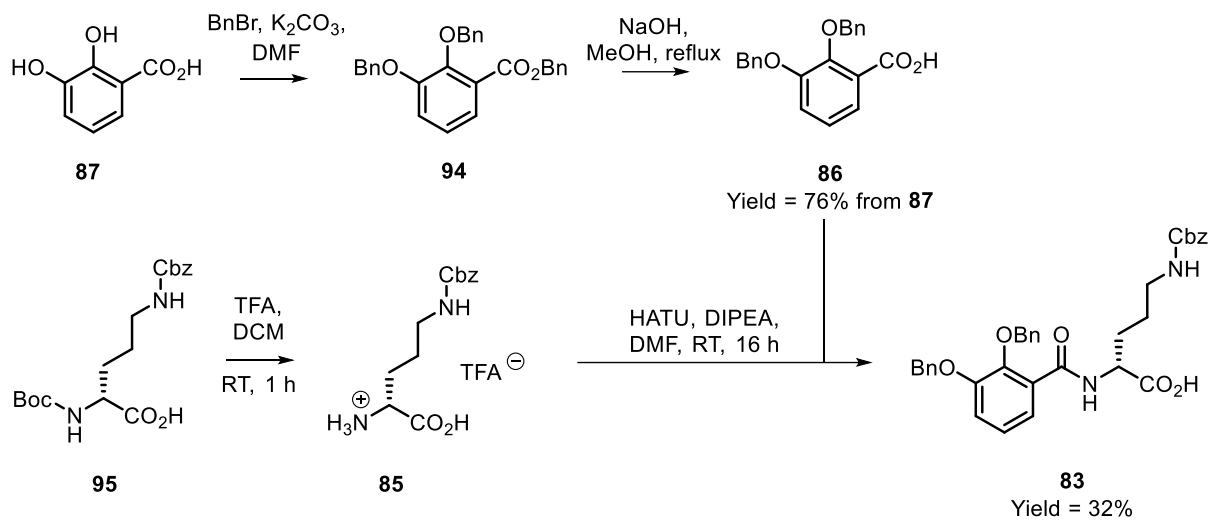
DEM30616/A was discovered during a screening study to find a novel LtaS inhibitor. After its discovery, we were able to solve its chemical structure *via* a mixture of HRMS and 1D and 2D NMR studies. The result of this de-novo structure determination was in keeping with the chemical structure preliminarily assigned by Fundación Medina. Upon determination of the chemical structure it was noted that DEM30616/A is very closely related to the chlorocatechelin's A and B as well as mirubactin. Indeed the chemical structure is so similar that, following the convention of the naming of the chlorocatechelins, DEM30616/A should be named mirubactin B. With the chemical structure solved, we then went on to assign the absolute stereochemistry of DEM30616/A through Marfey's analysis, showing that DEM30616/A contained two D-ornithine amino acids.



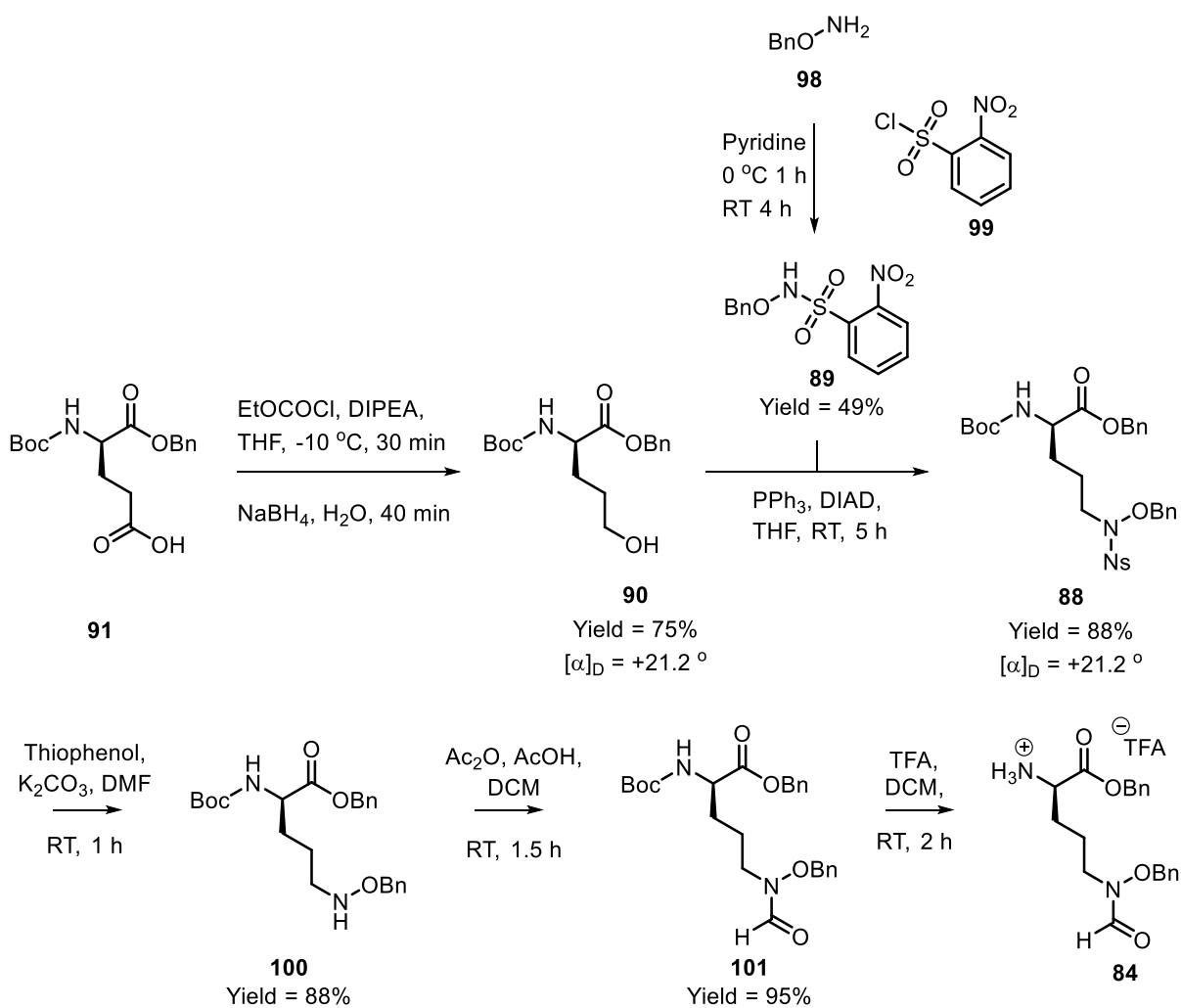
Scheme 33. Chemical structure of DEM30616/A.

With the chemical structure and absolute stereochemistry assigned for DEM30616/A, we next sought to complete the total synthesis of **79**. With this synthetic material (syn.30616) we hoped to be able to re-create the biological activity observed for the natural product, helping to prove the efficacy of (**79**) as an LtaS inhibitor. A retrosynthetic analysis was carried out, with disconnections being made at the amide bonds and the formyl group of the hydroxamic acid. We carried out the total synthesis of DEM30616/A using the approach used in the total synthesis of the chlorocatechelins and mirubactin.^{117–119} This utilised D-glutamic acid followed by activated reduction and Mitsunobu chemistry to generate the required formylated hydroxylamine ornithine amino acid. In addition to this, filtration of the crude product

(syn.30616) after the final hydrogenation reaction was carried out through the use of C8 SPE cartridges, as recommended to us by Prof. Marvin Miller.¹²¹ This prevented the degradation seen for synthetic madurastatin C1.



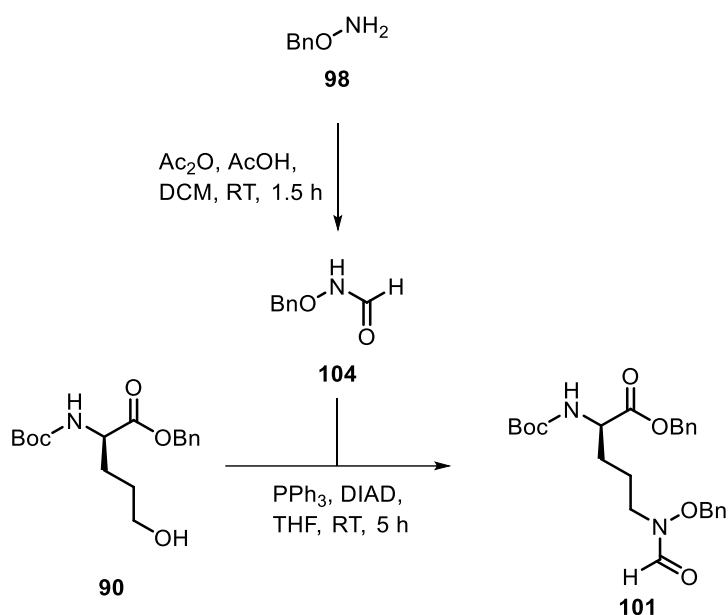
Scheme 34. Synthesis of the left-hand side of DEM30616/A (**83**).



Scheme 35. Synthesis of the right-hand side (formylated ornithine-hydroxylamine) of DEM30616/A (**84**)

rounds of column chromatography to isolate. Optimisation of the reaction conditions and isolation of (**83**) should improve the overall yield of this reaction.

Another area in which we believe improvements could be made to the overall yield could be in the synthesis of (**101**). We believe that this synthetic route could be reduced from five steps to three. This could be achieved *via* generation of amide (**104**, scheme 37) and then use of this in the Mitsunobu type reaction to generate (**101**). If this reaction can be completed successfully, then it would shorten the number of steps required to complete the synthesis of syn30616 and therefore give higher yields overall.



Scheme 37. Proposed alternative synthetic route to generate (**101**) in one step from (**90**).

5.5.2 Alternate synthetic targets.

Due to the role DEM30616/A as a potential LtaS inhibitor, the synthesis of structural derivatives is of interest. Modifications to syn30616 would allow us to probe the mode of action of this potential antibiotic molecule. For example, it would be interesting to discover if inversion of the stereochemistry of this molecule gave an active or inactive molecule. If this derivative with inverted stereochemistry was still active it could suggest that the role of this molecule is not as an enzyme inhibitor (as these are usually highly selective for a specific chirality of molecule). Further alterations could also be made by changing the functional groups, particularly the metal chelating catecholate and hydroxamic acid groups. The

catecholate could be modified by removing one or both hydroxyl groups, whilst the hydroxamic acid could be replaced with the corresponding free amine or a simple amide.

5.5.3 Microbiological studies

Due to the anticipated role as an LtaS inhibitor, several microbiological studies will need to be carried out in order to determine the mode of action of DEM30616/A. First of all, we need to account for the inherent flaw in the bioassay used to identify this potential LtaS inhibitor. This flaw is that the recovery of correct bacterial growth can be due to either the presence of high concentrations of Mg^{2+} or an LtaS inhibitor. If DEM30616/A is acting as a Mg^{2+} chelator, allowing transport into the bacterial cell, then this could lead to the observed bacterial growth without any inhibition of LtaS occurring at all. This problem could be investigated in several ways. Firstly, isolated DEM30616/A should be mixed with a source of Mg^{2+} and analysed to see whether DEM30616/A is indeed capable of chelating Mg^{2+} . If this is indeed the case then isolated DEM30616/A should be fed to several different bacterial strains including strain DEM30616. If DEM30616/A is indeed acting as an LtaS inhibitor then it should show antibiotic activity against the bacterial strains tested. Conversely, if DEM30616/A is merely acting as a Mg^{2+} shuttle, then it should not show any antibiotic activity. Modifying the metal chelating functional groups found in DEM30616/A to make them non-chelating and repeating the feeding studies against the Δmbl mutant could also prove useful, if no growth recovery is observed when fed with non-metal chelating DEM30616/A then it may suggest that the metal chelating and transport role is providing the bacterial recovery. However this result would need to be carefully examined as significantly changing the solubility, lipophilicity and molecular weight of DEM30616/A to make structural derivatives could stop its antibiotic activity, giving a false positive result toward a Mg^{2+} transport hypothesis.

Chapter 6 – Experimental

6.1 General experimental information

6.1.1 Analysis

Thin-layer chromatography was conducted on TLC silica gel 60 F₂₅₄ plates and visualised using UV light. ¹H and ¹³C{¹H} NMR spectra were recorded on a Bruker Avance III 700 MHz, Bruker Avance II HD 500 MHz, Bruker Avance II 400 MHz or Bruker Avance III 300 MHz spectrometer. Infrared spectra were recorded on a Varian 800 FT-IR Scimitar Series spectrometer. Melting points were obtained using a Stuart SMP3 melting point apparatus. High resolution mass spectra were obtained from the National Mass Spectrometry Facility (Swansea University) or Pinnacle (Newcastle University). LCMS was performed on an Agilent Infinity series HPLC, Agilent eclipse plus, using a C18 3.5 μM, 4.6 x 100 mm column with a Bruker micrOTOF II mass spectrometer. X-ray diffraction data were measured at 150 K on a Gemini ultra diffractometer equipped with an Enhance Ultra X-ray source ($\lambda\text{CuK}\alpha = 1.54184$). Through the Olex2 interface, the structures were solved with the XT structure solution program using intrinsic phasing and refined with the XL refinement package using least squares minimisation. Optical rotation measurements were obtained with a POLAAR 2001 polarimeter at $\lambda = 589$ nm using a 0.5 dm cell path length at 25 °C in spectrophotometric grade methanol.

6.1.2 Chemical procedures

Standard Schlenk techniques were used for all chemical reactions using air sensitive reagents under an atmosphere of nitrogen. Dry solvents were distilled under an atmosphere of nitrogen; THF and Et₂O were distilled from sodium/benzophenone, toluene was distilled from sodium whilst DCM was distilled from calcium hydride, all were then used directly. Manual column chromatography was carried out using Geduran silicagel 60 (40 – 63 μm). Celite Filter aid, Super-cel was used without additional pre-treatment. Automated flash column chromatography was performed using a biotage isolera One using KP-Sil SNAP C18 30 g cartridges. *m*CPBA was purified by dissolving 2 g of *m*CPBA in 20 mL of diethyl ether. This was then washed (3 x 10 mL) with pH 7.5 buffered aqueous solution (20.5 mL 0.1 M NaOH, 12.5 mL 0.2 M KH₂PO₄, 17 mL H₂O) and the ether layer evaporated under reduced pressure to give high purity *m*CPBA.

Isolation of DEM31376/A/madurastatin C1 (25)

The following isolation procedure is taken directly from the supporting information of our publication entitled: Structural Reassignment and Absolute Stereochemistry of Madurastatin C1 (MBJ-0034) and the Related Aziridine Siderophores: Madurastatins A1, B1, and MBJ-0035.⁹⁹

Actinomadura sp. DEM31376 was cultivated on ISP2-agar plates [4 g L⁻¹ Yeast extract, 10 g L⁻¹ malt extract, 4 g L⁻¹ glucose, 1% agar, dissolved in 1 L of distilled H₂O (pH 7.2) and sterilized by autoclaving for 30 min at 121 °C] at 30 °C for 7 days. A loopfull of vegetative cells from the ISP2 agar plate was taken and inoculated into 100 mL flask containing 10 mL ISP2 media and incubated at 30 °C for 3 days with rotatory shaking (140 rpm). This culture was used (250 µL) to inoculate a 500 mL flask containing 50 mL ISP2 media which was incubated at 30 °C for a further 3 days with orbital shaking. Finally, the seed culture of 500 mL ISP2 media (in 2.5 L baffled flask) was inoculated using 25 mL of the above culture and incubated at 30 °C for 3 days with orbital shaking. This was used to inoculate 18 L of ISP2 media (supplemented with 0.1% polypropylene glycol) in 20 L stirred tank reactor (Applikon). *Actinomadura sp.* DEM31376 was cultivated for 11 days at 30 °C. Twenty seven samples were collected over 11 days for further analysis. The pH was set to 7 at the beginning but was not maintained throughout the cultivation. The dissolved oxygen was controlled at 50% via the agitation speed (starting speed 400 rpm). Compressed air was applied to the vessel at 1 v/v/minute. The phosphatase concentration of samples collected from 20 L stir tank was measured by addition of 1 mL of Reagent ASA (0.25% Ammonium molybdate, 0.3 M sulphuric acid, and 1% ascorbic acid) to 85 µl of sample and KH₂PO₄ standards in the range of 0.0125 to 8 mM and incubated for 90 minutes at 37 °C. Reactions were stopped by adding 400 µL of 2 M sulphuric acid and absorbance was measured at 820 nm. The concentration was calculated from the KH₂PO₄ calibration curve. Glucose concentration of samples was measured using a SD Codefree Blood glucose monitoring system with disposable test strips. For the isolation of madurastatin C1, cultivation of *Actinomadura sp.* DEM31376 in a 20 L stirred tank reactor was repeated as described above and broth was collected after 5 days. The harvested culture broth was stirred with 320 g resin beads (Amberlite XAD16N, Sigma) for 16 hours at room temperature, followed by filtration. The beads were then washed with deionized H₂O (3 × 2 L) and extracted with MeOH (3.5 L) with stirring for three hours at room temperature. The MeOH extract was filtered and evaporated under reduced pressure to yield 5.48 g of crude material.

The crude was then dissolved in 50 mL of deionized H₂O and loaded onto a pre-hydrated 10 g HyperSep™ C8 cartridge (Thermo Scientific™) using a Vacuum manifold (Thames Restek). The cartridge was then washed with water (100 mL) and the aqueous collected. The cartridge was then washed with 100 mL of 25, 50 and 100% H₂O:MeOH. The 50 and 100% H₂O:MeOH fractions were combined, dried under reduced pressure and dissolved in 50 mL deionized H₂O. This was subjected to reversed phase chromatography using Biotage Isolera One system equipped with 30 g SNAP ultra C18 column (Biotage). Eluents A and B were 0.1% formic acid in water and 0.1% formic acid in MeCN respectively. The gradient consisted of wash with eluent A for 1 minute followed by linear gradient of 0 – 100% (B) over 10 minutes with a hold at 100% (B) for a final minute, with a flow rate of 25 mL/min. The major fraction, eluted between 40 - 60% MeCN, was dried under reduced pressure to yield 237.8 mg of madurastatin C1 (**25**).

NMR assignment of DEM31376/A/madurastatin C1 (25)

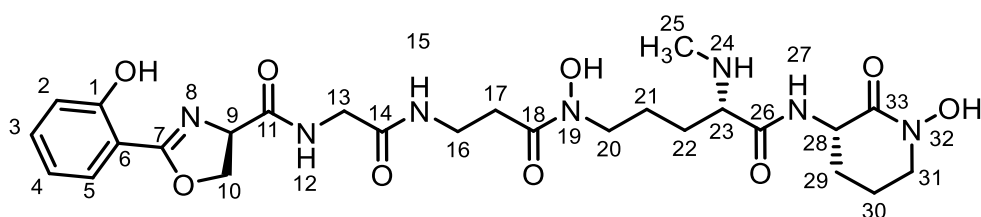
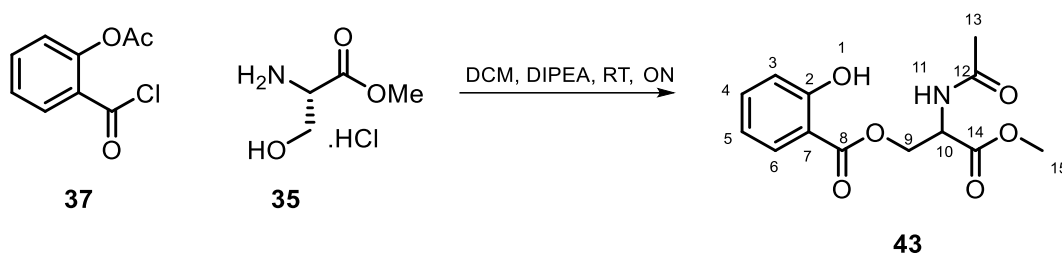


Table 15. NMR data for madurastatin C1 in D_6 -DMSO at 298 K, 700 MHz, 1H NMR collected at 700 MHz, $^{13}C\{^1H\}$ NMR collected at 176 MHz, ^{15}N shifts were measured indirectly by 1H - ^{15}N HMBC performed at both 8 and 12 Hz, referencing against liquid NH_3

Position	δ_{1H} multi, (J in Hz)	δ_{13C}	δ_{15N}	HMBC
1	-	159.1		
2	7.01 dd ($J = 8.3, 1.1$ Hz, 1H)	116.6		H to C6, 4, 1, 7
3	7.47 ddd ($J = 8.7, 7.3, 1.8$ Hz, 1H)	134.1		H to C6, 5, 1
4	6.97 – 6.93 (m, 1H)	119.1		H to C6, 2, 5, 3, 1
5	7.65 dd ($J = 7.8, 1.8$ Hz, 1H)	128.1		H to C2, 3, 1, 7
6	-	109.9		
7	-	165.9		
8	-	-	208.2	N to H9, 10
9	5.01 dd, ($J = 10.4, 7.7$ Hz, 1H)	67.4		H to C10, 6, 7, 11
10	4.65 dd ($J = 10.5, 8.4$ Hz, 1H) 4.52 t ($J = 8.0$ Hz, 1H)	69.4		H to C9, 7, 11, 10 H to C9, 7, 11, 10
11	-	170.2		
12	8.52 t ($J = 5.9$ Hz, 1H)	-	109.2	H to C13, 14, 11 N to H13
13	3.75 dd ($J = 16.5, 6.1$ Hz, 1H) 3.67 dd ($J = 16.5, 5.7$ Hz, 1H)	42.2		H to C14, 11 H to C14, 11
14	-	168.4		
15	7.93 t ($J = 5.8$ Hz, 1H),	-	112.5	H to C16, 14 N to H13, 17
16	3.28 – 3.22 (m, 2H)	34.6		H to C17, 14, 18
17	2.53 – 2.51 (m, 2H)	32.0		H to C16, 18
18	-	170.9		
19	-	-	175.9	N to H20, 21
20	3.49 – 3.42 (m, 4H)(2H)	47.0		H to C21, 22, 18
21	1.58 tt ($J = 16.5, 6.7$ Hz, 2H)	22.8		H to C22, 20, 23
22	1.40 ddd ($J = 15.9, 13.1, 6.8$ Hz, 1H) 1.48 ddt, ($J = 11.7, 9.8, 5.9$ Hz, 1H)	30.2		H to C20, 23, 26 H to C20, 23, 26
23	2.87 t ($J = 6.6$ Hz, 1H)	63.7		H to C21, 22, 25, 26
24	-	-	29.1	N to H25, 22
25	2.21 (s, 3H)	34.2		H to C23
26	-	173.5		
27	8.11 d ($J = 8.3$ Hz, 1H)	-	118.8	H to C28, 33, 26 N to H27, 28, 23, 29
28	4.32 ddd ($J = 10.9, 8.2, 5.3$ Hz, 1H)	49.4		H to C30, 29, 33, 26
29	1.96 – 1.82 (m, 3H) (1H) 1.67 qd ($J = 12.5, 4.3$, 1H)	27.8		H to C30, 29, 33 H to C30, 28, 31, 33
30	1.96 – 1.82 (m, 3H) (2H)	20.4		
31	3.49 – 3.42 (m, 4H) (2H)	51.2		H to C30, 29, 33
32	-	-	171.8	N to H31, 29
33	-	165.0		

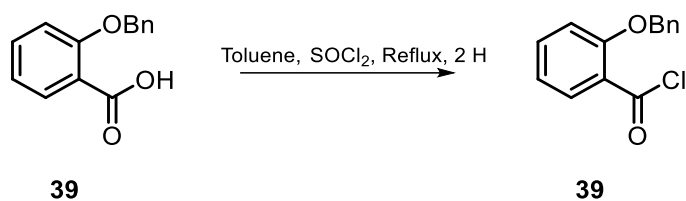
(S)-2-acetamido-3-methoxy-3-oxopropyl 2-hydroxybenzoate (43)



Following a modified procedure outlined by Miller *et al.*⁸⁹, to a stirred suspension of L-serine methyl ester hydrochloride (**35**) (0.78 g, 5.0 mmol, 1 eq) in DCM (10 mL) at 0 °C was added DIPEA (2.2 mL, 12.5 mmol, 2.5 eq) and the mixture stirred for 5 minutes. The resulting suspension was then added dropwise to a solution of 2-(chlorocarbonyl)phenyl acetate (**37**) (0.99 g, 5.0 mmol, 1 eq) in DCM (5 mL) and the resulting mixture allowed to warm to room temperature and stirred overnight. The solution was diluted with DCM (100 mL) and washed with 1 M HCl_(aq) (3 x 50 mL), saturated NaHCO_{3(aq)} (3 x 50 mL) and brine (30 mL). The organic layer was then dried over Na₂SO₃, filtered, and concentrated under reduced pressure to give a brown solid. This was then purified via silica gel column chromatography (EtOAc/DCM 9:1, R_f = 0.18, UV light) to give (S)-2-acetamido-3-methoxy-3-oxopropyl 2-hydroxybenzoate (**43**) (0.579 g, 2.06 mmol, 41%) as a white solid.

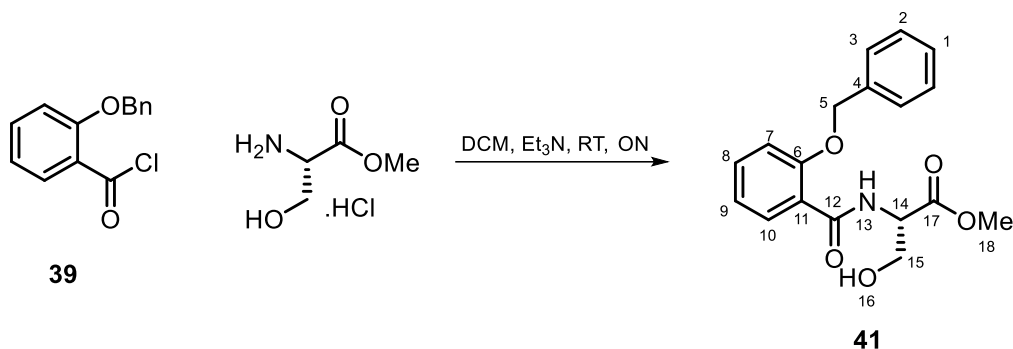
Mp = 89=91 °C. $[\alpha]_D = -3.63^\circ$ ($c = 1$, MeOH). ¹H NMR (300 MHz, Chloroform-*d*) δ 10.48 (d, $J = 1$ Hz, 1H¹), 7.73 (ddd, $J = 8.0, 1.8, 0.5$ Hz, 1H), 7.47 (ddd, $J = 8.7, 7.2, 1.7$ Hz, 1H), 6.98 (ddd, $J = 8.4, 1.1, 0.5$ Hz, 1H), 6.88 (ddd, $J = 8.2, 7.3, 1.1$ Hz, 1H), 6.41 (d, $J = 7.6$ Hz, 1H), 5.00 (dt, $J = 7.4, 3.6$ Hz, 1H), 4.70 (dd, $J = 11.3, 3.4$ Hz, 1H), 4.64 (dd, $J = 11.4, 3.8$ Hz, 1H), 3.81 (s, 3H), 2.06 (s, 3H). ¹³C NMR (75 MHz, Chloroform-*d*) δ 170.09, 170.07, 169.6⁸, 161.9, 136.4, 129.9, 119.5, 117.9, 111.8, 64.9, 53.2, 51.8, 23.3. IR (neat): $\nu_{\max}/\text{cm}^{-1}$ 3277.4, 3207.2, 1734.8, 1682.2. HRMS (pNSI) calcd for C₁₃H₁₆NO₆ [M+H]⁺: 282.0972, found 282.0971.

2-(benzyloxy)benzoyl chloride (**39**)



To a stirred suspension of 2-benzyloxybenzoic acid (**38**) (1.00 g, 4.38 mmol, 1.0 eq) in dry toluene (4 mL) was added thionyl chloride (0.32 ml, 4.42 mmol, 1.01 eq) and a reflux condenser added. The mixture was then stirred under reflux for 4 hours, after which time the sample was concentrated under reduced pressure to yield crude 2-(benzyloxy)benzoyl chloride (**39**) which was used without further purification.

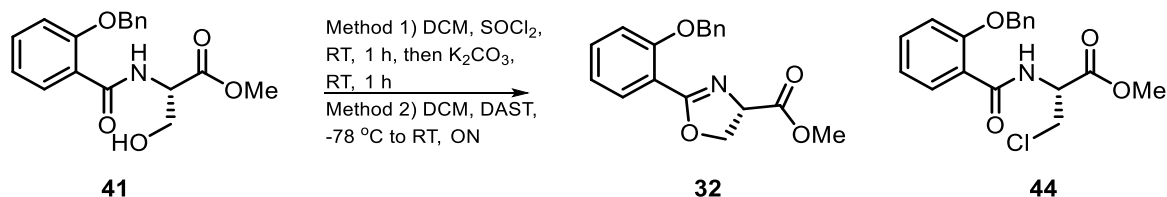
Methyl (2-(benzyloxy)benzoyl)-L-serinate (**41**)



Following the procedure outlined by Miller *et al.*⁸⁹, to a stirred suspension of L-serine methyl ester hydrochloride (1.343 g, 8.6 mmol, 1.0 eq) in DCM (5 mL) at 0 °C was added Et₃N (3.0 mL, 21.6 mmol, 2.5 eq) and the mixture stirred for 5 minutes. The resulting suspension was then added dropwise to a solution of 2-(benzyloxy)benzoyl chloride (**39**) (2.23 g, 8.6 mmol, 1 eq) in DCM (5 mL) at -78 °C and the resulting mixture allowed to warm to room temperature and stirred overnight. The solution was diluted with DCM (20 mL) and washed with 1 M HCl_(aq) (50 mL), saturated NaHCO_{3(aq)} (50 mL) and saturated brine (30 mL). The organic layer was then dried over Na₂SO₄, filtered, and concentrated under reduced pressure to give methyl (2-(benzyloxy)benzoyl)-L-serinate (**41**) (2.798 g, 8.5 mmol, 99%) as a white powder. X-Ray grade crystals were grown from slow evaporation of a 3mg/mL solution in DCM.

Mp = 125-127 °C [lit: 128-129 °C]^[89]. [α]_D +29.0 ° (c = 0.2, MeOH). R_f = 0.25(DCM/EtOAc 2:1, UV light) ¹H NMR (400 MHz, CDCl₃) δ 8.76 (d, J = 7.1 Hz, 1H¹³), 8.20 (dd, J = 7.8, 1.8 Hz, 1H^{Ar}), 7.54 – 7.33 (m, 6H^{Ar}), 7.17 – 7.04 (m, 2H^{Ar}), 5.30 – 5.21 (m, 2H⁵), 4.84 (dt, J = 7.1, 3.9 Hz, 1H¹⁴), 3.95 – 3.85 (m, 2H¹⁵), 3.70 (s, 3H¹⁸), 2.14 (s, 1H¹⁶). ¹³C NMR (101 MHz, CDCl₃) δ 170.9¹⁷, 165.7¹², 157.2^{Ar}, 135.7^{Ar}, 133.4^{Ar}, 132.6^{Ar}, 129.0², 128.8¹, 128.3³, 121.7^{Ar}, 121.4^{Ar}, 113.0^{Ar}, 71.6⁵, 63.9¹⁵, 55.4¹⁴, 52.7¹⁸. IR (neat): ν_{max}/cm⁻¹ 3325, 2930, 2851, 1736, 1625. HRMS (pNSI) calcd for C₁₈H₂₀NO₅ [M+H]⁺: 330.1336, found 330.1337

Methyl (S)-2-(2-(benzyloxy)phenyl)-4,5-dihydrooxazole-4-carboxylate (32) and methyl (R)-2-(2-(benzyloxy)benzamido)-3-chloropropanoate (44)

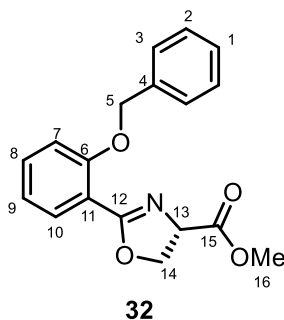


Method 1) Following the procedure outlined by Miller *et al.*⁸⁹, to a stirred solution of methyl (2-(benzyloxy)benzoyl)-L-serinate (**41**) (0.200 g, 0.6 mmol, 1 eq) in DCM (4 mL) under an atmosphere of nitrogen at room temperature was added SOCl₂ (0.31 mL, 4.3 mmol, 7.0 eq). The resulting mixture was stirred for 1 hour and then solid potassium carbonate (1.174 g, 8.5 mmol, 14.0 eq) was added in one portion and the mixture stirred at room temperature for one hour. After this time saturated NaHCO_{3(aq)} was added (10 mL) and the emulsion extracted with DCM (50 mL). The organics were then washed with water (50 mL) and saturated brine (20 mL). The organic layer was then dried over Na₂SO₄, filtered and concentrated under reduced pressure to give a white solid. This was then purified via silica gel column chromatography (DCM/EtOAc 9:1) to give methyl (S)-2-(2-(benzyloxy)phenyl)-4,5-dihydrooxazole-4-carboxylate (**32**) (0.064 g, 0.20 mmol, 34%) as a white solid and methyl (R)-2-(2-(benzyloxy)benzamido)-3-chloropropanoate (**44**) (0.095 g, 0.27 mmol, 45%) as a white solid.

Method 2) Following a modified procedure adapted from Williams *et al.*⁹¹, to a stirred solution of methyl (2-(benzyloxy)benzoyl)-L-serinate (**41**) (0.165 g, 0.5 mmol, 1 eq) in DCM (4 mL) under an atmosphere of nitrogen at -78 °C was added DAST (0.079 mL, 0.6 mmol, 1.2 eq). The resulting mixture was stirred for 2 hours and then solid potassium carbonate (0.192 g, 1.25 mmol, 2.5 eq) was added in one portion and the mixture allowed to warm to room temperature over one hour. After this time saturated NaHCO_{3(aq)} was added (10 mL) and the emulsion extracted with DCM (3 x 20 mL). The organics were then washed with water (2 x 20 mL) and saturated brine (10 mL), dried over Na₂SO₄, filtered and concentrated under reduced pressure to give a white solid. This was then purified via silica gel column chromatography

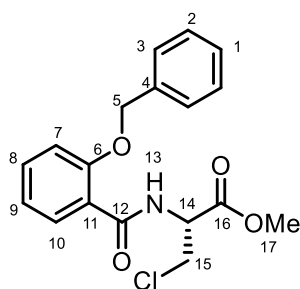
(EtOAc/DCM 1:9 R_f = 0.38, UV light) to give methyl (*S*)-2-(2-(benzyloxy)phenyl)-4,5-dihydrooxazole-4-carboxylate (**32**) (0.122 g, 0.39 mmol, 79%) as a white solid.

Methyl (*S*)-2-(2-(benzyloxy)phenyl)-4,5-dihydrooxazole-4-carboxylate (32**)**



Mp = 121-122 °C [lit: 121 – 123 °C]^[89]. $[\alpha]_D = +71.2^\circ$ (C = 0.5, MeOH) ¹H NMR (700 MHz, DMSO-d₆) δ 7.67 (dd, J = 7.6, 1.8 Hz, 1H), 7.53 – 7.51 (m, 2H³), 7.50 (ddd, J = 8.4, 7.4, 1.9 Hz, 1H), 7.41 – 7.35 (m, 2H²), 7.32 – 7.28 (m, 1H¹), 7.22 (dd, J = 8.5, 0.9 Hz, 1H), 7.03 (td, J = 7.5, 1.0 Hz, 1H), 5.22 (s, 2H⁵), 4.97 (dd, J = 10.3, 7.9 Hz, 1H¹³), 4.56 (dd, J = 10.3, 8.6 Hz, 1H^{14a}), 4.53 (dd, J = 8.6, 7.8 Hz, 1H^{14b}), 3.71 (s, 3H¹⁶). ¹³C NMR (176 MHz, DMSO-d₆) δ 171.5¹⁵, 164.2¹², 157.0⁶, 137.1⁴, 132.8^{Ar}, 131.0^{Ar}, 128.3², 127.4¹, 126.7³, 120.5, 116.7¹¹, 114.0, 69.5⁵, 69.0¹⁴, 68.2¹³, 52.2¹⁶. ¹H NMR (700 MHz, MeOD) δ 7.68 (dd, J = 7.7, 1.8 Hz, 1H), 7.50 – 7.44 (m, 3H), 7.38 – 7.34 (m, 2H), 7.30 – 7.25 (m, 1H), 7.16 (d, J = 8.4 Hz, 1H), 7.02 (td, J = 7.6, 0.9 Hz, 1H), 5.21 (s, 2H), 4.97 (dd, J = 10.5, 7.6 Hz, 1H), 4.67 (dd, J = 8.7, 7.6 Hz, 1H), 4.62 (dd, J = 10.5, 8.8 Hz, 1H), 3.79 (s, 3H). ¹³C NMR (176 MHz, MeOD) δ 173.0, 168.1, 159.0, 138.4, 134.2, 132.1, 129.4, 128.7, 128.1, 121.7, 118.1, 115.0, 71.5, 70.8, 69.3, 53.1. ¹H NMR (300 MHz, CDCl₃) δ 7.84 – 7.76 (m, 1H), 7.55 – 7.46 (m, 2H), 7.44 – 7.28 (m, 4H), 7.04 – 6.93 (m, 2H), 5.19 (s, 2H), 4.98 (dd, J = 10.7, 8.1 Hz, 1H), 4.68 (dd, J = 8.7, 8.1 Hz, 1H), 4.58 (dd, J = 10.7, 8.7 Hz, 1H), 3.81 (s, 3H). ¹³C NMR (75 MHz, CDCl₃) δ 171.9, 165.8, 157.8, 137.0, 132.9, 131.8, 128.6, 127.8, 126.9, 120.9, 117.4, 113.9, 77.2, 70.8, 69.4, 68.9, 52.8. IR (neat): $\nu_{\max}/\text{cm}^{-1}$ 3314, 3038, 2952, 2852, 1732, 1690, 1645. HRMS (pNSI) calcd for C₁₈H₁₈NO₄ [M+H]⁺: 312.1230, found 312.1230.

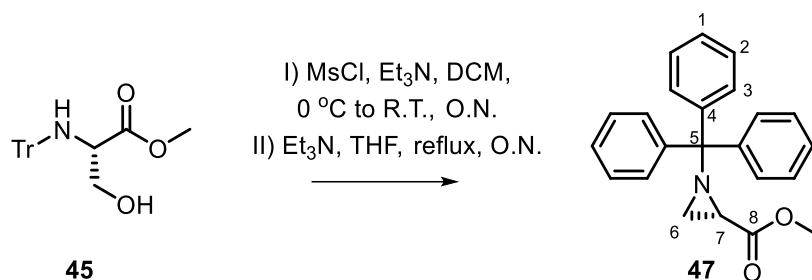
Methyl (*R*)-2-(2-(benzyloxy)benzamido)-3-chloropropanoate (44**)**



44

$[\alpha]_D = +20.0^\circ$ ($C = 0.05$, MeOH) $^1\text{H NMR}$ (300 MHz, Chloroform-*d*) δ 8.88 (d, $J = 7.6$ Hz, 1H^{13}), 8.29 – 8.14 (m, 1H^{Ar}), 7.53 – 7.31 (m, 6H^{Ar}), 7.09 (ddd, $J = 9.1, 7.8, 1.3$ Hz, 2H^{Ar}), 5.26 (s, 2H^5), 5.21 (dt, $J = 7.1, 3.3$ Hz, 1H^{14}), 3.97 (dd, $J = 11.3, 3.3$ Hz, $1\text{H}^{15\text{a}}$), 3.87 (dd, $J = 11.2, 3.5$ Hz, $1\text{H}^{15\text{b}}$), 3.69 (s, 3H^{17}). $^{13}\text{C NMR}$ (75 MHz, Chloroform-*d*) δ 169.4¹⁶, 165.1¹², 157.3^{Ar}, 135.4^{Ar}, 133.5^{Ar}, 132.6^{Ar}, 128.9^{Ar}, 128.7^{Ar}, 128.4^{Ar}, 121.6^{Ar}, 120.9^{Ar}, 112.9^{Ar}, 71.5⁵, 53.8¹⁴, 52.9¹⁷, 45.3¹⁵. IR (neat): $\nu_{\text{max}}/\text{cm}^{-1}$ 3359.0, 1745.0, 1645.1, 753.6. HRMS (pNSI) calcd for $\text{C}_{18}\text{H}_{19}\text{ClNO}_4$ $[\text{M}+\text{H}]^+$: 348.0997, found 348.1007.

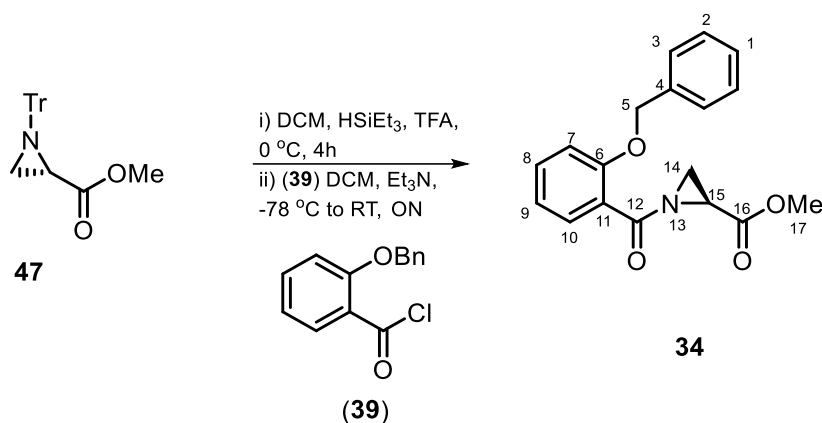
Methyl (S)-1-tritylaziridine-2-carboxylate (**47**)



Following a modified procedure adapted from Carlson *et al.*⁹³, to a stirred solution of *N*-Trityl-L-serine methyl ester (**45**) (9.036 g, 25.0 mmol, 1 eq) in DCM (20 mL) at room temperature was added Et₃N (5.27 mL, 37.5 mmol, 1.5 eq). The solution was then cooled to 0 °C in an ice bath and methanesulphonyl chloride (2.32 mL, 60.0 mmol, 2.4 eq) was added dropwise. After complete addition, the ice bath was removed and the reaction stirred at room temperature overnight. The reaction was quenched via the addition of saturated NaHCO_{3(aq)} and the slurry extracted with DCM (20 mL). The organic layer was collected, washed with water (2 x 40 mL), saturated brine (40 mL), dried over Na₂SO₃, filtered, and the organics removed under reduced pressure to yield the crude mesylate as a yellow oil. This oil was then taken and dissolved in THF (10 mL) and trimethylamine (7.02 mL, 50.0 mmol, 2 eq) was added. The reaction was then heated to reflux overnight, after which time the reaction mix was concentrated under reduced pressure. The product was then crystallised from EtOAc, filtered, washed with hexane and dried under vacuum to yield the product, methyl (S)-1-tritylaziridine-2-carboxylate (**47**) as a pale yellow coloured powder (6.037 g, 70%).

Mp = 127-129 °C [lit. 127-128 °C]¹²⁰. [α]_D = -11.6 (c 0.1, MeOH). R_f = 0.10 (EtOAc:Petrol (40-60 °C) 9:1, UV light). ¹H NMR (300 MHz, CDCl₃): δ_H 7.54 – 7.46 (m, 6H), 7.36 – 7.16 (m, 9H), 3.77 (s, 3H), 2.26 (dd, *J* = 2.7, 1.6 Hz, 1H), 1.89 (dd, *J* = 6.2, 2.7 Hz, 1H), 1.42 (dd, *J* = 6.2, 1.6 Hz, 1H). ¹³C NMR (75 MHz, CDCl₃) δ 172.1, 143.7, 129.5, 127.8, 127.1, 77.2, 74.5, 52.3, 31.8, 28.9. IR (neat): ν_{max}/cm⁻¹ 2996, 2951, 1742, 1179. HRMS (pNSI) calcd for C₂₃H₂₁NNaO₂ [M+Na]⁺: 366.1470, found 366.1467.

Methyl (S)-1-(2-(benzyloxy)benzoyl)aziridine-2-carboxylate (**34**)

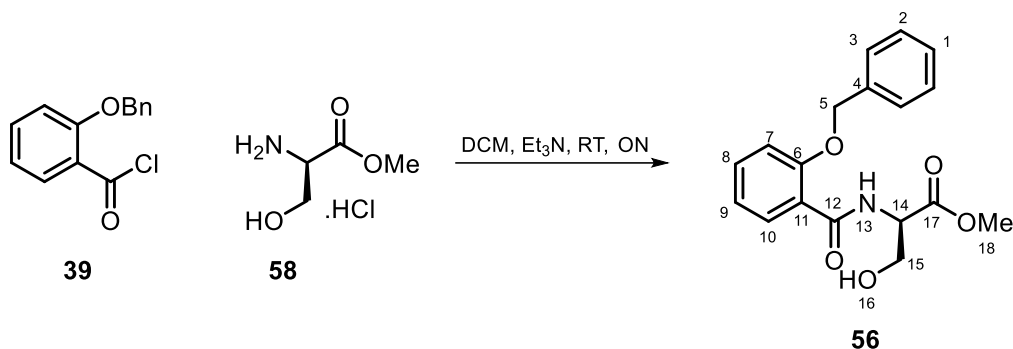


Following a modified procedure adapted from Weiss *et al.*⁹⁸, to a stirred solution of methyl 1-tritylaziridine-2-carboxylate (**47**) (0.515 g, 1.5 mmol, 1eq) in DCM (5 mL) at 0 °C was added triethylsilane (1.02 mL, 1.5 mmol, 1eq) followed by the dropwise addition of TFA (3 mL, 4.5 mmol, 3eq). After 4 hours the mixture was cooled to -78 °C and Et₃N (1.05 mL, 7.5 mmol, 5eq) was added and the reaction left stirring for a further 10 minutes. After this time 2-(benzyloxy)benzoyl chloride (**39**) (0.407 g, 1.65 mmol, 1.1eq) in DCM (2 mL) was added. The mixture was left stirring at room temperature overnight, and concentrated under reduced pressure to give a brown solid. This was then purified via silica gel column chromatography (diethyl ether/petrol 1:1, R_f = 0.25, UV light) to give methyl (S)-1-(2-(benzyloxy)benzoyl)aziridine-2-carboxylate (**34**) (0.164 g, 0.53 mmol, 35%) as a yellow oil.

¹H NMR (700 MHz, MeOD) δ 7.83 (dd, *J* = 7.8, 1.8 Hz, 1H), 7.52 – 7.46 (m, 3H), 7.41 – 7.35 (m, 2H), 7.32 – 7.28 (m, 1H), 7.18 – 7.15 (m, 2H), 7.03 (ddd, *J* = 7.8, 7.3, 1.0 Hz, 1H), 5.23 – 5.17 (m, 2H), 3.59 (s, 3H¹⁷), 3.23 (dd, *J* = 5.3, 3.1 Hz, 1H), 2.63 (dd, *J* = 5.3, 1.3 Hz, 1H), 2.62 (dd, *J* = 3.1, 1.3 Hz, 1H). ¹³C NMR (176 MHz, MeOD) δ 178.1, 170.3, 159.1, 138.1, 135.1, 132.7, 129.6, 129.0, 128.5, 123.9, 121.8, 115.1, 71.7, 52.9, 49.0, 37.5, 33.1. ¹H NMR (700 MHz, DMSO-d₆) δ 7.75 (dd, *J* = 7.8, 1.7 Hz, 1H), 7.51 (ddd, *J* = 8.4, 7.3, 1.9 Hz, 1H), 7.49 – 7.47 (m, 2H), 7.41 – 7.36 (m, 2H), 7.34 – 7.30 (m, 1H), 7.21 (dd, *J* = 8.6, 0.9 Hz, 1H), 7.04 (td, *J* = 7.5, 1.0 Hz, 1H), 5.29 – 5.15 (m, 2H), 3.57 (s, 3H), 3.29 (dd, *J* = 5.5, 3.1 Hz, 1H), 2.66 (dd, *J* = 5.4, 1.4 Hz, 1H), 2.54 (dd, *J* = 3.1, 1.4 Hz, 1H). ¹³C NMR (176 MHz, DMSO-d₆) δ 175.0, 168.5, 157.0, 136.7, 133.7, 131.2, 128.4, 127.7, 127.2, 122.4, 120.5, 114.0, 69.7, 52.2, 35.8, 32.0. ¹H NMR (300 MHz, CDCl₃) δ 7.94 (ddd, *J* = 7.7, 1.9, 0.5 Hz, 1H), 7.51 – 7.28 (m, 6H), 7.07 – 6.95 (m, 2H), 5.19 (d, *J* = 0.9 Hz,

2H), 3.61 (s, 3H), 3.20 (dd, $J = 5.5, 3.1$ Hz, 1H), 2.67 (dd, $J = 3.1, 1.3$ Hz, 1H), 2.62 (dd, $J = 5.5, 1.3$ Hz, 1H). ^{13}C NMR (75 MHz, CDCl_3) δ 176.0, 169.0, 157.8, 136.6, 133.9, 132.3, 128.7, 128.1, 127.1, 122.8, 121.1, 113.8, 70.9, 52.5, 36.3, 32.5. IR (neat): $\nu_{\text{max}}/\text{cm}^{-1}$ 3067, 3032, 3007, 2953, 2876, 1740, 1660, 1200, 697. HRMS (pNSI) calcd for $\text{C}_{18}\text{H}_{18}\text{NO}_4$ $[\text{M}+\text{H}]^+$: 312.1230, found 312.1230.

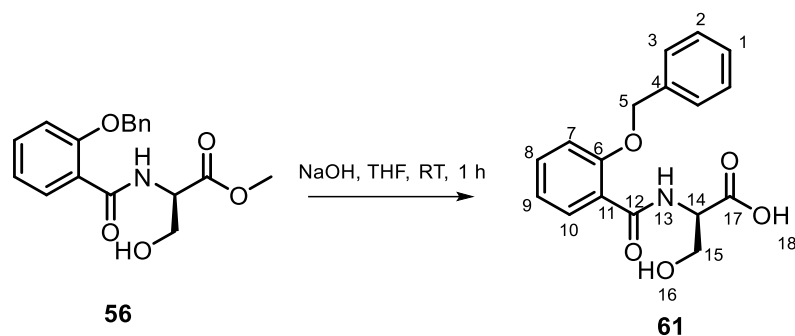
Methyl (2-(benzyloxy)benzoyl)-D-serinate (**56**)



Following a modified procedure outlined by Miller *et al.*⁸⁹, to a stirred suspension of D-serine methyl ester hydrochloride (**58**) (1.50 g, 9.64 mmol, 1.1 eq) in DCM (10 mL) at 0 °C was added Et₃N (3.1 mL, 21.9 mmol, 2.5 eq) and the mixture stirred for 5 minutes. The resulting suspension was then added dropwise to a solution of 2-(benzyloxy)benzoyl chloride (**39**) (2.17 g, 8.8 mmol, 1 eq) in DCM (5 mL) at -78 °C and the resulting mixture allowed to warm to room temperature and stirred overnight. The solution was diluted with DCM (100 mL) and washed with 1 M HCl_(aq) (3 x 50 mL), saturated NaHCO_{3(aq)} (3 x 50 mL) and brine (30 mL). The organic layer was then dried over Na₂SO₃, filtered, and concentrated under reduced pressure to give a brown solid. This was then purified via silica gel column chromatography (EtOAc/DCM 1:2, R_f = 0.25, UV light) to give methyl (2-(benzyloxy)benzoyl)-D-serinate (**56**) (1.94 g, 5.9 mmol, 67%) as a white solid. X-Ray grade crystals were grown from slow evaporation of a 10mg/mL solution in methanol.

Mp = 127-129 °C. [α]_D = -21.6 ° (c = 1, MeOH). ¹H NMR (300 MHz, Chloroform-*d*) δ 8.76 (d, *J* = 7.2 Hz, 1H¹³), 8.19 (dd, *J* = 7.8, 1.8 Hz, 1H^{Ar}), 7.55 – 7.31 (m, 6H^{Ar}), 7.15 – 6.95 (m, 2H^{Ar}), 5.32 – 5.14 (m, 2H⁵), 4.84 (dt, *J* = 7.6, 4.0 Hz, 1H¹⁴), 3.95 – 3.83 (m, 2H¹⁵), 3.69 (s, 3H¹⁸), 2.24 (s, 1H¹⁶). ¹³C NMR (75 MHz, Chloroform-*d*) δ 170.9¹⁷, 165.7¹², 157.1, 135.7, 133.3, 132.5, 128.9², 128.8¹, 128.3³, 121.7, 121.3, 112.9, 71.5⁵, 63.8¹⁵, 55.4¹⁴, 52.7¹⁸. IR (neat): $\nu_{\max}/\text{cm}^{-1}$ 3370.8, 3324.8, 1735.0, 1632.9.

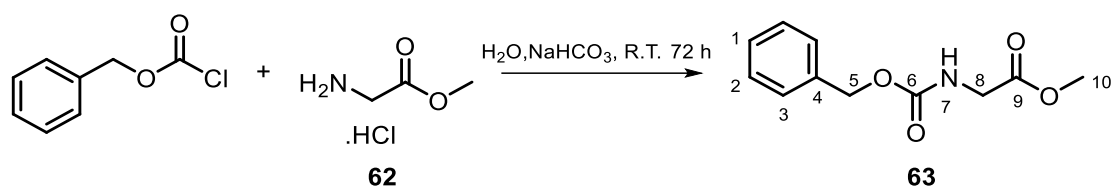
(2-(Benzyloxy)benzoyl)-D-serine (61)



To a stirred suspension of methyl (2-(benzyloxy)benzoyl)-D-serinate (**56**) (1.01 g, 3.06 mmol) in THF (6 mL) was added 2 M NaOH (1.5 mL) and the mixture stirred for 1 hour. After this time the mixture was diluted with EtOAc (20 mL) and extracted with saturated NaHCO_{3(aq)} (20 mL). The aqueous was then taken, acidified to pH 2 with 2 M HCl and extracted with EtOAc (3 x 20 mL). The combined organic layers were washed with water (20 mL), brine (20 mL), dried over sodium sulphate, filtered and evaporated under reduced pressure to give ((benzyloxy)carbonyl)glycine (**61**) (0.693 g, 2.20 mmol, 72%) as a white solid.

$[\alpha]_D = -22.4^\circ$ ($c = 1$, MeOH).. ¹H NMR (300 MHz, Chloroform-*d*) δ 8.88 (d, $J = 6.3$ Hz, 1H¹³), 8.18 (dd, $J = 7.9, 1.8$ Hz, 1H), 7.58 – 7.31 (m, 6H), 7.13 – 7.00 (m, 2H), 5.21 (d, $J = 2.7$ Hz, 2H⁵), 4.68 (dt, $J = 6.3, 4.1$ Hz, 1H¹⁴), 3.96 (dd, $J = 11.5, 3.9$ Hz, 1H^{15a}), 3.72 (dd, $J = 11.5, 4.3$ Hz, 1H^{15b}). ¹³C NMR (75 MHz, Chloroform-*d*) δ 172.7¹⁷, 167.5¹², 157.4, 135.3, 134.0, 132.5, 129.0, 121.8, 120.2, 113.0, 71.7⁵, 62.2¹⁵, 55.3¹⁴.

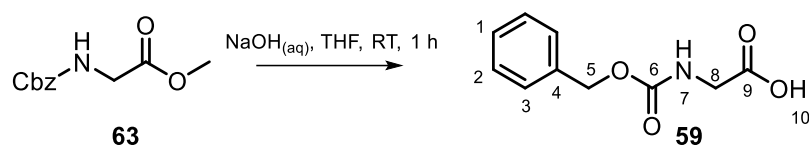
Methyl ((benzyloxy)carbonyl)glycinate (**63**)



To a stirred solution of glycine methyl ester hydrochloride (**62**) (3.00 g, 23.8 mmol) in water (10 mL) was added benzyl chloroformate (4.6 mL, 31.0 mmol 1.3 eq) and the mixture stirred rapidly. Sodium hydrogen carbonate (4.20 g, 50.0 mmol, 2.1 eq) suspended in water (20 mL) was then added to the reaction mixture and the solution stirred at room temperature for 72 hours. After this time the mixture was diluted with water (50 mL), acidified to pH 3 with 2 M HCl and extracted with diethyl ether (2 x 50 mL). The combined organic layers were washed water (50 mL), brine (50 mL), dried over sodium sulphate, filtered and evaporated under reduced pressure to give crude methyl ((benzyloxy)carbonyl)glycinate as a mixture with residual benzyl chloroformate. The crude mixture was subjected to column chromatography (ethyl acetate/40-60 petrol 1:1, 40-60 R_f = 0.65) to give pure methyl ((benzyloxy)carbonyl)glycinate (**63**) (5.251 g, 23.5 mmol, 99%) as a clear oil.

¹H NMR (400 MHz, Chloroform-*d*) δ 7.45 – 7.29 (m, 5H¹⁻³), 5.28 (s br, 1H⁷), 5.13 (s, 2H⁵), 3.99 (d, *J* = 5.6 Hz, 2H⁸), 3.76 (s, 3H¹⁰). ¹³C NMR (101 MHz, Chloroform-*d*) δ 170.4⁹, 156.2⁶, 136.2⁴, 128.5², 128.2¹, 128.1³, 67.1⁵, 52.3¹⁰, 42.7⁸. IR (neat): $\nu_{\max}/\text{cm}^{-1}$ 3352.2, 1704.0, 1521.0. HRMS (pNSI) calcd for C₁₁H₁₃NO₄Na [M+Na]⁺: 246.0737, found 246.0738.

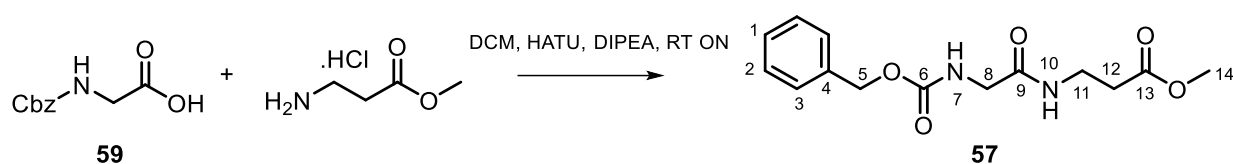
((benzyloxy)carbonyl)glycine (59)



To a stirred suspension of methyl ((benzyloxy)carbonyl)glycinate (**63**) (1.339 g, 6 mmol) in THF (5 mL) was added 2 M NaOH (5 mL) and the mixture stirred for 1 hour. After this time the mixture was diluted with EtOAc (20 mL) and extracted with NaHCO_{3(aq)} (20 mL). The aqueous layer was collected, acidified to pH 2 (2 M HCl) and extracted with EtOAc (3 x 20 mL). The combined organic layers were washed with water (20 mL), brine (20 mL), dried over sodium sulphate, filtered and evaporated under reduced pressure to give ((benzyloxy)carbonyl)glycine (**59**) (1.013g, 4.8 mmol, 83%) as a white solid.

Mp = 116-118 °C. ¹H NMR (300 MHz, DMSO-*d*₆) δ 12.58 (s, 1H¹⁰), 7.57 (t, *J* = 6.2 Hz, 1H⁷), 7.50 – 7.08 (m, 5H¹⁻³), 5.04 (s, 2H⁵), 3.67 (d, *J* = 6.2 Hz, 2H⁸). ¹³C NMR (75 MHz, DMSO-*d*₆) δ 171.6⁹, 156.5⁶, 137.0⁴, 128.4², 127.8¹, 127.7³, 65.5⁵, 42.1⁸. IR (neat): $\nu_{\text{max}}/\text{cm}^{-1}$ 3327.1, 1724.4, 1533.1. HRMS (pNSI) calcd for C₁₀H₁₀NO₃ [M-H]⁻: 208.0615, found 208.0616.

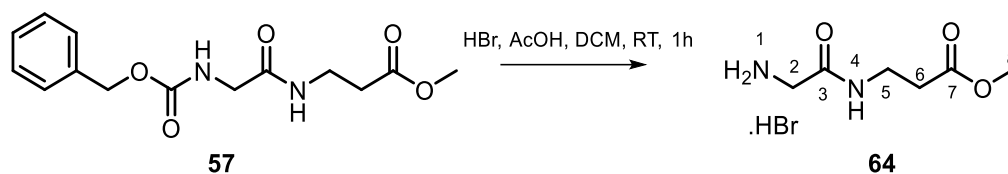
methyl 3-(2-(((benzyloxy)carbonyl)amino)acetamido)propanoate (57)



To a stirred solution of ((benzyloxy)carbonyl)glycine (**59**) (1.00 g, 4.78 mmol) in DCM (20 mL) was added HATU (2.00 g, 5.26, mmol 1.1 eq) and the mixture stirred for 10 minutes. To this mixture was added β -alanine methyl ester hydrochloride (0.734 g, 5.26 mmol, 1.1 eq) and the reaction mix stirred for an additional 20 minutes. To this was added DIPEA (3.3 mL, 19.12 mmol, 4.0 eq) and the mixture stirred at room temperature overnight. After this time the mixture was diluted with DCM (20 mL) and washed with saturated $\text{NH}_4\text{Cl}_{(\text{aq})}$ (2 x 20 mL), saturated $\text{NaHCO}_3_{(\text{aq})}$ (2 x 20 mL) and brine (50 mL). The organics were then dried over sodium sulphate, filtered and evaporated under reduced pressure and crude mixture subjected to silica gel column chromatography (ethyl acetate/40-60 petrol 2:1, $R_f = 0.2$) to give pure methyl 3-(2-(((benzyloxy)carbonyl)amino)acetamido)propanoate (**57**) (1.175 g, 4.0 mmol, 84%) as a white solid.

Mp = 93-95 °C. ^1H NMR (300 MHz, Chloroform-*d*) δ 7.42 – 7.27 (m, 5H^{1-3}), 6.78 (t, $J = 6.0$ Hz, 1H^{10}), 5.74 (t, $J = 5.7$ Hz, 1H^7), 5.09 (s, 2H^5), 3.81 (d, $J = 5.7$ Hz, 2H^8), 3.65 (s, 3H^{14}), 3.49 (q, $J = 6.1$ Hz, 2H^{11}), 2.50 (t, $J = 6.1$ Hz, 2H^{12}). ^{13}C NMR (75 MHz, Chloroform-*d*) δ 172.8 13 , 169.2 9 , 156.6 6 , 136.2 4 , 128.5 1 , 128.2 2 , 128.1 3 , 67.1 5 , 51.8 14 , 44.5 8 , 34.9 11 , 33.7 12 . IR (neat): $\nu_{\text{max}}/\text{cm}^{-1}$ 3314.4, 1732.2, 1689.5, 1534.7. HRMS (pNSI) calcd for $\text{C}_{14}\text{H}_{18}\text{N}_2\text{O}_5\text{Na}$ $[\text{M}+\text{Na}]^+$: 317.1108, found 317.1107.

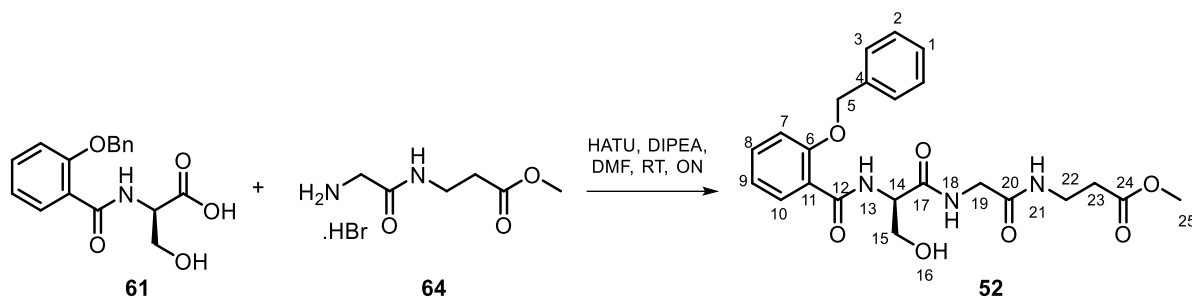
2-((3-methoxy-3-oxopropyl)amino)-2-oxoethan-1-aminium bromide (**64**)



To a stirred solution of methyl 3-(2-(((benzyloxy)carbonyl)amino)acetamido)propanoate (**57**) (0.500 g, 1.7 mmol) in DCM (12 mL) was added 33% HBr in acetic acid (12 mL) and the mixture stirred for 1 hour. After this time, the reaction mixture was evaporated using a flow of air, before being dissolved in CHCl₃ (10 mL) and concentrated under reduced pressure. The residue was dissolved in CHCl₃ concentrated under reduced pressure a second time. The residue was triturated by dissolving in the minimum amount of MeOH followed by the addition of an equal volume of hexane and the stoppered solution left to stir overnight. The resulting solid was then collected via filtration to yield 2-((3-methoxy-3-oxopropyl)amino)-2-oxoethan-1-aminium bromide (**64**) (0.340 g, 1.41 mmol, 83 %) as an orange solid.

¹H NMR (400 MHz, DMSO-*d*₆) δ 8.45 (t, *J* = 5.8 Hz, 1H⁴), 7.97 (br-s, 3H¹), 3.61 (s, 3H⁸), 3.51 (s, 2H²), 3.35 (q, *J* = 6.6 Hz, 2H – overlaps with residual water peak), 2.51 (t, *J* = 6.2 Hz, 2H – overlaps with residual DMSO peak). ¹³C NMR (101 MHz, DMSO-*d*₆) δ 171.5⁷, 165.9⁹, 51.43⁸, 40.1², 34.7⁵, 33.3⁶. HRMS (pNSI) calcd for C₆H₁₃N₂O₃ [M+H]⁺: 161.0921, found 161.0918.

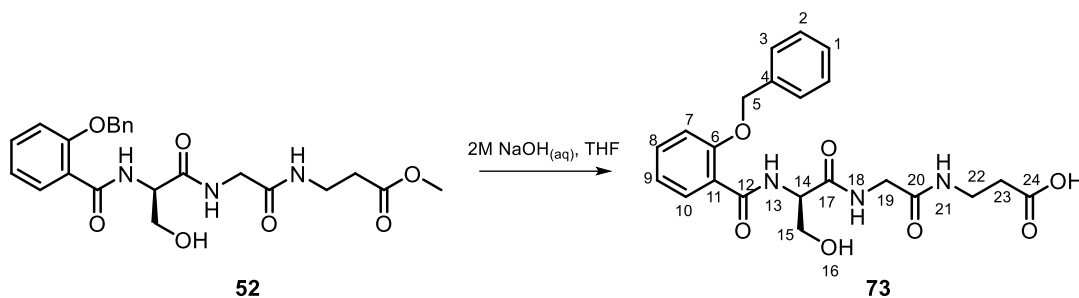
(R)-3-(2-(2-(2-(benzyloxy)benzamido)-3-hydroxypropanamido)acetamido)propanoate (52)



To a stirred solution of (2-(benzyloxy)benzoyl)-D-serine (**61**) (0.392 g, 1.24 mmol, 1eq) in DMF (12 mL) was added HATU (0.519 g, 1.36 mmol, 1.1 eq) and the mixture stirred for 10 minutes. To this mixture was added methyl 3-(2-aminoacetamido)propanoate hydrobromide (**64**) (0.300 g, 1.24 mmol, 1eq) and the reaction mix stirred for an additional 20 minutes. After this time DIPEA (0.86 mL, 4.96 mmol, 4eq) was added dropwise and the mixture stirred at room temperature overnight. After this time, the mixture was diluted with brine (10 mL) and the resulting slurry extracted with EtOAc (3 x 50 mL). The combined organic layers were then washed with 0.2 M HCl (30 mL), saturated NaHCO_{3(aq)} (30 mL) and brine (50 mL). The organics were then dried over sodium sulphate, filtered and evaporated under reduced pressure. The crude mixture was then subjected to silica gel column chromatography (EtOAc/Meoh 9:1, R_f = 0.43) to give methyl (R)-3-(2-(2-(2-(benzyloxy)benzamido)-3-hydroxypropanamido)acetamido)propanoate (**52**) (0.381 g, 0.83 mmol, 67%) as a white solid.

[α]_D = -34.6 ° (c = 1, MeOH). ¹H NMR (300 MHz, Chloroform-*d*) δ 8.69 (d, *J* = 6.6 Hz, 1H¹³), 8.13 (dd, *J* = 7.8, 1.8 Hz, 1H), 7.57 – 7.31 (m, 6H), 7.15 – 7.03 (m, 3H^{18+Ar}), 6.89 (t, *J* = 5.9 Hz, 1H²¹), 5.22 (s, 2H⁵), 4.65 – 4.49 (m, 1H¹⁴), 4.01 (dd, *J* = 11.1, 3.3 Hz, 1H^{15a}), 3.84 (d, *J* = 5.8 Hz, 2H¹⁹), 3.65 (s, 3H²⁵), 3.59 (dd, *J* = 11.1, 5.1 Hz, 1H^{15b}), 3.55 – 3.40 (m, 2H²²), 2.72 (br-s, 1H¹⁶), 2.53 (dd, *J* = 6.9, 5.5 Hz, 2H²³). ¹³C NMR (75 MHz, Chloroform-*d*) δ 173.1²⁴, 171.8¹⁷, 168.9²⁰, 166.4¹², 157.1, 135.5, 133.6, 132.3, 129.03, 128.95, 128.4, 121.8, 121.1, 113.0, 71.6⁵, 62.6¹⁵, 55.5¹⁴, 52.0²⁵, 43.3¹⁹, 35.1²², 33.8²³. HRMS (pNSI) calcd for C₂₃H₂₈N₃O₇ [M+H]⁺: 458.1922, found 458.1922.

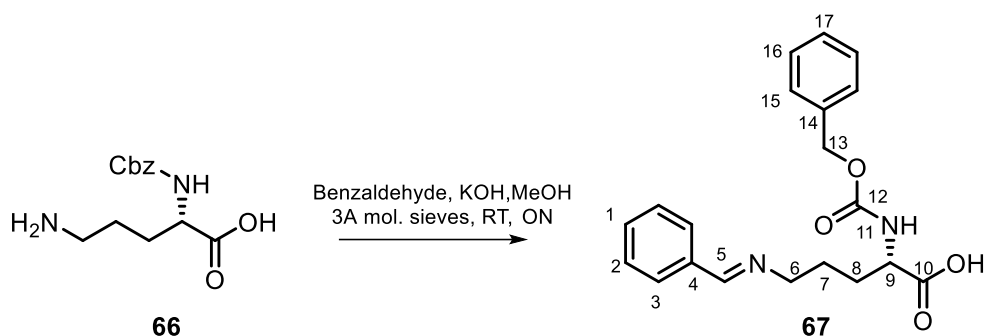
(*R*)-3-(2-(2-(2-(benzyloxy)benzamido)-3-hydroxypropanamido)acetamido)propanoate (73**)**



To a stirred suspension of methyl (*R*)-3-(2-(2-(2-(benzyloxy)benzamido)-3-hydroxypropanamido)acetamido)propanoate (**52**) (0.261 g, 0.57 mmol, 1eq) in THF (5 mL) was added aqueous 2 M NaOH solution (5 mL). The mixture was stirred for 30 minutes after which time water (50 mL) was added and the reaction mixture was washed with EtOAc (2 x 50 mL). The aqueous layer was then acidified to pH 2 (HCl_{aq}) and extracted with EtOAc (3 x 50 mL) and the combined organic layers concentrated under reduced pressure yielding (*R*)-3-(2-(2-(2-(benzyloxy)benzamido)-3-hydroxypropanamido)acetamido)propanoic acid (**73**) (0.216 g, 0.49 mmol, 86%) as a colourless oil.

$[\alpha]_D -13.2^\circ$ ($c = 1$, MeOH). $^1\text{H NMR}$ (300 MHz, Methanol- d_4) δ 8.00 (dd, $J = 7.9, 1.8$ Hz, 1H), 7.55 – 7.28 (m, 6H), 7.21 (dd, $J = 8.5, 1.0$ Hz, 1H), 7.06 (td, $J = 7.6, 1.0$ Hz, 1H), 5.29 (s, 2H), 4.53 (t, $J = 5.2$ Hz, 1H), 3.94 – 3.76 (m, 3H), 3.76 – 3.61 (m, 1H), 3.48 – 3.39 (m, 2H), 2.52 (t, $J = 6.9$ Hz, 2H). $^{13}\text{C NMR}$ (75 MHz, Chloroform- d) δ 174.9, 171.9, 170.3, 166.3, 157.1, 135.6, 133.5, 132.0, 128.9, 128.7, 128.0, 121.6, 120.9, 113.1, 71.4, 62.4, 55.9, 43.1, 35.5, 33.7.

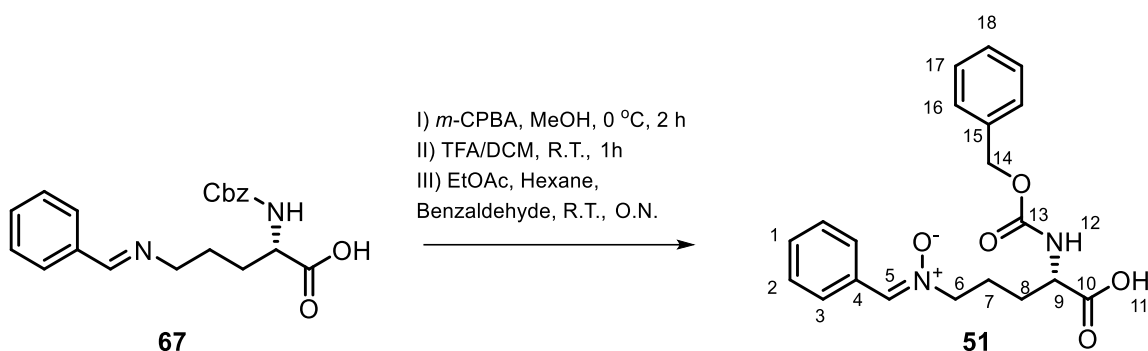
(*S,E*)-5-(benzylideneamino)-2-(((benzyloxy)carbonyl)amino)pentanoic acid (67**)**



To a stirred solution of KOH (1.10 g, 19.53 mmol, 1.04 eq) in methanol (42 mL) was added (*S*)-5-amino-2-(((benzyloxy)carbonyl)amino)pentanoic acid (**66**) (5.00 g, 18.78 mmol, 1.0 eq). After the solids had dissolved, benzaldehyde (2 mL, 19.72 mmol, 1.05 eq) was added followed by 3 Å mol. sieves. The mixture was then stirred at room temperature overnight after which time the molecular sieves were filtered off and washed with methanol. The filtrate was then evaporated under reduced pressure to give (*S,E*)-5-(benzylideneamino)-2-(((benzyloxy)carbonyl)amino)pentanoic acid (**67**) (7.254 g, 18.48 mmol, 98%) as a hygroscopic white foam.

^1H NMR (300 MHz, Methanol- d_4) δ 8.35 (s, 1H⁵), 7.79 – 7.70 (m, 2H), 7.50 – 7.40 (m, 3H), 7.40 – 7.22 (m, 5H), 5.08 (d, J = 3.4 Hz, 2H¹³), 4.09 (dd, J = 7.0, 4.3 Hz, 1H⁹), 3.70 – 3.58 (m, 2H⁶), 2.03 – 1.86 (m, 1H^{8a}), 1.86 – 1.63 (m, 3H^{8b+7}). ^{13}C NMR (75 MHz, Methanol- d_4) δ 192.9, 177.9, 163.0, 156.8, 137.0, 135.7, 134.3, 130.6, 128.3, 128.0, 127.9, 127.5, 127.4, 66.0, 60.5, 56.1, 30.5, 26.7. ^1H NMR (300 MHz, DMSO- d_6) δ 8.29 (s, 1H⁵), 7.83 – 7.63 (m, 2H), 7.54 – 7.39 (m, 3H), 7.39 – 7.20 (m, 5H), 6.36 (d, J = 6.2 Hz, 1H¹¹), 4.98 (s, 2H¹³), 3.77 – 3.43 (m, 3H⁹⁺⁶), 1.81 – 1.62 (m, 1H^{8a}), 1.56 (t, J = 6.0 Hz, 3H^{8b+7}). ^{13}C NMR (75 MHz, DMSO- d_6) δ 172.5, 160.2, 155.0, 137.5, 136.2, 130.4, 128.6, 128.3, 127.8, 127.6, 127.5, 64.9¹³, 60.9⁶, 55.5⁹, 30.7⁸, 26.7⁷. IR (neat): $\nu_{\text{max}}/\text{cm}^{-1}$ 3661.0, 1694.1. HRMS (pNSI) calcd for C₂₀H₂₃N₂O₄[M+H]⁺: 355.1652, found 355.1655.

(S,Z)-N-(4-(((benzyloxy)carbonyl)amino)-4-carboxybutyl)-1-phenylmethanimine oxide (51)

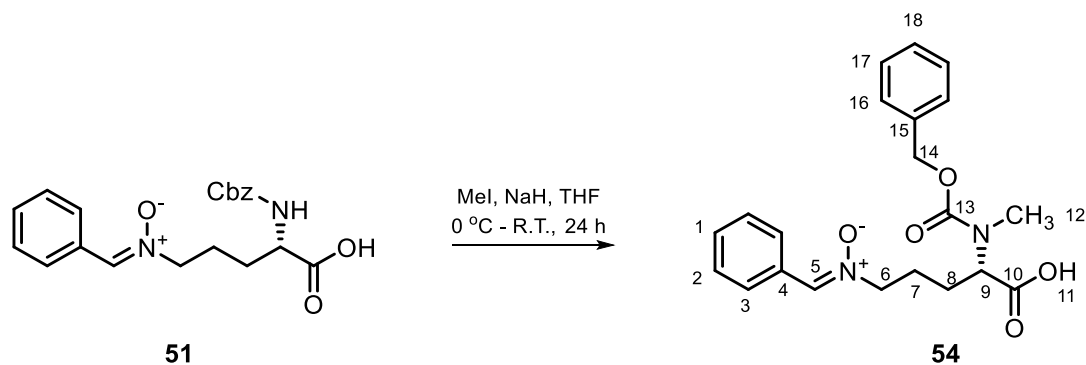


A stirred solution of (S,E)-5-(benzylideneamino)-2-(((benzyloxy)carbonyl)amino)pentanoic acid (**67**) (6.93 g, 17.65 mmol, 1 eq) in methanol (32 mL) was cooled to 0 °C in an ice bath. A pressure equalising dropping funnel was fitted to which was added freshly prepared *m*CPBA (3.42 g, 19.8 mmol, 1.12 eq) in methanol (13 mL) and the dropping funnel stoppered. The *m*CPBA solution was then added dropwise to the reaction mix over an hour. Upon complete addition of the *m*CPBA solution the reaction mix was allowed to stir at 0 °C for an additional hour. After this time the reaction mix was concentrated under reduced pressure and partitioned between EtOAc (50 mL) and water (50 mL) and the aqueous layer acidified to pH2 (HCl_{aq}). The layers were then separated and the aqueous layer extracted with a EtOAc (50 mL). The combined organic layers were washed with brine (50 mL), dried over sodium sulphate, filtered and concentrated to give crude oxaziridine as a white solid that was used without further purification.

To the crude oxaziridine was added TFA (8 mL) followed by DCM (8 mL) and the resulting solution was stirred at room temperature for 1 hour. After this time the solution was evaporated under reduced pressure and the resulting slurry was dissolved in EtOAc (32 mL). Hexane (64 mL) was then added, followed by the addition of benzaldehyde (1 mL, 9.84 mmol) and the mixture was then stirred at room temperature overnight, yielding a cloudy suspension. The solution was cooled in an ice bath for 2 h and the solid collected via filtration, washed with EtOAc (3 x 50 mL) and dried to give (S,Z)-N-(4-(((benzyloxy)carbonyl)amino)-4-carboxybutyl)-1-phenylmethanimine oxide (**51**) (5.171 g, 14.0 mmol, 76% from Cbz-L-Ornithine) as an off white solid. X-ray grade crystals were grown from slow evaporation in methanol.

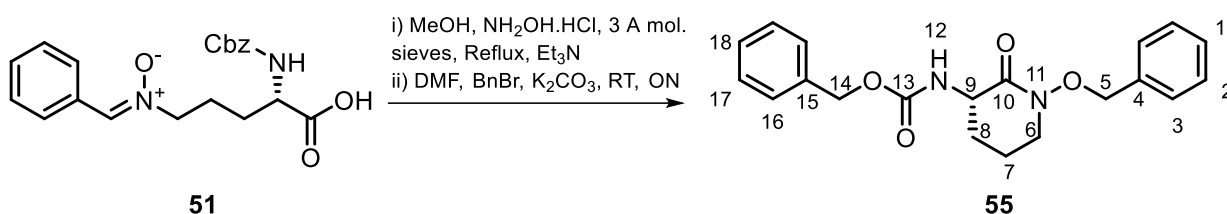
Mp = 148 – 151 °C. $[\alpha]_D = -4.4^\circ$ ($c = 1.0$, MeOH). ^1H NMR (300 MHz, DMSO- d_6) δ 12.65 (s, 1H¹¹), 8.28 – 8.20 (m, 2H), 7.86 (s, 1H⁵), 7.66 (d, $J = 8.1$ Hz, 1H¹²), 7.49 – 7.25 (m, 8H), 5.03 (s, 2H¹⁴), 4.07 – 3.95 (m, 1H⁹), 3.91 (t, $J = 6.7$ Hz, 2H⁶), 1.96 – 1.85 (m, 2H⁷), 1.82 – 1.68 (m, 1H⁸), 1.68 – 1.55 (m, 1H⁸). ^{13}C NMR (75 MHz, DMSO- d_6) δ 173.6¹⁰, 156.1¹³, 137.0, 133.3⁵, 131.0, 129.8, 128.3, 127.9, 127.8, 127.7¹⁴, 65.5⁶, 65.4, 59.8, 53.5⁹, 27.8⁸, 24.1⁷. IR (neat): $\nu_{\text{max}}/\text{cm}^{-1}$ 2952.7, 1710.0, 1660.2, 1200.1, 697.1. HRMS (pNSI) calcd for C₂₀H₂₃N₂O₅ [M+H]⁺: 371.1607, found 371.1601.

(*S,Z*)-*N*-(4-(((benzyloxy)carbonyl)(methyl)amino)-4-carboxybutyl)-1-phenylmethanimine oxide (54**)**



To a stirred suspension of (*S,Z*)-*N*-(4-(((benzyloxy)carbonyl)amino)-4-carboxybutyl)-1-phenylmethanimine oxide (**51**) (1.00 g, 2.70 mmol, 1.0 eq) in THF (40 mL) under nitrogen at 0 °C was added methyl iodide (1.3 mL, 21.6 mmol) followed by sodium hydride (0.324 g, 8.1 mmol, 60 % weight dispersion in mineral oil). The solution was then stirred at room temperature for 24 h. After this time the reaction was quenched via the addition of methanol. The reaction mix was concentrated under a flow on nitrogen until a yellow residue resulted. The residue was partitioned between Et₂O (75 mL) and H₂O (40 mL). After separation of the layers, the aqueous layer was acidified with 2 M HCl and extracted with 3 x 30 mL EtOAc. The organic layers were combined, washed with brine, dried with sodium sulphate, filtered and evaporated under reduced pressure. The sample was then taken and stirred overnight in Et₂O/hexane to give (*S,Z*)-*N*-(4-(((benzyloxy)carbonyl)(methyl)amino)-4-carboxybutyl)-1-phenylmethanimine oxide (**54**) (0.644 g, 1.68 mmol, 62%) as a yellow powder

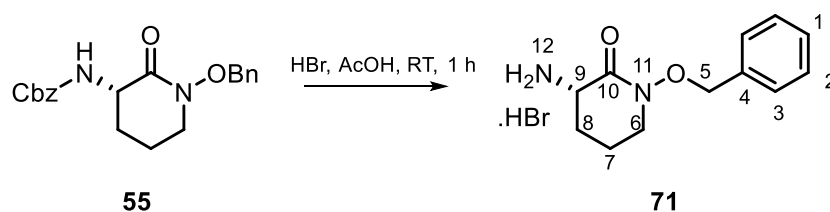
[α]_D = -13.2 (*c* = 1.0, MeOH) ¹H NMR (700 MHz, DMSO-*d*₆, 352 K) δ 8.24 (dd, *J* = 8.0, 1.7 Hz, 2H), 7.96 (dd, *J* = 8.3, 1.4 Hz, 1H), 7.92 – 7.89 (m, 2H), 7.78 (d, *J* = 3.3 Hz, 1H), 7.68 (ddd, *J* = 8.0, 2.1, 1.2 Hz, 1H), 7.62 (tt, *J* = 7.6, 1.4 Hz, 1H), 7.56 – 7.52 (m, 1H), 7.52 – 7.48 (m, 1H), 7.44 – 7.39 (m, 3H), 7.36 (t, *J* = 3.8 Hz, 3H), 7.33 – 7.28 (m, 1H), 5.12 (s, 2H), 4.57 (s, 1H), 3.95 (t, *J* = 6.6 Hz, 2H), 2.84 (s, 3H), 2.00 – 1.90 (m, 1H), 1.90 – 1.76 (m, 3H). ¹³C NMR (176 MHz, DMSO-*d*₆, 352 K) δ 172.5, 167.7, 166.4, 156.6, 137.4, 133.9, 133.6, 133.5, 133.1, 133.0, 131.6, 131.0, 130.0, 129.7, 129.3, 128.9, 128.8, 128.7, 128.2, 127.8, 67.0, 66.0, 58.9, 31.2, 25.8, 24.8. IR (neat): ν_{\max} /cm⁻¹ 1948.0, 1688.2, 1604.4 HRMS (pNSI) calcd for C₂₁H₂₃N₂O₅ [M-H]⁻: 383.1612, found 383.1606.

benzyl (S)-(1-(benzyloxy)-2-oxopiperidin-3-yl)carbamate (55)

To a stirred solution of (S,Z)-N-(4-(((benzyloxy)carbonyl)amino)-4-carboxybutyl)-1-phenylmethanimine oxide (**51**) (1.00 g, 2.70 mmol) in methanol (27 mL) was added hydroxylamine hydrochloride (0.20 g, 2.84 mmol, 1.05 eq) and the reaction heated to reflux for 20 minutes. After this time 3 Å mol. sieves were added followed by Et₃N and the mixture stirred for an additional hour. After this time the mixture was filtered through a pad of celite and the filtrate evaporated under reduced pressure. This was taken and partitioned between EtOAc (30 mL) and water (15 mL) and the organics separated, dried (Na₂SO₄) and evaporated to give the crude hydroxamic acid as a orange/red residue. The residue was dissolved in DMF (4 mL) followed by the addition of K₂CO₃ (3.73 g, 27 mmol, 10 eq) and benzyl bromide (1.44 mL, 13.5 mmol, 5 eq). The mixture was stirred at room temperature overnight and then diluted with EtOAc (50 mL). The resulting slurry was then washed with water (3 x 50 mL), brine (50 mL), dried over sodium sulphate, filtered and concentrated under reduced pressure. The crude residue was then subjected to silica gel column chromatography (EtOAc/DCM 1:8, R_f = 0.2), to yield benzyl (S)-(1-(benzyloxy)-2-oxopiperidin-3-yl)carbamate (**55**) (0.546 g, 1.54 mmol, 57%) as a white solid. X-Ray grade crystals were grown from slow evaporation of a 10mg/mL solution in methanol.

Mp = 86-89 °C. $[\alpha]_D = +23.2^\circ$ (c = 1.0, MeOH). ¹H NMR (400 MHz, Chloroform-*d*) δ 7.64 – 7.14 (m, 10H^{1-3, 15-18}), 5.70 (br-s, 1H¹²), 5.12 (s, 2H¹⁴), 4.97 (d, J = 10.6 Hz, 1H^{5a}), 4.89 (d, J = 10.6 Hz, 1H^{5b}), 4.17 (dt, J = 11.6, 5.2 Hz, 1H⁹), 3.55 – 3.37 (m, 1H^{6a}), 3.37 – 3.22 (m, 1H^{6b}), 2.53 – 2.33 (m, 1H^{8a}), 1.94 – 1.72 (m, 2H⁷), 1.54 (qd, J = 12.5, 4.0 Hz, 1H^{8b}). ¹³C NMR (101 MHz, Chloroform-*d*) δ 167.8¹⁰, 156.4¹³, 156.3, 136.3, 135.2, 128.8, 128.1, 76.0⁵, 66.9¹⁴, 52.8⁹, 51.4⁶, 28.2⁸, 20.8⁷. IR (neat): $\nu_{\max}/\text{cm}^{-1}$ 3304.1, 1688.0, 1658.5. HRMS (pNSI) calcd for C₂₀H₂₃N₂O₅ [M+Na]⁺: 377.1472, found 377.1464.

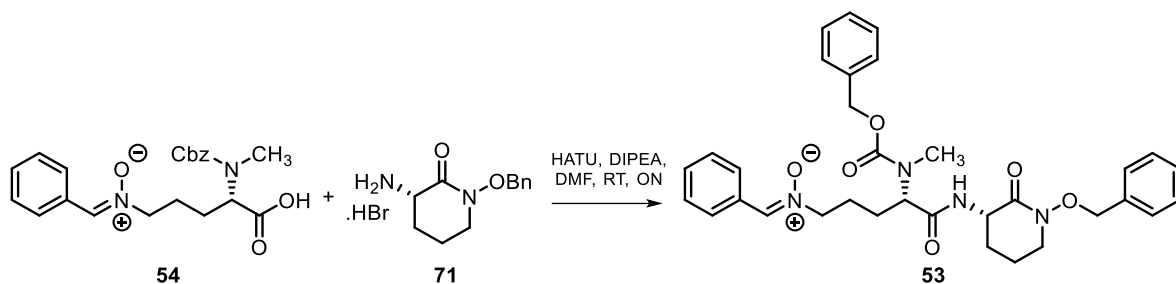
(S)-1-(benzyloxy)-2-oxopiperidin-3-aminium bromide (71)



To a 100 mL round bottomed flask fitted with a subaseal was added benzyl (S)-1-(benzyloxy)-2-oxopiperidin-3-yl)carbamate (**55**) (1.00 g, 2.82 mmol, 1.0 eq) and DCM (20 mL) and a nitrogen atmosphere was introduced. To this was added HBr 33% in acetic acid (20 mL) dropwise via syringe. The reaction mix was stirred at room temperature for 1 hour and after this time the reaction mix was concentrated under a flow on nitrogen until a dark orange solid resulted. The solid was then dissolved in chloroform (40 mL) and evaporated under reduced pressure and repeated twice more. The residue was then dissolved in chloroform, hexane added and the mixture stirred overnight, yielding the product as a triturated powder. The powder was filtered, washed with petrol and dried to yield pure 3-amino-1-(benzyloxy)piperidin-2-one hydrobromide (**71**) (8.05 g, 2.43 mmol, 86%) as a red solid. X-Ray grade crystals were grown from slow evaporation in methanol.

$[\alpha]_D = +43.0^\circ$ ($c = 1$, MeOH). $^1\text{H NMR}$ (300 MHz, Deuterium Oxide) δ 7.61 – 7.37 (m, 5H), 5.00 (s, 2H), 4.10 (dd, $J = 11.7, 5.7$ Hz, 1H), 3.75 – 3.53 (m, 2H), 2.38 – 2.22 (m, 1H), 2.18 – 2.06 (m, 1H), 2.04 – 1.70 (m, 2H). $^{13}\text{C NMR}$ (75 MHz, Deuterium Oxide) δ 164.8, 134.0, 130.0, 129.4, 128.8, 75.8, 50.3, 49.7, 24.6, 19.7. IR (neat): $\nu_{\text{max}}/\text{cm}^{-1}$ 3080.5, 1676.8. HRMS (pNSI) calcd for $\text{C}_{12}\text{H}_{17}\text{N}_2\text{O}_2$ [M-Br] $^+$: 221.1285, found 221.1288

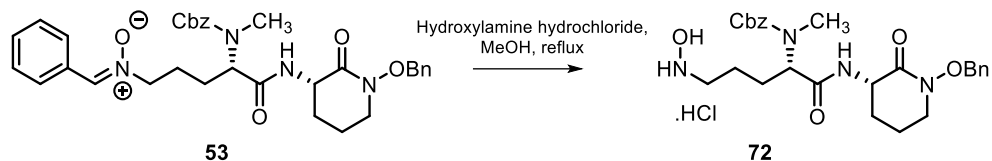
(Z)-N-((S)-5-(((S)-1-(benzyloxy)-2-oxopiperidin-3-yl)amino)-4-(((benzyloxy)carbonyl)(methyl)amino)-5-oxopentyl)-1-phenylmethanimine oxide (53)



To a stirred suspension of benzyl (S)-1-(1-(benzyloxy)-2-oxopiperidin-3-yl)carbamate (**54**) (0.313 g, 1.04 mmol, 1.0 eq) in DMF (5 mL) under nitrogen at room temperature was added HATU (0.435 g, 1.14 mmol, 1.1 eq) and the yellow coloured solution stirred for 5 minutes. After this time 3-amino-1-(benzyloxy)piperidin-2-one hydrobromide (**71**) (0.400 g, 1.04 mmol, 1.0 eq) was added and the reaction took on a darker colouration. The reaction was stirred for an additional 20 minutes at room temperature followed by the injection of DIPEA (0.53 mL, 3.02 mmol, 2.9 eq) and the resulting dark orange reaction mix stirred at room temperature overnight. After this time, the reaction mix was diluted with water (20 mL) and extracted with DCM (2 x 50 mL). The organic layers were combined, washed with sat. NaHCO_{3(aq)} (50 mL), hydrochloric acid (50 mL) and then washed a further three times with water (3 x 50 mL). The organic later was then washed with brine, dried over sodium sulphate, filtered and concentrated under reduced pressure to yield the crude product. The crude material was then taken and purified via column chromatography (DCM/MeOH 9.5:0.5) and gave pure (Z)-N-((S)-5-(((S)-1-(benzyloxy)-2-oxopiperidin-3-yl)amino)-4-(((benzyloxy)carbonyl)(methyl)amino)-5-oxopentyl)-1-phenylmethanimine oxide (**53**) as an off white foam. (0.426 g, 0.727 mmol) 70%.

¹H NMR (700 MHz, DMSO-*d*₆, 348 K) δ 8.32 – 8.15 (m, 2H), 8.00 (d, *J* = 8.2 Hz, 1H), 7.80 (d, *J* = 6.4 Hz, 1H), 7.50 – 7.20 (m, 14H), 5.20 – 5.09 (m, 2H), 4.90 – 4.82 (m, 2H), 4.63 (s, 1H), 4.40 – 4.26 (m, 1H), 3.95 (t, *J* = 7.1 Hz, 2H), 3.52 – 3.42 (m, 2H), 2.85 (d, *J* = 1.0 Hz, 3H), 2.02 – 1.91 (m, 1H), 1.91 – 1.76 (m, 4H), 1.76 – 1.64 (m, 2H). ¹³C NMR (176 MHz, DMSO-*d*₆) δ 170.4, 166.5, 137.4, 136.2, 133.5, 131.6, 130.0, 129.5, 128.8, 128.7, 128.7, 128.6, 128.4, 128.1, 127.8, 75.2, 67.0, 66.1, 50.9, 50.5, 30.4, 27.9, 26.1, 24.7, 21.1. HRMS (pNSI) calcd for C₃₃H₃₉N₄O₆ [M+H]⁺: 587.2864, found 587.2869.

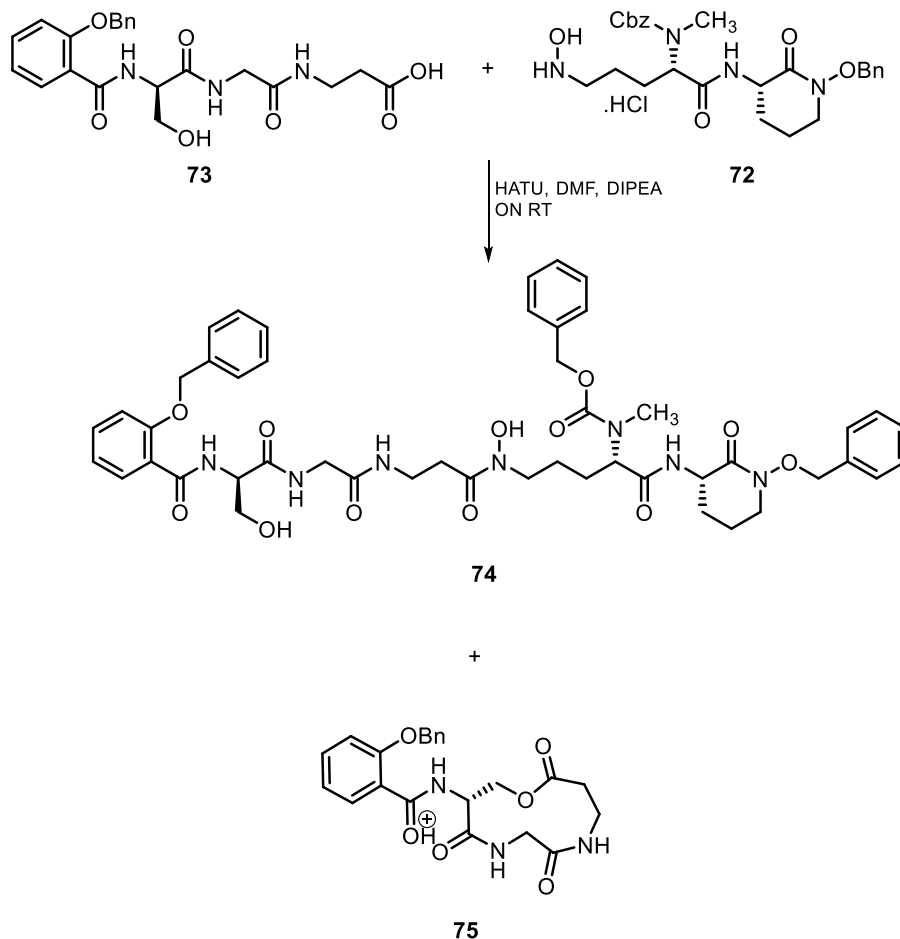
***N*-((*S*)-5-(((*S*)-1-(benzyloxy)-2-oxopiperidin-3-yl)amino)-4-(((benzyloxy)carbonyl)(methyl)amino)-5-oxopentyl)hydroxylammonium chloride (**72**)**



To a stirred suspension of (*Z*)-*N*-((*S*)-5-(((*S*)-1-(benzyloxy)-2-oxopiperidin-3-yl)amino)-4-(((benzyloxy)carbonyl)(methyl)amino)-5-oxopentyl)-1-phenylmethanimine oxide (**53**) (0.193 g, 0.329 mmol, 1.0 eq) in methanol (5 mL) under nitrogen at room temperature was added hydroxylamine hydrochloride (0.024 g, 0.345 mmol, 1.05 eq) and reaction mix refluxed for 20 minutes. After this time, the reaction mix was concentrated under reduced pressure and the residue triturated with MeOH/Et₂O (1:3) and the solid collected by vacuum filtration. This solid was then dissolved again in methanol and evaporated under reduced pressure give crude *N*-((*S*)-5-(((*S*)-1-(benzyloxy)-2-oxopiperidin-3-yl)amino)-4-(((benzyloxy)carbonyl)(methyl)amino)-5-oxopentyl)hydroxylammonium chloride (**72**) which was used without further purification.

HRMS (pNSI) calcd for C₂₆H₃₅N₄O₆ [M+H]⁺: 499.2551, found 499.2535

benzyl ((3R,16S)-17-(((S)-1-(benzyloxy)-2-oxopiperidin-3-yl)amino)-1-(2-(benzyloxy)phenyl)-12-hydroxy-3-(hydroxymethyl)-1,4,7,11,17-pentaoxo-2,5,8,12-tetraazaheptadecan-16-yl)(methyl)carbamate (**74**)



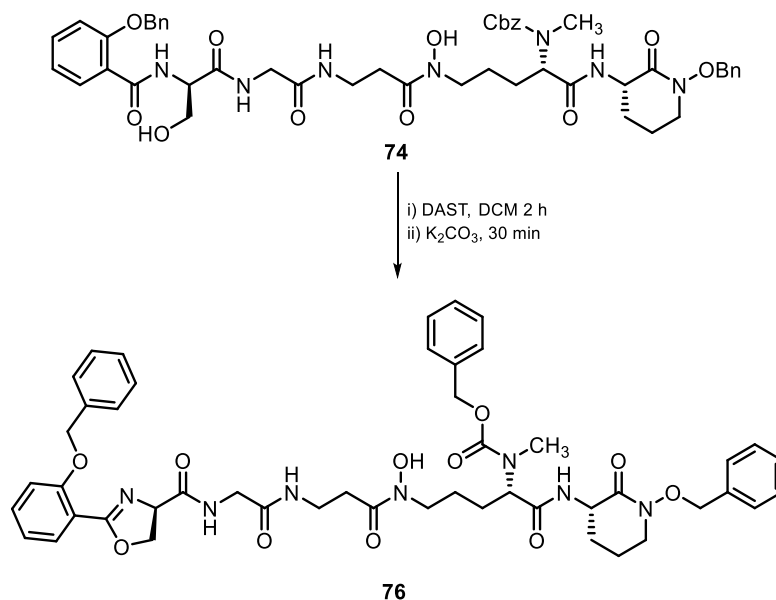
To a solution of (*R*)-3-(2-(2-(2-(benzyloxy)benzamido)-3-hydroxypropanamido)acetamido)propanoic acid (**73**) (0.155 g, 0.35 mmol, 1.0eq) in DMF (3 mL) under nitrogen at room temperature was added HATU (0.146 g, 0.384 mmol, 1.1eq) and the solution stirred for 10 minutes. After this time *N*-((*S*)-5-(((*S*)-1-(benzyloxy)-2-oxopiperidin-3-yl)amino)-4-(((benzyloxy)carbonyl) (methyl)amino)-5-oxopentyl)hydroxylammonium chloride (**72**) (0.176 g, 0.363 mmol, 1.4eq) was added and the reaction was stirred for an additional 20 minutes. After this time DIPEA (0.24 mL, 1.36 mmol, 3.9 eq) was added and the reaction mix stirred at room temperature overnight. After this time, the reaction mix was diluted with water (20 mL) and extracted with DCM (2 x 50 mL). The organic layers were combined, washed with sat. NaHCO_{3(aq)} (50 mL), 0.2 M hydrochloric acid (50 mL) and then washed a further three times with water (3 x 50 mL). The organic later was then washed with brine, dried over sodium

sulphate, filtered and concentrated under reduced pressure. The crude material was then subjected to silica gel column chromatography (DCM/MeOH 9:1 $R_f = 0.1$) to give pure benzyl ((3*R*,16*S*)-17-(((*S*)-1-(benzyloxy)-2-oxopiperidin-3-yl)amino)-1-(2-(benzyloxy)phenyl)-12-hydroxy-3-(hydroxymethyl)-1,4,7,11,17-pentaoxo-2,5,8,12-tetraazaheptadecan-16-yl)(methyl)carbamate (**74**) (0.120 g, 0.13 mmol 38%) as a yellow tinted oil.

^1H NMR (300 MHz, Chloroform-*d*) δ 9.39 – 9.08 (m, 1H), 8.72 – 8.49 (m, 1H), 8.17 – 7.96 (m, 1H), 7.76 – 7.58 (m, 1H), 7.56 – 7.19 (m, 17H), 7.12 – 6.95 (m, 2H), 5.20 (s, 2H), 5.11 (s, 2H), 4.91 (d, $J = 10.5$ Hz, 1H), 4.83 (d, $J = 10.5$ Hz, 1H), 4.69 – 4.51 (m, 1H), 4.53 – 4.39 (m, 1H), 4.35 – 4.13 (m, 1H), 3.97 – 3.74 (m, 3H), 3.67 – 3.54 (m, 3H), 3.45 – 3.36 (m, 2H), 3.35 – 3.21 (m, 1H), 2.93 (s, 3H), 2.90 – 2.78 (m, 1H), 2.63 – 2.46 (m, 1H), 2.36 – 2.17 (m, 1H), 2.15 – 1.97 (m, 1H), 1.97 – 1.27 (m, 8H). ^{13}C NMR (75 MHz, Chloroform-*d*) δ 172.8, 172.0, 171.9, 169.9, 167.9, 166.1, 157.0, 136.6, 135.6, 135.0, 133.4, 131.9, 129.5, 129.0, 128.9, 128.7, 128.67, 128.6, 128.1, 128.0, 127.9, 127.8, 121.6, 121.3, 113.1, 76.0, 71.4, 67.7, 62.8, 57.7, 56.0, 53.6, 51.0, 50.7, 48.4, 46.7, 43.4, 35.7, 32.2, 29.8, 27.6, 25.5, 22.6, 22.6, 21.0. HRMS (pNSI) calcd for $\text{C}_{40}\text{H}_{58}\text{N}_7\text{O}_{12}$ $[\text{M}+\text{H}]^+$: 924.4138, found 924.4143.

In addition to (**74**), compound (**75**) was also isolated as a co-eluting mixture of by-products and as such does not have an accurate isolated yield or NMR. However the structure was solved via X-ray crystallography (see appendix)

benzyl ((*S*)-1-(((*S*)-1-(benzyloxy)-2-oxopiperidin-3-yl)amino)-5-(3-(2-((*R*)-2-(2-(benzyloxy)phenyl)-4,5-dihydrooxazole-4-carboxamido)acetamido)-*N*-hydroxypropanamido)-1-oxopentan-2-yl)(methyl) carbamate (**76**)



To a solution of benzyl ((3*R*,16*S*)-17-(((*S*)-1-(benzyloxy)-2-oxopiperidin-3-yl)amino)-1-(2-(benzyloxy)phenyl)-12-hydroxy-3-(hydroxymethyl)-1,4,7,11,17-pentaoxo-2,5,8,12-tetraazah-*heptadecan-16-yl*)(methyl)carbamate (**74**) (30 mg, 0.033 mmol, 1.0eq) in dry DCM (1 mL) under nitrogen at -78 °C was added DAST (5.2 μL, 0.039 mmol, 1.2eq). After addition the reaction was removed from the acetone/dry ice bath and the solution stirred for a further 2 hours. After this time K₂CO₃ (11 mg, 0.08 mmol, 2.5eq) was added in one portion and the solution stirred for an additional 30 minutes. The reaction mix was then diluted with DCM (10 mL) and washed with water (20 mL), brine (20 mL), dried over sodium sulphate and concentrated under reduced pressure to yield benzyl ((*S*)-1-(((*S*)-1-(benzyloxy)-2-oxopiperidin-3-yl)amino)-5-(3-(2-(2-(((*R*)-2-(2-(benzyloxy)phenyl)-4,5-dihydrooxazol-4-yl)amino)acetamido)acetamido)-*N*-hydroxypropanamido)-1-oxopentan-2-yl)(methyl)carbamate (**76**) (7 mg, 0.008 mmol, 23%) as a yellow oil.

HRMS (pNSI) calcd for C₄₈H₅₆N₇O₁₁ [M+H]⁺: 906.4032, found 906.4036.

NMR assignment of DEM30616/A (79)

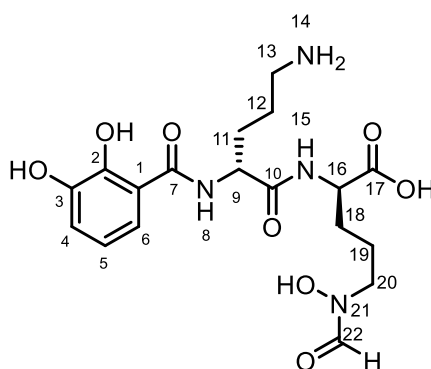
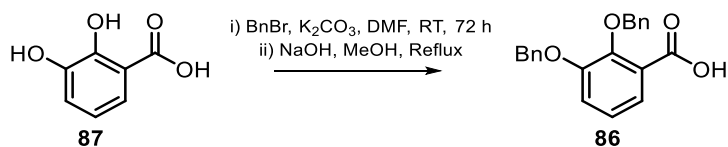


Table 16. NMR data for DEM30616/A in D₂O at 298 K, 700 MHz, ¹H NMR collected at 700 MHz, ¹³C{¹H} NMR collected at 176 MHz, ¹⁵N shifts were measured indirectly by ¹H-¹⁵N HMBC performed at both 8 and 12 Hz, referencing against nitromethane

Position	δ_{1H} multi, (J in Hz)	δ_{13C}	δ_{15N}	HMBC
1	-	116.4		
2	-	146.3 or		
3	-	144.4		
4	6.98 (dd, J = 7.9, 1.5 Hz, 1H)	119.5		H to C1, 2, 3, 5, 6
5	6.76 (t, J = 8.0 Hz, 1H)	119.6		H to C1, 2, 3, 4, 6, 7
6	7.18 (dd, J = 8.1, 1.6 Hz, 1H)	119.2		H to C1, 2, 3, 4, 5, 7
7	-	169.8		
8	-	-	-260.5	
9	4.53 (dd, J = 7.8, 6.4 Hz, 1H)	53.2		H to C1, 7, 10, 11, 12
10	-	172.6		-
11	1.98 – 1.91 (m, 1H) 1.89 – 1.82 (m, 1H)	27.8		H to C9, 10, 12, 13
12	a) 1.80 – 1.71 (m, 3H) (2H)	23.1		*
13	2.99 (ddd, J = 8.6, 6.9, 2.1 Hz, 2H)	38.8		H to C11, 12
14	-	-	-348.8	
15	-	-	-252.9	
16	4.21 – 4.13 (m, 1H)	54.6		H to C10, 17, 18, 19
17	-	178.1		
18	b) 1.80 – 1.71 (m, 3H) (1H) b) 1.69 – 1.60 (m, 3H) (1H)	28.2		*
19	a) 1.69 – 1.60 (m, 3H) (2H)	22.7		*
20	3.56 – 3.44 (m, 2H)	50.0		H to C16, 18, 19, 22
21	-	-	-199.3	
22	7.83 and 8.18 (2 x s, 1H)	159.4		H to C20

*Unknown due to signal overlap

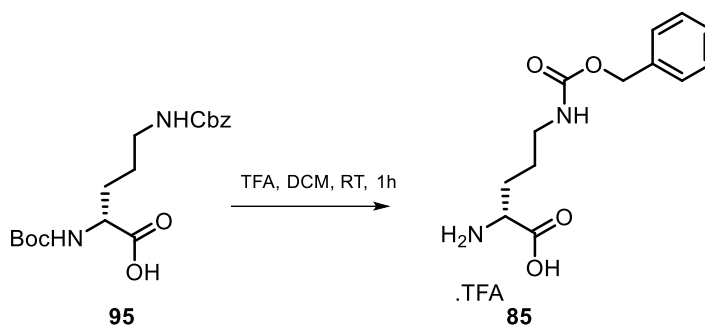
2,3-bis(benzyloxy)benzoic acid (**86**)



To a schlenk flask under nitrogen was added K₂CO₃ (2.142 g, 15.5 mmol, 3.1 eq) and 2,3-dihydroxybenzoic acid (**87**) (0.771 g, 5.0 mmol, 1 eq) and the mixture suspended in dry DMF (5 mL). Benzyl bromide (1.84 mL, 15.5 mmol, 3.1 eq) was added dropwise and the reaction stirred for 72 hours at room temperature. After this time the reaction mixture was diluted with water (75 mL) and the aqueous extracted with EtOAc (3 x 25 mL) to obtain the benzyl ester. The combined organic layers were then washed with water (3 x 25 mL), brine (50 mL), dried (Na₂SO₄), filtered and then evaporated under reduced pressure to yield the crude benzyl ester. The crude benzyl ester was then dissolved in methanol (8.33 mL) and 2 M NaOH (8.33 mL) was added and. The reaction mixture was then stirred and heated to reflux for 8 hours. After this time the mixture was allowed to cool to room temperature, diluted with water (20 mL) and the aqueous layer washed with diethyl ether (2 x 20 mL). The aqueous layer was then acidified to pH 2 (2 M HCl) and extracted with ethyl acetate (3 x 25 mL). The combined organic layers were then washed with brine (50 mL), dried (Na₂SO₄), filtered and evaporated under reduced pressure to yield 2,3-bis(benzyloxy)benzoic acid (**86**) (1.271 g, 1.80 mmol, 76%) as a white solid.

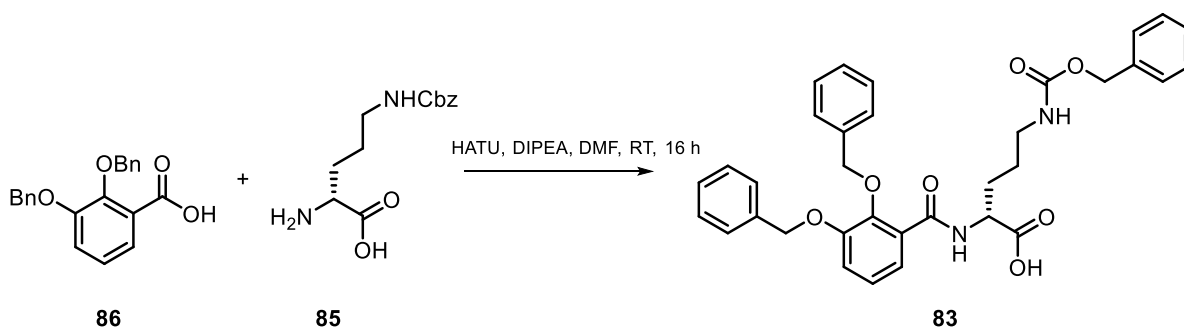
¹H NMR (300 MHz, Chloroform-*d*) δ 11.38 (br-s, 1H), 7.80 (dd, *J* = 7.8, 1.7 Hz, 1H), 7.59 – 7.17 (m, 12H), 5.32 (s, 2H), 5.25 (s, 2H). ¹³C NMR (75 MHz, Chloroform-*d*) δ 165.2, 151.4, 147.2, 136.0, 134.7, 129.5, 129.5, 129.0, 129.0, 128.7, 127.9, 125.2, 124.6, 123.1, 119.1, 77.3, 71.7. IR (neat): $\nu_{\text{max}}/\text{cm}^{-1}$ 3325, 2930, 2851, 1736, 1625, 1216, 736 HRMS (pNSI) calcd for C₁₈H₂₀NO₅ [M+H]⁺: 330.1336, found 330.1337

4-(((benzyloxy)carbonyl)amino)-1-carboxybutan-1-aminium 2,2,2-trifluoroacetate (85)



To a solution of ((R)-5-(((benzyloxy)carbonyl)amino)-2-((tert-butoxycarbonyl)amino)pentanoic acid (**95**) (1.415 g, 4.1 mmol) in dry DCM (22 mL) was added TFA (22 mL). The mixture was stirred at RT for 1 h after which time the solvent was removed under reduced pressure. The residue was then triturated with Et₂O to yield 4-(((benzyloxy)carbonyl)amino)-1-carboxybutan-1-aminium 2,2,2-trifluoroacetate (**85**) (0.974 g) as a pink solid that was used without further purification.

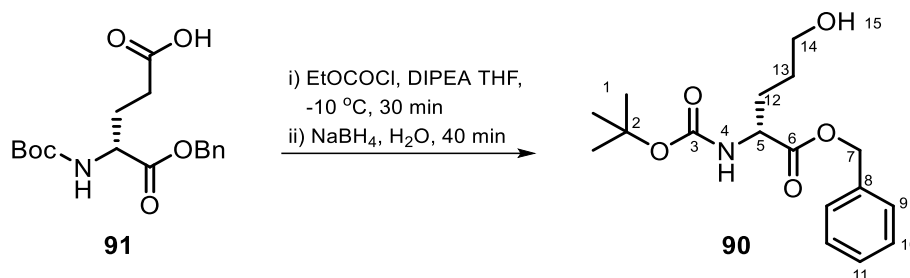
(*R*)-5-(((benzyloxy)carbonyl)amino)-2-(2,3-bis(benzyloxy)benzamido)pentanoic acid (83**)**



In a RBF 2,3-bis(benzyloxy)benzoic acid (**86**) (1.00g, 2.99 mmol, 1eq) was added dry DMF (25 mL). HATU (1.14 g, 2.99 mmol, 1eq) and the reaction mix stirred at room temperature for 10 mins. 2-amino-5-(((benzyloxy)carbonyl)amino)pentanoic acid (**85**) (0.679 g, 2.99 mmol, 1eq) was dissolved in 5 mL dry DMF and added followed by the addition of DIPEA (1.70 mL, 9.87 mmol) and the reaction mix stirred for 16 h at room temperature. The reaction was quenched with H₂O before being diluted with EtOAc (30 mL). This was then washed with 0.2M NaOH (3 x 30 mL), 0.4M HCl (3 x 30 mL) and then and brine (30 mL). The organics were then dried over sodium sulphate, filtered and evaporated under reduced pressure to give a yellow oil. The crude mixture was then purified via silica gel column chromatography (MeOH/DCM/Acetic acid 0.5:9.5:0.1 *R_f* = 0.30) to give (*R*)-5-(((benzyloxy)carbonyl)amino)-2-(2,3-bis(benzyloxy)benzamido)pentanoic acid (**83**) (0.550 g, 0.94 mmol, 32%) as a yellow foam.

¹H NMR (700 MHz, DMSO-*d*₆) δ 8.52 (d, *J* = 7.5 Hz, 1H), 7.55 – 7.46 (m, 2H), 7.45 – 7.22 (m, 18H), 7.16 (t, *J* = 8.0 Hz, 2H), 5.21 (s, 2H), 5.09 (d, *J* = 10.4 Hz, 1H), 5.01 (d, *J* = 10.4 Hz, 1H), 4.99 (s, 2H), 4.34 (q, *J* = 6.8 Hz, 1H), 2.94 (dq, *J* = 13.5, 6.7 Hz, 2H), 1.81 – 1.73 (m, 1H), 1.56 (dq, *J* = 15.0, 7.9 Hz, 1H), 1.42 (p, *J* = 7.3 Hz, 2H). ¹³C NMR (176 MHz, DMSO-*d*₆) δ 174.2, 165.1, 156.5, 152.1, 146.1, 137.7, 137.1, 129.5, 129.1, 128.9, 128.8, 128.5, 128.5, 128.5, 128.2, 124.6, 121.9, 116.9, 75.6, 70.8, 65.6, 53.1, 38.7, 29.4, 26.4. HRMS (pNSI) calcd for C₃₄H₃₃N₂O₇ [M-H]⁻: 581.2293, found 581.2284

benzyl (R)-2-((tert-butoxycarbonyl)amino)-5-hydroxypentanoate (90)

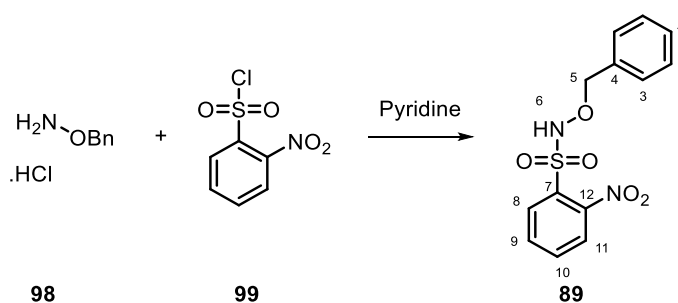


To a 100 mL round bottomed flask under an atmosphere of nitrogen was added (*R*)-5-(benzyloxy)-4-((tert-butoxycarbonyl)amino)-5-oxopentanoic acid (**91**) (0.765 g, 2.27 mmol, 1 eq) and dry THF (11 mL) was added. The mixture was cooled to -10 °C and stirred for 20 minutes. After this time, DIPEA (2.35 mmol, 0.41 mL, 1.04 eq) and ethyl chloroformate (2.58 mmol, 0.25 mL, 1.14 eq) were added dropwise from two separate syringes at the same time over 10 minutes. Upon complete addition the reaction mix was stirred for a further 30 minutes, after which time sodium borohydride (6.75 mmol, 0.255 g, 3 eq) was added in one portion. The reaction mix then removed from the cold bath and allowed to warm to room temperature, after which point, H₂O (5 mL) was added dropwise over 10 minutes. Upon complete addition the mixture was left to stir for 30 minutes before brine (5 mL) was added. The mixture was then extracted with EtOAc (3 x 50 mL) and the combined organic layers were washed with saturated sodium bicarbonate (20 mL), saturated ammonium chloride (20 mL) and finally brine (20 mL). The organics were then dried over sodium sulphate, filtered and evaporated under reduced pressure to give a clear colourless oil. The crude mixture was then purified via column chromatography (ethyl acetate/petrol 40-60 1:2, R_f = 0.12) to give benzyl (*R*)-2-((tert-butoxycarbonyl)amino)-5-hydroxypentanoate (**90**) (0.550 g, 1.70 mmol, 75%) as a clear colourless oil.

[α]_D = +21.2° ¹H NMR (300 MHz, Chloroform-*d*) δ 7.32 (d, *J* = 3.1 Hz, 5H⁹⁻¹¹), 5.29 (d, *J* = 8.4 Hz, 1H⁴), 5.21 – 5.09 (m, 2H⁷), 4.44 – 4.24 (m, 1H⁵), 3.58 (t, *J* = 6.1 Hz, 2H¹⁴), 2.37 (s, 1H¹⁵), 2.01 – 1.80 (m, 1H¹²), 1.80 – 1.65 (m, 1H¹²), 1.65 – 1.48 (m, 2H¹³), 1.41 (s, 9H¹). ¹³C NMR (75 MHz, Chloroform-*d*) δ 172.7⁶, 155.6³, 135.4, 128.6, 128.5, 128.3, 80.0², 67.1⁷, 61.9¹⁴, 53.3⁵, 29.3¹²,

28.4¹³, 28.3¹. IR (neat): $\nu_{\max}/\text{cm}^{-1}$ 3373.8 (OH), 1737.7 (C=O ester), 1693.4 (C=O amide). HRMS (pNSI) calcd for C₁₇H₂₆N₁O₅ [M+H]⁺: 324.1805, found 324.1809.

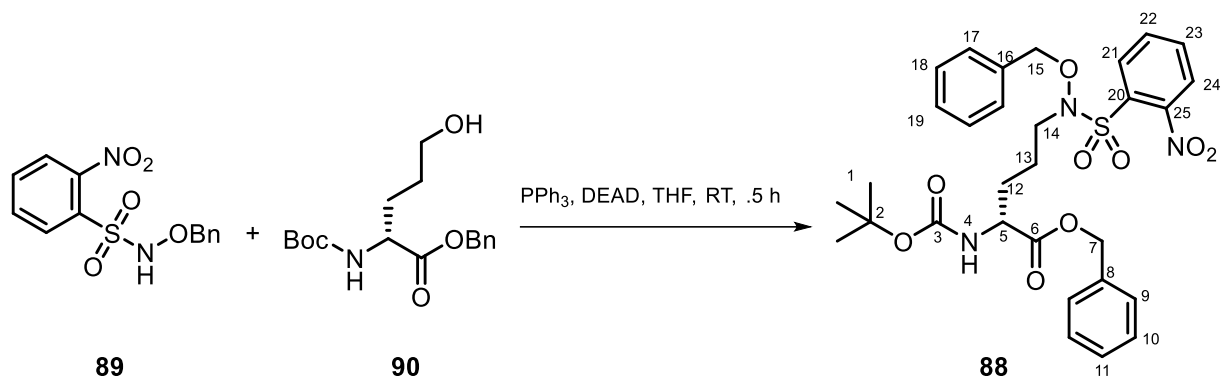
N-(benzyloxy)benzenesulfonamide (**89**)



A stirred solution of *O*-benzylhydroxylamine hydrochloride (**98**) (2.400 g, 15.0 mmol, 1eq) in dry pyridine (20 mL) (0.2 mL) was cooled to 0 °C in an ice bath. To this solution was added dropwise a solution of 2-nitrobenzenesulfonyl chloride (**99**) (3.37 g, 15.2 mmol, 1.1eq) in dry pyridine (20 mL) over 20 minutes. The reaction mixture was stirred at 0 °C for an additional hour after which the ice bath was removed, and the reaction mix left to stir for an additional 4 hours. After this time, the reaction mix was quenched with the addition of water (40 mL) and the mixture extracted with DCM (2 x 20 mL). The organic layers were combined, washed with 0.2 M HCl (3 x 10 mL), dried over sodium sulphate and concentrated under reduced pressure. The resulting solids were then dissolved in the minimum amount of CHCl₃ and methanol added to promote crystallisation. The crystals were collected via filtration and washed with cold methanol (30 mL) to give *N*-(benzyloxy)benzenesulfonamide (**89**) (2.26 g, 7.4 mmol, 49%) as colourless crystals. X-Ray grade crystals were generated at the interface of a mixture of 1:1:1 CHCl₃, MeOH and H₂O.

Mp = 151-152 °C. ¹H NMR (300 MHz, Chloroform-*d*) δ 8.32 – 8.19 (m, 1H), 8.12 (s, 1H⁶), 7.95 – 7.85 (m, 1H), 7.84 – 7.72 (m, 2H), 7.42 – 7.32 (m, 3H¹⁻³), 5.07 (s, 2H⁵). ¹³C NMR (75 MHz, Chloroform-*d*) δ 148.6, 134.9, 134.8, 133.8, 133.0, 130.5, 129.6, 129.0, 128.8, 125.7, 80.0. HRMS (pNSI) calcd for C₁₃H₁₃N₂O₅S [M+H]⁺: 309.0540, found 309.0543.

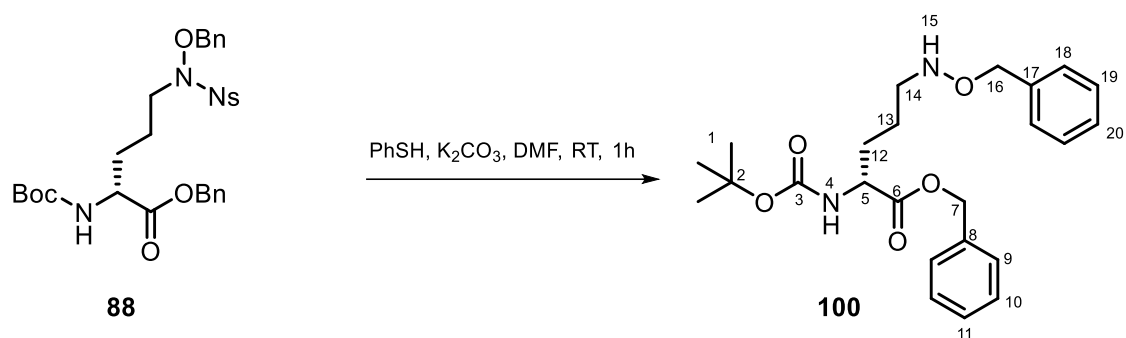
**benzyl (*R*)-5-((*N*-(benzyloxy)-2-nitrophenyl)sulfonamido)-2-((*tert*-butoxycarbonyl)amino)pentanoate
(88)**



To a 50 mL round bottomed flask under an atmosphere of nitrogen was added benzyl (*R*)-2-((*tert*-butoxycarbonyl)amino)-5-hydroxypentanoate (**90**) (0.225 g, 0.700 mmol, 1 eq), triphenylphosphine (**89**) (0.193 g, 0.735 mmol, 1.05 eq) and *N*-(benzyloxy)-2-nitrobenzenesulfonamide (0.223 g, 0.735 mmol, 1.05 eq). The solids were then dissolved in dry THF (7 mL) and the reaction mixture cooled to 0 °C. To the reaction mix was added DEAD (0.120 mL, 0.756 mmol, 1.08 eq) dropwise over 30 minutes. After this time the reaction mix was allowed to warm to room temperature, stirred for one hour and then quenched with the addition of saturated ammonium chloride (15 mL). The resulting mixture was then extracted with ethyl acetate (3 x 5 mL) and the combined organic layers were washed with saturated ammonium chloride (30 mL), brine (20 mL) dried over sodium sulphate, filtered and concentrated under reduced pressure to give a colourless oil. The crude mixture was then purified via column chromatography (ethyl acetate/petrol 40-60, 1:2) R_f: 0.38 to give benzyl (*R*)-5-((*N*-(benzyloxy)-2-nitrophenyl)sulfonamido)-2-((*tert*-butoxycarbonyl)amino)pentanoate (**88**) (0.380 g, 0.619 mmol, 88%) as a colourless oil.

$[\alpha]_D = +21.2^\circ$ ¹H NMR (400 MHz, Chloroform-*d*) δ 7.99 (dd, $J = 8.0, 1.4$ Hz, 1H), 7.74 (td, $J = 7.7, 1.5$ Hz, 1H), 7.63 (td, $J = 7.8, 1.3$ Hz, 1H), 7.53 (dd, $J = 7.9, 1.3$ Hz, 1H), 7.42 – 7.28 (m, 10H^{9-11 + 17-19}), 5.15 (s, 2H⁷), 5.06 – 4.97 (m, 3H¹⁵⁺⁴), 4.29 (q, $J = 7.2$ Hz, 1H⁵), 3.07 (br-s, 2H¹⁴), 1.99 – 1.76 (m, 1H¹²), 1.71 – 1.57 (m, 1H¹²), 1.56 – 1.46 (m, 2H¹³), 1.43 (s, 9H¹). ¹³C NMR (101 MHz, Chloroform-*d*) δ 172.1, 155.3, 149.7, 135.3, 134.9, 134.7, 132.6, 131.0, 130.0, 129.1, 128.7, 128.7, 128.5, 128.3, 125.9, 123.7, 80.3, 80.0, 67.2, 53.2, 52.9, 29.9, 28.3, 22.8. IR (neat): $\nu_{\text{max}}/\text{cm}^{-1}$ 3373.8 (OH), 1737.7 (C=O ester), 1693.4 (C=O amide). HRMS (pNSI) calcd for C₃₀H₃₆N₃O₉S [M+H]⁺: 614.2167, found 614.2167

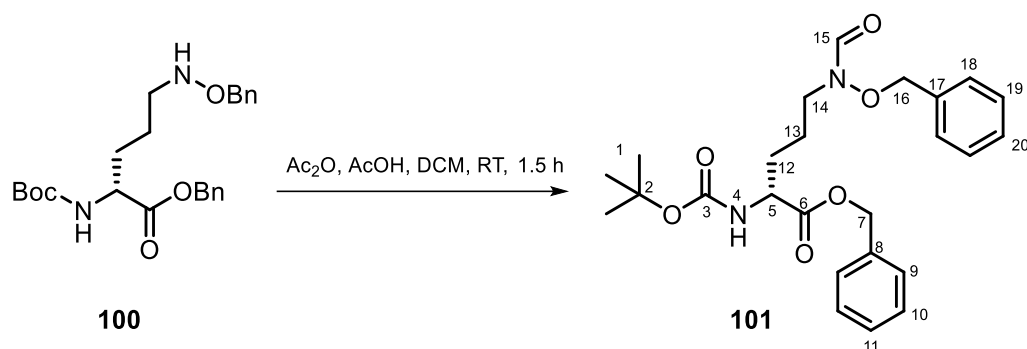
benzyl (*R*)-5-((benzyloxy)amino)-2-((tert-butoxycarbonyl)amino)pentanoate (**100**)



To a 50 mL schlenk flask under an atmosphere of nitrogen was added benzyl (*R*)-5-((*N*-(benzyloxy)-2-nitrophenyl)sulfonamido)-2-((tert-butoxycarbonyl)amino)pentanoate (**88**) (0.220 g, 0.358 mmol, 1 eq), K₂CO₃ (0.054 g, 0.387 mmol, 1.08 eq) and DMF (2 mL). The reaction was stirred for 5 minutes and then thiophenol (45 μ L, 1.437 mmol, 1.22 eq) was added via syringe. The reaction mix was then stirred for an additional 50 minutes, after which time the reaction was quenched with saturated ammonium chloride (10 mL). The reaction mixture was then extracted with EtOAc (3 x 5 mL) and the combined organic layers were washed with saturated ammonium chloride (30 mL), brine (20 mL) dried over sodium sulphate, filtered and concentrated under reduced pressure to give a colourless oil. The crude mixture was then purified via column chromatography (ethyl acetate/ petrol 40-60, 1:2 R_f = 0.2) to give benzyl (*R*)-5-((benzyloxy)amino)-2-((tert-butoxycarbonyl)amino)pentanoate (**100**) (0.135 g, 0.315 mmol, 88%) as a colourless oil.

¹H NMR (300 MHz, Chloroform-*d*) δ 7.79 – 7.19 (m, 10H⁹⁻¹¹⁺¹⁸⁻²⁰), 5.36 – 5.06 (m, 3H⁷⁺⁴), 4.67 (s, 2H¹⁶), 4.35 (q, *J* = 7.3 Hz, 1H⁵), 2.90 (t, *J* = 6.8 Hz, 2H¹⁴), 2.01 – 1.80 (m, 1H^{12a}), 1.77 – 1.63 (m, 1H^{12b}), 1.59 – 1.49 (m, 2H¹³), 1.44 (s, 9H¹). ¹³C NMR (75 MHz, Chloroform-*d*) δ 172.7⁶, 155.5³, 138.0, 135.5, 128.7, 128.5, 128.5, 128.4, 127.9, 79.9², 76.4¹⁶, 67.1⁷, 53.5⁵, 51.5¹⁴, 30.4¹², 28.4¹, 23.3¹³.

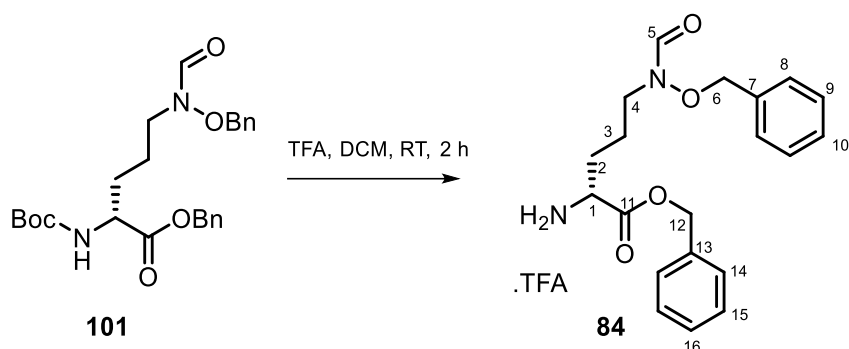
Benzyl (R)-5-(N-(benzyloxy)formamido)-2-((tert-butoxycarbonyl)amino)pentanoate (101)



A mixed anhydride solution was prepared by mixing of acetic anhydride (41 μ L, 0.44 mmol, 2eq) and formic acid (33 μ L, 0.88 mmol, 4eq) for one hour. After this time the mixture was poured into a solution of benzyl (R)-5-((benzyloxy)amino)-2-((tert-butoxycarbonyl)amino)pentanoate (**100**) (93 mg, 0.22 mmol) in dry DCM (1 mL). The reaction mix was then left to stir at room temperature for 1.5 hours after which time the mixture was diluted with DCM (10 mL) and washed with saturated NaHCO₃ (20 mL), dried over sodium sulphate and concentrated under reduced pressure to give benzyl (R)-5-(N-(benzyloxy)formamido)-2-((tert-butoxycarbonyl)amino)pentanoate (**101**) (97 mg, 0.21 mmol, 95%) as a colourless oil.

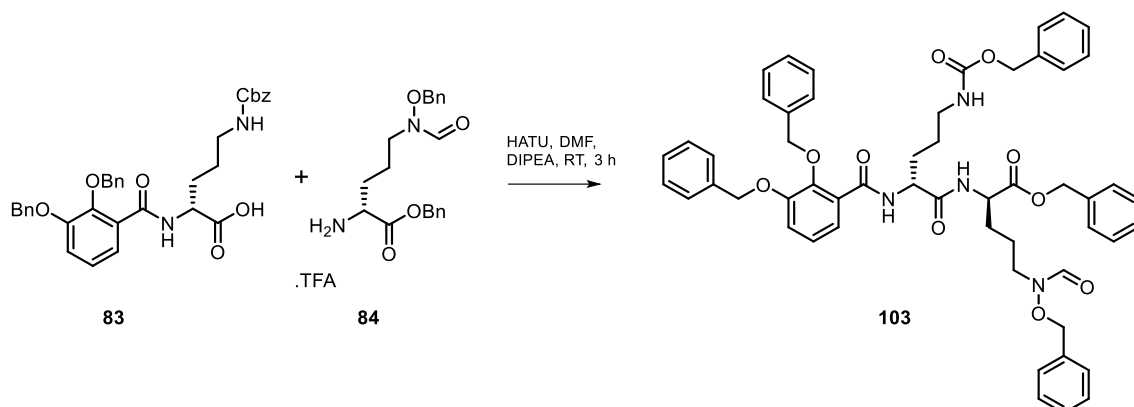
¹H NMR (300 MHz, Chloroform-*d*) δ 8.16 (s, 1H), 7.48 – 7.22 (m, 17H), 5.19 – 5.02 (m, 5H), 4.78 (s, 2H), 4.47 – 4.24 (m, 1H), 3.55 (s, 2H), 1.83 (d, *J* = 10.5 Hz, 2H), 1.65 (d, *J* = 7.8 Hz, 4H), 1.42 (s, 12H). ¹³C NMR (75 MHz, Chloroform-*d*) δ 172.3, 163.2, 155.4, 135.3, 134.3, 129.5, 129.1, 128.8, 128.6, 128.5, 128.3, 78.0, 77.7, 67.1, 53.2, 43.6, 29.9, 28.3, 23.0. HRMS (pNSI) calcd for C₂₅H₃₃N₂O₆ [M+H]⁺: 457.2333, observed 457.2331.

(R)-1-(benzyloxy)-5-(N-(benzyloxy)formamido)-1-oxopentan-2-aminium trifluoroacetate (84**)**



To a 5 mL Schlenk flask under an atmosphere of nitrogen at room temperature containing benzyl (*R*)-5-(*N*-(benzyloxy)formamido)-2-((*tert*-butoxycarbonyl)amino)pentanoate (**101**) (50 mg, 0.110 mmol) was added dry DCM (0.2 mL) followed by TFA (0.2 mL). The reaction mix was stirred at room temperature for 2 hours after which time the reaction mix was concentrated under reduced pressure to yield (*R*)-1-(benzyloxy)-5-(*N*-(benzyloxy)formamido)-1-oxopentan-2-aminium trifluoroacetate (**84**) (51 mg) as a pale pink solid which was used without further purification.

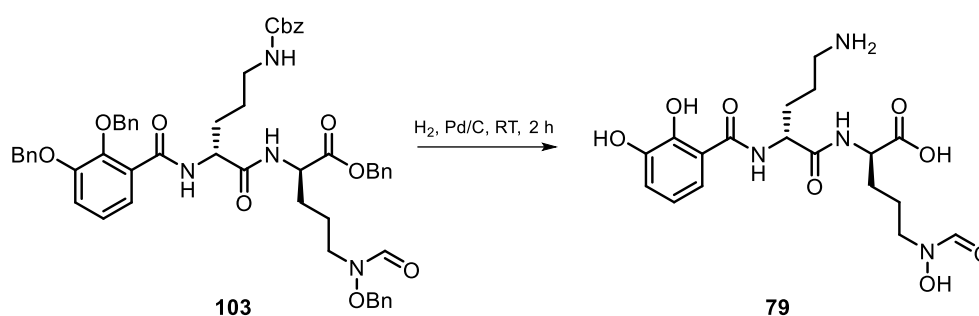
Benzyl (*R*)-2-((*R*)-5-(((benzyloxy)carbonyl)amino)-2-(2,3-bis(benzyloxy)benzamido)pentanamido)-5-(*N*-(benzyloxy)formamido)pentanoate (103**)**



To a stirred solution of (*R*)-5-(((benzyloxy)carbonyl)amino)-2-(2,3-bis(benzyloxy)benzamido)pentanoic acid (**83**) (64 mg, 0.11 mmol, 1 eq) under an atmosphere of nitrogen in DMF (0.2 mL) was added HATU (36 mg, 0.12 mmol, 1.1 eq) and the mixture left to stir for 10 minutes. To this mixture was added (*R*)-1-(benzyloxy)-5-(*N*-(benzyloxy)formamido)-1-oxopentan-2-aminium trifluoroacetate (**84**) (51 mg, 0.11 mmol, 1.0 eq) and the reaction mix stirred for an additional 20 minutes. After this time DIPEA (77 μ L, 0.44 mmol, 4.0 eq) was added and the mixture stirred at room temperature for 2.5 h. After this time the mixture was diluted with saturated ammonium chloride (4 mL) and water (2 mL) and the resulting slurry extracted with EtOAc (3 x 10 mL). The combined organic layers were then washed with saturated ammonium chloride (40 mL), brine (40 mL) dried over sodium sulphate, filtered and evaporated under reduced pressure. The crude mixture was then subjected to silica gel column chromatography (chloroform/acetone/methanol 50:10:1, R_f = 0.68) to give benzyl (*R*)-2-((*R*)-5-(((benzyloxy)carbonyl)amino)-2-(2,3-bis(benzyloxy)benzamido)pentanamido)-5-(*N*-(benzyloxy)formamido)pentanoate (**103**) (64 mg, 0.069 mmol, 63 %) as a colourless solid. It is noted that many of the ^{13}C signals are duplicated leading to a higher than expected number of signals.

^1H NMR (700 MHz, $\text{DMSO-}d_6$) δ 8.54 (dd, J = 44.9, 7.5 Hz, 1H), 8.47 (dd, J = 20.1, 8.1 Hz, 1H), 7.54 – 7.46 (m, 2H), 7.45 – 7.11 (m, 24H), δ 5.23 – 5.19 (m, 2H), 5.15 – 5.05 (m, 3H), 4.97 (d, J = 7.0 Hz, 3H), 4.88 – 4.83 (m, 2H), 4.64 – 4.49 (m, 1H), 4.40 – 4.25 (m, 1H), 3.59 – 3.41 (m, 2H), 2.99 – 2.76 (m, 2H), 1.78 – 1.68 (m, 1H), 1.67 – 1.53 (m, 4H), 1.51 – 1.31 (m, 3H). ^{13}C NMR (176

MHz, DMSO-*d*₆) δ 171.7, 171.6, 171.5, 171.5, 164.6, 164.3, 162.6, 156.1, 156.1, 151.6, 151.6, 145.6, 145.5, 137.2, 137.2, 136.7, 136.6, 136.6, 136.4, 135.8, 135.8, 134.7, 129.6, 129.2, 129.1, 128.7, 128.6, 128.5, 128.4, 128.3, 128.3, 128.1, 128.0, 128.0, 128.0, 127.8, 127.7, 127.7, 124.2, 121.6, 121.5, 116.6, 116.5, 79.2, 79.0, 76.6, 75.1, 75.1, 70.3, 70.3, 66.0, 66.0, 65.1, 52.2, 51.7, 42.4, 30.3, 29.9, 28.1, 25.8, 23.0, 22.8 (pNSI) calcd for C₅₄H₅₆N₄O₁₀ [M+H]⁺: 921.4069, found 921.4074.

Syn.30616/A (79)

To a stirred solution of benzyl (*R*)-2-((*R*)-5-(((benzyloxy)carbonyl)amino)-2-(2,3-bis(benzyloxy)benzamido)pentanamido)-5-(*N*-(benzyloxy)formamido)pentanoate (**103**) (12 mg, 0.011 mmol) in THF (0.2 mL) was added 10% Pd/C (5 mg) and the resulting suspension stirred vigorously under an atmosphere of hydrogen gas for 2 hours. After this time, the catalyst was removed via filtration through a SPE C8 cartridge and the solids washed with methanol (2 mL). The filtrate was then concentrated under reduced pressure to give approximately 3 mg of crude material. This was then subjected to HPLC chromatography and a peak at 32.9 minutes was collected as it matched that of the natural product DME30616/A (33.3 minutes) (Injection vol 100 μ L, 1.25 mL/min, MeCN:H₂O 95%:5%, to 85%:15% over 50 min, to 0%:100% over 10 min, C18, column diameter = 4.6 mm, column length 100 mm, scanning at 254 nm) to give 1 mg of purified syn.DEM30616/A (**79**) as a pale brown solid.

¹H NMR (700 MHz, Deuterium Oxide) δ 8.24 (s, 0.5H), 7.90 (s, 0.7H), 7.34 – 7.29 (m, 1H), 7.08 (d, *J* = 7.7 Hz, 1H), 6.83 (d, *J* = 7.7 Hz, 1H), 4.62 (dd, *J* = 7.9, 6.2 Hz, 1H), 4.23 (q, *J* = 7.3 Hz, 1H), 3.62 – 3.49 (m, 2H), 3.06 (t, *J* = 7.6 Hz, 2H), 2.06 – 1.97 (m, 1H), 1.97 – 1.90 (m, 1H), 1.87 – 1.79 (m, 3H), 1.76 – 1.63 (m, 3H).

References

- 1 D. A. Dias, S. Urban and U. Roessner, *Metabolites*, 2012, **2**, 303–36.
- 2 J. I. Scherz, *Der Schmerz*, 2003, **17**, 280–283.
- 3 M. C. Wani, H. L. Taylor, M. E. Wall, P. Coggon and A. T. McPhail, *J. Am. Chem. Soc.*, 1971, **93**, 2325–2327.
- 4 Alexander Fleming, *Br. Journal Exp. Pathol.*, 1929, **10**, 226–236.
- 5 J. W. Medley and M. Movassaghi, *Chem. Commun.*, 2013, **49**, 10775–10777.
- 6 R. Robinson, *J. Chem. Soc., Trans.*, 1917, **111**, 762–768.
- 7 C. A. G. N. Montalbetti and V. Falque, *Tetrahedron*, 2005, **61**, 10827–10852.
- 8 J. C. Sheehan and K. R. Henery-Logan, *J. Am. Chem. Soc.*, 1959, **81**, 3089–3094.
- 9 J. C. Sheehan and K. R. Henery-Logan, *the Total Synthesis of Penicillin V*, 1957, vol. 79.
- 10 J. H. Comroe, *Am. Rev. Respir. Dis.*, 1978, **117**, 773–781.
- 11 V. M. D’Costa, C. E. King, L. Kalan, M. Morar, W. W. L. Sung, C. Schwarz, D. Froese, G. Zazula, F. Calmels, R. Debruyne, G. B. Golding, H. N. Poinar and G. D. Wright, *Nature*, 2011, **477**, 457–461.
- 12 C. L. Ventola, *Pharm. Ther.*, 2015, **40**, 277–83.
- 13 Y. Y. Liu, Y. Wang, T. R. Walsh, L. X. Yi, R. Zhang, J. Spencer, Y. Doi, G. Tian, B. Dong, X. Huang, L. F. Yu, D. Gu, H. Ren, X. Chen, L. Lv, D. He, H. Zhou, Z. Liang, J. H. Liu and J. Shen, *Lancet Infect. Dis.*, 2016, **16**, 161–168.
- 14 P. Hinchliffe, Q. E. Yang, E. Portal, T. Young, H. Li, C. L. Tooke, M. J. Carvalho, N. G. Paterson, J. Brem, P. R. Niumsup, U. Tansawai, L. Lei, M. Li, Z. Shen, Y. Wang, C. J. Schofield, A. J. Mulholland, J. Shen, N. Fey, T. R. Walsh and J. Spencer, *Sci. Rep.*, 2017, **7**, 39392.
- 15 J. F. Fisher and S. Mobashery, *Medchemcomm*, 2016, **7**, 37–49.
- 16 E. D. Brown and G. D. Wright, *Nature*, 2016, **529**, 336–343.
- 17 Douglas Morier, Antibiotic resistance | Britannica.com, <https://www.britannica.com/science/antibiotic-resistance>, (accessed 20 November 2018).
- 18 J. Bérdy, *J. Antibiot. (Tokyo)*, 2005, **58**, 1–26.
- 19 A. L. Demain and S. Sanchez, *J. Antibiot. (Tokyo)*, 2009, **62**, 5–16.
- 20 O. Genilloud, *Nat. Prod. Rep.*, 2017, **34**, 1203–1232.
- 21 L. F. W. Roesch, R. R. Fulthorpe, A. Riva, G. Casella, A. K. M. Hadwin, A. D. Kent, S. H. Daroub, F. A. O. Camargo, W. G. Farmerie and E. W. Triplett, *ISME J.*, 2007, **1**, 283–290.
- 22 D. Barua, in *Cholera. Current Topics in Infectious Disease*, eds. D. Barua and W. B. Greenough, Springer US, Boston, MA, 1992, pp. 1–36.
- 23 J. W. Peterson, in *Medical Microbiology*, ed. S. Baron, University of Texas Medical Branch at Galveston, 4th edn., 1996.
- 24 R. C. Hider and X. Kong, *Nat. Prod. Rep.*, 2010, **27**, 637–657.

- 25 M. F. Kreuzer, H. Kage and M. Nett, *J. Am. Chem. Soc.*, 2012, **134**, 5415–5422.
- 26 K. Matsumoto, T. Ozawa, K. Jitsukawa and H. Masuda, *Inorg. Chem.*, 2004, **43**, 8538–8546.
- 27 K. Poole and G. A. McKay, *Front. Biosci.*, 2003, **8**, 661–686.
- 28 M. Miethke and M. a. Marahiel, *Microbiol. Mol. Biol. Rev.*, 2007, **71**, 413–451.
- 29 T. W. Giessen, K. B. Franke, T. a. Knappe, F. I. Kraas, M. Bosello, X. Xie, U. Linne and M. a. Marahiel, *J. Nat. Prod.*, 2012, **75**, 905–914.
- 30 E. J. Dimise, P. F. Widboom and S. D. Bruner, *Proc. Natl. Acad. Sci. U. S. A.*, 2008, **105**, 15311–6.
- 31 M. Saha, S. Sarkar, B. Sarkar, B. K. Sharma, S. Bhattacharjee and P. Tribedi, *Environ. Sci. Pollut. Res.*, 2016, **23**, 3984–3999.
- 32 T. A. Wencewicz and M. J. Miller, in *Topic*, eds. J. Fisher, S. Mobashery and M. Miller, Springer, Cham, 2017, vol. 26, pp. 151–183.
- 33 T. F. Moraes, R. Yu, N. C. J. Strynadka and A. B. Schryvers, *Mol. Cell*, 2009, **35**, 523–33.
- 34 C. Calmettes, J. Alcantara, R.-H. Yu, A. B. Schryvers and T. F. Moraes, *Nat. Struct. Mol. Biol.*, 2012, **19**, 358–60.
- 35 C. P. Owens, J. Du, J. H. Dawson and C. W. Goulding, *Biochemistry*, 2012, **51**, 1518–1531.
- 36 N. D. Hammer and E. P. Skaar, *Annu. Rev. Microbiol.*, 2011, **65**, 129–147.
- 37 J. B. Neilands, *J. Biol. Chem.*, 1995, **270**, 26723–26726.
- 38 I. G. O’Brien and F. Gibson, *BBA - Gen. Subj.*, 1970, **215**, 393–402.
- 39 J. R. Pollack and J. B. Neilands, *Biochem. Biophys. Res. Commun.*, 1970, **38**, 989–992.
- 40 M. R. Seyedsayamdost, M. F. Traxler, S.-L. L. Zheng, R. Kolter and J. Clardy, *J. Am. Chem. Soc.*, 2011, **133**, 11434–11437.
- 41 Z. L. Reitz, M. Sandy and A. Butler, *Metallomics*, 2017, **9**, 824–839.
- 42 A. H. Delcour, *Biochim. Biophys. Acta - Proteins Proteomics*, 2009, 1794, 808–816.
- 43 H. Nikaido, *Microbiol. Mol. Biol. Rev.*, 2003, **67**, 593–656.
- 44 R. Annamalai, B. Jin, Z. Cao, S. M. C. Newton and P. E. Klebba, *J. Bacteriol.*, 2004, **186**, 3578–89.
- 45 V. Braun, *Drug Resist. Updat.*, 1999, **2**, 363–369.
- 46 B. C. H. Chu, R. Otten, K. D. Krewulak, F. A. A. Mulder and H. J. Vogel, *J. Biol. Chem.*, 2014, **289**, 29219–34.
- 47 T. Fukushima, B. E. Allred, A. K. Sia, R. Nichiporuk, U. N. Andersen and K. N. Raymond, *Proc. Natl. Acad. Sci.*, 2013, **110**, 13821–13826.
- 48 T. Fukushima, B. E. Allred and K. N. Raymond, *ACS Chem. Biol.*, 2014, **9**, 2092–2100.
- 49 R. C. Hider, D. Bickar, I. E. G Morrison and J. Silver, *J. Am. Chem. Soc.*, 1984, **106**, 6983–6987.
- 50 F. Hallé and J. -M Meyer, *Eur. J. Biochem.*, 1992, **209**, 621–627.
- 51 K. N. Raymond and C. J. Carrano, *Acc. Chem. Res.*, 1979, **12**, 183–190.

- 52 A. D’Onofrio, J. M. Crawford, E. J. Stewart, K. Witt, E. Gavriš, S. Epstein, J. Clardy and K. Lewis, *Chem. Biol.*, 2010, **17**, 254–264.
- 53 T. Kaeberlein, K. Lewis and S. S. Epstein, *Science*, 2002, **296**, 1127–9.
- 54 D. Nichols, K. Lewis, J. Orjala, S. Mo, R. Ortenberg, P. O’Connor, C. Zhao, P. Vouros, T. Kaeberlein and S. S. Epstein, *Appl. Environ. Microbiol.*, 2008, **74**, 4889–97.
- 55 S. R. Vartoukian, A. Adamowska, M. Lawlor, R. Moazzez, F. E. Dewhirst and W. G. Wade, *PLoS One*, 2016, **11**, e0146926.
- 56 J. Francis, J. Madinaveitia, H. M. Macturk and G. A. Snow, *Nature*, 1949, **163**, 365–366.
- 57 J. B. Neilands, *J. Am. Chem. Soc.*, 1952, **74**, 4846–4847.
- 58 L. L. Ling, T. Schneider, A. J. Peoples, A. L. Spoering, I. Engels, B. P. Conlon, A. Mueller, T. F. Schäberle, D. E. Hughes, S. Epstein, M. Jones, L. Lazarides, V. A. Steadman, D. R. Cohen, C. R. Felix, K. A. Fetterman, W. P. Millett, A. G. Nitti, A. M. Zullo, C. Chen and K. Lewis, *Nature*, 2015, **517**, 455–459.
- 59 T. Zheng and E. M. Nolan, *Metallomics*, 2012, **4**, 866.
- 60 D. D. Doorneweerd, W. A. Henne, R. G. Reifenger and P. S. Low, *Langmuir*, 2010, **26**, 15424–15429.
- 61 P. Bhadra, M. S. Shajahan, P. N. Patel, E. Bhattacharya, A. Chadha and P. K. Sekhar, *J. Electrochem. Soc.*, 2018, **165**, B3017–B3022.
- 62 N. Mobarra, M. Shanaki, H. Ehteram, H. Nasiri, M. Sahmani, M. Saeidi, M. Goudarzi, H. Pourkarim and M. Azad, *A Review on Iron Chelators in Treatment of Iron Overload Syndromes*, 2016, vol. 10.
- 63 G. J. Kontoghiorghes, A. Kolnagou, A. Skiada and G. Petrikos, *Hemoglobin*, 2010, **34**, 227–239.
- 64 V. Braun, A. Pramanik, T. Gwinner, M. Köberle and E. Bohn, *BioMetals*, 2009, **22**, 3–13.
- 65 A. D. Ferguson, V. Braun, H. P. Fiedler, J. W. Coulton, K. Diederichs and W. Welte, *Protein Sci*, 2000, **9**, 956–963.
- 66 A. Hartmann, H. -P Fielder and V. Braun, *Eur. J. Biochem.*, 1979, **99**, 517–524.
- 67 V. Braun, K. Gunthner, K. Hantke and L. Zimmermann, *J. Bacteriol.*, 1983, **156**, 308–315.
- 68 C. Ji, R. E. Juárez-Hernández and M. J. Miller, *Future Med. Chem.*, 2012, **4**, 297–313.
- 69 N. J. Yang and M. J. Hinner, in *Site-Specific Protein Labeling: Methods and Protocols*, 2015, pp. 29–53.
- 70 H. I. Zgurskaya, C. A. López and S. Gnanakaran, *ACS Infect. Dis.*, 2016, **1**, 512–522.
- 71 M. Ghosh, P. A. Miller, U. Möllmann, W. D. Claypool, V. A. Schroeder, W. R. Wolter, M. Suckow, H. Yu, S. Li, W. Huang, J. Zajicek and M. J. Miller, *J. Med. Chem.*, 2017, **60**, 4577–4583.
- 72 T. Zheng and E. M. Nolan, *J. Am. Chem. Soc.*, 2014, **136**, 9677–9691.
- 73 R. Liu, P. A. Miller, S. B. Vakulenko, N. K. Stewart, W. C. Boggess and M. J. Miller, *J. Med. Chem.*, 2018, **61**, 3845–3854.
- 74 L. A. Maldonado, J. E. M. Stach, W. Pathom-aree, A. C. Ward, A. T. Bull and M. Goodfellow, *Antonie Van Leeuwenhoek*, 2005, **87**, 11–18.

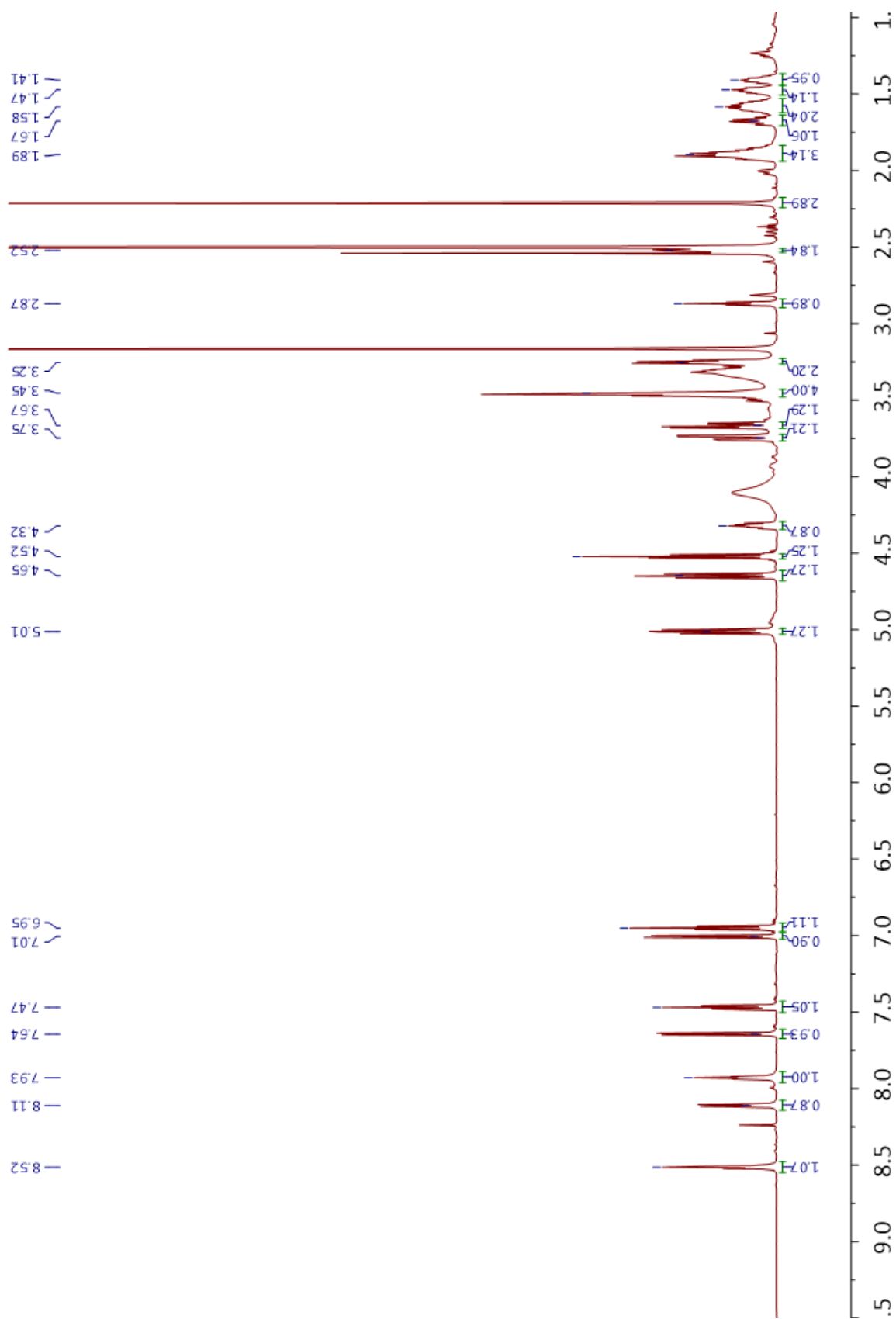
- 75 C. R. Chitambar, *Biochim. Biophys. Acta - Mol. Cell Res.*, 2016, **1863**, 2044–2053.
- 76 O. Olakanmi, J. S. Gunn, S. Su, S. Soni, D. J. Hassett and B. E. Britigan, *Antimicrob. Agents Chemother.*, 2010, **54**, 244–53.
- 77 T. Emery, *Biochemistry*, 1986, **25**, 4629–4633.
- 78 N. Basavraj and V. Deepak, *Eur. J. Gen. Med.*, 2011, **8**, 229–235.
- 79 R. Soares, E. Pires, A. M. Almeida, R. Santos, R. Gomes, K. Ko, C. F. Franco and A. V. Coelho, in *Tandem Mass Spectrometry - Applications and Principles*, ed. J. Prasain, 2001, pp. 35–56.
- 80 P. Marfey, *Carlsberg Res. Commun.*, 1984, **49**, 591–596.
- 81 K. Harada, K. Fujii, K. Hayashi, M. Suzuki, Y. Ikai and H. Oka, *Tetrahedron Lett.*, 1996, **37**, 3001–3004.
- 82 H. Stephan, S. Freund, J.-M. Meyer, G. Winkelmann and G. Jung, *Liebigs Ann. der Chemie*, 1993, **1993**, 43–48.
- 83 K. Harada, K. Tomita, K. Fujii, K. Masuda, Y. Mikami, K. Yazawa and H. Komaki, *J. Antibiot. (Tokyo)*, 2004, **57**, 125–133.
- 84 E. Mazzei, M. Iorio, S. I. Maffioli, M. Sosio and S. Donadio, *J. Antibiot. (Tokyo)*, 2012, **65**, 267–269.
- 85 X. Zhang, H. He, R. Ma, Z. Ji, Q. Wei, H. Dai, L. Zhang and F. Song, *J. Ind. Microbiol. Biotechnol.*, 2017, **44**, 589–594.
- 86 Y. Chen, M. Unger, I. Ntai, R. A. McClure, J. C. Albright, R. J. Thomson and N. L. Kelleher, *Medchemcomm*, 2013, **4**, 233–238.
- 87 K. Schneider, I. Rose, S. Vikineswary, A. L. Jones, M. Goodfellow, G. Nicholson, W. Beil, R. D. Süßmuth and H.-P. Fiedler, *J. Nat. Prod.*, 2007, **70**, 932–5.
- 88 A. Mukai, T. Fukai, Y. Matsumoto, J. Ishikawa, Y. Hoshino, K. Yazawa, K. Harada and Y. Mikami, *J. Antibiot. (Tokyo)*, 2006, **59**, 366–369.
- 89 P. J. Maurer and M. J. Miller, *J. Am. Chem. Soc.*, 1983, **105**, 240–245.
- 90 J. Hu and M. J. Miller, *J. Am. Chem. Soc.*, 1997, **119**, 3462–3468.
- 91 A. J. Phillips, Y. Uto, P. Wipf, M. J. Reno and D. R. Williams, *Org. Lett.*, 2000, **2**, 1165–1168.
- 92 D. Foley, M. Pieri, R. Pettecrew, R. Price, S. Miles, H. K. Lam, P. Bailey and D. Meredith, *Org. Biomol. Chem.*, 2009, **7**, 3652–3656.
- 93 U. Larsson and R. Carlson, *Acta Chem. Scand.*, 1994, **48**, 551–516.
- 94 B. McKeever and G. Pattenden, *Tetrahedron Lett.*, 1999, **40**, 9317–9320.
- 95 L. Marzorati, G. C. Barazzone, M. a. Bueno Filho, B. Wladislaw and C. Di Vitta, *Tetrahedron Lett.*, 2007, **48**, 6509–6513.
- 96 N. J. Church and D. W. Young, *J. Chem. Soc. - Perkin Trans. 1*, 1998, 1475–1482.
- 97 B. S. Axelsson, K. J. O’Toole, P. A. Spencer and D. W. Young, *J. Chem. Soc. Perkin Trans. 1*, 1994, 807.
- 98 E. Vedejs, A. Klapars, D. L. Warner and A. H. Weiss, *J. Org. Chem.*, 2001, **66**, 7542–7546.
- 99 A. R. Tyler, H. Mosaei, S. Morton, P. G. Waddell, C. Wills, W. McFarlane, J. Gray, M.

- Goodfellow, J. Errington, N. Allenby, N. Zenkin and M. J. Hall, *J. Nat. Prod.*, 2017, **80**, 1558–1562.
- 100 G. J. Sharman, D. H. Williams, D. F. Ewing, C. Ratledge, D. H. Williams', D. F. Ewing and C. Ratledge, *Chem. Biol.*, 1995, **2**, 553–561.
- 101 R. M. Hall and C. Ratledge, *Microbiology*, 1987, **133**, 193–199.
- 102 S. Dhungana, M. J. Miller, L. Dong, C. Ratledge and A. L. Crumbliss, *J. Am. Chem. Soc.*, 2003, **125**, 7654–7663.
- 103 L. Dong and M. J. Miller, *J. Org. Chem.*, 2002, **67**, 4759–4770.
- 104 H.-U. Naegeli and W. Keller-Schierlein, *Helv. Chim. Acta*, 1978, **61**, 2088–2095.
- 105 Y.-M. M. Lin and M. J. Miller, *J. Org. Chem.*, 1999, **64**, 7451–7458.
- 106 H. D. Flack and G. Bernardinelli, *Chirality*, 2008, **20**, 681–690.
- 107 J. Clayden, N. Greeves, S. Warren and P. Wothers, *Organic Chemistry*, Oxford University Press, 1st ed., 2012.
- 108 T. Kolasa and M. J. Miller, *J. Org. Chem.*, 1990, **55**, 1711–1721.
- 109 P. R. Sridhar, B. C. Venkatesh, S. Kalesha and C. Sudharani, *Org. Biomol. Chem.*, 2018, **16**, 3732–3740.
- 110 A. Gründling and O. Schneewind, *Proc. Natl. Acad. Sci. U. S. A.*, 2007, **104**, 8478–83.
- 111 D. Lu, M. E. Wormann, X. Zhang, O. Schneewind, A. Grundling and P. S. Freemont, *Proc. Natl. Acad. Sci.*, 2009, **106**, 1584–1589.
- 112 S. G. Richter, D. Elli, H. K. Kim, A. P. A. Hendrickx, J. A. Sorg, O. Schneewind and D. Missiakas, *Proc. Natl. Acad. Sci.*, 2013, **110**, 3531–3536.
- 113 C. R. Vickery, B. M. K. Wood, H. G. Morris, R. Losick and S. Walker, *J. Am. Chem. Soc.*, 2018, **140**, 876–879.
- 114 F. L. Paganelli, T. van de Kamer, E. C. Brouwer, H. L. Leavis, N. Woodford, M. J. M. Bonten, R. J. L. Willems and A. P. A. Hendrickx, *Int. J. Antimicrob. Agents*, 2017, **49**, 355–363.
- 115 K. Schirner and J. Errington, *J. Bacteriol.*, 2009, **191**, 1404–1413.
- 116 K. Schirner, J. Marles-Wright, R. J. Lewis and J. Errington, *EMBO J.*, 2009, **28**, 830–842.
- 117 S. Kishimoto, S. Nishimura, A. Hattori, M. Tsujimoto, M. Hatano, M. Igarashi and H. Kakeya, *Org. Lett.*, 2014, **16**, 6108–6111.
- 118 S. Kishimoto, S. Nishimura, M. Hatano, M. Igarashi and H. Kakeya, *J. Org. Chem.*, 2015, **80**, 6076–6082.
- 119 S. Kishimoto, S. Nishimura and H. Kakeya, *Chem. Lett.*, 2015, **44**, 1303–1305.
- 120 K. D. Park, P. Morieux, C. Salomé, S. W. Cotten, O. Reamtong, C. Evers, S. J. Gaskell, J. P. Stables, R. Liu and H. Kohn, *J. Med. Chem.*, 2009, **52**, 6897–6911.
- 121 M. Miller, Private communication, 256th American Chemical Society meeting in Boston USA, 2018.

Appendix

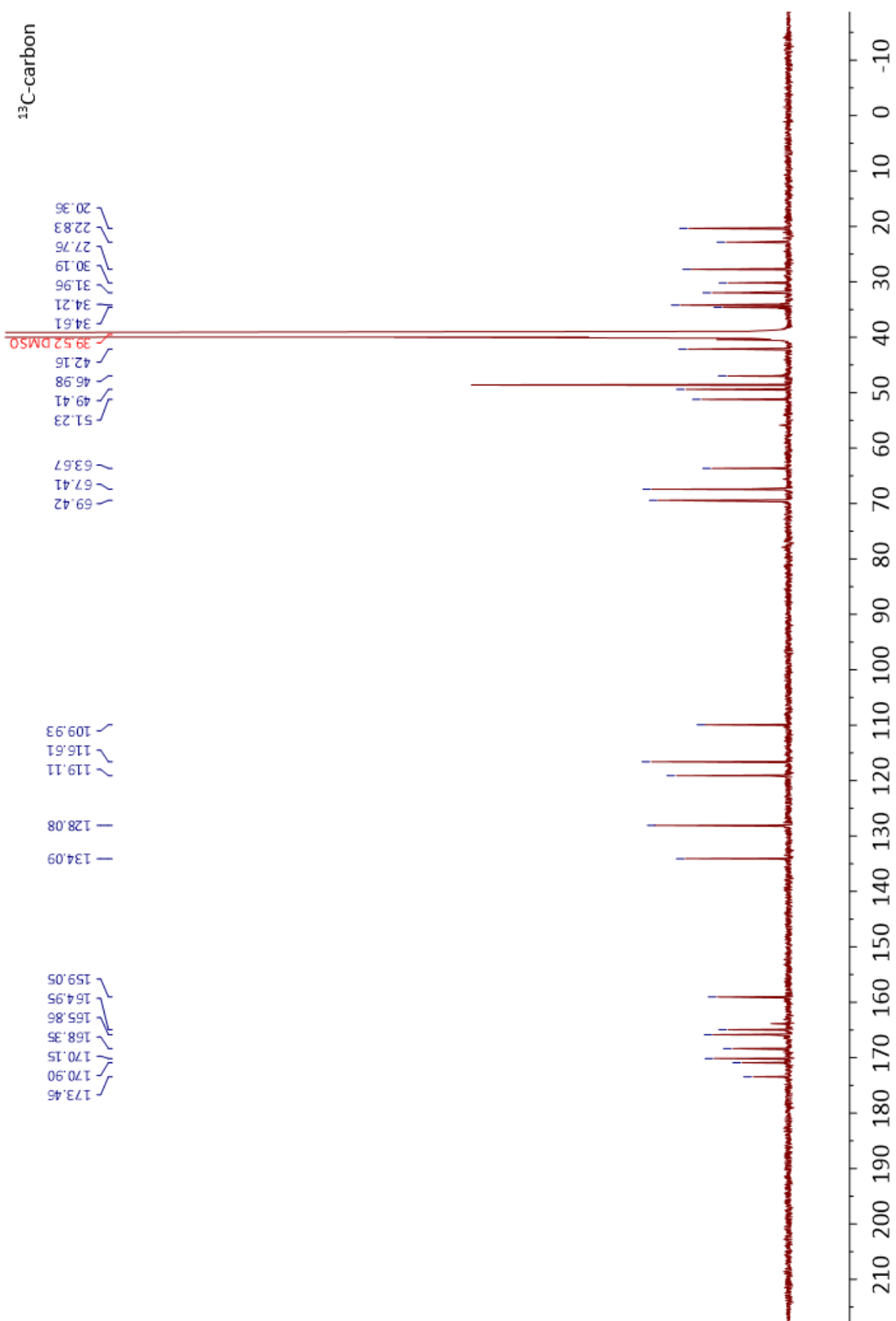
¹H NMR of DEM31376/A (madurastatin C1)

D6-DMSO, 298K, 700 MHz



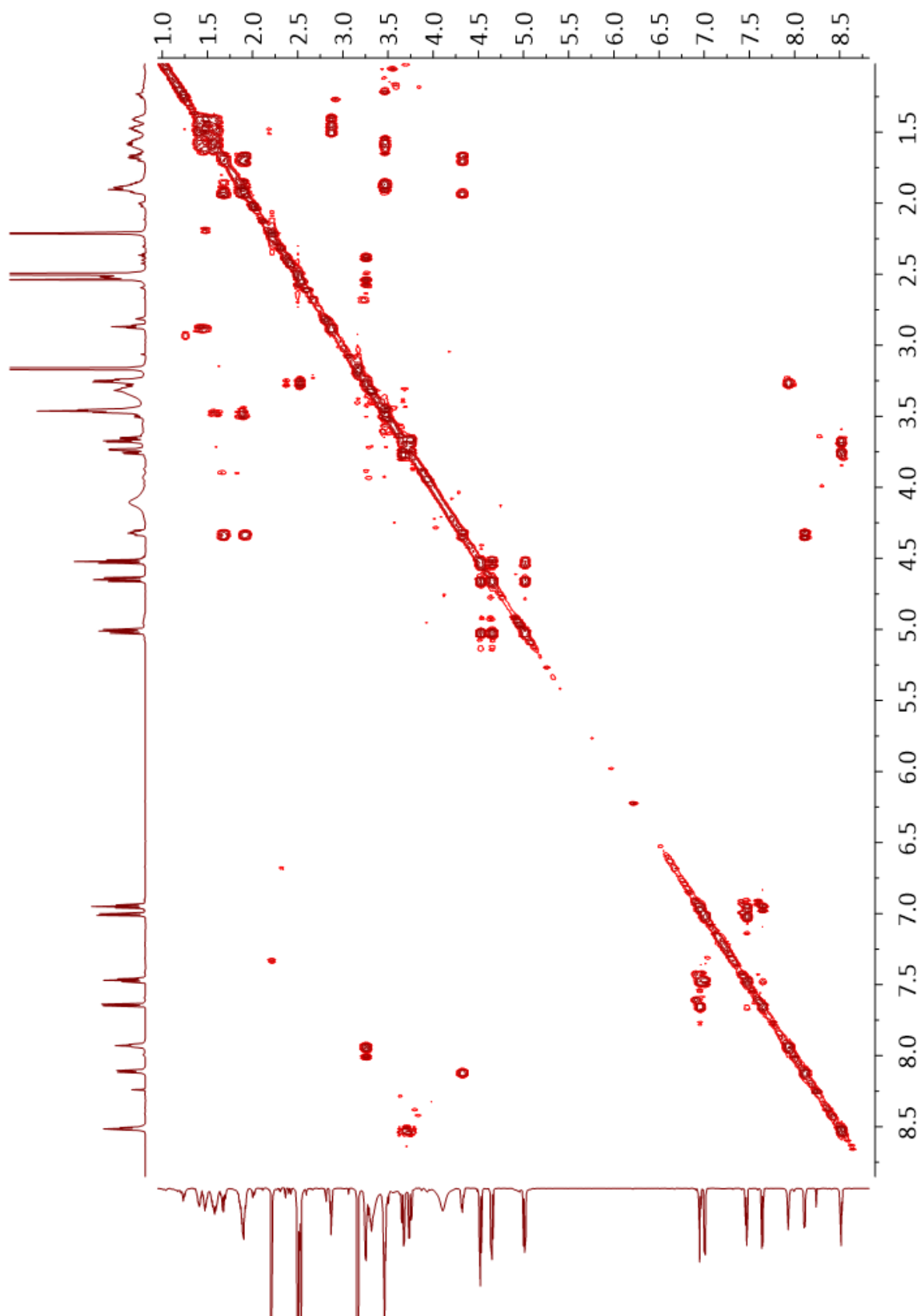
¹³C NMR of DEM31376/A (madurastatin C1)

D6-DMSO, 298K, 176 MHz



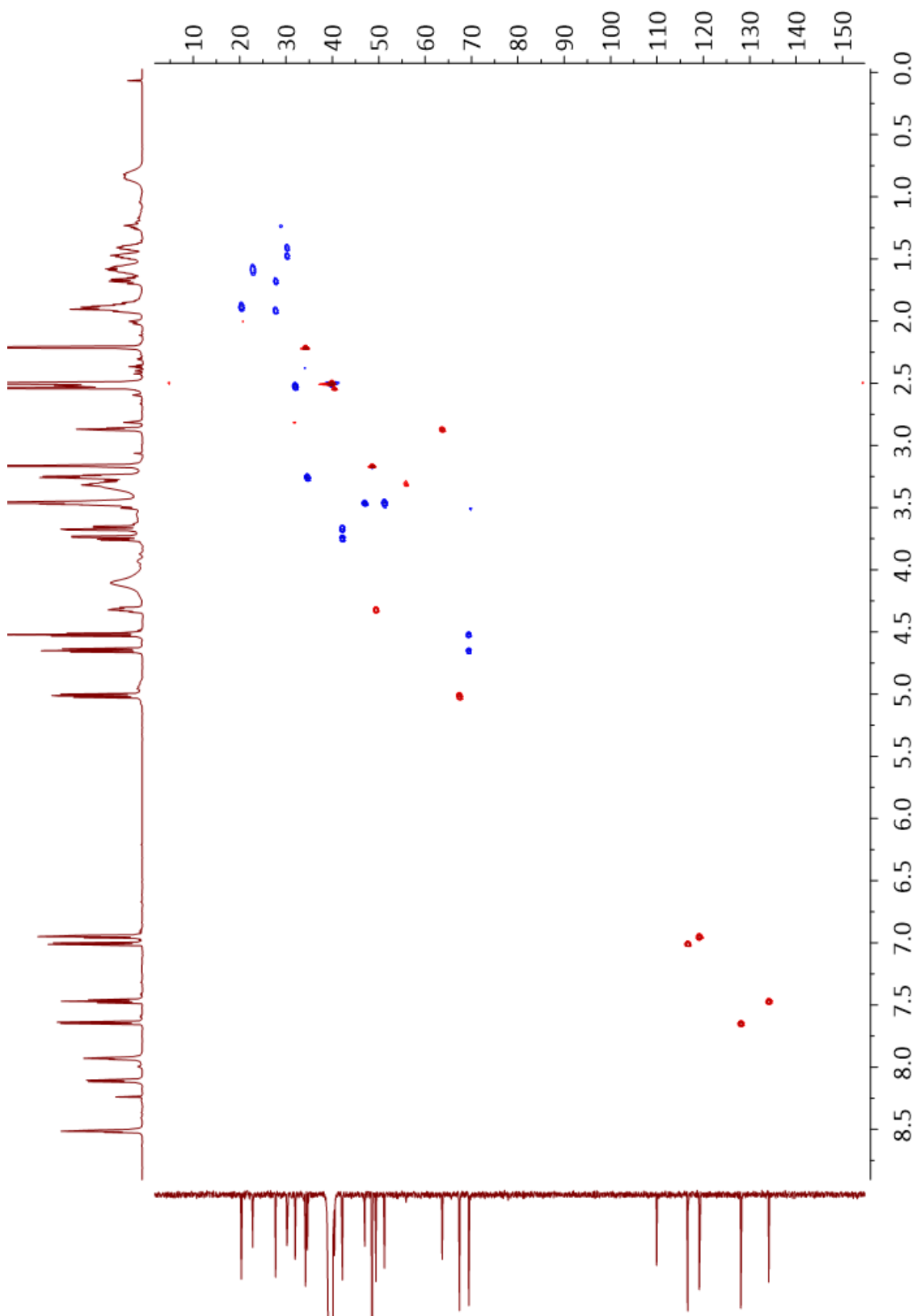
COSY NMR of DEM31376/A (madurastatin C1)

D6-DMSO, 298K, 700 MHz



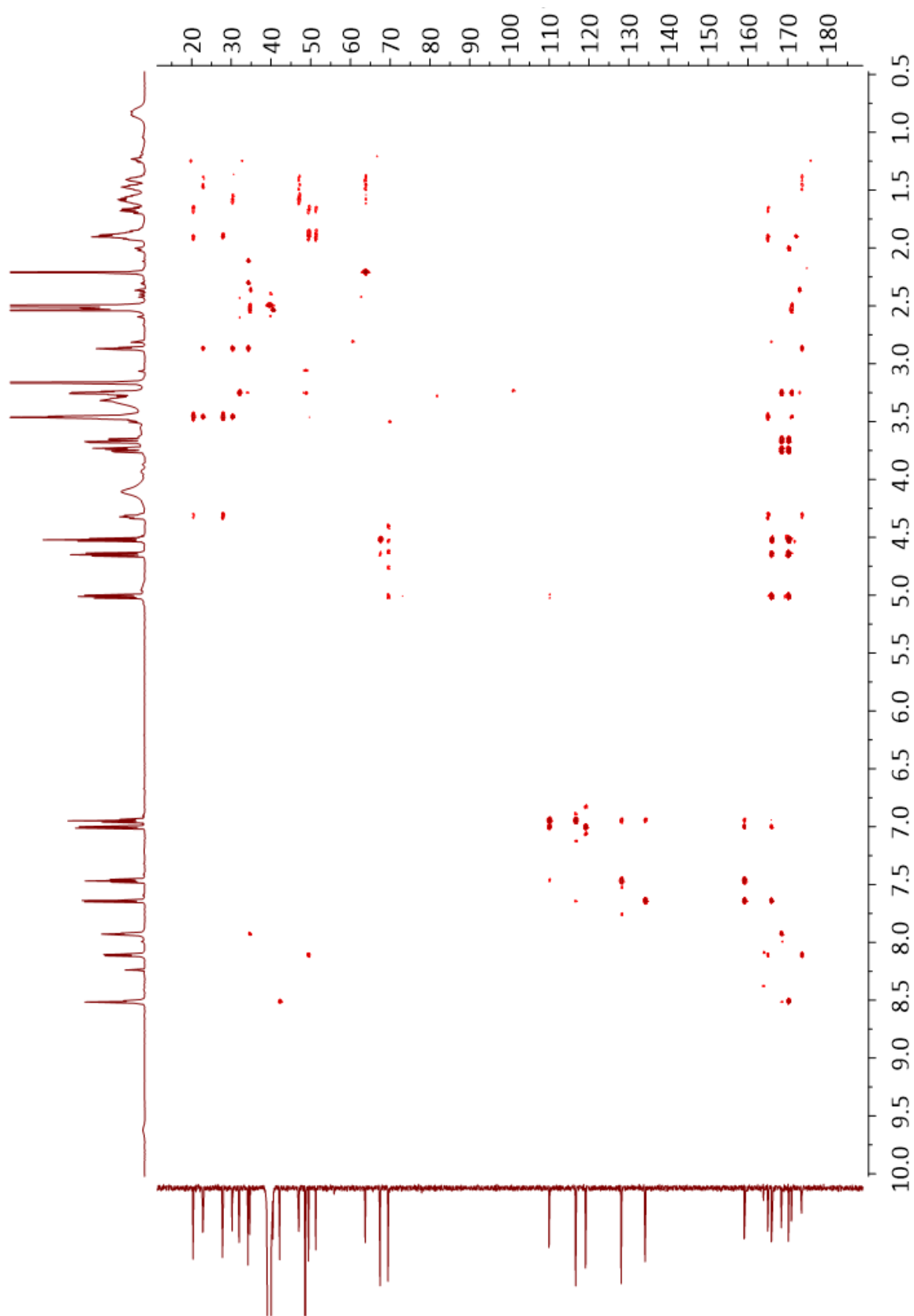
HSQC NMR of DEM31376/A (madurastatin C1)

D6-DMSO, 298K, 700 MHz



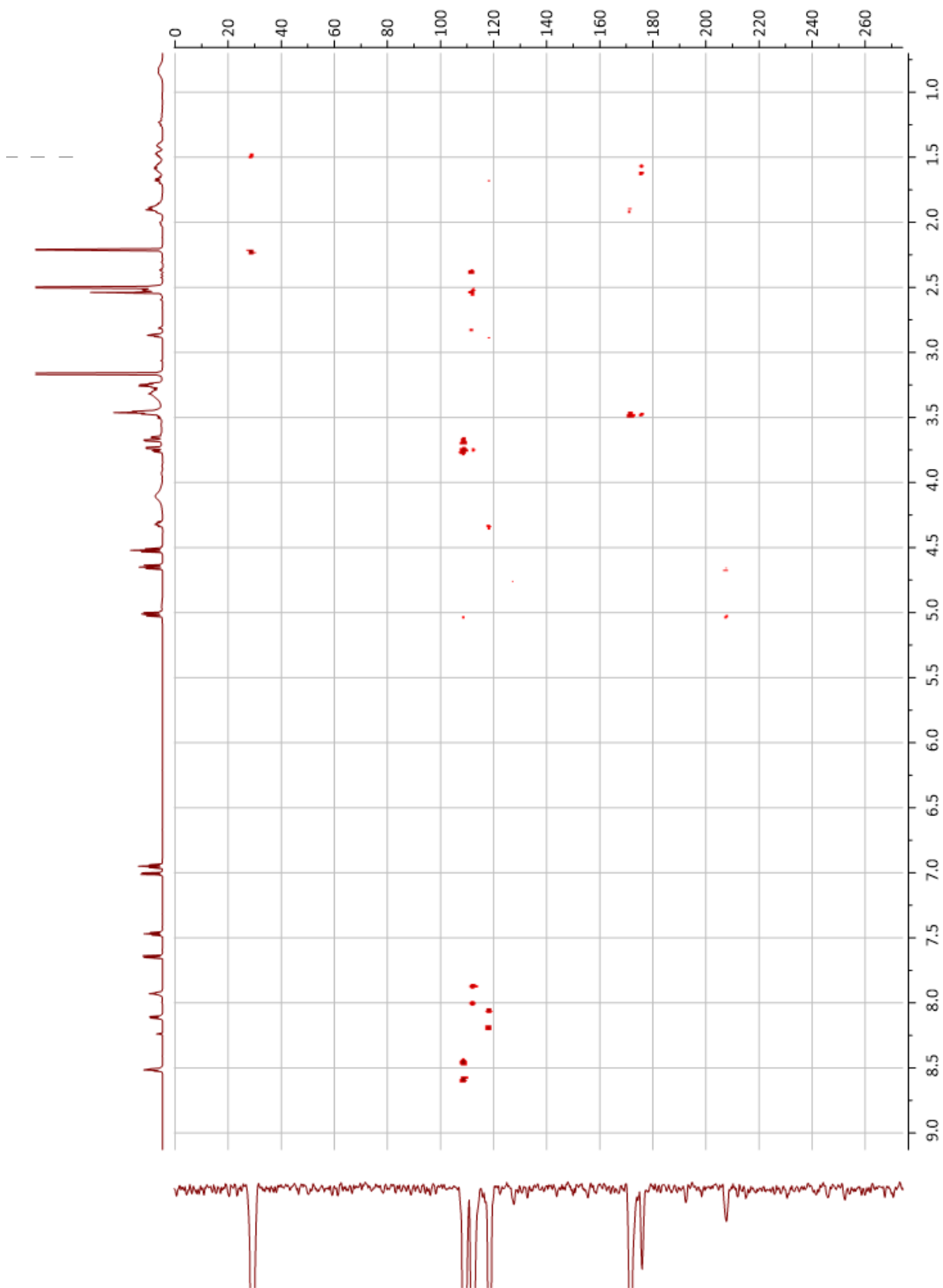
HMBC_10Hz NMR of DEM31376/A (madurastatin C1)

D6-DMSO, 298K, 700 MHz



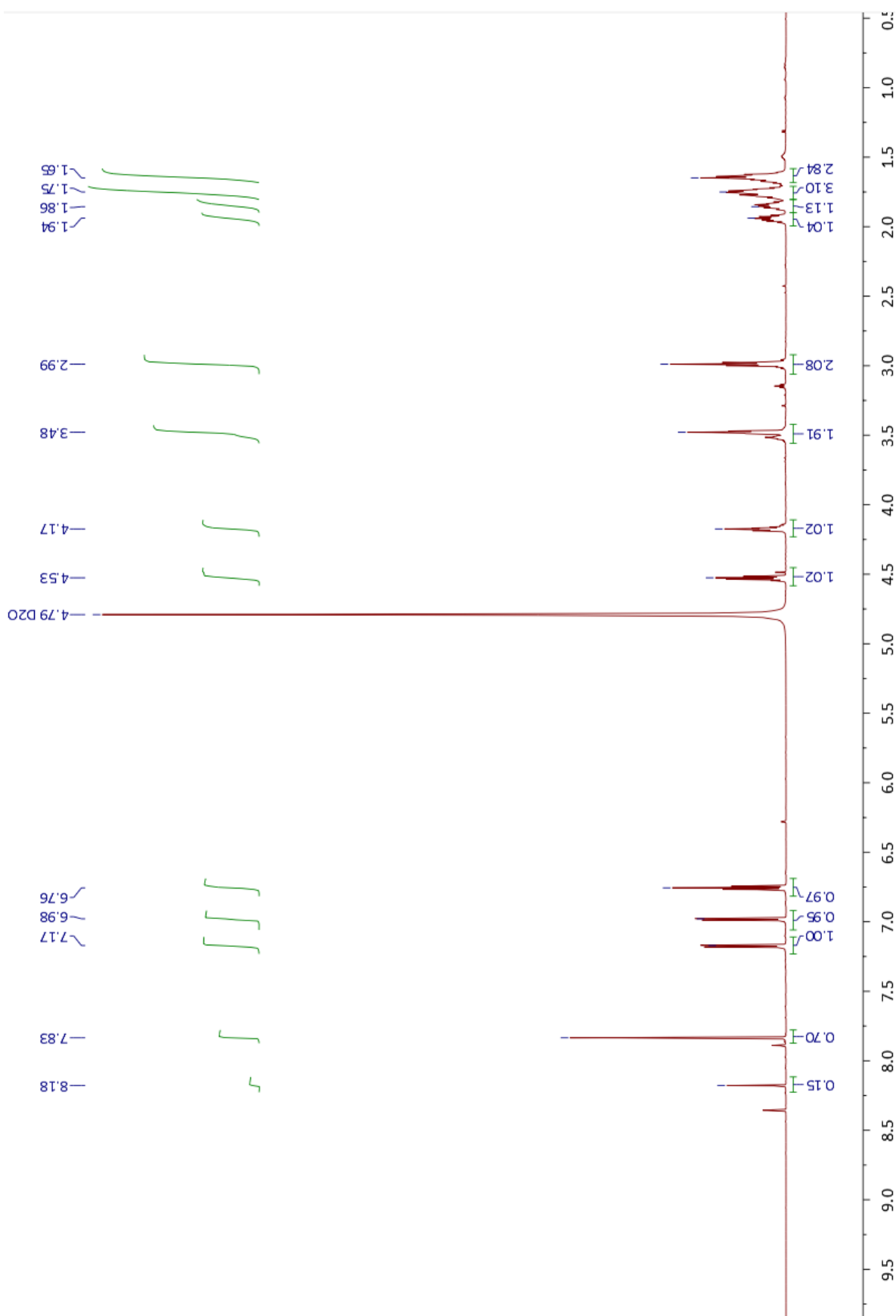
NH long range correlation 3Hz, NMR of DEM31376/A (madurastatin C1)

D6-DMSO, 298K, 700 MHz, N = 236



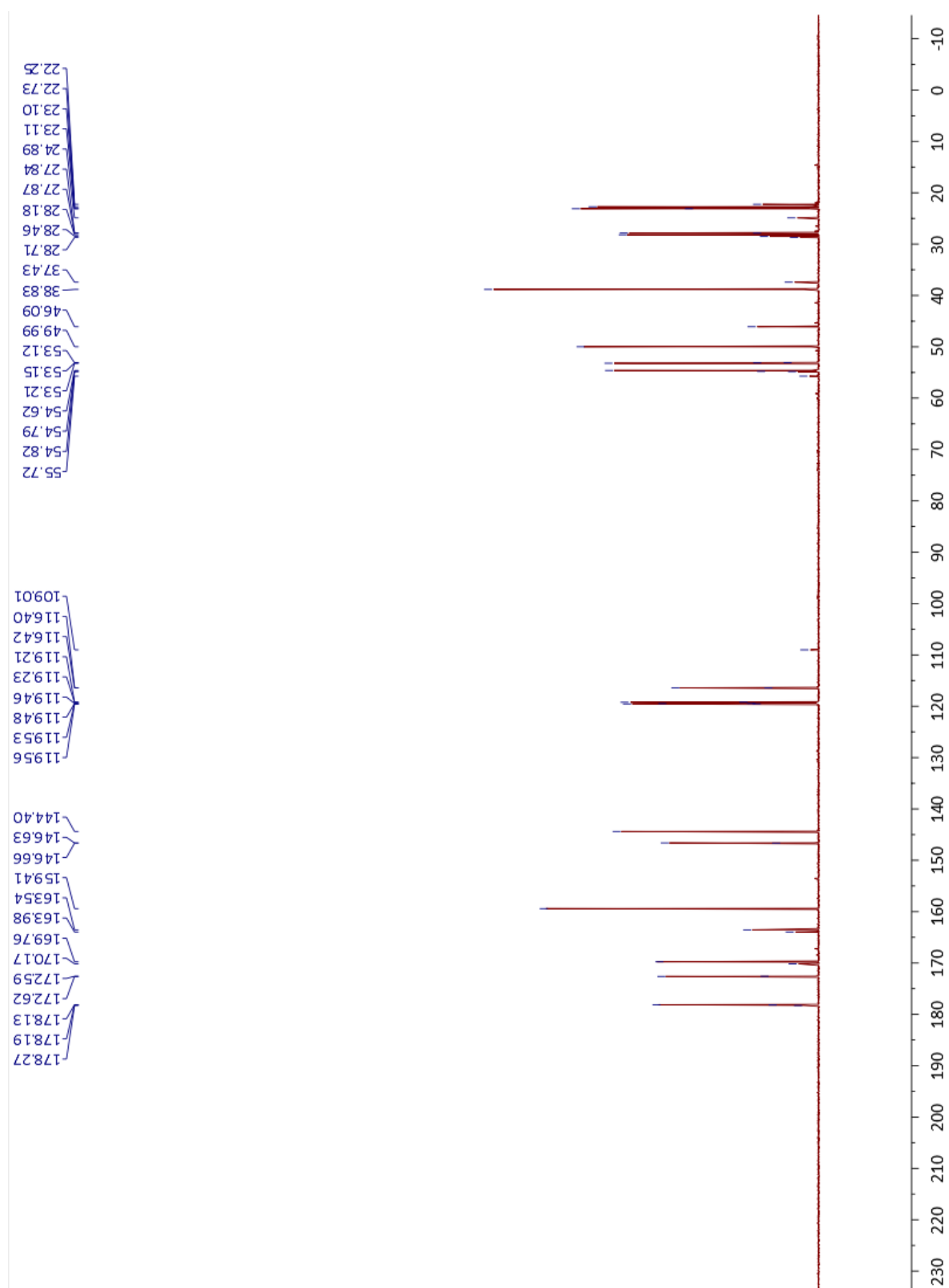
^1H NMR of DEM30616/A

D_2O , 298K, 700 MHz



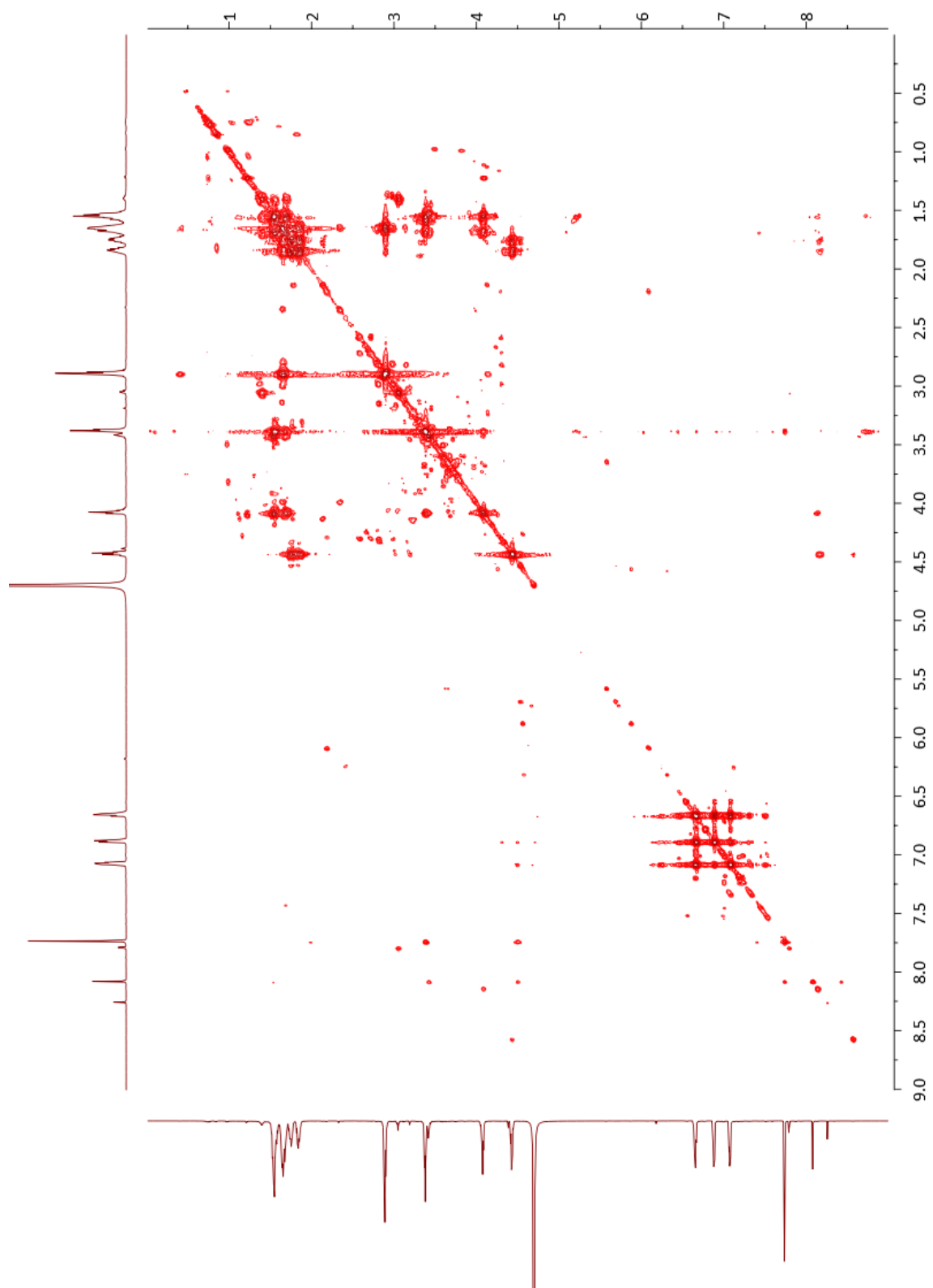
^{13}C NMR of DEM30616/A

D_2O , 298K, 176 MHz



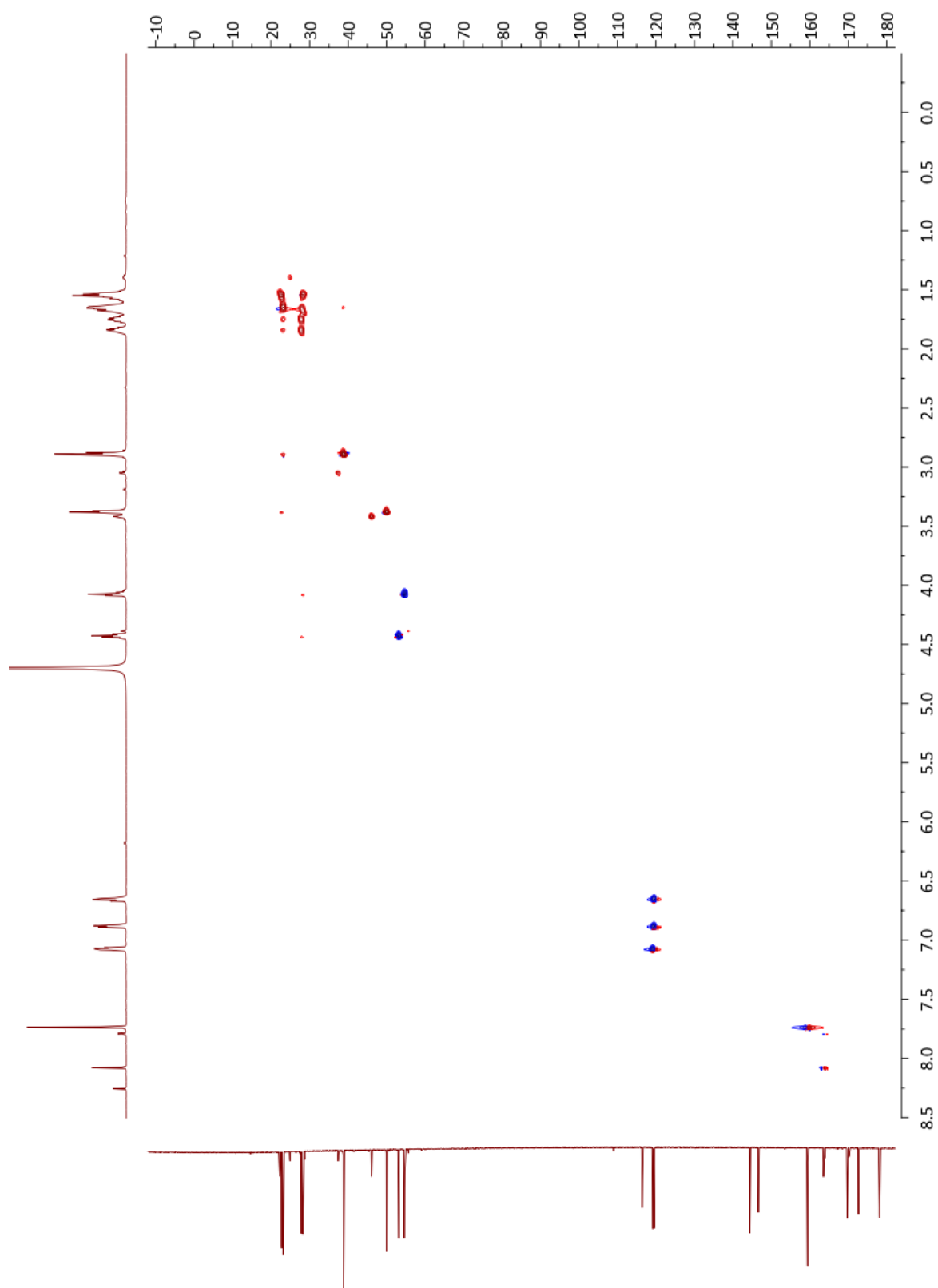
COSY NMR of DEM30616/A

D₂O, 298K, 700 MHz



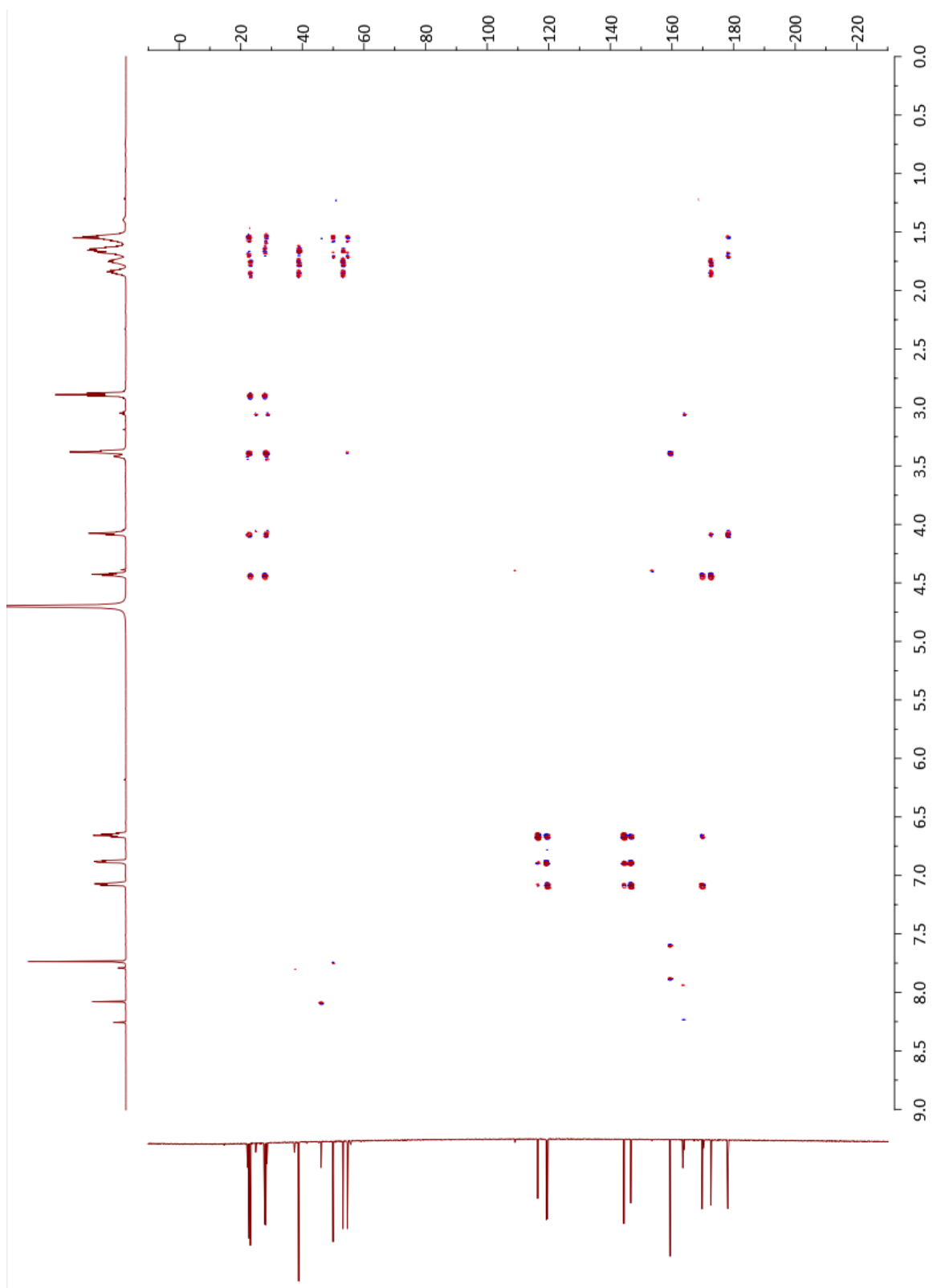
HSQC NMR of DEM30616/A

D₂O, 298K, 700 MHz



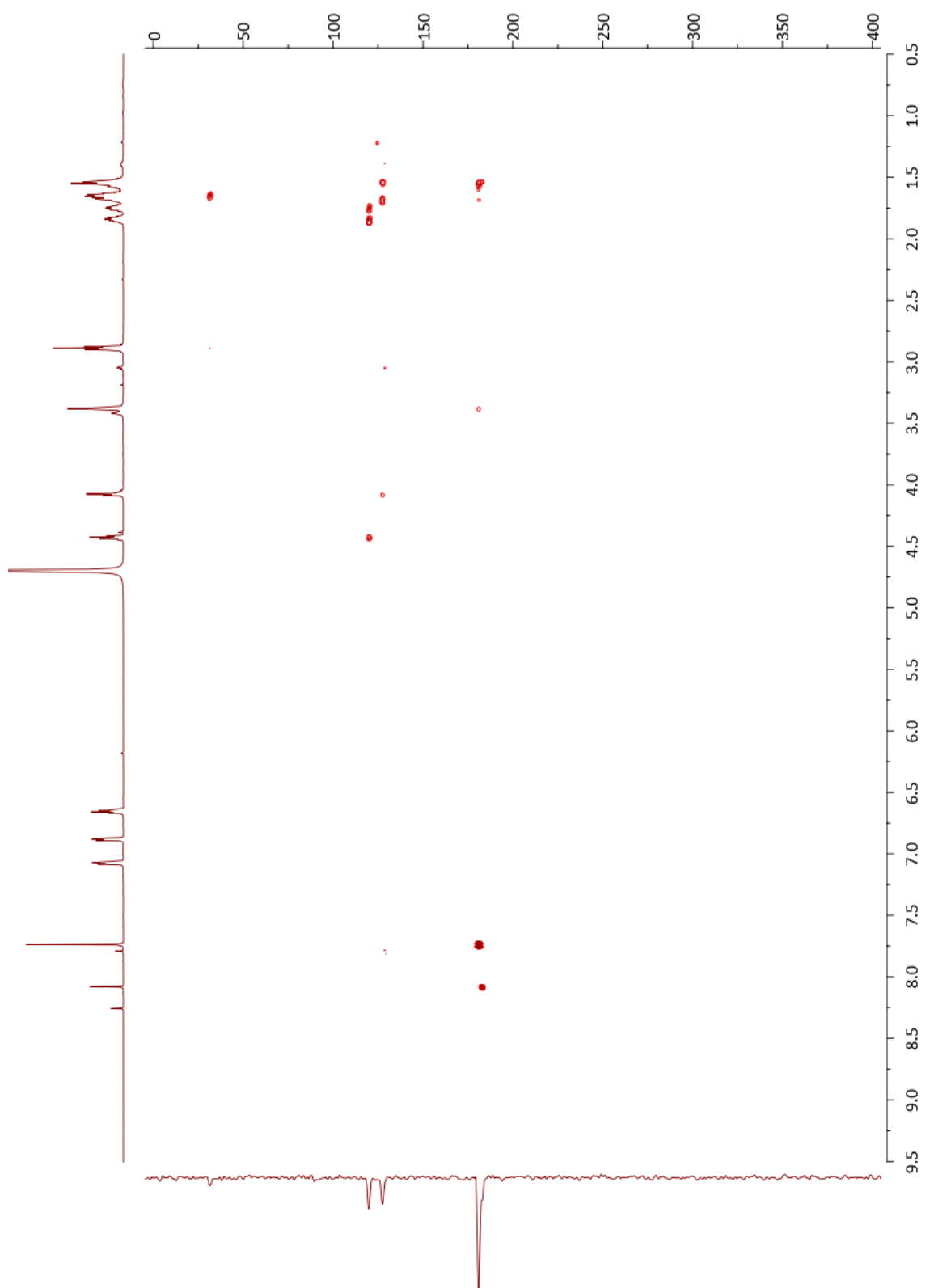
HMBC NMR of DEM30616/A

D₂O, 298K, 700 MHz

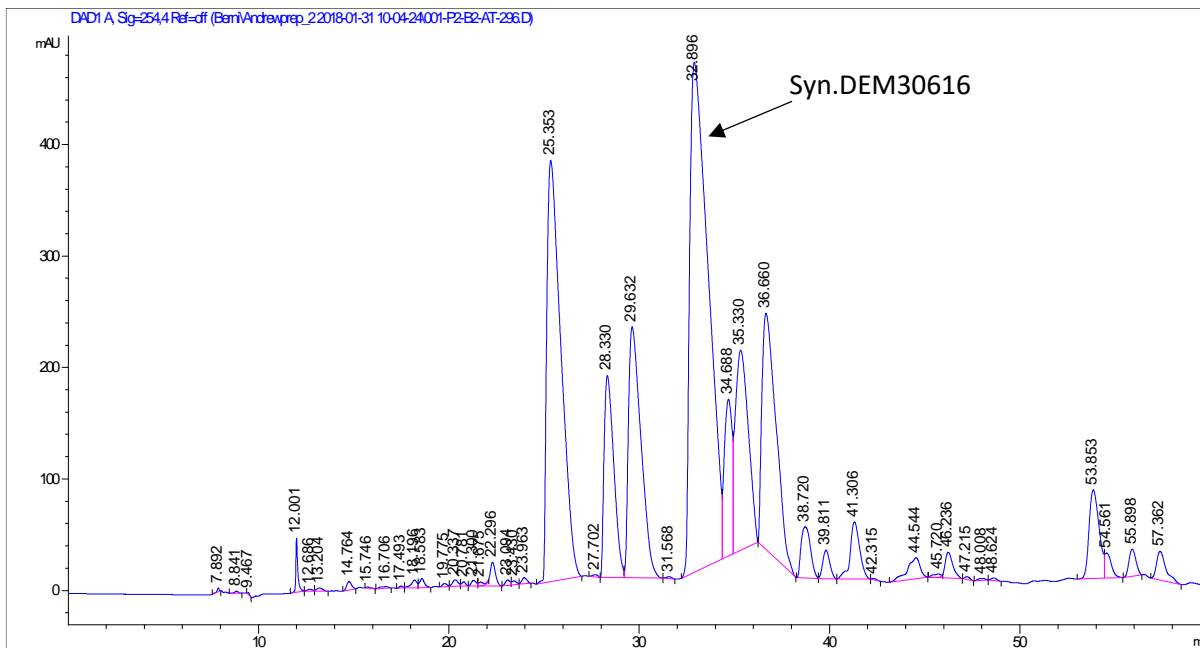


NH long range correlation 8Hz, NMR of DEM30616/A

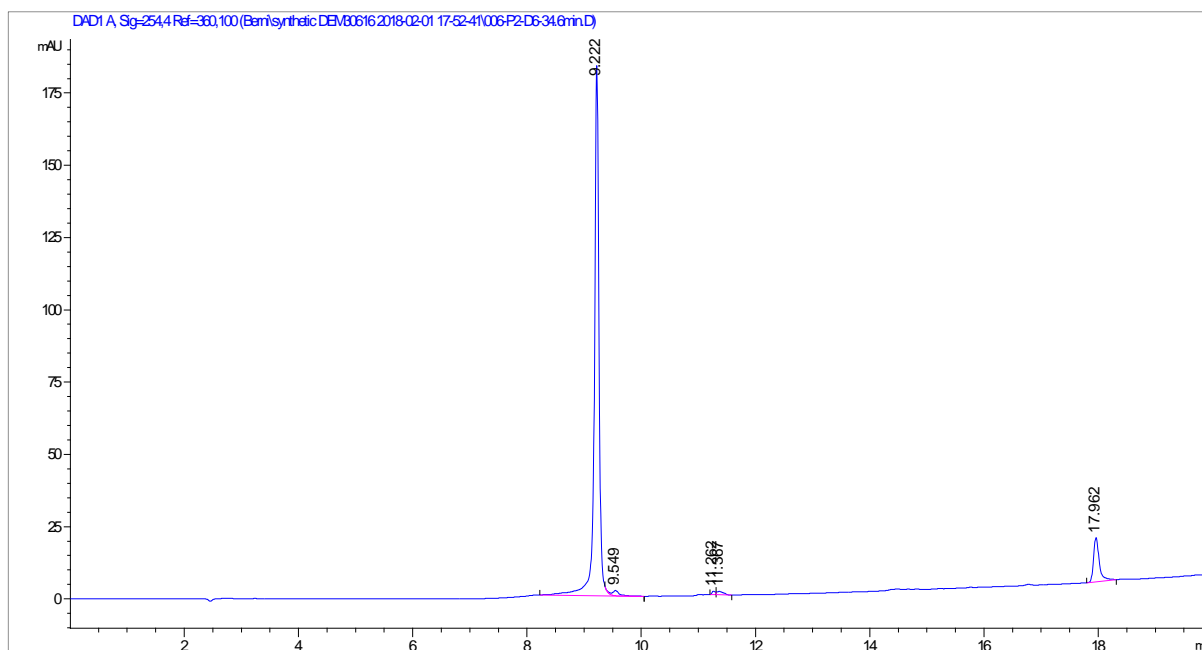
D₂O, 298K, 700 MHz, N = 236



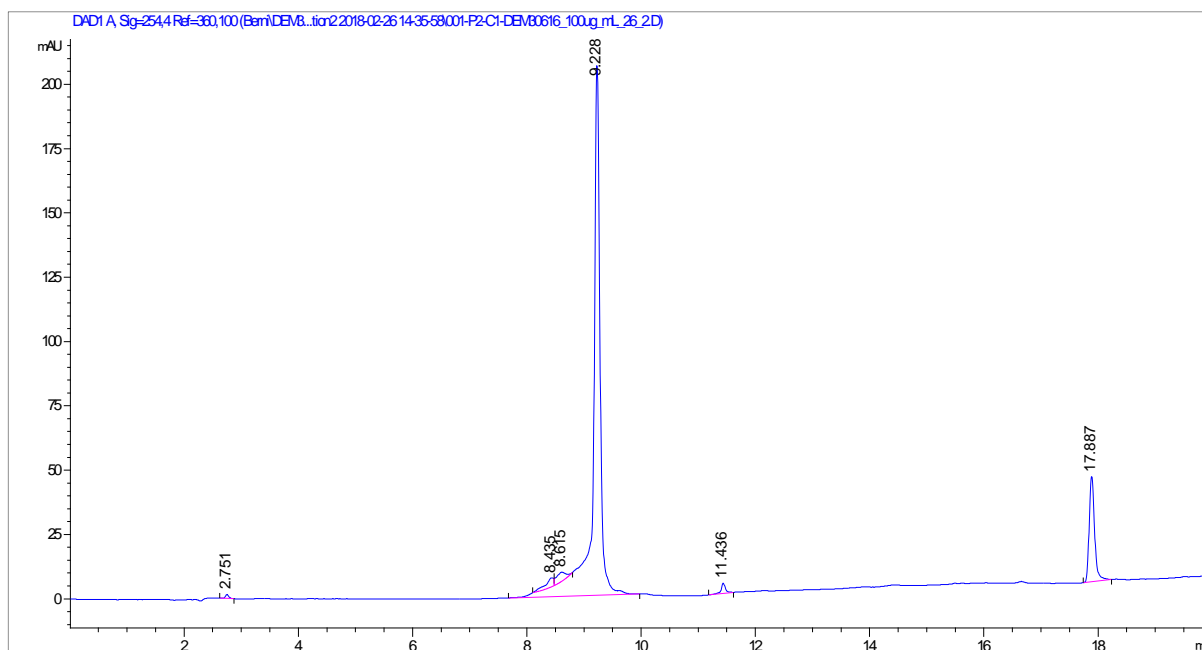
HPLC chromatogram of crude syn.30626/A. HPLC 1260 Infinity II. Injection volume 100 μ L, Flow rate 1.25 mL/min, Solvent A: MeCN, Solvent B: H₂O. Time 0-50 minutes, 95% A:5% B to 85% A: 15% B. Time 50-60 minutes 85% A: 15% B to 0% A: to 100% B. DAD at 254 nM. Column conditions Eclipse Plus C18, 3.5 μ M, column length 4.6 x 100 mm, 40°C.



HPLC chromatogram of Isolated syn.30616/A. HPLC 1260 Infinity II. Injection volume 100 μ L, Flow rate 0.5 mL/min, Solvent A: MeCN, Solvent B: H₂O. Time 0-15 minutes, 100% A:0% B to 0% A: 100% B. Time 15-20 minutes 0% A: 100% B. DAD at 254 nM. Column conditions Eclipse Plus C18, 3.5 μ M, column length 4.6 x 100 mm, 40°C.

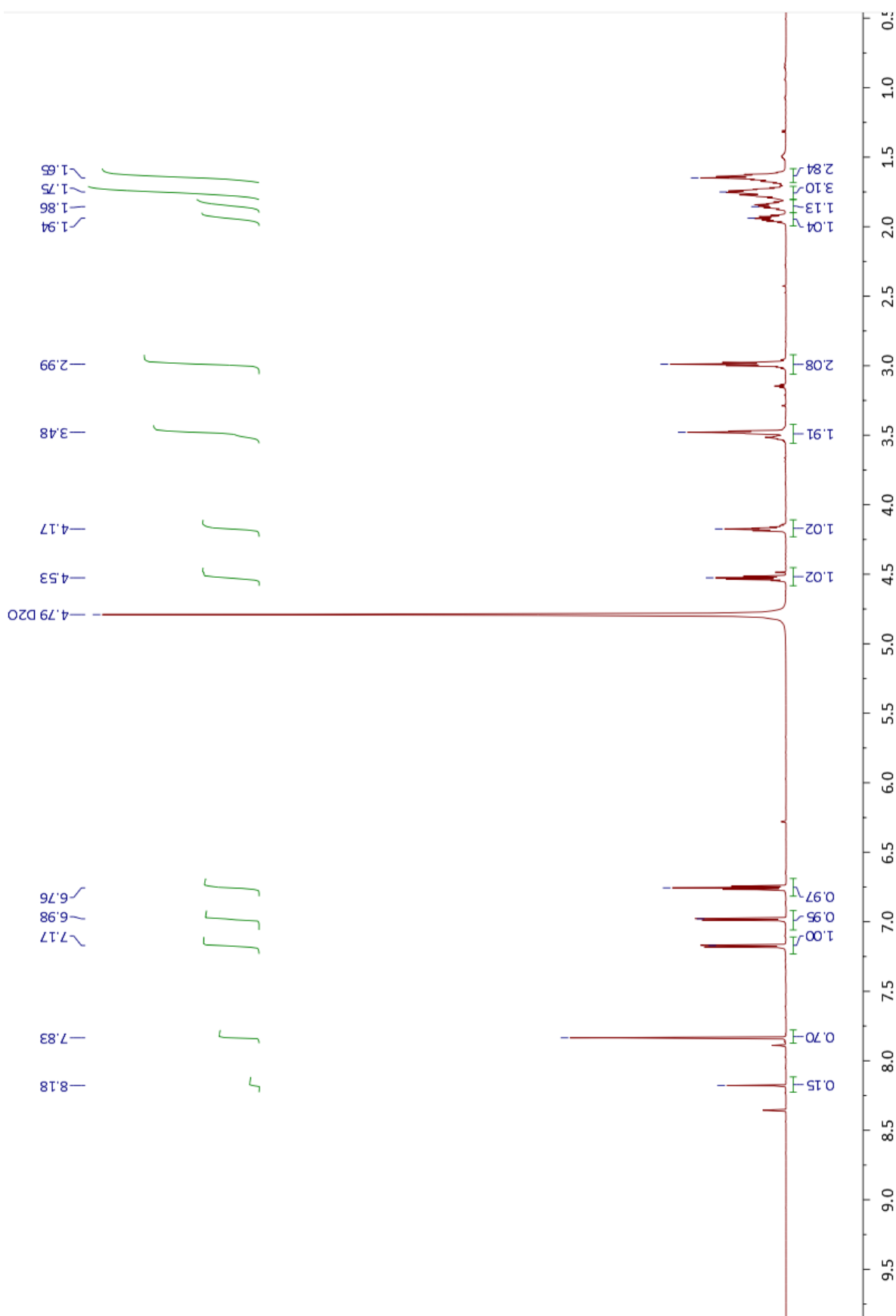


HPLC chromatogram of Isolated DEM30616/A. HPLC 1260 Infinity II. Injection volume 100 μ L, Flow rate 0.5 mL/min, Solvent A: MeCN, Solvent B: H₂O. Time 0-15 minutes, 100% A:0% B to 0% A: 100% B. Time 15-20 minutes 0% A: 100% B. DAD at 254 nM. Column conditions Eclipse Plus C18, 3.5 μ M, column length 4.6 x 100 mm, 40°C.



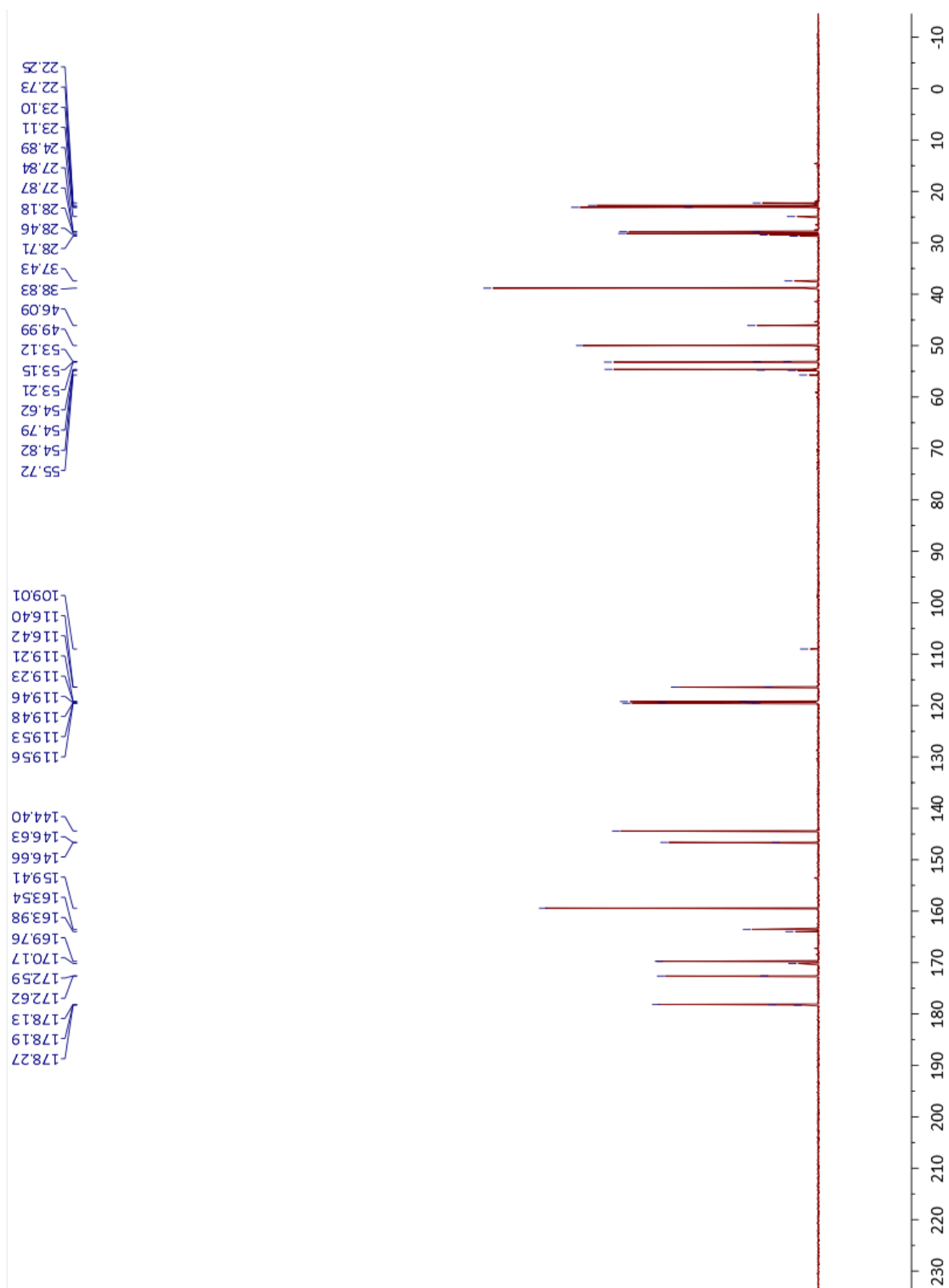
^1H NMR of DEM30616/A

D_2O , 298K, 700 MHz



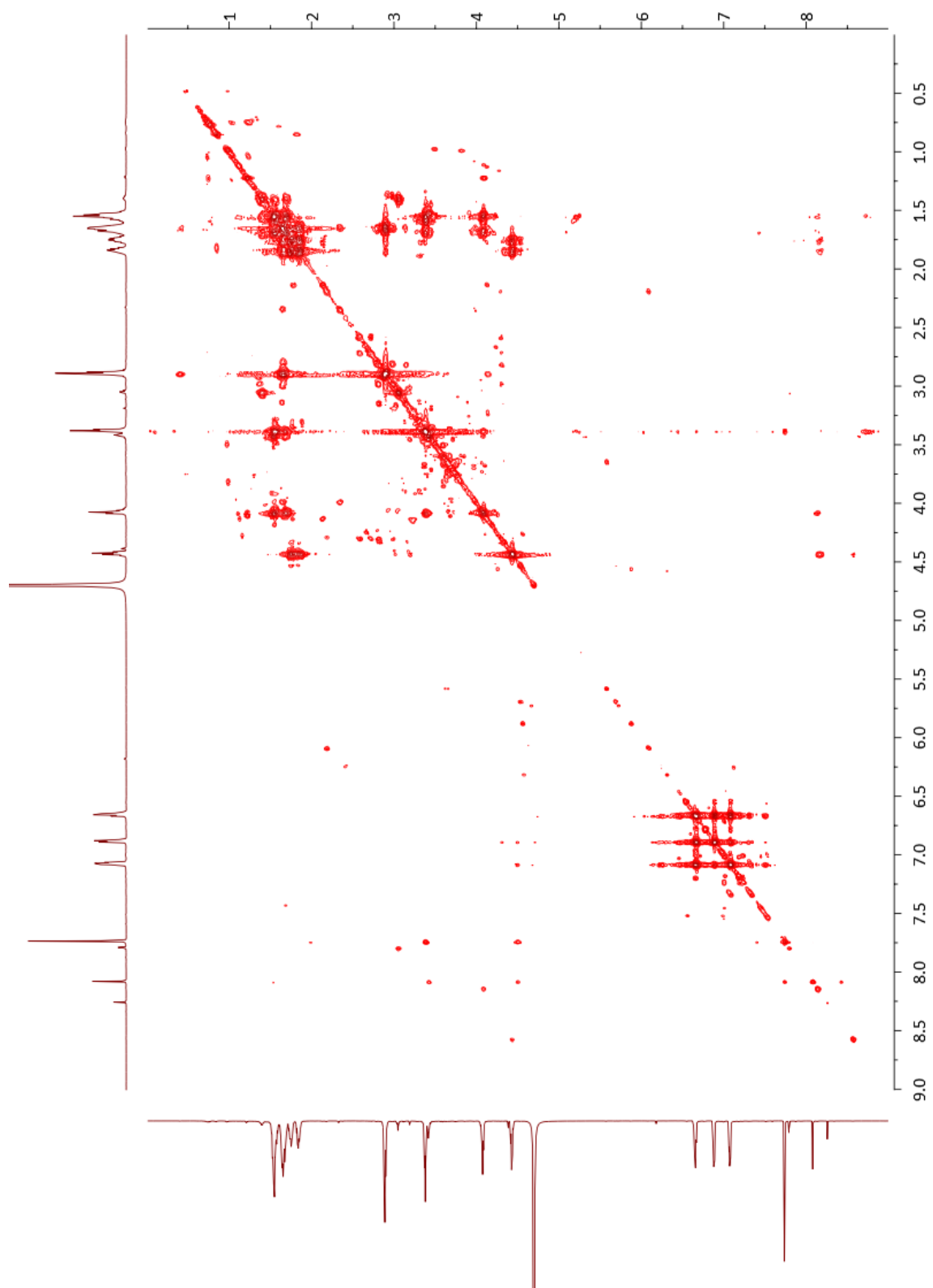
¹³C NMR of DEM30616/A

D₂O, 298K, 176 MHz



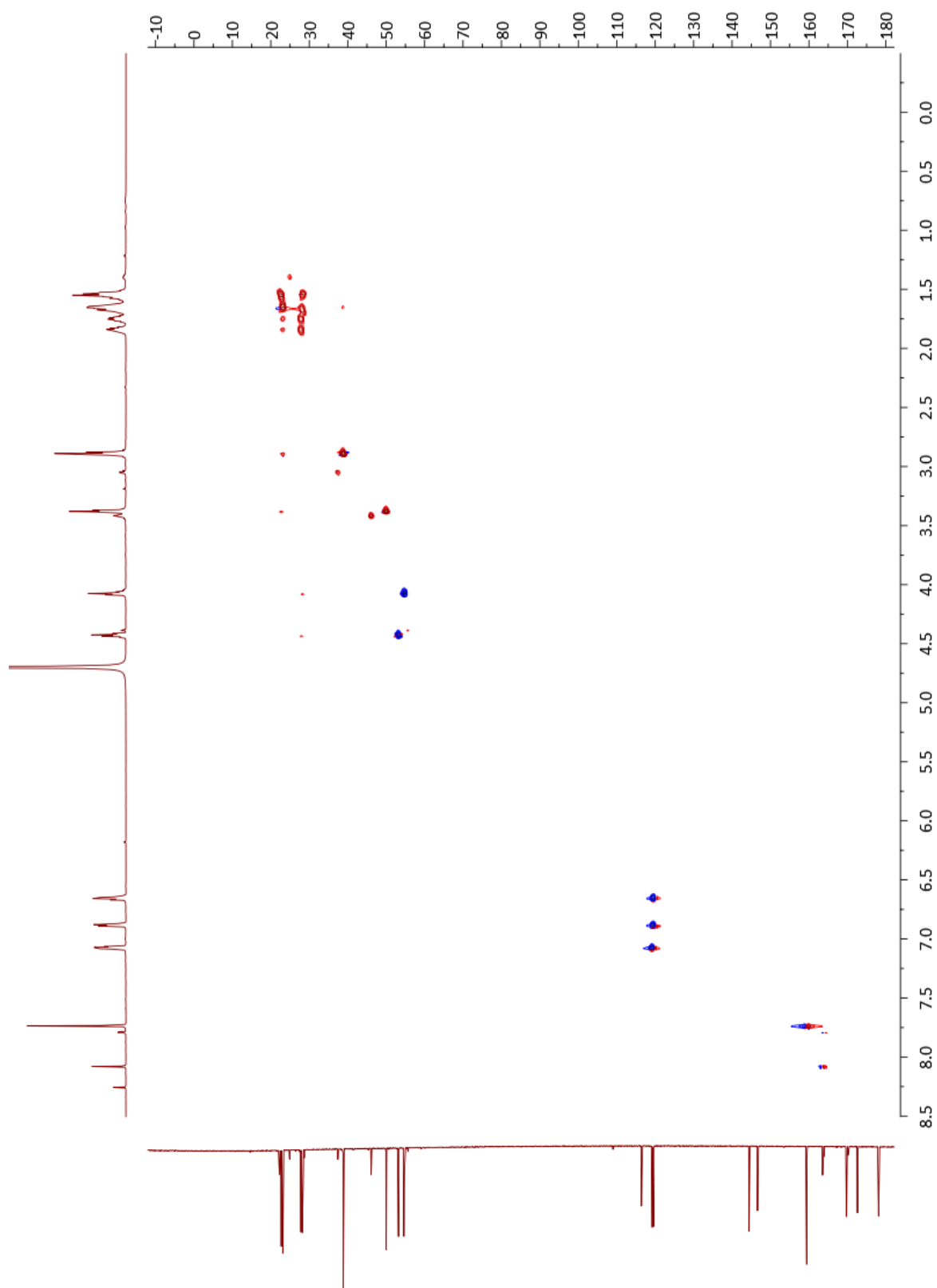
COSY NMR of DEM30616/A

D₂O, 298K, 700 MHz



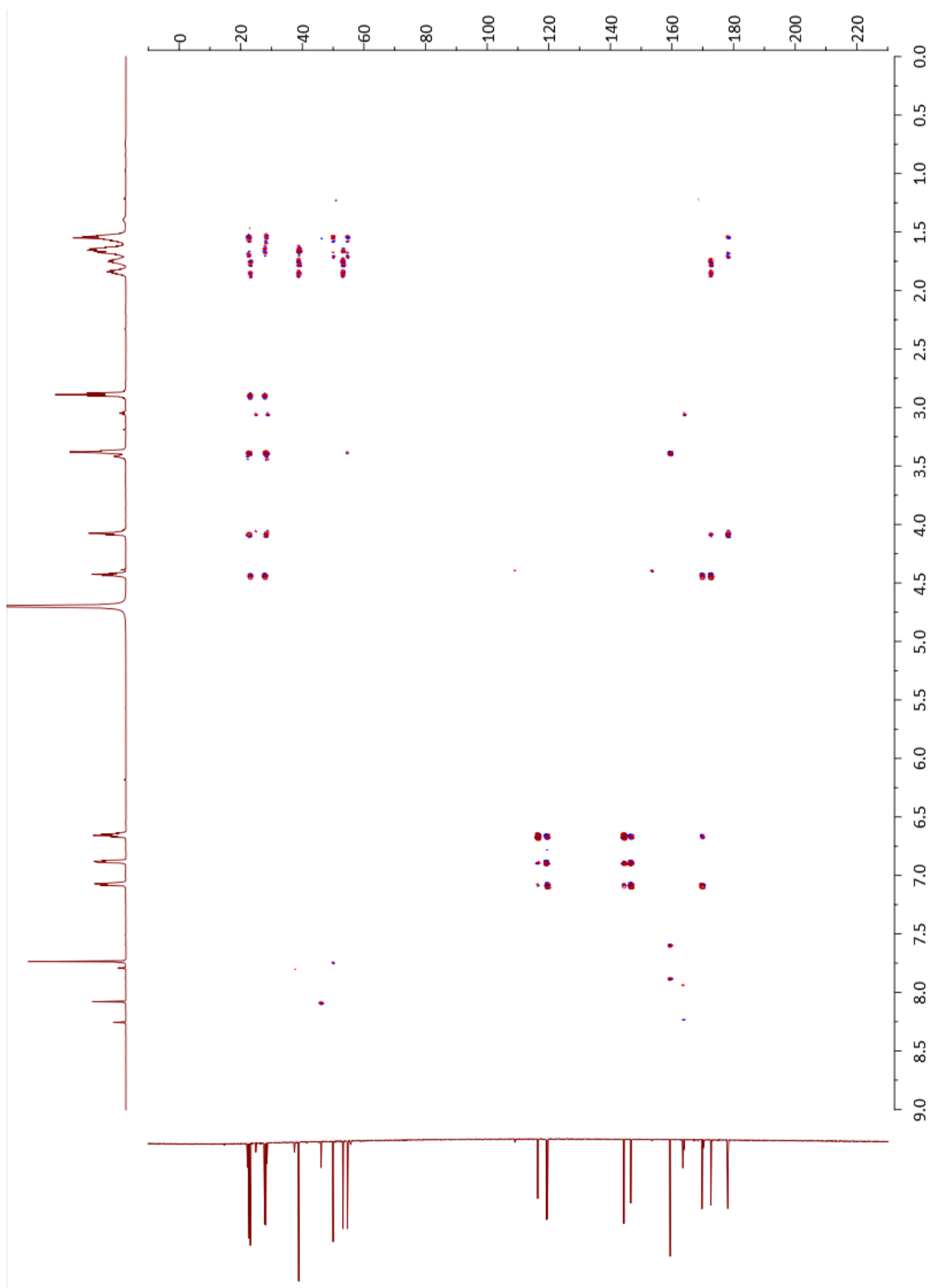
HSQC NMR of DEM30616/A

D₂O, 298K, 700 MHz



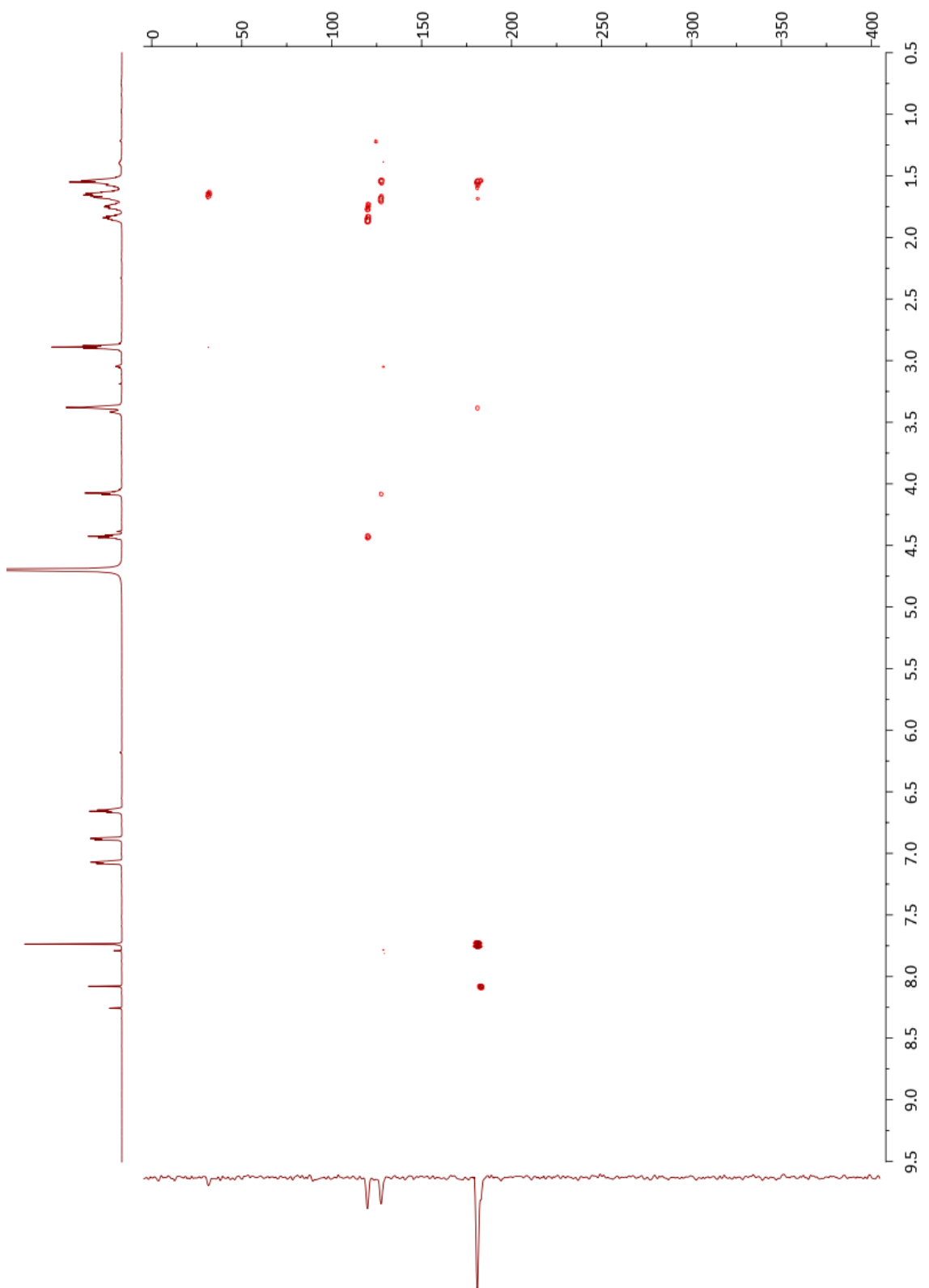
HMBC NMR of DEM30616/A

D₂O, 298K, 700 MHz



NH long range correlation 8Hz, NMR of DEM31376/A (madurastatin C1)

D₂O, 298K, 700 MHz, N = 236



Methyl (S)-2-(2-(benzyloxy)phenyl)-4,5-dihydrooxazole-4-carboxylate (32)

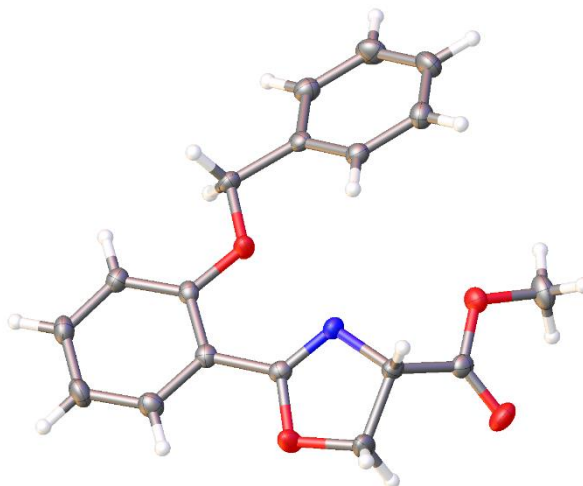


Table 1. Crystal data and structure refinement for mjh150026.

Identification code	mjh150026
Empirical formula	C ₁₈ H ₁₇ NO ₄
Formula weight	311.32
Temperature/K	150.0(2)
Crystal system	orthorhombic
Space group	P2 ₁ 2 ₁ 2 ₁
a/Å	7.10991(7)
b/Å	9.99847(11)
c/Å	21.2273(2)
α/°	90
β/°	90
γ/°	90
Volume/Å ³	1509.01(3)
Z	4
ρ _{calc} /cm ³	1.370
μ/mm ⁻¹	0.800
F(000)	656.0
Crystal size/mm ³	0.4 × 0.34 × 0.18
Radiation	CuKα (λ = 1.54184)

2 θ range for data collection/ $^{\circ}$	9.778 to 133.674
Index ranges	$-5 \leq h \leq 8, -11 \leq k \leq 11, -25 \leq l \leq 25$
Reflections collected	9614
Independent reflections	2672 [$R_{\text{int}} = 0.0249, R_{\text{sigma}} = 0.0205$]
Data/restraints/parameters	2672/0/209
Goodness-of-fit on F^2	1.085
Final R indexes [$I \geq 2\sigma(I)$]	$R_1 = 0.0270, wR_2 = 0.0680$
Final R indexes [all data]	$R_1 = 0.0277, wR_2 = 0.0684$
Largest diff. peak/hole / $e \text{ \AA}^{-3}$	0.17/-0.23
Flack parameter	-0.06(7)

Methyl (2-(benzyloxy)benzoyl)-L-serinate (41)

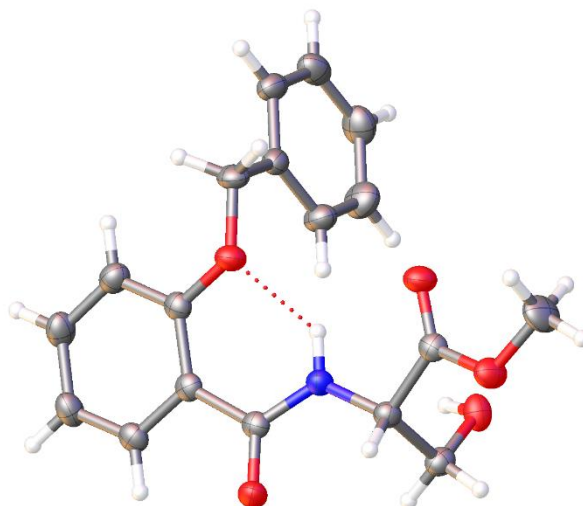


Table 1. Crystal data and structure refinement for mjh150018.

Identification code	mjh150018
Empirical formula	C ₁₈ H ₁₉ NO ₅
Formula weight	329.34
Temperature/K	150.0(2)
Crystal system	orthorhombic
Space group	P2 ₁ 2 ₁ 2 ₁
a/Å	8.31571(8)
b/Å	12.57373(12)
c/Å	15.66923(15)
α/°	90
β/°	90
γ/°	90
Volume/Å ³	1638.37(3)
Z	4
ρ _{calc} /g/cm ³	1.335
μ/mm ⁻¹	0.811
F(000)	696.0
Crystal size/mm ³	0.43 × 0.25 × 0.22
Radiation	CuKα (λ = 1.54184)

2 θ range for data collection/ $^{\circ}$	9.018 to 134.53
Index ranges	$-9 \leq h \leq 7, -15 \leq k \leq 14, -18 \leq l \leq 18$
Reflections collected	11667
Independent reflections	2898 [$R_{\text{int}} = 0.0234, R_{\text{sigma}} = 0.0177$]
Data/restraints/parameters	2898/0/224
Goodness-of-fit on F^2	1.113
Final R indexes [$I \geq 2\sigma(I)$]	$R_1 = 0.0273, wR_2 = 0.0676$
Final R indexes [all data]	$R_1 = 0.0285, wR_2 = 0.0688$
Largest diff. peak/hole / $e \text{ \AA}^{-3}$	0.14/-0.23
Flack parameter	0.00(6)

Methyl (*R*)-2-(2-(benzyloxy)benzamido)-3-chloropropanoate(44)

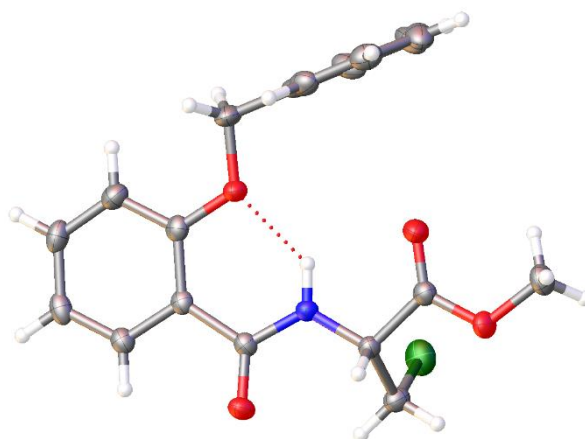


Table 1 : Crystal data and structure refinement for mjh150038.

Identification code	mjh150038
Empirical formula	C ₁₈ H ₁₈ ClNO ₄
Formula weight	347.78
Temperature/K	150.0(2)
Crystal system	orthorhombic
Space group	P2 ₁ 2 ₁ 2 ₁
a/Å	6.34313(11)
b/Å	11.79295(19)
c/Å	22.2052(4)
α/°	90
β/°	90
γ/°	90
Volume/Å ³	1661.04(5)
Z	4
ρ _{calc} /cm ³	1.391
μ/mm ⁻¹	2.230
F(000)	728.0
Crystal size/mm ³	0.38 × 0.1 × 0.07
Radiation	CuKα (λ = 1.54184)

2 θ range for data collection/ $^{\circ}$	7.964 to 133.896
Index ranges	$-7 \leq h \leq 7$, $-14 \leq k \leq 13$, $-26 \leq l \leq 25$
Reflections collected	11687
Independent reflections	2954 [$R_{\text{int}} = 0.0488$, $R_{\text{sigma}} = 0.0391$]
Data/restraints/parameters	2954/0/221
Goodness-of-fit on F^2	1.060
Final R indexes [$I \geq 2\sigma(I)$]	$R_1 = 0.0321$, $wR_2 = 0.0750$
Final R indexes [all data]	$R_1 = 0.0381$, $wR_2 = 0.0792$
Largest diff. peak/hole / $e \text{ \AA}^{-3}$	0.18/-0.23
Flack parameter	-0.004(10)

Methyl (*S*)-1-tritylaziridine-2-carboxylate (47)

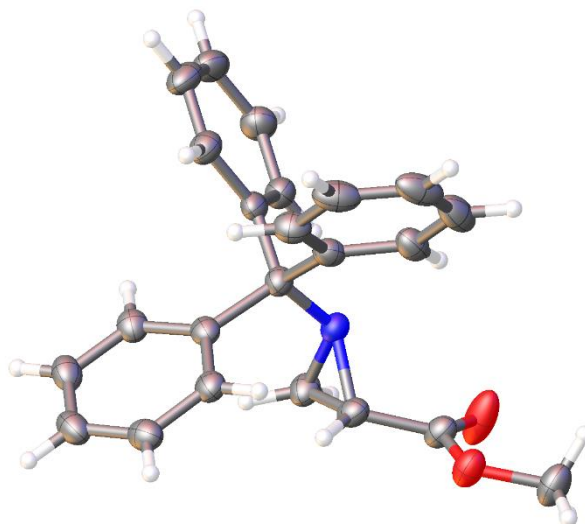


Table 1. Crystal data and structure refinement for mjh150004.

Identification code	mjh150004
Empirical formula	C ₂₃ H ₂₁ NO ₂
Formula weight	343.41
Temperature/K	150.0(2)
Crystal system	orthorhombic
Space group	P2 ₁ 2 ₁ 2 ₁
a/Å	9.85701(14)
b/Å	10.71346(15)
c/Å	17.4921(2)
α/°	90
β/°	90
γ/°	90
Volume/Å ³	1847.21(4)
Z	4
ρ _{calc} /cm ³	1.235
μ/mm ⁻¹	0.620
F(000)	728.0
Crystal size/mm ³	0.26 × 0.14 × 0.08
Radiation	CuKα (λ = 1.54184)

2 θ range for data collection/ $^{\circ}$	9.68 to 133.976
Index ranges	-11 \leq h \leq 11, -12 \leq k \leq 11, -20 \leq l \leq 20
Reflections collected	13238
Independent reflections	3270 [R _{int} = 0.0302, R _{sigma} = 0.0223]
Data/restraints/parameters	3270/0/236
Goodness-of-fit on F ²	1.061
Final R indexes [I \geq 2 σ (I)]	R ₁ = 0.0288, wR ₂ = 0.0684
Final R indexes [all data]	R ₁ = 0.0318, wR ₂ = 0.0705
Largest diff. peak/hole / e \AA^{-3}	0.10/-0.17
Flack parameter	0.06(11)

(S,Z)-N-(4-(((benzyloxy)carbonyl)amino)-4-carboxybutyl)-1-phenylmethanimine oxide (51)

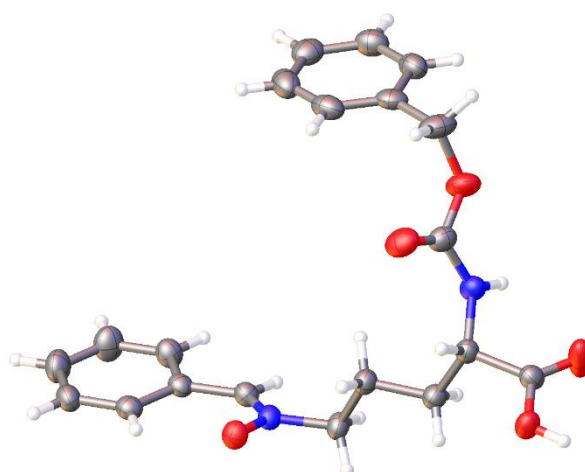


Table 1. Crystal data and structure refinement for mjh180049.

Identification code	mjh180049
Empirical formula	C ₂₀ H ₂₂ N ₂ O ₅
Formula weight	370.39
Temperature/K	150.0(2)
Crystal system	monoclinic
Space group	P21
a/Å	14.4192(5)
b/Å	5.18265(16)
c/Å	15.1106(5)
α /°	90
β /°	116.713(5)
γ /°	90
Volume/Å ³	1008.69(7)
Z	2
ρ calc/g cm ³	1.220
μ /mm ⁻¹	0.729
F(000)	392.0
Crystal size/mm ³	0.48 × 0.07 × 0.05
Radiation	CuK α (λ = 1.54184)

2 θ range for data collection/ $^{\circ}$	11.43 to 133.844
Index ranges	$-16 \leq h \leq 17$, $-5 \leq k \leq 6$, $-17 \leq l \leq 14$
Reflections collected	13813
Independent reflections	3466 [Rint = 0.0335, Rsigma = 0.0278]
Data/restraints/parameters	3466/2/250
Goodness-of-fit on F2	1.061
Final R indexes [$I \geq 2\sigma(I)$]	R1 = 0.0307, wR2 = 0.0776
Final R indexes [all data]	R1 = 0.0339, wR2 = 0.0797
Largest diff. peak/hole / e \AA^{-3}	0.12/-0.14
Flack parameter	-0.05(10)

Benzyl (S)-(1-(benzyloxy)-2-oxopiperidin-3-yl)carbamate (55)

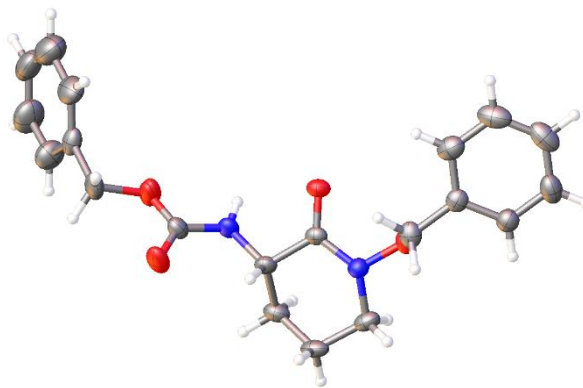


Table 1. Crystal data and structure refinement for mjh150031_fa.

Identification code	mjh150031_fa
Empirical formula	C ₂₀ H ₂₂ N ₂ O ₄
Formula weight	354.39
Temperature/K	150.0(2)
Crystal system	monoclinic
Space group	P2 ₁
a/Å	5.8565(2)
b/Å	4.74886(17)
c/Å	32.8637(12)
α/°	90
β/°	90.461(3)
γ/°	90
Volume/Å ³	913.96(6)
Z	2
ρ _{calc} /g/cm ³	1.288
μ/mm ⁻¹	0.738
F(000)	376.0
Crystal size/mm ³	0.19 × 0.13 × 0.04
Radiation	CuKα (λ = 1.54184)
2θ range for data collection/°	5.378 to 135.358
Index ranges	-6 ≤ h ≤ 6, -5 ≤ k ≤ 5, -39 ≤ l ≤ 38

Reflections collected	11002
Independent reflections	3239 [R _{int} = 0.0323, R _{sigma} = 0.0297]
Data/restraints/parameters	3239/92/305
Goodness-of-fit on F ²	1.087
Final R indexes [I ≥ 2σ (I)]	R ₁ = 0.0328, wR ₂ = 0.0730
Final R indexes [all data]	R ₁ = 0.0379, wR ₂ = 0.0759
Largest diff. peak/hole / e Å ⁻³	0.12/-0.13
Flack parameter	0.35(12)

Methyl (2-(benzyloxy)benzoyl)-D-serinate (56)

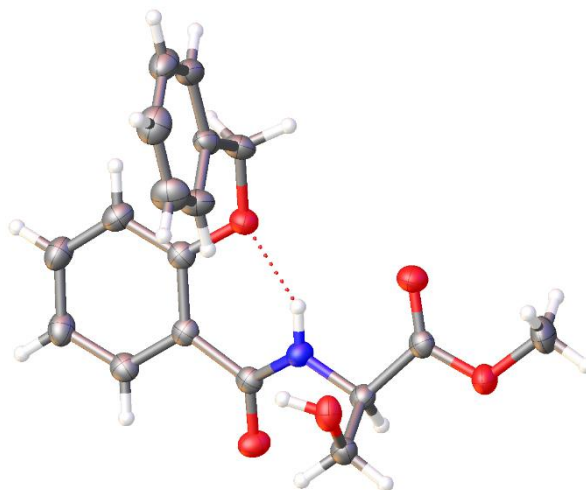


Table 1. Crystal data and structure refinement for mjh170005_fa.

Identification code	mjh170005_fa
Empirical formula	C ₁₈ H ₁₉ NO ₅
Formula weight	329.34
Temperature/K	150.0(2)
Crystal system	orthorhombic
Space group	P2 ₁ 2 ₁ 2 ₁
a/Å	8.31712(6)
b/Å	12.57172(10)
c/Å	15.66621(14)
α/°	90
β/°	90
γ/°	90
Volume/Å ³	1638.07(2)
Z	4
ρ _{calc} /cm ³	1.335
μ/mm ⁻¹	0.812
F(000)	696.0
Crystal size/mm ³	0.28 × 0.16 × 0.13
Radiation	CuKα (λ = 1.54184)

2 θ range for data collection/ $^{\circ}$	9.02 to 133.508
Index ranges	$-8 \leq h \leq 9, -14 \leq k \leq 15, -18 \leq l \leq 18$
Reflections collected	14353
Independent reflections	2889 [$R_{\text{int}} = 0.0228, R_{\text{sigma}} = 0.0159$]
Data/restraints/parameters	2889/0/225
Goodness-of-fit on F^2	1.077
Final R indexes [$I \geq 2\sigma(I)$]	$R_1 = 0.0233, wR_2 = 0.0581$
Final R indexes [all data]	$R_1 = 0.0241, wR_2 = 0.0588$
Largest diff. peak/hole / $e \text{ \AA}^{-3}$	0.14/-0.13
Flack parameter	0.08(5)

(S)-1-(benzyloxy)-2-oxopiperidin-3-aminium bromide (71)

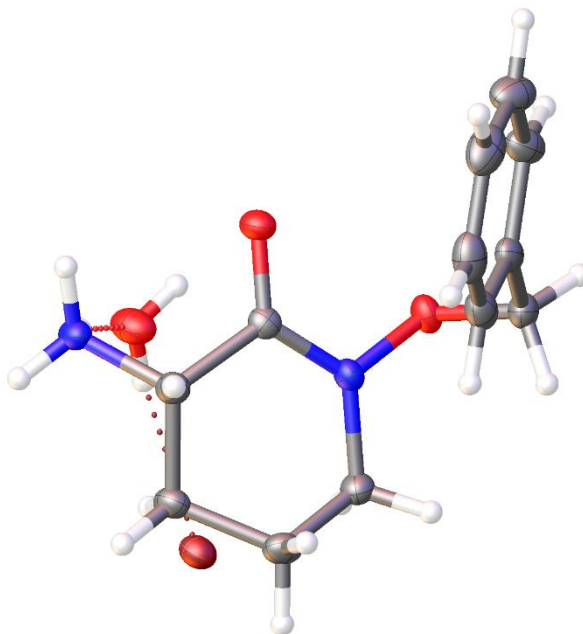


Table 1. Crystal data and structure refinement for mjh180048.

Identification code	mjh180048
Empirical formula	C ₁₂ H ₁₉ BrN ₂ O ₃
Formula weight	319.20
Temperature/K	150.0(2)
Crystal system	orthorhombic
Space group	P212121
a/Å	6.27186(7)
b/Å	13.02097(16)
c/Å	16.9228(2)
α /°	90
β /°	90
γ /°	90
Volume/Å ³	1382.02(3)
Z	4
ρ calcg/cm ³	1.534
μ /mm ⁻¹	4.095

F(000)	656.0
Crystal size/mm ³	0.39 × 0.1 × 0.05
Radiation	CuK α (λ = 1.54184)
2 θ range for data collection/°	8.568 to 133.83
Index ranges	-7 ≤ h ≤ 7, -15 ≤ k ≤ 15, -19 ≤ l ≤ 20
Reflections collected	19643
Independent reflections	2461 [Rint = 0.0385, Rsigma = 0.0192]
Data/restraints/parameters	2461/0/178
Goodness-of-fit on F ²	1.045
Final R indexes [$I \geq 2\sigma(I)$]	R1 = 0.0172, wR2 = 0.0422
Final R indexes [all data]	R1 = 0.0183, wR2 = 0.0430
Largest diff. peak/hole / e Å ⁻³	0.17/-0.22
Flack parameter	-0.030(9)

(R)-2-(benzyloxy)-N-(4,7,11-trioxo-1-oxa-5,8-diazacycloundecan-3-yl)benzamide (75)

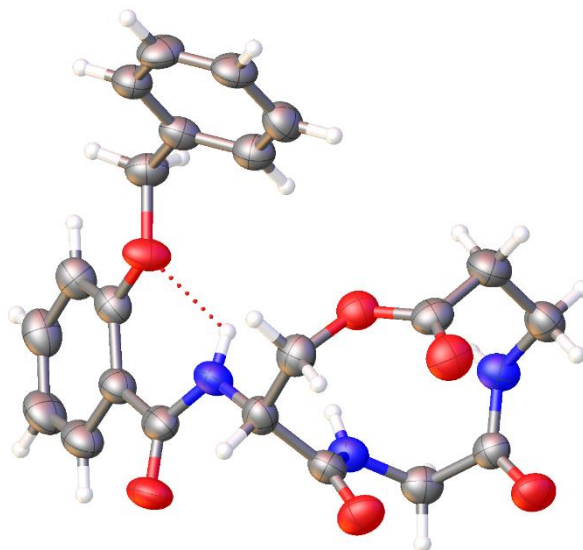


Table 1. Crystal data and structure refinement for mjh180034_2_fa.

Identification code	mjh180034_2_fa
Empirical formula	C ₂₂ H ₂₃ N ₃ O ₆
Formula weight	425.43
Temperature/K	150.0(2)
Crystal system	monoclinic
Space group	P2 ₁
a/Å	9.3116(7)
b/Å	18.9840(13)
c/Å	11.8019(9)
α/°	90
β/°	94.865(8)
γ/°	90
Volume/Å ³	2078.7(3)
Z	4
ρ _{calc} /cm ³	1.359
μ/mm ⁻¹	0.834
F(000)	896.0
Crystal size/mm ³	0.09 × 0.08 × 0.02

Radiation	CuK α ($\lambda = 1.54184$)
2 θ range for data collection/ $^\circ$	7.518 to 133.862
Index ranges	$-8 \leq h \leq 11$, $-22 \leq k \leq 21$, $-14 \leq l \leq 14$
Reflections collected	14785
Independent reflections	6517 [$R_{\text{int}} = 0.0748$, $R_{\text{sigma}} = 0.0943$]
Data/restraints/parameters	6517/16/577
Goodness-of-fit on F^2	1.014
Final R indexes [$I \geq 2\sigma(I)$]	$R_1 = 0.0607$, $wR_2 = 0.1271$
Final R indexes [all data]	$R_1 = 0.0954$, $wR_2 = 0.1488$
Largest diff. peak/hole / $e \text{ \AA}^{-3}$	0.24/-0.22
Flack parameter	-0.1(3)

N-(benzyloxy)-2-nitrobenzenesulfonamide (89)

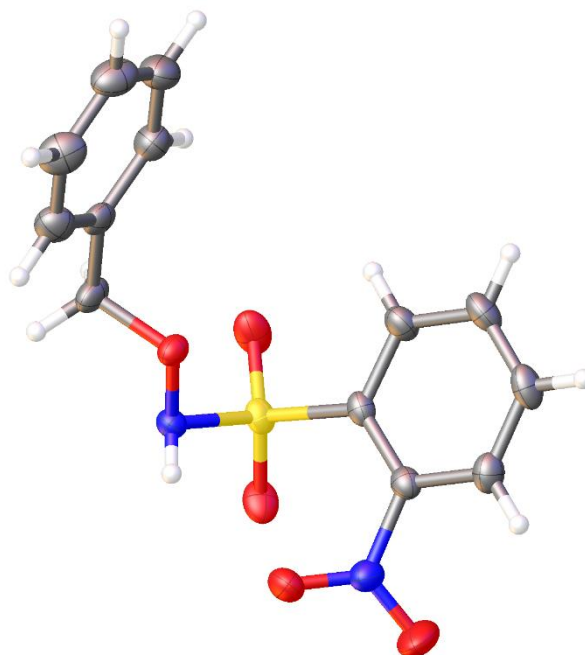


Table 1. Crystal data and structure refinement for mjh170033.

Identification code	mjh170033
Empirical formula	C ₁₃ H ₁₂ N ₂ O ₅ S
Formula weight	308.31
Temperature/K	150.0(2)
Crystal system	monoclinic
Space group	P2 ₁ /n
a/Å	13.35590(9)
b/Å	7.85194(5)
c/Å	13.94732(12)
α/°	90
β/°	104.5616(7)
γ/°	90
Volume/Å ³	1415.668(18)
Z	4
ρ _{calc} /g/cm ³	1.447
μ/mm ⁻¹	2.264
F(000)	640.0

Crystal size/mm ³	0.33 × 0.18 × 0.15
Radiation	CuKα (λ = 1.54184)
2θ range for data collection/°	8.194 to 133.866
Index ranges	-15 ≤ h ≤ 15, -9 ≤ k ≤ 9, -15 ≤ l ≤ 16
Reflections collected	51635
Independent reflections	2507 [R _{int} = 0.0272, R _{sigma} = 0.0079]
Data/restraints/parameters	2507/0/194
Goodness-of-fit on F ²	1.047
Final R indexes [I ≥ 2σ (I)]	R ₁ = 0.0254, wR ₂ = 0.0647
Final R indexes [all data]	R ₁ = 0.0265, wR ₂ = 0.0655
Largest diff. peak/hole / e Å ⁻³	0.28/-0.29

Structural Reassignment and Absolute Stereochemistry of Madurastatin C1 (MBJ-0034) and the Related Aziridine Siderophores: Madurastatins A1, B1, and MBJ-0035

Andrew R. Tyler,[†] Hamed Mosaei,[‡] Stephanie Morton,[†] Paul G. Waddell,[†] Corinne Wills,[†] William McFarlane,[†] Joe Gray,[§] Michael Goodfellow,[‡] Jeff Errington,^{||,‡} Nick Allenby,^{||} Nikolay Zenkin,[‡] and Michael J. Hall^{*,†,⊙}

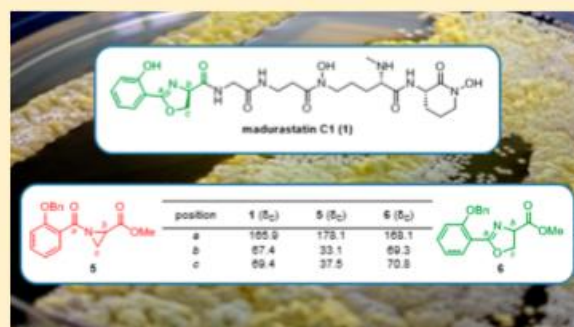
[†]School of Chemistry and [‡]School of Biology, Newcastle University, Newcastle upon Tyne, NE1 7RU, U.K.

[‡]Centre for Bacterial Cell Biology and [§]Pinnacle Laboratory, Institute for Cell and Molecular Biosciences, Newcastle University, Newcastle Upon Tyne, NE2 4AX, U.K.

^{||}Demuris Limited, Newcastle Biomedicine Bio-Incubators, Framlington Place, Newcastle upon Tyne, NE2 4HH, U.K.

Supporting Information

ABSTRACT: The madurastatins are pentapeptide siderophores originally described as containing an unusual salicylate-capped N-terminal aziridine ring. Isolation of madurastatin C1 (**1**) (also designated MBJ-0034), from *Actinomadura* sp. DEM31376 (itself isolated from a deep sea sediment), prompted structural reevaluation of the madurastatin siderophores, in line with the recent work of Thorson and Shaaban. NMR spectroscopy in combination with partial synthesis allowed confirmation of the structure of madurastatin C1 (**1**) as containing an N-terminal 2-(2-hydroxyphenyl)oxazoline in place of the originally postulated aziridine, while absolute stereochemistry was determined via Harada's advanced Marfey's method. Therefore, this work further supports Thorson and Shaaban's proposed structural revision of the madurastatin class of siderophores (madurastatins A1 (**2**), B1 (**3**), C1 (**1**), and MBJ-0036 (**4**)) as N-terminal 2-(2-hydroxyphenyl)oxazolines.



Siderophores are key components of the bacterial endogenous secondary metabolome, facilitating intracellular uptake of Fe³⁺ and other essential metals from the surrounding environment.¹ Pathogenic bacteria also employ siderophores to sequester metals from the host organism, thus playing an important role in virulence.² The genus *Actinomadura*,³ from the family *Thermomonosporaceae*, contains both environmental (predominately soil dwelling) and opportunistically pathogenic species and are a source of a number of bioactive secondary metabolites⁴ including the madurastatin⁵ and maduraferrin⁶ siderophores.

As part of a program to identify new natural products from actinobacteria,⁷ we have investigated the secondary metabolite production of a marine isolate, *Actinomadura* sp. DEM31376. Along with the known cyclic heptapeptide RNAP inhibitor GE23077,⁸ we isolated the siderophore madurastatin C1 (**1**)^{5b} (also designated MBJ-0034).^{5c} Spectroscopic analysis of isolated **1** was however not consistent with the originally reported structure. Recent work by Thorson and Shaaban proposed a structural revision for the madurastatins as containing a 2-(2-hydroxyphenyl)oxazoline moiety, based on an analysis of the NMR data pertaining to both related bacterial siderophores and synthetic intermediates.⁹ Thus, as part of our

investigations we compared isolated madurastatin C1 (**1**) to both aziridine- and 2-(2-hydroxyphenyl)oxazoline-containing synthetic analogues, as well as examined the absolute stereochemistry of madurastatin C1 (**1**) via a Marfey's analysis.

RESULTS AND DISCUSSION

Madurastatin C1 (**1**) was first isolated from the fermentation broth of *Actinomadura* sp. DSMZ 13491 by Sosio *et al.* in 2012^{5b} and again by Shin-ya *et al.* in 2014 (as MBJ-0034, along with the related siderophore MBJ-0035 (**4**))^{5c} and was originally assigned as a linear pentapeptide containing a salicylate-capped N-terminal aziridine ring by spectroscopic analysis and analogy with the previously reported madurastatins A1 (**2**) and B1 (**3**) (Figure 1).

In our hands, madurastatin C1 (**1**) was reisolated from *Actinomadura* sp. DEM31376, a strain originally isolated from deep sea marine sediment (Canary Basin, Atlantic Ocean).¹⁰ On the basis of 16S rRNA analysis, strain DEM31376 was recovered in the genus *Actinomadura*, forming a subgroup with

Received: January 26, 2017

Published: April 11, 2017

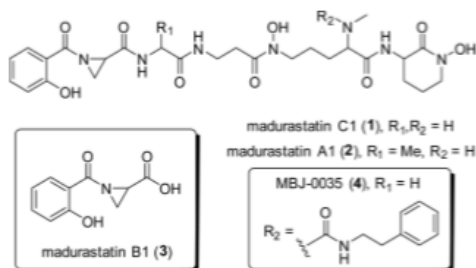


Figure 1. Previously proposed structures of the “aziridine”-containing madurastatin siderophores.

the type strains *A. mexicana*, *A. citrea*, and *A. scrupuli*. Although closely related to both *A. mexicana* and *A. citrea* (99.4% 16S rRNA gene similarity), taxonomic analysis suggests that strain DEM31376 may form the nucleus of a novel species within the genus *Actinomadura* (Figure 2).¹¹

Strain DEM31376 was cultivated in ISP2 media in a 20 L bioreactor. Absorption of the fermentation broth onto Amberlite XAD16N beads (elution MeOH), solid-phase capture on C_8 SPE cartridges (elution with 50–100% MeOH), and finally reversed-phase column chromatography (gradient elution, H_2O to MeOH, Biotage Isolera SNAP C_{18}) provided 238 mg of 1. ESIHRMS showed an $[M + H]^+$ ion at 592.2732 m/z , confirming the molecular formula ($C_{26}H_{37}O_9N_7$). MS/MS gave fragments at 462, 434, 403, 349, and 318 m/z in line with a previous analysis,^{5b} while HPLC-ESIMS showed the presence of a related molecule at 610 m/z , formed via hydrolysis of the parent ion. ^{13}C NMR revealed 26 carbon signals, six corresponding to an *ortho*-disubstituted benzene and six to carbonyl-like carbons, three of which were shown to be primary amides though HMBC correlations with exchangeable protons at 8.52, 8.11, and 7.93 ppm. Thus, the remaining two degrees of unsaturation are due to the presence of a further two ring systems. 1H NMR, COSY, and ^{15}N - 1H HSQC revealed five amino acid spin systems, namely, glycine, β -alanine, a modified serine, and two modified ornithines. Indirect measurement of the natural abundance ^{15}N spectra by 1H - ^{15}N HMBC showed the presence of seven nitrogen atoms in four different chemical shift ranges, indicative of three amides, two hydroxamic acids, one amine, and an unusual imine-like nitrogen. The role of 1 as a hexadentate siderophore was confirmed through chelation with both $Fe(acac)_3$ and $Ga(acac)_3$, HPLC-ESIMS showing signals at 645.2 and 658.2 m/z corresponding to the protonated 1:1 complexes of 1 with

Fe^{3+} and Ga^{3+} , respectively. Interestingly chelation with $Fe(acac)_3$ gave rise to an additional compound (663.2 m/z), demonstrating that hydrolyzed 1 is also a competent ligand for Fe^{3+} . Furthermore, 1 showed growth reduction against *Bacillus subtilis* (disk diffusion assay) presumably through an inhibition of Fe^{3+} uptake.

The NMR data of 1 did however highlight a number of discrepancies with the originally proposed structure. In particular the ^{13}C NMR shifts for the α - and β -carbons of the serine residue are observed at 67 and 69 ppm, highly atypical of an aryl-substituted aziridine ring (shift range 25–45 ppm).¹³ Thorson and Shaaban recently proposed that the madurastatin siderophores contain an N-terminal 2-(2-hydroxyphenyl)-oxazoline ring,⁹ a bidentate coordination moiety present in a number of other mixed ligand siderophores (e.g., acinetobactin,¹⁴ the amamistatins,¹⁵ the amychelins,¹⁶ brasilibactin A,¹⁷ gobichelins A and B,¹⁸ nocardichelins A and B,¹⁹ transvalencin Z,²⁰ and the spoxazomicins A–C²¹), in which the corresponding ^{13}C shifts typically occur from 65 to 72 ppm (Table 1).

To test this hypothesis, we synthesized the salicylate-containing fragment of 1 as both an aziridine 5 and as an oxazoline 6 for comparison. *N*-Trityl-L-serine methyl ester 7 was activated with mesyl chloride followed by base-catalyzed intramolecular ring closure to give methyl (S)-1-tritylaziridine-2-carboxylate 8, confirmed by single-crystal X-ray analysis.²² Trityl deprotection with TFA/ Et_3SiH in DCM²³ followed by *in situ* reaction with 2-(benzyloxy)benzoyl chloride gave the desired aziridine-containing fragment 5 (Scheme 1).

Synthesis of the oxazoline-containing fragment 6 involved reaction of L-serine methyl ester 9 with 2-(benzyloxy)benzoyl chloride to give amide 10. Attempted oxazoline formation with thionyl chloride gave only low yields of 6 alongside an unwanted chlorinated derivative, 11.²⁴ Treatment of 10 with diethylaminosulfur trifluoride (DAST) provided the desired oxazoline 6 in 79% yield.²⁵ Confirmation of the structure of 6 was given by single-crystal X-ray analysis,²² including comparison to the closely related X-ray structure of spoxazomicin C (Scheme 2).^{21a}

Comparison of the 1H and ^{13}C NMR spectra of 1, 5, and 6 confirmed the presence of an oxazoline in the natural product. Both the ^{13}C NMR shifts of the ring carbons (C-2 and C-3) and carbonyl-like carbon (C-1) and the 1H NMR shifts for H_a , H_b , and H_c of 1 align well with those of synthetic oxazoline 6. In addition, coupling constant analysis of 6 shows J_{cis} , J_{trans} , and J_{gem} of 10.5, 7.6, and 8.8 Hz, respectively,²⁶ corresponding closely to those observed in 1 (note that in 5 $J_{cis} = 5.3$, $J_{trans} = 3.1$, and $J_{gem} = 1.3$ Hz, demonstrating the small geminal coupling characteristic of an aziridine).²⁷ Analysis of the

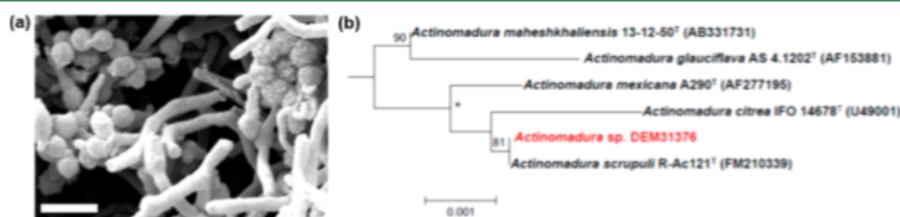
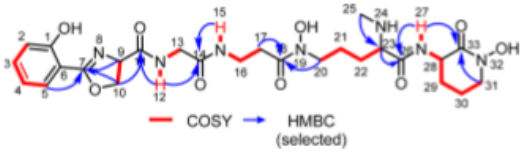
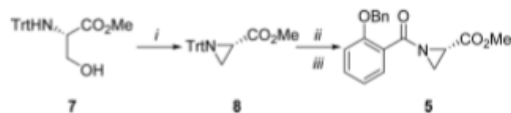


Figure 2. (a) Scanning electron micrograph of strain DEM31376 showing spiral chains of warty ornamented spores following growth on ISP3 agar; bar indicates 2 μm . (b) Neighbor-joining tree based on nearly complete 16S rRNA gene sequences showing relationships between strain DEM31376 and closely related type strains of *Actinomadura* species. Asterisks indicate branches also recovered using maximum likelihood and maximum parsimony tree making methods. Numbers at nodes indicate bootstrap values based on neighbor-joining analysis of 1000 resampled data sets.

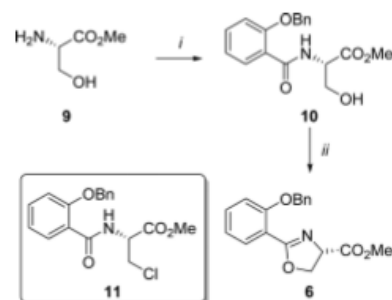
Table 1. Revised Structure and NMR Data for Madurastatin C1 (DMSO-*d*₆, 298 K, 700 MHz)


position	δ_C type	δ_H (J in Hz)	δ_N^c
1	159.1, C		
2	116.6, CH	7.01, dd (8.3, 1.1)	
3	134.1, CH	7.47, ddd (8.7, 7.3, 1.8)	
4	119.1, CH	6.95, td (7.5, 1.1)	
5	128.1, CH	7.65, dd (7.8, 1.8)	
6	109.9, C		
7	165.9, C		
8			208.2
9	67.4, CH	5.01, dd (10.4, 7.7)	
10	69.4, CH ₂	4.65, dd (10.5, 8.4) 4.52, t (8.0)	
11	170.2, C		
12		8.52, t (5.9)	109.2
13	42.2, CH ₂	3.75, dd (16.5, 6.1) 3.67, dd (16.5, 5.7)	
14	168.4, C		
15		7.93, t (5.8 Hz)	112.5
16	34.6, CH ₂	3.28–3.22, m	
17	32.0, CH ₂	2.53–2.51, m	
18	170.9, C		
19			175.9
20	47.0, CH ₂	3.51–3.42, m ^b	
21	22.8, CH ₂	1.63–1.53, m	
22	30.2, CH	1.50–1.45, m 1.43–1.38, m	
23	63.7, CH	2.87, t (6.6)	
24			29.1
25	34.2, CH ₃	2.21, s	
26	173.5, C		
27		8.11, d (8.3)	118.8
28	49.4, CH	4.32, ddd (10.9, 8.2, 5.3)	
29	27.8, CH ₂	1.96–1.82, m ^b 1.67 qd (12.5, 4.3)	
30	20.4, CH ₂	1.96–1.82, m ^b	
31	51.2, CH ₂	3.51–3.42, m ^b	
32			171.8
33	165.0, C		

^aHMBC performed at 10 Hz. ^bSignals overlapping. ^c¹⁵N shifts measured indirectly by ¹H–¹⁵N HMBC performed at both 8 and 12 Hz, referenced against liquid NH₃.

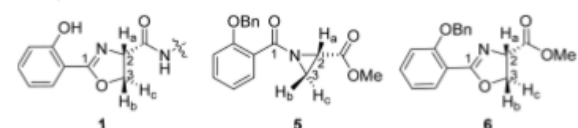
Scheme 1. Formation of the Aziridine-Containing Fragment 5^a

^aConditions: (i) MsCl, Et₃N, DCM, 0 °C to RT, 18 h, then Et₃N, THF, reflux, 16 h, 70%. (ii) Et₃SiH, Et₃N, DCM, 0 °C to RT, 5 h. (iii) 2-(benzyloxy)benzoyl chloride, Et₃N, –78 °C to RT, 48 h, 35% over 2 steps.

Scheme 2. Synthesis of the Oxazoline-Containing Fragment 6^a

^aConditions: (i) 2-(benzyloxy)benzoyl chloride, Et₃N, –78 °C to RT, 18 h, 95%. (ii) DCM, DAST, –78 °C to RT, 2 h, 79%.

literature pertaining to the madurastatin siderophores A1 and MBJ-0036 reveals that the ¹H and ¹³C NMR data of these compounds also closely match those of oxazoline 6, suggesting that, in agreement with Thorson and Shaaban,⁹ these structures should also be similarly revised as containing an N-terminal 2-(2-hydroxyphenyl)oxazoline (Table 2).

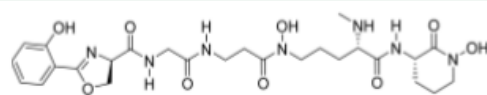
Table 2. ¹H and ¹³C NMR Comparison of 1 with Synthetic Compounds 5 and 6

position	1	5	6
1, δ_C	165.9	178.1	168.1
2, δ_C	67.4	33.1	69.3
3, δ_C	69.4	37.5	70.8
H _a , δ_H (J in Hz)	5.05 dd (10.7, 8.1)	3.23 dd (5.3, 3.1)	4.97 dd (10.5, 7.6)
H _b , δ_H (J in Hz)	4.69 dd (10.7, 8.5)	2.63 dd (5.3, 1.3)	4.62 dd (10.5, 8.8)
H _c , δ_H (J in Hz)	4.61 t (8.3) ^b	2.62 dd (3.1, 1.3)	4.67 dd (8.8, 7.6)

^a700 MHz, CD₃OD. ^bSignal is an apparent triplet due to similar values of *J*_{trans} and *J*_{gem}.

Finally Harada's advanced Marfey's method was employed to determine the absolute stereochemistry of madurastatin C1 (1).²⁸ Hydrolysis of 1 with concentrated HI²⁹ and derivatization with *N*α-(5-fluoro-2,4-dinitrophenyl)-L-leucinamide was followed by analysis by HPLC-ESIMS. Comparison to prepared amino acid standards revealed the presence of D-serine, L-N-methylornithine, and L-ornithine, allowing absolute stereochemical determination of all three stereocenters (Figure 3).

In conclusion, we have confirmed Thorson and Shaaban's revised structure of madurastatin C1 (1) as an oxazoline-

**Figure 3.** Revised structure of madurastatin C1 (1) including absolute stereochemistry.

containing mixed ligand N-terminal 2-(2-hydroxyphenyl)-oxazoline hexadentate siderophore and have determined its absolute stereochemistry. On the basis of NMR analysis, similar structural revisions should also be applied across the madurastatin family of natural products including madurastatins A1, B1, and MBJ-0035.^{5,9}

■ ASSOCIATED CONTENT

Supporting Information

The Supporting Information is available free of charge on the ACS Publications website at DOI: 10.1021/acs.jnatprod.7b00082.

Characterization details for DEM31376, isolation procedures and analysis (including 1D and 2D NMR spectra) for madurastatin C1 (1), experimental details for the synthesis and characterization of compounds 5, 6, 8, and 10, crystal data for 6, 8, and 10 (PDF)

■ AUTHOR INFORMATION

Corresponding Author

*Tel (M. J. Hall): +44 (0) 191 208 7321. Fax: +44 (0) 191 208 6929. E-mail: michael.hall@newcastle.ac.uk.

ORCID

Jeff Errington: 0000-0002-6977-9388

Michael J. Hall: 0000-0001-6475-9161

Notes

The authors declare no competing financial interest.

■ ACKNOWLEDGMENTS

The authors thank Newcastle University for funding including Ph.D. studentships (A.T. and S.M.), the Wellcome Trust (102851) and Leverhulme Trust (PLP-2014-229) for funding (N.Z.), the EPSRC UK National Mass Spectrometry Facility at Swansea University, and EPSRC for X-ray crystallography facilities (EP/F03637X/1).

■ REFERENCES

- Hider, R. C.; Konga, X. *Nat. Prod. Rep.* **2010**, *27*, 637–657.
- Miethke, M.; Marahiel, M. A. *Microbiol. Mol. Biol. Rev.* **2007**, *71*, 413–451.
- Trujillo, M. E.; Goodfellow, M. *Actinomadura*. *Bergey's Manual of Systematics of Archaea and Bacteria*; Lechevalier and Lechevalier, 400th ed.; Kropfenstedt, Stackebrandt and Goodfellow, 156, John Wiley & Sons, Inc., in association with Bergey's Manual Trust, 2015; pp 1–32.
- (a) Gerber, N. N. *Tetrahedron Lett.* **1970**, *11*, 809–812. (b) Zein, N.; Solomon, W.; Colson, K. L.; Schroeder, D. R. *Biochemistry* **1995**, *34*, 11591–11597. (c) Simmons, L.; Kaufmann, K.; Garcia, R.; Schwär, G.; Huch, V.; Müller, R. *Bioorg. Med. Chem.* **2011**, *19*, 6570–6575. (d) Wyche, T. P.; Piotrowski, J. S.; Hou, Y.; Braun, D.; Deshpande, R.; McIlwain, S.; Ong, I. M.; Myers, C. L.; Guzei, I. A.; Westler, W. M.; Andes, D. R.; Bugni, T. S. *Angew. Chem., Int. Ed.* **2014**, *53*, 11583–11586. (e) Shaaban, K. A.; Elshahawi, S. I.; Wang, X.; Horn, J.; Kharel, M. K.; Leggas, M.; Thorson, J. S. *J. Nat. Prod.* **2015**, *78*, 1723–1729. (f) Shin, B.; Kim, B.-Y.; Cho, E.; Oh, K.-B.; Shin, J.; Goodfellow, M.; Oh, D.-C. *J. Nat. Prod.* **2016**, *79*, 1886–1890. (g) Kimura, T.; Iwatsuki, M.; Asami, Y.; Ishiyama, A.; Hokari, R.; Otaguro, K.; Matsumoto, A.; Sato, N.; Shiomi, K.; Takahashi, Y.; Omura, S.; Nakashima, T. *J. Antibiot.* **2016**, *69*, 818–824. (h) Kodani, S.; Komaki, H.; Ishimura, S.; Hemmi, H.; Ohnishi-Kameyama, M. *J. Ind. Microbiol. Biotechnol.* **2016**, *43*, 1159–1165.
- (a) Harada, K.; Tomita, K.; Fujii, K.; Masuda, K.; Mikami, Y.; Yazawa, K.; Komaki, H. *J. Antibiot.* **2004**, *57*, 125–135. (b) Mazzei, E.; Iorio, M.; Maffioli, S. I.; Sosio, M.; Donadio, S. *J. Antibiot.* **2012**, *65*, 267–269. (c) Kawahara, T.; Itoh, M.; Izumikawa, M.; Sakata, N.; Tsuchida, T.; Shin-ya, K. *J. Antibiot.* **2014**, *67*, 577–580.
- Keller-Schierlein, W.; Hagmann, L.; Zähler, H.; Huhn, W. *Helv. Chim. Acta* **1988**, *71*, 1528–1540.
- Baksh, A.; Keppinger, B.; Isah, H. A.; Probert, M. R.; Clegg, W.; Wills, C.; Goodfellow, M.; Errington, J.; Allenby, N.; Hall, M. J. *Nat. Prod. Res.* **2017**, 10.1080/14786419.2016.1263854.
- (a) Marazzi, A.; Kurz, M.; Stefanelli, S.; Colombo, L. *J. Antibiot.* **2005**, *58*, 260–267. (b) Mariani, R.; Granata, G.; Maffioli, S. I.; Serina, S.; Brunati, C.; Sosio, M.; Marazzi, A.; Vannini, A.; Patel, D.; White, R.; Ciabatti, R. *Bioorg. Med. Chem. Lett.* **2005**, *15*, 3748–3752. (c) Zhang, Y.; Degen, D.; Ho, M. X.; Sineva, E.; Ebricht, K. Y.; Ebricht, Y. W.; Mekler, V.; Vahedian-Movahed, H.; Feng, Y.; Yin, R.; Tuske, S.; Irschik, H.; Jansen, R.; Maffioli, S.; Donadio, S.; Arnold, E.; Ebricht, R. H. *eLife* **2014**, *3*, e02450.
- Shaaban, K. A.; Saunders, M. A.; Zhang, Y.; Tran, T.; Elshahawi, S. I.; Ponomareva, L. V.; Wang, X.; Zhang, J.; Copley, G. C.; Sunkara, M.; Kharel, M. K.; Morris, A. J.; Hower, J. C.; Tremblay, M. S.; Prendergast, M. A.; Thorson, J. S. *J. Nat. Prod.* **2017**, *80*, 2–11.
- Maldonado, L. A.; Stach, J. E.; Pathom-aree, W.; Ward, A. C.; Bull, A. T.; Goodfellow, M. *Antonie van Leeuwenhoek* **2005**, *87*, 11–18.
- The 16S rRNA sequence for *Actinomadura* sp. DEM31376 was deposited with the NCBI, GenBank accession number KY512569.
- Production of madurastatin C1 from *Actinomadura* sp. DEM31376 was estimated at 19 mg/L (bioreactor, ISP2 media), in comparison to the reported 65 mg/L from *Actinomadura* sp. DSMZ 13491 (shake flask, AFT media) [ref 5b] and 32 mg/L from *Streptosporangium* sp. 32552 (shake flasks, custom media) [ref 5c].
- Fong, C. F.; Grant, H. G. *Aust. J. Chem.* **1981**, *34*, 2307–2312.
- (a) Yamamoto, S.; Okujo, N.; Sakakibara, Y. *Arch. Microbiol.* **1994**, *162*, 249–254. (b) Shapiro, J. A.; Wenciewicz, T. A. *ACS Infect. Dis.* **2016**, *2*, 157–168.
- (a) Suenaga, K.; Kokubo, S.; Shinohara, C.; Tsuji, T.; Uemura, D. *Tetrahedron Lett.* **1999**, *40*, 1945–1948. (b) Kokubo, S.; Suenaga, K.; Shinohara, C.; Tsuji, T.; Uemura, D. *Tetrahedron* **2000**, *56*, 6435–6440.
- Seyedsayamdost, M. R.; Traxler, M. F.; Zheng, S.-L.; Kolter, R.; Clardy, J. *J. Am. Chem. Soc.* **2011**, *133*, 11434–11437.
- Tsuda, M.; Yamakawa, M.; Oka, S.; Tanaka, Y.; Hoshino, Y.; Mikami, Y.; Sato, A.; Fujiwara, H.; Ohizumi, Y.; Kobayashi, J. *J. Nat. Prod.* **2005**, *68*, 462–464.
- Chen, Y.; Unger, M.; Ntai, I.; McClure, R. A.; Albright, J. C.; Thomson, R. J.; Kelleher, N. L. *MedChemComm* **2013**, *4*, 233–238.
- Schneider, K.; Rose, I.; Vikineswary, S.; Jones, A. L.; Goodfellow, M.; Nicholson, G.; Beil, W.; Süßmuth, R. D.; Fiedler, H.-P. *J. Nat. Prod.* **2007**, *70*, 932–935.
- Mukai, A.; Fukai, T.; Matsumoto, Y.; Ishikawa, J.; Hoshino, Y.; Yazawa, K.; Harada, K.; Mikami, Y. *J. Antibiot.* **2006**, *59*, 366–369.
- (a) Inahashi, Y.; Iwatsuki, M.; Ishiyama, A.; Namatame, M.; Nishihara-Tsukashima, A.; Matsumoto, A.; Hirose, T.; Sunazuka, T.; Yamada, H.; Otaguro, K.; Takahashi, Y.; Omura, S.; Shiomi, K. *J. Antibiot.* **2011**, *64*, 303–7. (b) Zhang, J.; Hughes, R. R.; Saunders, M. A.; Elshahawi, S. I.; Ponomareva, L. V.; Zhang, Y.; Winchester, S. R.; Scott, S. A.; Sunkara, M.; Morris, A. J.; Prendergast, M. A.; Shaaban, K. A.; Thorson, J. S. *J. Nat. Prod.* **2017**, *80*, 12–18.
- CCDC 1525889–1525891 contain the supplementary crystallographic data for compounds 5, 6, and 10. These data can be obtained free of charge from the Cambridge Crystallographic Data Centre via www.ccdc.cam.ac.uk/structures.
- Vedejs, E.; Klapars, A.; Warner, D. L.; Weiss, A. H. *J. Org. Chem.* **2001**, *66*, 7542–7546.
- Hu, J.; Miller, M. J. *J. Am. Chem. Soc.* **1997**, *119*, 3462–3468.
- Phillips, A. J.; Uto, Y.; Wipf, P.; Reno, M. J.; Williams, D. R. *Org. Lett.* **2000**, *2*, 1165–1168.
- Wohl, R. A.; Cannie, J. *J. Org. Chem.* **1973**, *38*, 1787–1790.
- Lwowsky, W. In *Comprehensive Heterocyclic Chemistry*; Katritzky, A. R.; Rees, C. W., Eds.; Pergamon Press: Oxford, 1984; Vol. 7, Chapter 5.

(28) Harada, K.; Fujii, K.; Hayashi, K.; Suzuki, M.; Ikai, Y.; Oka, H. *Tetrahedron Lett.* **1996**, *37*, 3001–3004.

(29) (a) Stephan, H.; Freund, S.; Meyer, J.-M.; Winkelmann, G.; Jung, G. *Liebigs Ann. Chem.* **1993**, *1993*, 43–48. (b) Kreuzer, M. F.; Kage, H.; Nett, M. *J. Am. Chem. Soc.* **2012**, *134*, 5415–5422.